Magnetorheological Properties of Sterically Stabilized Ferrofluids

By

LEONA J FELICIA

Enrolment No: PHYS02 2010 04012

Indira Gandhi Centre for Atomic Research, Kalpakkam,
Tamil Nadu, India 603 102

A Thesis submitted to the
Board of Studies in Physical Sciences
In partial fulfillment of requirements
For the degree of

DOCTOR OF PHILOSOPHY

of

HOMI BHABHA NATIONAL INSTITUTE

May, 2015

Homi Bhabha National Institute

Recommendations of the Viva Voce Board

As members of the Viva Voce Board, we certify that we have read the dissertation prepared by **Leona J Felicia** entitled "**Magnetorheological Properties of Sterically Stabilized Ferrofluids**" and recommend that it may be accepted as fulfilling the dissertation requirement for the Degree of Doctor of Philosophy.

____**Date:**

Chairman-**Dr. T. Jayakumar**

____**Date:**

Convener-**Dr. John Philip**

____**Date:**

Member 1-Examiner

____**Date:**

Member 2-**Dr. B. V. R. Tata**

____**Date:**

Member 3- **Dr. T. R. Ravindran**

Final approval and acceptance of this dissertation is contingent upon the candidate's submission of the final copies of the dissertation to HBNI.

I hereby certify that I have read this thesis prepared under my direction and recommend that it may be accepted as fulfilling the thesis requirement.

Date: **Dr. John Philip**

Place: (Guide)

CERTIFICATE

I hereby certify that I have read this thesis prepared under my direction and recommend that it may be accepted as fulfilling the thesis requirement.

Date: **Dr. John Philip**

Place: (Guide)

STATEMENT BY AUTHOR

This dissertation has been submitted in partial fulfillment of requirements for an advanced degree at Homi Bhabha National Institute (HBNI) and is deposited in the Library to be made available to borrowers under rules of the HBNI.

Brief quotations from this dissertation are allowable without special permission, provided that accurate acknowledgement of source is made. Requests for permission for extended quotation from or reproduction of this manuscript in whole or in part may be granted by the Competent Authority of HBNI when in his or her judgment the proposed use of the material is in the interests of scholarship. In all other instances, however, permission must be obtained from the author.

Kalpakkam **(LEONA J FELICIA)**

May, 2015

DECLARATION

I, hereby declare that the investigation presented in the thesis has been carried out by me. The work is original and has not been submitted earlier as a whole or in part for a degree/diploma at this or any other Institution/University.

Kalpakkam **(LEONA J FELICIA)**

May, 2015

List of Publications arising from the thesis

1. "Effect of Hydrophilic Silica Nanoparticles on the Magnetorheological Properties of Ferrofluids: A Study Using Opto-magnetorheometer", **Leona J Felicia** and John Philip, *Langmuir,* **2015**, 31, 3343-3353.

2. "Probing of Field Induced Structures and their Dynamics in Ferrofluids using Oscillatory Rheology", **Leona J Felicia** and John Philip, *Langmuir,* **2014**, 30, 12171-12179.

3. "Magnetorheological Properties of a Magnetic Nanofluid with Dispersed Carbon Nanotubes", **Leona J Felicia** and John Philip, *Phys. Rev. E,* **2014**, 89, 022310.

4. "Probing of Field-Induced Structures and Tunable Rheological Properties of Surfactant Capped Magnetically Polarizable Nanofluids", **Leona J Felicia** and John Philip, *Langmuir,* **2013**, 29, 110-120.

Communicated/in preparation

5. "Correlation between the macroscopic rheology and microstructure of ferrofluids under magnetic field using Rheomicroscope", **Leona J. Felicia** and John Philip.

6. "Temporal evolution of field induced structures and their effect on the magnetorheology of ferrofluids", **Leona J. Felicia** and John Philip.

7. "Effect of nanofillers on the rheological properties of Poly vinyl alcohol hydrogels". **Leona J. Felicia** and John Philip,

Conferences

1. **Leona J Felicia** and John Philip, "*Magnetorheological Properties of ferroseals*", 24th Annual General Meeting (AGM) of the Materials Research Society of India (MRSI), held at the Indira Gandhi Centre for Atomic Research, Kalpakkam, India, during February 11-13, 2013, P-138.

2. **Leona J Felicia** and John Philip, "*Magnetorheological Properties of ferrofluids*", 13th International Conference on Magnetic Fluids- ICMF-13, held at National Physical Laboratory, New Delhi, during January 7-11, 2013, P-351.
3. **Leona J Felicia** and John Philip, "*Magnetorheological Properties of Nanofluids*" International Conference on Nanoscience and Technology (ICONSAT)-2012, held at Hotel Taj Krishna, Hyderabad, during January 20-23, 2012, P-256.
4. **Leona J Felicia** and John Philip, "*Magnetorheological Properties of ferrofluids*", Invited presentation at the Department of Materials & Interfaces (Professor Jacob Klein's lab), Weizmann Institute of Science, Israel, during March 15-18, 2015.

Other Publications (not included in the thesis)

1. "Effect of Surfactant on the Size, Zeta Potential and Rheology of Alumina Nanofluids", **Leona J. Felicia**, Jeena C Johnson and John Philip, *J. Nanofluids*, **2014**, 3, 328-335.
2. "Rheological Properties of Magnetorheological Fluid with Silica Nanoparticles Stabilizers – A Comparison with Ferrofluid", **Leona J. Felicia**, Reji John, and John Philip, *J. Nanofluids*, **2013**, 2, 75-84.
3. "A Simple, In-Expensive and Ultrasensitive Magnetic Nanofluid Based Sensor for Detection of Cations, Ethanol and Ammonia ", J. Philip, V. Mahendran, and **Leona J. Felicia**, *J. Nanofluids*, **2013**, 2, 112-119.

Kalpakkam **(LEONA J FELICIA)**

May, 2015

DEDICATED

To my parents,

M. Jayaprakash & R. Lakshmi

ACKNOWLEDGEMENTS

First of all, I praise and thank my Lord Jesus Christ, for His grace in providing me this opportunity and granting me the capability to proceed successfully. I thank the former centre directors, **Dr. Baldev Raj** and **Shri. C. Chetal** and the present Director, **Dr. P. R. Vasudeva Rao** for allowing me to carry out my research work at the Indira Gandhi Centre for Atomic Research.

I express my deepest sense of gratitude to **Dr. John Philip**, my esteemed supervisor, for grooming me as a PhD student, his warm encouragement, thoughtful guidance, insightful decisions, critical comments and correction of the thesis.

I am thankful to my doctoral committee chairman **Dr. T. Jayakumar** and members **Dr. B. V. R. Tata**, **Dr. T. R. Ravindran** and **Dr. V. P. Venugopalan** for their valuable comments and support.

I gratefully acknowledge the financial assistance from **DAE-BRNS** through a perspective research grant **(2009/38/01/BRNS)**. I thank **Dr. Sai Baba** for the wonderful hospitality during my stay at JRF enclave. I also thank all the members of **SMARTS** and **RTS** for their support and for creating a cordial working environment.

I wish to thank my friends, **Ms. S. Anbumozhi Angayarkanni**, for the everyday fun we had and **Ms. R. Pratibha Nalini,** for her prayers. They were with me through some of my toughest moments, supporting me by their love and encouraging words. I deeply acknowledge my aunt **Mrs. Carolin William**, for her moral support, prayers and for listening and offering me advice. I thank **Dr. Isaac Samuel**, **Mrs. Cynthia Isaac** and **Miss. Johanna Afreena** for the love, prayerful support and homely atmosphere which I enjoyed at their place. I am thankful to my seniors **Dr. Sudhanshu** and **Dr. Joy** for the

many discussions and helping me with learning instruments. I also thank all my friends who in each big or small means helped me throughout this entire research period.

Finally but most importantly, I am indebted to my parents **Mr. Jayaprakash** and **Mrs. Lakshmi** and brother, **Mr. Godwin JP**, for their love and care in all aspects of my life and for their support of all my life choices.

CONTENTS

Chapter 1

Introduction

Chapter 2

Materials and Experimental Techniques

Chapter 3

Probing of Field Induced Structures and Tunable Rheological Properties of Ferrofluid

Chapter 4

Study of Field Induced Structures in Ferrofluid using Rheomicroscope

Chapter 5

Probing the Dynamics in Ferrofluid using Oscillatory Rheology

Chapter 6

Effect of Multiwalled Carbon Nanotubes on the Magnetorheological Properties of Ferrofluid

Chapter 7

Effect of Hydrophilic Silica Nanoparticles on the Magnetorheological Properties of Ferrofluid

Chapter 8

Conclusions and Recommendations for Future Work

SYNOPSIS

Ferrofluids are suspensions of nanometer sized magnetic particles dispersed in carrier fluids. The particles used in ferrofluids are single-domain, surfactant or polymer coated magnetic particles in the size range of 3-15 nm. Ferrofluids can be manipulated by an external magnetic field and thereby tune their physical properties such as optical, thermal and rheological and hence find use in several applications. An understanding of the rheological properties of ferrofluids under an external magnetic field is very important from both fundamental understanding as well as application point of view. Most experimental studies report results on the magnetorheological behavior of dilute ferrofluids. In addition the non availability of model ferrofluids with minimum polydispersity and well stabilized magnetic nanoparticles has led to non-reproducible results. This served as one of the motivations to carry out a systematic study of the magnetorheological properties of ferrofluids. Further, the relaxation dynamics in ferrofluids under oscillatory deformation and the effect of non magnetic additives have not been probed which is another motivation for the thesis. The thesis consists of eight chapters and the details of each chapter are summarized below. **Chapter 1** gives an introduction to ferrofluids with a focus on the initial studies on viscosity measurements on ferrofluids in the presence of an external magnetic field with discussion on the concepts of rotational viscosity, magnetoviscosity, negative viscosity and the relaxation mechanisms involved and the factors affecting the magnetorheological properties of ferrofluids. **Chapter 2** describes methods of preparation of ferrofluids and the experimental techniques used for their characterization. **Chapter 3** discusses the magnetorheological properties of the ferrofluid containing Fe_3O_4 nanoparticles of size ~12 nm coated with oleic acid and dispersed in kerosene at volume fractions of 0.038 and 0.05. **Chapter 4** discusses the results on the study of magnetic field induced structures in dilute ferrofluids (φ = 0.00078 to 0.0063) using a rheomicroscope with custom-made solenoid set up. **Chapter 5** presents the results of field-induced structures and their dynamics in ferrofluid (φ = 0.046) using oscillatory rheology. **Chapter 6** discusses the effect of multiwalled carbon nanotubes on the magnetorheological properties of an oil based ferrofluid of volume fraction φ = 0.087. **Chapter 7** discusses the effect of network forming hydrophilic silica nanoparticles on the rheology of a nonpolar oil based ferrofluid under varying magnetic field using magnetorheometer and rheomicroscope. **Chapter 8** summarizes the results obtained, conclusions drawn and the recommendations for future work. The key findings of this thesis work are: The application of magnetic field to a ferrofluid results in the increase in the viscosity of the ferrofluid due to the alignment of the magnetic moments of the particles along the field direction leading to the formation of chains and columns. When subjected to a shear force, the ferrofluid exhibits a shear thinning behavior due to the breaking of the field induced structures and their reorientation along the shear flow. A shear resistant “plateau-like region” due to the peculiar alignment of the chains with respect to the field direction is observed at high magnetic field. Mason number scaling shows a collapse of viscosity curves at different magnetic fields onto a single master curve. The hysteresis area decreases with shear rate as a power law. Under oscillatory shear, the ferrofluid exhibits a viscoelastic behavior. The amplitude sweep measurements show elastic behavior at low strain amplitudes and viscous response due to the destruction of field induced structures at higher strains. A transition from the high frequency elastic to low frequency viscous response is observed in the frequency dependent measurements. The microstructure of the ferrofluid under magnetic field and shear, observed along the field direction perpendicular to the plane of shear, shows columnar aggregates whose diameter increases with magnetic field due to the

zippering transitions and form larger size aggregates with diameter varying from 7 to 37 μm. Under shear, the columns begin to dealign from the direction of the magnetic field and reorient along the shear flow direction. The changes in the ferrofluid microstructure are evident from the increase in the macroscopic viscosity and shear thinning response. Using the SRFS, the relaxation occurring at low frequencies was shifted to an accessible frequency regime. The structural relaxation resulting from rearrangement of particles occurred more easily as the strain-rate increases. The magnetic field dependence of the relaxation time and crossover modulus showed two distinct regions, indicating the different microstructures in those regions. In the presence of magnetic field, the ferrofluid containing CNTs shows lower viscosity, yield stress, hysteresis and viscoelastic moduli due to weakening of the ferrofluid microstructure. The weakened dipolar interaction in presence of silica lowers the viscosity, yield stresses and viscoelastic moduli of the ferrofluid. The silica network hampers the zippering transition in ferrofluids which is confirmed from the diameter of the columns. The ferrofluid with silica exhibits a dominant elastic behavior in frequency sweep measurements and a longer viscoelastic regime in strain dependent measurements. The findings of this thesis provide new insights into the magnetorheological properties of oil based ferrofluids that would enable their better utilization in applications such as electronic cooling for micro- and nanomechanical devices, smart dampers, dynamic liquid seals, etc. The fast switching of Brownian particles to linear structures and their retention under flow are essential for cooling and also dynamic sealing applications.

LIST OF FIGURES

LIST OF TABLES

LIST OF ABBREVIATIONS

CCD	Charge coupled device
CI	Carbonyl iron
CNT	Carbon nanotubes
CNT-FF	Ferrofluid with CNT
CR	Controlled strain
CS	Controlled stress
DC	Direct Current
EC	Electrically Commuted
ER	Electrorheological
FF	Ferrofluid
FF-silica	Ferrofluid with silica
LDS	Lithium dodecyl sulfate
LVE	Linear viscoelastic
MCR	Modular Compact Rheometer
MHT	Modified Halsey-Toor
MR	Magnetorheological
MRD	Magnetorheological Device
MVE	Magnetoviscous Effect
MWCNT	Multiwalled carbon nanotubes
PANI	Polyaniline
PMMA	Poly methyl methacrylate

PS	Polystyrene
rpm	Rotations per minute
SANS	Small angle neutron scattering
SDS	Sodium dodecyl sulfate
SRFS	Strain-rate frequency superposition
SWNT	Single walled carbon nanotubes
TEM	Transmission electron microscopy
TGA	Thermogravimetric Analysis
TMAOH	Tetramethylammonium hydroxide
TMV	Tobacco Mosaic Virus
VSM	Vibrating Sample Magnetorheometer
YS	Yield stress

LIST OF SYMBOLS

H	Magnetic field strength
φ	Volume fraction of particles
η_c	Viscosity of carrier fluid
η_R	Rotational viscosity
v	Velocity of a liquid element
Ω	Angular Velocity of the liquid element
Θ	Angular Velocity of particles
α	Angle between H and Ω
μ_0	Permeability of free space
m	Magnetic moment of the particle
k_B	Boltzmann constant
T	Temperature

d	Diameter of the nanoparticle
a	Radius of the nanoparticle
χ	Effective magnetic susceptibility of the particle
$U(r,\theta)$	Dipolar interaction energy
r	Distance between centres of two particles
θ	Angle between H and line joining the particle centres
λ	Coupling constant
t_B	Characteristic time for Brownian motion
t_{BW}	Characteristic time for Brownian motion accounting for dipolar interactions
D	Diffusion coefficient of the particle
ρ	Distance between two chains
s	Size of the cluster
D_s	Diffusion coefficient of a cluster of size s
t_c*	Cross-over time
τ_B	Brownian relaxation time
τ_N	Neel relaxation time
$\tilde{V}$	Hydrodynamic volume of the particle
V	Magnetic volume of the particle
f_0	Attempt frequency
K	Anisotropy constant
τ_{eff}	Effective relaxation time
F_m	Magnetic force
F_v	Viscous force
M_0	Spontaneous magnetization of the particle
b	Thickness of the surfactant layer

N	Number of particles in a chain
N_{max}	Maximum number of particles in a chain
$\dot{\gamma}$	Shear rate
h	Gap between the plates of the rheometer
F	Tangential force
A	Area of the plate
σ	Shear stress
η	Viscosity
Pe	Peclet number
G	Rigidity modulus
γ	Strain
τ_K	Retardation time
τ_M	Relaxation time
γ_0	Strain amplitude
σ_0	Stress amplitude
ω	Angular frequency
δ	Damping factor
G^*	Complex modulus
G'	Storage/elastic modulus
G''	Loss/viscous modulus
θ_{cp}	Angle of the cone
R	Radius of the cone/plate
Ω'	Angular velocity of cone/plate/cylinder
r_o	Radius of outer cylinder
r_1	Radius of inner cylinder

t'	Thickness of the specimen
δ'	Phase shift
$\mathit{\Delta}$	Optical path difference
n_1	Refractive index of medium
n_2	Refractive index of specimen
λ'	Wavelength of light
t	Time
δt	Time difference
$g^{(1)}(q,t)$	Electric field auto correlation function
$g^{(2)}(q,t)$	Intensity auto correlation function
$\mathit{\Gamma}$	Relaxation rate
q	Scattering vector
U	Interaction energy per unit length
L_{max}	Maximum chain length
Mn	Mason number
β	Contrast factor
μ_c	Relative permeability of the carrier fluid
μ_p	Relative permeability of the particle
N^*	Maximum number particles for gap-spanning chain
Mn^*	Critical Mason number
θ_c	Maximum chain tilt angle
τ_y	Yield stress
k	Consistency factor
n	Power law index
M_s	Saturation magnetization of the particle

η_∞	Viscosity of ferrofluid at infinite shear rate in the absence of magnetic field
η_F	Field specific viscosity
B	Magnetic field
γ_c	Critical strain
$\dot{\gamma}_0$	Strain-rate amplitude
G_{scaled}	Scaled modulus
ω_{scaled}	Scaled angular frequency
G_c	Cross-over modulus
ω_c	Cross-over frequency
t_r	Structural relaxation time
H_c	Critical magnetic field strength

Chapter 1 Introduction

1.1 Soft Matter

Soft matters comprise a wide range of systems including emulsions, foams, colloidal suspensions, polymers, surfactants, liquid crystals, gels, granular and biological materials which self-organize into mesoscopic length scales ranging from a few nanometer to micrometers wherein the forces involved are weaker as compared to interatomic or intermolecular forces.[1] They have neither the three-dimensional atomic long-range order of crystalline solids nor the uniform disorder of liquids. Soft matter is easily deformable by thermal fluctuations. The lower energy scale allows a plethora of symmetries and morphologies in soft matter. The macroscopic behavior of soft matter is determined by the overall properties and interactions of the mesoscopic structures. A schematic picture showing the different classes of soft matter is provided in **Fig. 1.1**.

Some soft materials have an ability to alter their physico-chemical properties by responding to external stimuli such as light, temperature, pH, ionic strength, electric and magnetic fields.[2-5] For example, liquid crystals and block copolymer solutions exhibit one or more mesophases upon heating or changing solvent conditions.[6-9] The optical and rheological properties of a class of soft materials called electrorheological (ER) fluids can be tuned by an electric field.[10-14] The hydrogels can swell or collapse under varying pH[15] and can change their viscoelastic moduli significantly under varying ionic strength.[16, 17] Tuning the rheological properties of surfactant solutions has been achieved by exposure to light.[18] For instance, when the surfactant solution of cetyl trimethylammonium bromide together with a photosensitive organic acid is irradiated with an ultra violet light its viscosity decreases by almost 4 orders of magnitude due to the trans to cis photoisomerisation.[18] The stop bands of colloidal photonic crystals can be magnetically tuned to cover the entire visible spectrum.[19, 20] Telechelic cationic polyelectrolytes exhibit pH tuning of their rheology.[21] The degradability of hydrogels can be tuned by varying the cross-linker molecular weight, functionality and polymer density.[22]

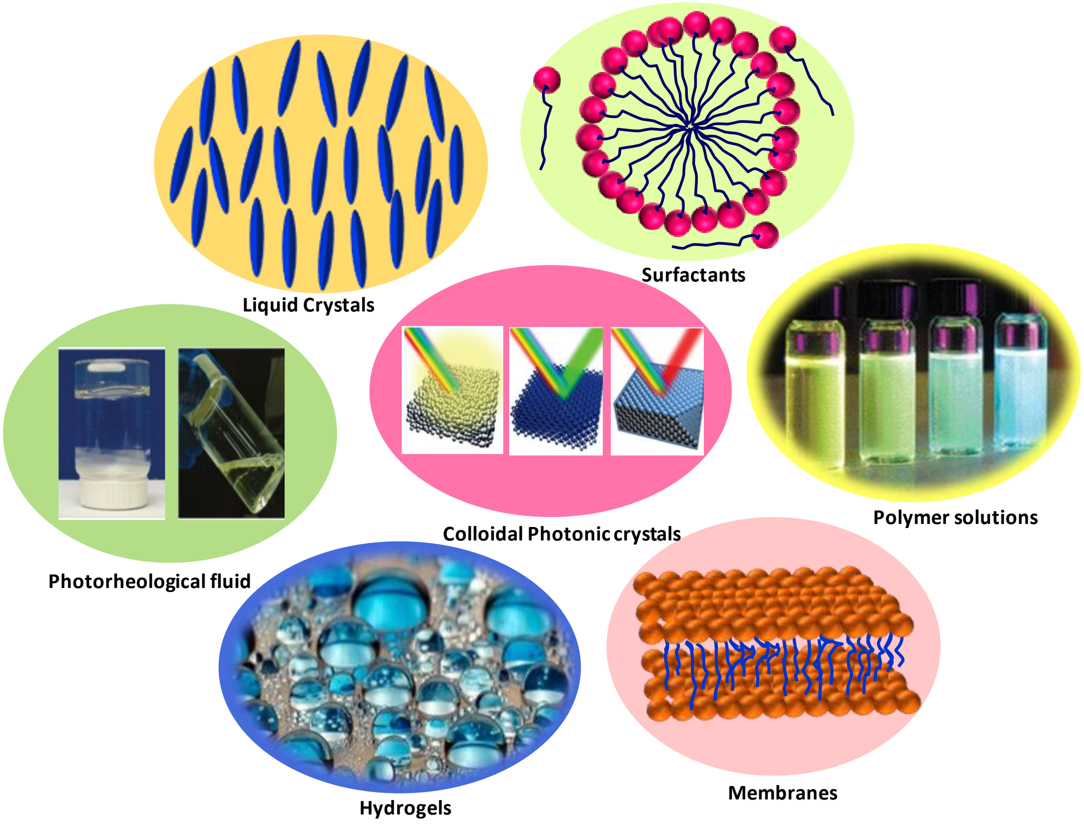

Figure 1.1: Schematic showing the different types of soft matter.

1.2 Magnetic Field Tunable Soft Matter

There exists a class of soft matter whose properties can be tuned by applying a magnetic field. Magnetic fluids and magnetic gels fall under this category.[23-32] Magnetic fluids are suspensions of micro[33, 34] or nano[35-37] sized magnetic particles in a base fluid. The former are called Magnetorheological (MR) fluids and the latter are called Ferrofluids. Magnetic gels are formed by incorporating magnetic particles within gel forming matrices which have several biomedical applications such as biomimetic actuators, drug release etc.[38-43]

1.2.1 Magnetorheological Fluids

Magnetorheological fluids were first developed by Jacob Rabinow.[44, 45] They exhibit reversible and very fast (fraction of a millisecond) transition from a liquid to a nearly solid state in the presence of external magnetic fields and hence have applications in seismic vibration dampers, shock absorbers, torque transducers, clutches, brakes, ultrafine polishing technology, clutches and thermal energy transfer.[46-48] **Fig. 1.2 (a)** shows the viscosity variation of an MR fluid with increasing magnetic field. The schematic of an MR fluid damper is shown in **Fig. 1.2 (b)**.

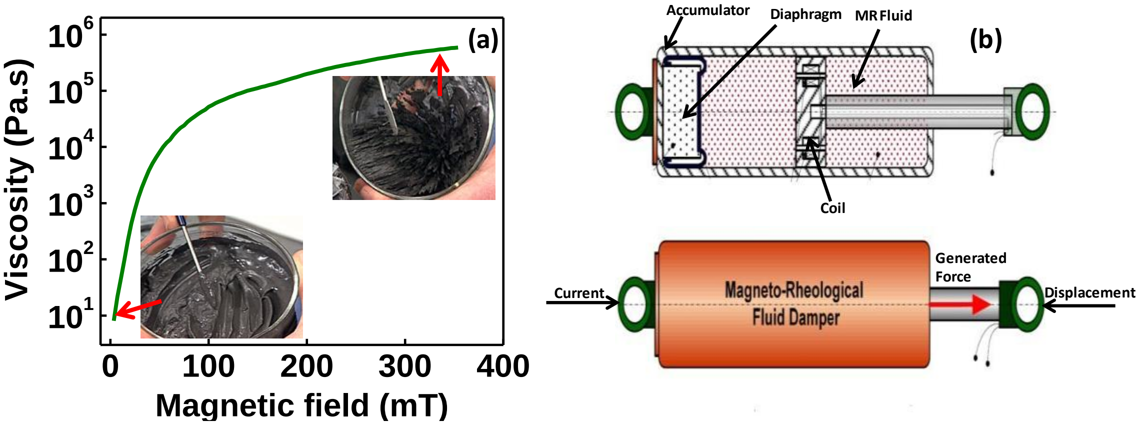

Figure 1.2: (a) Variation of viscosity of Magnetorheological fluid with magnetic field.[49] (b) Schematic showing the set up of an MR fluid damper. Inset of (a) shows the MR fluid in the absence and presence of magnetic field.

Carbonyl iron (CI) is one of the most commonly used particles in MR fluids due to its high magnetic permeability, soft magnetic property and common availability. Mineral oil, silicone oil, polyesters, polyethers, synthetic hydrocarbons, vegetable oils, water etc. are used as carrier fluids. However, MR fluids suffer from a serious problem of sedimentation owing to the large sized particles used. The sedimentation problem in MR fluids was overcome by several ways such as addition of surfactants to provide electrostatic or steric repulsion, addition of magnetic nanoparticles, addition of thickening agents like carbon fibers, silica nanoparticles, use of ionic carrier liquids etc.[50-54] E.g. Choi et al.[55] found that the addition of fumed silica to MR fluids reduced the sedimentation of micron-sized CI particles and improved the flocculation stability. Organoclay additives in MR fluid was also found to prevent sedimentation due to the formation of three dimensional network.[54] Polymer coatings on the CI particles were found to decrease their sedimentation rate due to decreased density of the CI-polymer composite.

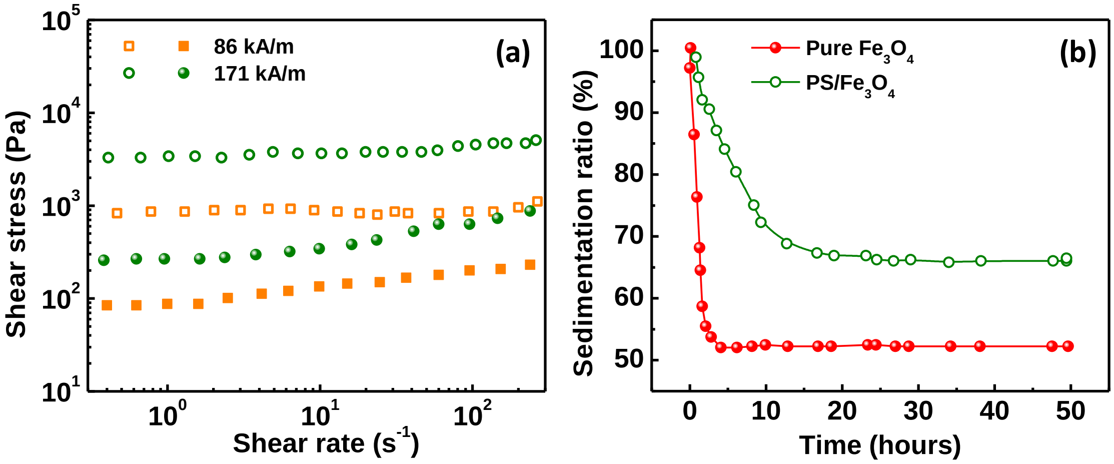

Figure 1.3: (a) Flow curves of CI-PMMA based MR fluids at CI:PMMA ratio of 2:1 (open symbols) and 1:2 (closed symbols)[56] (b) Sedimentation ratio as a function of time for pure Fe_3O_4 and PS/Fe_3O_4 based MR fluids.[57]

For example, Poly methyl methacrylate (PMMA) encapsulated CI particles showed a larger yield stress and an enhanced sedimentation stability.[58] Core-shell structured Polystyrene(PS)/Fe_3O_4[57] and multi walled carbon nanotubes (MWCNT)/Polyaniline/CI[59] particles used in MR fluids displayed remarkable stability against sedimentation. Another method of improving the stability of MR fluids was by the use of magnetizable fibers that have good sedimentation stability as against the spheres.[60] Single walled carbon nanotubes (SWNTs) added to MR suspensions were also able to reduce the sedimentation of the CI particles.[61] Enhancement of yield stress in CI-PMMA based MR fluids and better sedimentation stability of PS/Fe_3O_4 MR fluids are shown in **Fig. 1.3**. The magnetorheological studies on MR fluids showed that the addition of 3 wt% of stearic acid to silicone oil based MR fluid resulted in 92 % stability enhancement of the suspensions which is eight times more than that of common MR fluids.[62] The maximum observed yield stress of 27 kPa was more than the yield stress of common MR fluids.

The viscosity and yield stress values decreased with increase in temperature. MR fluids containing rod shaped particles showed an enhanced MR performance under oscillatory shear when compared to MR suspensions containing spheres.[63] A lower magnetic field strength is sufficient for the structuration of rod-based MR fluid. The viscoelastic moduli are almost one order of magnitude larger for the rod-based fluid than that of the sphere based fluid. Magnetorheological properties of MR fluids containing cobalt wires and rigid filaments of chemically linked iron microspheres were compared with those of suspensions containing spherical cobalt or iron particles.[64] It was observed that the yield stress of suspensions of cobalt wires is three times higher than that of cobalt spheres suspension. On the other hand, suspension of iron filaments showed a lower yield stress than that of iron spheres suspension, probably due to the lower magnetization of the former. Time dependent rheological measurements on MR fluids showed that slippage and phase separation of the fluid occurred under high magnetic fields and shear rates leading to a decrease in the magnitude of the shear stress.[65]

Table 1.1: Summary of the magnetorheological studies on MR fluids. (YS- Yield stress, M_S – saturation magnetization)

S. No.	Particle/base fluid	Size (µm)	Concentration (vol%)	Key findings	Ref
1.	CI@PMMA/silicone oil	4.3	30	Larger YS and enhanced sedimentation stability	58
2.	Iron microwires/ silicone oil	5.4 & 7.6	2-6	Larger YS and enhanced sedimentation stability for wires than spheres	60
3.	CI@SWNT/Yubase 8 lubricant oil	4.25	20	• YS α $H^{3/2}$ • G' & G'' independent of ω	61
4.	CI/ silicone oil	2.7	15	• YS = 27 kPa • YS decreases with T	62
5.	Magnetite spheres/ silicone oil	0.68±0.15	0.5 -5	Enhanced MR performance of rods than spheres	63
	Magnetite rods/ silicone oil	0.56±0.12 ×6.9±3.8 (dia ×length)			
6.	Cobalt wires/ silicone oil	32-69 ×1.8-5.1 (Length × width)	5	YS of Co wires = 3 times YS of Co spheres	64
	Cobalt spheres	1.34 ± 0.4			
7.	CI/ silicone oil	4.5	46-50	Compression leads to high YS of 800 kPa	66
8.	Iron / silicone oil	-	0.5-2.1	YS scales with M_s	67

As the yield stress of the MR fluid depends on the magnetic field induced structure, a change in the fluid microstructure can improve the yield stress. Tang et al.[66] reported that compressing the MR fluid along the field direction, soon after the application of magnetic field, pushes the thick columns together resulting in a static yield stress value of 800 kPa under moderate magnetic field while the uncompressed fluid had a yield stress of 80 kPa.

Vereda et al.[67] reported that the average particle magnetization is a parameter for the scaling of the yield stress of MR fluid at low particle concentration. They observed a collapse of the yield stress values of suspensions containing iron spheres and plates of different saturation magnetization. For highly anisotropic iron rods, the yield stress of suspensions did not scale with magnetization due to interparticle mechanical friction. The key findings of the studies on the magnetorheological properties of MR fluids are summarized in **Table 1.1**.

1.2.2 Ferrofluids

The suspensions containing nanometer sized magnetic particles dispersed in carrier fluids are called ferrofluids. The particles used in ferrofluids are single-domain, surfactant or polymer coated magnetic particles in the size range of 3-15 nm.[68] The commonly used particles are ferrites such as Fe_3O_4, Fe_2O_3, $CoFe_2O_4$ etc. Ferrofluid was invented in 1963 by NASA's Steve Papell[69] with an idea of controlling liquids in gravity free space as their properties can be maneuvered by an external magnetic field. The smaller size of the particles in ferrofluids keeps them under constant Brownian motion thus preventing their gravitational settling while MR fluids, due to larger size of the particles, are prone to settling. However, the large surface area to volume ratio of magnetic nanoparticles leads to aggregation due to van der Waals attraction. The larger aggregates subsequently settle down thus rendering the fluid unstable. This problem was overcome by inducing either electrostatic or steric repulsion between particles in the fluid by making the particles charged or coating them with surfactants. Ferrofluids can be manipulated by an external magnetic field and thereby have tunable physical properties such as optical,[70] thermal[71] and rheological.[72] This has lead to the use of ferrofluids in numerous applications which exploit the change in the physical properties of the ferrofluid in the presence of an external magnetic field. Some of the interesting applications of ferrofluids are magnetofluidic leak free seals,[73] lubricants,[74] density separation,[75] ink jet printers,[76] refrigeration,[77] clutches,[78] tunable dampers,[79] tunable heat transfer fluids,[80] optical filters,[81] optical grating[82], defect sensors,[83] biosensors,[84, 85] cell separation,[86] magnetic resonance imaging based drug targeting,[87] quantification of biomolecule agglutination,[88] ultrasound contrast agents,[89] diagnostics in medicine,[90] hyperthermia agents,[91] magnetic field activated gels[92] and single-nucleotide polymorphism genotyping.[93] A schematic depicting some of the applications of ferrofluids is shown in **Fig. 1.4**. Their applications span a wide range of industrial sectors including defense, space, refrigeration and medicine. The field induced changes in the properties of ferrofluids have been studied using several techniques such as light scattering,[36] thermal conductivity measurements,[71] rheology[94] and Brownian dynamics.[95]

Of the several interesting physical properties of the ferrofluid, their rheology has drawn considerable interests from both fundamental understanding as well as application point of view. Rheology is the study of deformation and flow of matter.[96] Rheology is a mechanical method of probing the structure and dynamics of soft matter in general. In rheology the material is subject to a shear and the resulting stress is measured, from which quantities such as viscosity, shear stress, viscoelastic moduli and yield stress are determined. Magnetorheology is the study of rheological properties of the material under the action of an applied magnetic field. Since ferrofluids respond to an external magnetic field, their rheology is strongly influenced by the magnetic field. The detailed description of rheological techniques is given in **Chapter 2** of this thesis.

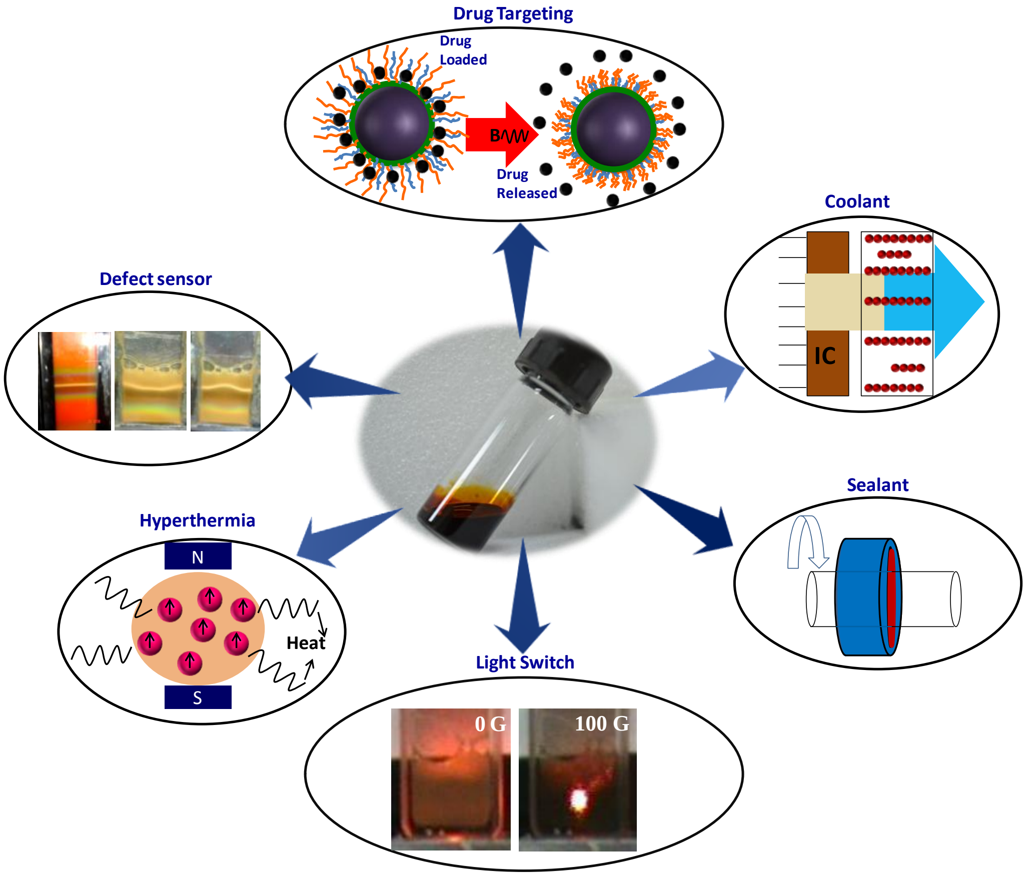

Figure 1.4: Schematic showing the different applications of ferrofluid such as coolants, sealants, light switch, hyperthermia, defect sensor and drug targeting.

1.2.3 Inverse Ferrofluids

A class of fluids containing nonmagnetic particles dispersed in ferrofluids is called "inverse ferrofluids".[97-100] The nonmagnetic particles used are silica and polystyrene latex spheres which are typically several orders of magnitude larger in size than the magnetic nanoparticles that constitute the ferrofluid and hence they experience a magnetically and hydrodynamically continuous medium. On application of a magnetic field, dipolar interactions are induced between the nonmagnetic particles, whose strength can be varied by changing the magnetic field or the saturation magnetization of the ferrofluid. A schematic of an inverse ferrofluid is shown in **Fig. 1.5**.

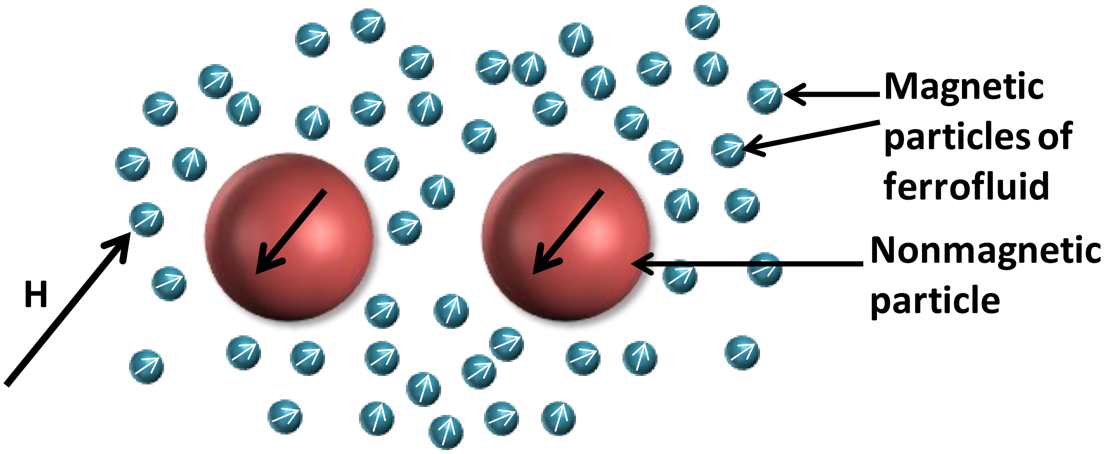

Figure 1.5: Schematic picture of an inverse ferrofluid. The arrows represent the magnetic moment of the particles.

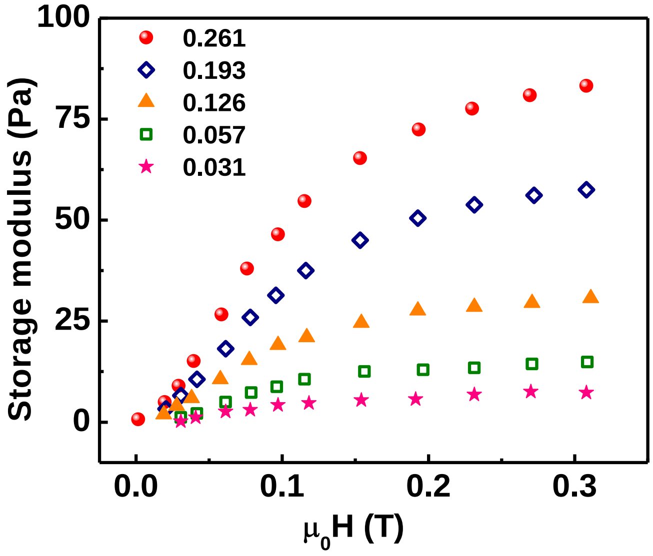

Figure 1.6: Storage modulus as a function of magnetic field strength and volume fraction of nonmagnetic silica particles in the inverse ferrofluid at a frequency of 1 Hz.[98]

The formation of linear particle chains under magnetic field in inverse ferrofluids was first reported by Skjeltorp.[101] Inverse ferrofluids produce viscosity enhancements comparable to MR fluids.[100] Since the size and shape of the nonmagnetic particles are well defined, inverse ferrofluids also serve as suitable systems for model studies of the magnetorheological effect.[98] The variation of storage modulus with H for an inverse ferrofluid[98] is shown in **Fig. 1.6**.

Table 1.2: Summary of the magnetorheological studies on inverse ferrofluids. (η – viscosity, Mn – Mason number)

S. No.	Particle/ base fluid	Size of non magnetic particle (µm)	Concentra-tion	Key findings	Ref
1.	Polystyrene spheres/ Hydrocarbon oil based ferrofluid	1.9	10^7 spheres/ cm^2	Attractive or repulsive dipolar interactions by tuning B	101
2.	Silica/ Nonaqueous ferrofluid	0.104-0.378	5.5 vol%	• Mason number scaling with η • Low Mn – monotonic increase in η with decreasing $\dot{\gamma}$ shear rate or low shear plateau • Medium Mn values – $\eta/\eta\infty\ \alpha\ Mn\Delta$; $1 < \Delta < 2/3$	100
3.	Silica/ Decalin based ferrofluid	0.053-0.189	5.7 and18 vol %	• small particles - strong increase of η • Beyond critical size-limited size dependence • Crossover occurs when chain length equals gap height	99
4.	Silica/ Cyclohexane based ferrofluid	0.177	3.1 to 26.1 vol%	• $G' >> G''$ • G' weakly dependent on ω	98
5.	Silica/ Cyclohexane based ferrofluid	0.199	1.1 to 18.1 vol%	• YS , $\eta\ \alpha\ \varphi$ • YS, $\eta\ \alpha\ m^2$ • Mason number scaling of η curves • Agreement with Bead-rod model	102
6.	Silica/ Ferrofluid	0.76	12.6 to 26.1vol%	η depends on flow point	103

There are also reports on a strong increase of viscosity of inverse ferrofluids with increase in magnetic field and size of the nonmagnetic particles.[99] Beyond a certain particle size and field strength, the dependence of viscosity on particle size saturates. The transition to saturation occurs when the average chain length approaches the gap size of the measuring geometry. The summary of the studies on inverse ferrofluids is given in **Table 1.2**.

1.3 Studies on Magnetorheological Properties of Ferrofluids

1.3.1 Rotational Viscosity

The first systematic study on the viscosity of ferrofluid was done by McTague[104] where the capillary viscosity of a dilute cobalt ferrofluid with the magnetic field either parallel or perpendicular to the flow direction was investigated. It was observed that the viscosity of the ferrofluid increased in the presence of a magnetic field. The increase was almost two times in the parallel mode than in the perpendicular mode. The increase in viscosity under magnetic field is termed "*rotational viscosity*" (η_R). The particles were assumed to be non-interacting and the rotational viscosity was accounted for by the hindrance to particle rotation caused by the magnetic torque which tries to align the particles magnetic moment in the direction of the applied field.[105] When a ferrofluid is subjected to a shear flow, the particles in the fluid will rotate about an axis parallel to the vorticity of the flow. If a magnetic field is applied along the direction of the vorticity as in **Fig. 1.7 (a)**, the magnetic moment of the particle will align along the direction of the field and the particle will rotate around the field direction with no effect of the flow. However, when the field is applied perpendicular to the vorticity as in **Fig. 1.7 (b)**, the magnetic moment of the particle will be tilted by the viscous force acting on it, causing it to deviate from the field direction. This results in a magnetic torque that counteracts the viscous torque and tries to realign the moment along the field direction. The free rotation of the particle is thus hindered by the counteraction of the magnetic and mechanical torques leading to an increase in the viscosity of the fluid.

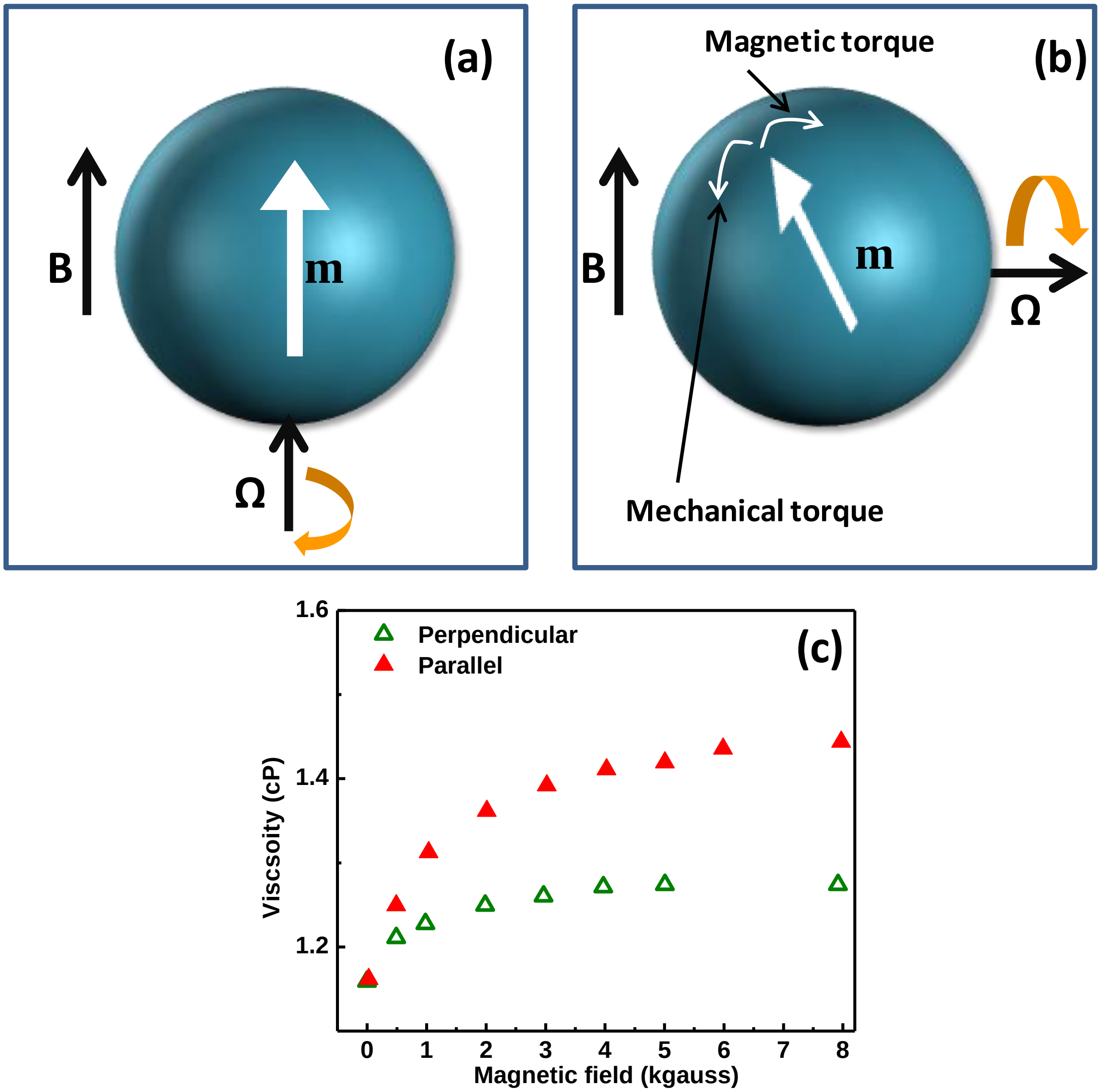

Figure 1.7: Schematic showing the direction of the magnetic moment of the particle when the magnetic field is (a) parallel and (b) perpendicular to the vorticity direction. (c) Viscosity of cobalt based ferrofluid as function of magnetic field directed perpendicular and parallel to the flow from the work of McTague.[104]

In the parallel mode, the magnetic field is perpendicular to the flow gradient preventing the particle rotation while in the perpendicular field there is a spatial distribution of angles between the magnetic field and the flow gradient. The variation of viscosity of cobalt ferrofluid as a function of magnetic field for parallel and perpendicular orientations of the magnetic field and shear flow from the work of McTague [104] is shown in **Fig. 1.7 (c)**. The expression for the viscosity increase in dilute magnetic suspensions under a magnetic field was derived by Shliomis[106] in 1972. The applied field orients the particles thus impeding their rotation resulting in an increase in the effective viscosity while the Brownian and hydrodynamic forces try to disorient the particles' magnetic moment. For a liquid moving with a velocity *v*, an element of the liquid volume rotates with an angular velocity $\Omega = \nabla \mathrm{x}\, \mathrm{v}/2$. In the absence of a magnetic field, the particles in the liquid rotate with an angular velocity $\Theta = \Omega$. But when the particles are oriented by the magnetic field which prevents their free rotation, a difference $(\Theta - \Omega)$ in angular velocity between the liquid and particles arises leading to energy dissipation and an effective increase in viscosity.

Considering all these factors, the contribution from rotational viscosity is given by

$$\Delta\eta = \frac{3}{2}\varphi\eta_c \frac{\xi - \tanh\xi}{\xi + \tanh\xi}\sin^2\alpha \tag{1. 1}$$

where φ is the volume fraction of the particles, η_c is the viscosity of the carrier fluid, α is the angle between the magnetic field strength H and the angular velocity of the rotation of the liquid Ω, $\xi = \frac{\mu_0 m H}{k_B T}$, μ_0 is the permeability of free space, m is the magnetic moment of the particle, k_B is the Boltzmann constant and T is the temperature. When H is parallel to Ω, the viscosity is independent of the magnetic field. When H is perpendicular to Ω, maximum increase in viscosity is observed. This theory could satisfactorily explain the observation of McTague.[104] Using the effective field method, Shliomis et al.[107] derived the magnetization equation microscopically and obtained a more accurate expression for rotational viscosity.

Miguel et al.[108] obtained an expression for the rotational viscosity of the ferrofluid as a function of the anisotropy parameter. Later Felderhof,[109, 110] Shliomis,[111] Muller et al.,[112] Patel et al.[113] and Embs et al.[114] proposed modifications and also verified the ferrofluid magnetization equations with experiments.

1.3.2 Magnetoviscosity

While the above theories could explain the origin of rotational viscosity in dilute ferrofluids, they failed to account for the observations in concentrated suspensions. Odenbach et al.[115] observed a large increase in viscosity in a ferrofluid containing 6.7 vol % of magnetite with increasing magnetic field. The viscosity increase was much larger than Shliomis'[106] predictions. Such large increase in viscosity in concentrated suspensions under magnetic field is termed as "*magnetoviscous effect*" (MVE). The failure of the theories to predict the much larger viscosity increase in ferrofluid is attributed to the omission of the interactions between particles. In their subsequent work, Odenbach et al.[116-118] found that the concept of rotational viscosity was insufficient to explain their experimental observations in ferrofluids where a large increase in viscosity under magnetic field and a shear thinning with increasing shear rate were observed. **Fig. 1.8** shows the variation of viscosity change with magnetic field for a ferrofluid of φ = 7.2 vol% for a shear rate = 500 s^{-1} from the work of Odenbach.[118] It is seen that Shliomis predictions of viscosity increment according to **Eqn. (1.1)** underestimates the experimental observations.

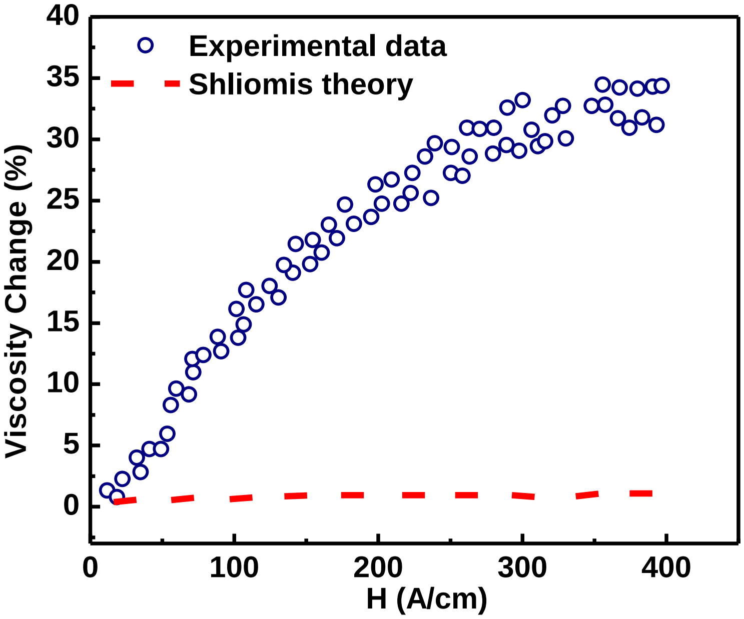

Figure 1.8: Variation of viscosity change as a function of magnetic field strength for a ferrofluid of concentration 7.2 vol% for a shear rate = 500 s^{-1} from the work of Odenbach.[118] The dotted lines are values obtained from **Eqn. (1.1)**.

The magnetic nanoparticles are under random Brownian motion in the absence of magnetic field. When an external magnetic field is applied, the particles acquire dipole moments. The magnitude of the induced dipole moment of an individual particle is given by $m = \frac{\pi}{6} d^3 \chi H$ where d is the diameter of the particle and χ is the effective magnetic susceptibility of the particle. For two particles with aligned dipole moments, the interaction energy is given by[119]

$$U(r,\theta) = \frac{m^2 \mu_0}{4\pi} \left(\frac{1 - 3\cos^2\theta}{r^3} \right) \qquad (1.\,2)$$

where r is the distance between the centres of the two particles and θ is the angle between the magnetic field direction and the line joining the centers of the particles. The interaction is attractive when the dipoles are in a head-to-tail configuration and repulsive when they are side-by-side. The maximum attraction occurs when the separation between the particles equals their diameter i.e., $r = d$ and $\theta = 0$. The interaction strength is quantified by the dimensionless dipole strength also called the coupling constant (λ) given by[33]

$$\lambda = \frac{\pi\mu_0 d^3 \chi^2 H^2}{72 k_B T} \tag{1. 3}$$

The coupling constant quantifies the magnitude of the dipolar interaction relative to the thermal motion. The growth kinetics of the field induced structures depends on the dipolar interaction. In the absence of dipolar interaction between particles in a dilute suspension, the particle motion is purely Brownian with a characteristic time t_B given by

$$t_B = \frac{1}{6}\frac{a^2}{D\varphi} \tag{1. 4}$$

where a is the radius of the particle and D is the diffusion coefficient of the particle given by

$$D = \frac{k_B T}{3\pi\eta_c d} \tag{1. 5}$$

In the presence of attractive interactions, a transition between a random and a ballistic motion occurs when the interparticle distance is such that $U(r)/k_B T = O(1)$. The coagulation flux is thus modified by the long range interparticle interactions so as to alter the characteristic time scale. The characteristic time scale accounting for the dipolar interactions is thus given by[119]

$$t_{BW} = \frac{9.16}{6}\frac{a^2}{D\varphi\lambda^{4/3}} \tag{1. 6}$$

When the separation between chains is such that long chains are close enough, a sideways coalescence of chains is observed resulting in thickening of the chains to form fibers of particles. This lateral aggregation called zippering occurs at sufficient particle concentration since the attraction between chains is a short range interaction which decays exponentially as $exp(-\rho/a)/\rho^{3/2}$ where ρ is the distance between two chains. On the other hand the aggregation of particles into chains in a tip-to-tip fashion occurs through long range dipolar interaction which decays much slower as r^3. Thus when the average chain length is such that the chains need to travel a long distance to undergo tip-to-tip aggregation, this process slows down. With large enough number density of chains the lateral aggregation of chains occurs resulting in the formation of thick columns of particles.[119, 120] The rate of lateral aggregation is limited by diffusion as the lateral attraction is short range. Hence the time scale for lateral aggregation is long when compared to the tip-to-tip aggregation.[119] The time scales for tip-to-tip and lateral aggregation are given by

$$t_{tip} = s^5 \frac{a^2}{D\lambda} \tag{1. 7}$$

$$t_{lat} = \frac{d_i^4}{a^2 D_s} \tag{1. 8}$$

where s is the size of a cluster, $d_i = \frac{d}{2}\varphi_e^{-1/2}$, and D_s is the diffusion coefficient of a cluster of size s.

The crossover time t_c^* is given by

$$t_c^* = \frac{\sqrt{\lambda}}{\varphi} \tag{1. 9}$$

From the **Eqn. (1.9)** it is seen that the transition from tip-to-tip to lateral aggregation occurs when the concentration of the particles (φ) is higher. The interaction between fluctuating chains is stronger than that between rigid chains and has a longer range than the exponentially decaying interaction between rigid chains.[119, 121, 122] This is also a factor that favors lateral aggregation. Further, zippering leads to a lowering of the energy of the system.[33, 123] Junaid et al.[124] showed that the energy of the ferrofluid system before aggregation at the first critical field where the first instance of zippering occurs was $1.22\times10^{-}$

^{26} J while that after zippering was -5.36×10^{-25} J. Similarly at the second critical field, the energies before and after zippering were -1.2×10^{-24} J and -1.05×10^{-24} J, respectively. The interaction energy for two rigid parallel chains consists of two parts, approach energy for all chains that approach one another laterally and an attractive energy well if the chains have a net attraction once they are zipped.[33] At larger separations, the chains have repulsive interaction. As they approach each other, the repulsion increases. The interaction remains repulsive when the chains are of same length and not shifted vertically with respect to one another (on registry). On the other hand, when the chains are of different length or shifted with respect to one another (off registry), the interaction energy curve has a ‘zipped’ energy well. The presence of chains and thick columns offers hindrance to the flow of the ferrofluid leading to an increase in the viscosity under magnetic field. In the presence of shear, the field induced chains and columns are broken down by the hydrodynamic force resulting in a decrease of viscosity.[116]

1.3.3 Negative viscosity

As described in **Section 1.3.1**, the application of a stationary magnetic field increases the viscosity of the ferrofluid due to the hindrance of the free rotation of the particle which gives rise to a positive component to the total viscosity of the ferrofluid. However, in an alternating magnetic field the additional component to viscosity is positive at low frequencies of the alternating field and negative at high frequencies. Ferrofluids thus exhibit a decrease in viscosity in the presence of an alternating magnetic field which was first predicted by Shliomis et al.[125] The experimental evidence for the existence of negative viscosity was provided by Bacri et al. in 1995.[126] Brownian motion prevents the complete alignment of particles dipole moment along the direction of the magnetic field. Hence when the field changes in either magnitude or direction, the particle magnetization is unable to follow the field. This lag between the applied field and the particle magnetization is responsible for the appearance of negative viscosity.[127] The linearly polarized alternating magnetic field does not prefer a particular direction of rotation of the particle. At any instant, one half of the particles rotate clockwise while the other half rotates anti-clockwise and hence the average velocity is zero. This degeneracy in the direction of rotation is valid only as long as the fluid is motionless. A flow with non-zero vorticity breaks the degeneracy and leads to a nonzero macroscopic spin rate of the particles. A part of the magnetic energy is transformed into the angular momentum of the particles, which in turn is converted into the hydrodynamic motion of the fluid. This leads to a decrease in the viscosity of the ferrofluid. In presence of a constant magnetic field, the vorticity is balanced by the field and the rotation of the magnetic particles is impeded while an alternating magnetic field increases the vorticity and the particle rotation is favored.

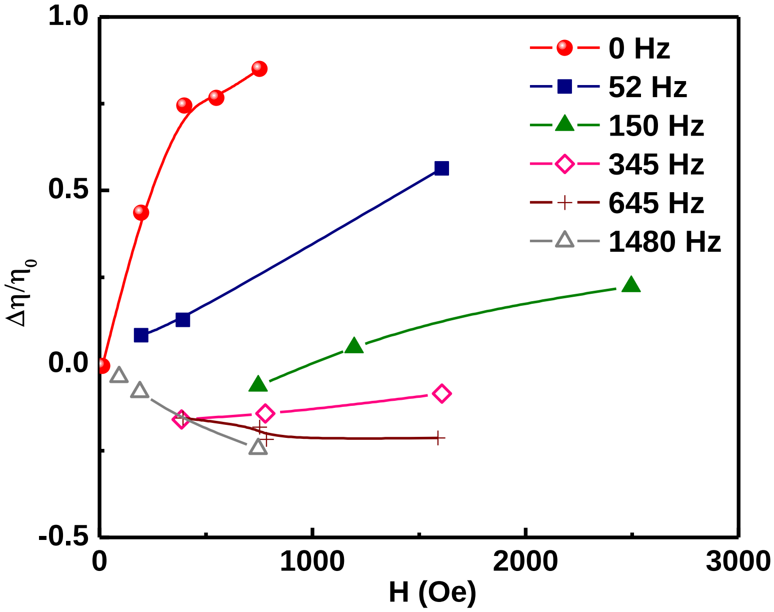

Figure 1.9: Reduced viscosities as function of magnetic field strength for different frequencies of the alternating magnetic field.[126] Full lines are guides for the eye.

The decrease in viscosity of the ferrofluid is more pronounced as the frequency of the oscillating field is increased as seen in **Fig. 1.9**. Rosensweig[127] observed that the viscosity of a magnetic fluid increased from 0.077 N s m^{-2} in the absence of field to 0.22 N s m^{-2} at a field of 0.2 T. However the viscosity reduced to 0.100, 0.077 and 0.058 N s m^{-2} at the alternating field frequencies of 50, 250 and 700 Hz, respectively. The studies on the rotational, magneto and negative viscosity in ferrofluids are summarized in **Table 1.3**.

Table 1.3: Summary of the results on rotational, magneto and negative viscosity in ferrofluids. ($\eta_{\parallel}$ and $\eta_{\perp}$ - viscosity in parallel and perpendicular mode, respectively)

Rotational viscosity				
Particle/base fluid	**Size (nm)**	**Concentration**	**Key findings**	**Ref**
Cobalt /organic solvent	5.5-12	10^{15} particles/ cm^3	$\eta_{\parallel} > \eta_{\perp}$	104
Fe_3O_4 / water	15.3	18-42 vol%	1. Larger rotational viscosity for water based ferrofluid 2. $\eta_R \propto \frac{1}{Capillary\,diameter}$ 3. $\eta_R \propto \exp(\alpha)$	128
Fe_3O_4/Kerosene	13	11-17 vol%		
-	-	-	$\Delta\eta = \frac{3}{2}\varphi\eta\frac{\xi - \tanh\xi}{\xi + \tanh\xi}\sin^2\alpha$	106
Fe_3O_4 / water	10	7 vol%	Competition between magnetic and mechanical torques	105
Magnetoviscosity				
Fe_3O_4 / di-ester	10	6.7	Chain formation under magnetic field. Shear thinning in ferrofluids	116
Fe_3O_4 / petroleum oil	8.3-10.1	7.2	Depends on the amount of larger particles (greater than critical size) present	105, 129, 130
Fe_3O_4 / di-ester	10	6.7		131

Negative viscosity				
Cobalt ferrite / water	10	20	η decrease under AC field	126
Magnetite/ water	12.2	3.9	η decrease under AC field	132
Theoretical studies			AC field aids the free rotation of particles	125
			η decreases as the frequency of the AC field increases	125, 127, 132-134
			1. Frequency range of negative η effect widens with amplitude of B field. 2. $\Theta > \Omega$	135

1.3.4 Magnetization Relaxation in Ferrofluids

Magnetoviscous effect is attributed to the ability of particles to interact with each other. In order for the dipolar interaction between particles to be significant, it is required that particles size should be above a certain critical size. This was demonstrated by Odenbach et al.[129, 131] who showed that the magnetoviscous effect in the ferrofluids is due to contributions from larger particles. In their study, five ferrofluids (designated as F_1 to F_5) each containing different concentration (0.09, 0.14, 0.22, 0.26 and 0.8 vol%) of large particles were used. The viscosity change $\left(\frac{\Delta\eta}{\eta_0}\right)$ at H = 22 kA/m was about 0.4 and 0.05 for the ferrofluid concentrations of 0.8 and 0.09 vol%, respectively indicating that the larger particles are responsible for the magnetoviscous effect. The magnetoviscosity has its origin in the magnetization relaxation of the magnetic particles. When the magnetic moment of the particle is fixed within the particle, the relaxation occurs by the rotation of particle as a whole. This process is called the Brownian relaxation which is characterized by the time

$$\tau_B = \frac{3\tilde{V}\eta_c}{k_B T} \tag{1. 10}$$

where $\tilde{V}$ is the hydrodynamic volume of the particle. On the other hand, the magnetic moment is free to rotate within the particle without the rotation of the particle. This process is termed the Neel relaxation and is characterized by the time

$$\tau_N = \frac{1}{f_0}\exp\left(\frac{KV}{k_B T}\right) \tag{1. 11}$$

where f_0 is the attempt frequency typically 10^9 Hz, K is the anisotropy constant and V is the magnetic volume of the nanoparticle. In general, the Neel and Brownian mechanisms occur in parallel with the effective relaxation time (τ_{eff}) given by

$$\frac{1}{\tau_{eff}} = \frac{1}{\tau_N} + \frac{1}{\tau_B} \tag{1. 12}$$

From **Eqn 1.12** it is clear that the magnetization relaxation is dominated by the process with the shortest relaxation time.[136] A plot of the size dependence of Brownian, Neel and effective relaxation times from literature[136] is shown in **Fig. 1.10**.

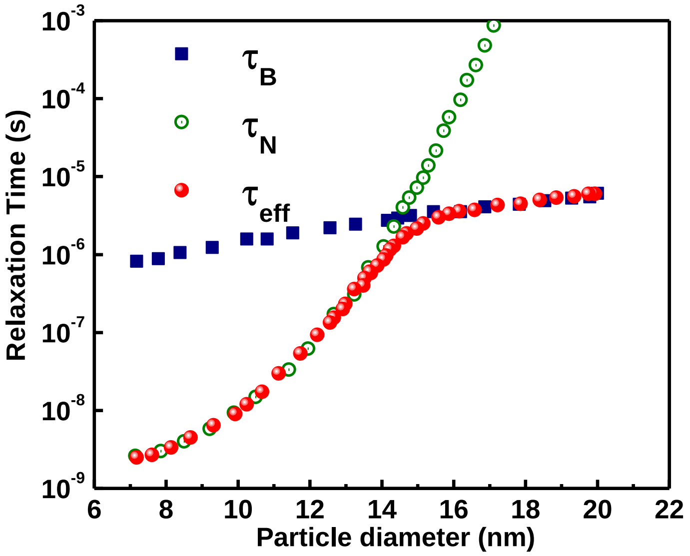

Figure 1.10: Relaxation time as a function of particle diameter for single domain magnetite nanoparticles.[136]

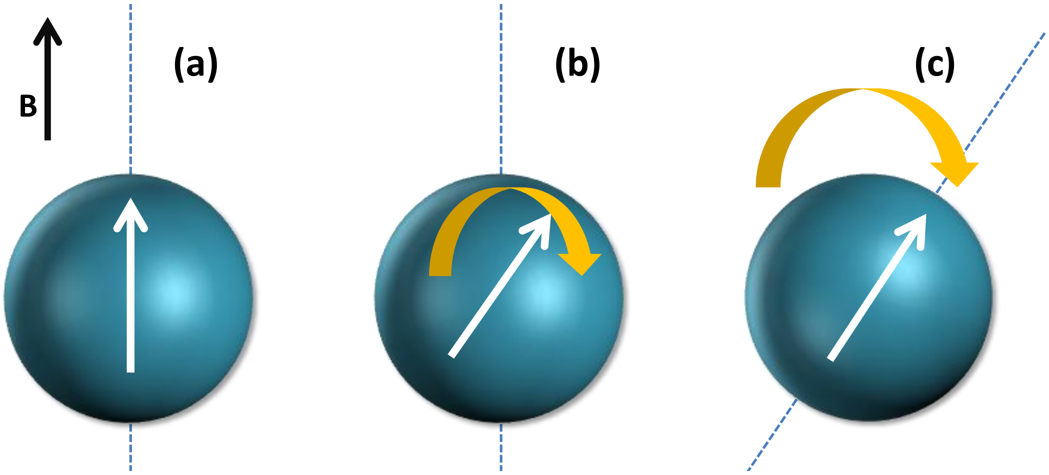

Figure 1.11: Schematic showing (a) the magnetic moment of the particle aligned along the direction of magnetic field (b) rotation of the moment within the particle (Neel relaxation) and (c) rotation of the particle as a whole (Brownian relaxation).

From **Fig 1.10**, it is seen that Brownian relaxation dominates for larger particles while Neel relaxation dominates for smaller particles. There exists a critical size for the transition from

Neel to Brownian process. Particles smaller than the critical size relax by Neel process while those larger than that relax by Brownian process.[137] The schematic of the mechanism of Neel and Brownian relaxation is shown in **Fig. 1.11**. Particles relaxing by the Neel process do not contribute to the field dependent viscosity increase as their free rotation is not hindered by the magnetic torque produced by the interaction between the applied field and magnetic moment. Such particles are considered to be magnetically weak. On the other hand, particles relaxing by the Brownian process are acted upon by the magnetic torque which impedes their rotation. Such particles contribute to both rotational and magnetoviscosity. The critical size depends upon the particle used. For example, Cobalt particles have a critical size of 5 nm for the Neel to Brown transition while for magnetite (Fe_3O_4) particles the critical size is14 nm.[129] Thus only particles larger than the critical size contribute to the rotational viscosity. Moreover, the magnetoviscous effect also requires certain critical size for the particles to overcome the thermal energy and form chains.[105, 129]

1.3.5 Nature of Field Induced Structures in Ferrofluids

Over the years researchers have focused on ascertaining the nature of the field induced structures such as linear chains, droplike aggregates, etc. that are formed in the ferrofluid. The nature of field induced structures were initially reported in model systems of inverse ferrofluids where they are shown to evolve from linear to zippered aggregates.[119, 120] In ferrofluids, Zubarev et al.[138] reported that the increase in viscosity of the ferrofluid composed of particles with frozen magnetic moment (i.e., those that follow Brownian relaxation) is due the formation of straight and rigid chainlike aggregates without any interchain interaction. They also showed that the hydrodynamical relaxation time increases in the presence of a magnetic field. Under a weak or moderate magnetic field, normal stresses responsible for the

Weissenberg effect in ferrofluids arise and disappear under strong field. The behavior of a free ferrofluid surface at a rotating axis immersed in the liquid depends on whether or not the fluid exhibits normal stress differences.[139] For liquids without normal stress differences, the fluid surface will bend downward due to action of centrifugal forces while for liquids that exhibit normal stress differences, the centrifugal forces is countered by a force radially inward which drives the surface to bend upward. This effect is called the Weissenberg effect.

However, there are also reports that under specific conditions the linear chainlike aggregates are transformed to bulk dense drops due to condensation phase transitions.[140] When the ratio ($\varepsilon = \frac{\mu_0 m^2}{2\pi d^3 k_B T}$) of the energy of magnetic particle interaction and thermal energy is lower than a critical value ε', the system is spatially homogenous with chainlike aggregates. If $\varepsilon > \varepsilon'$, the system undergoes phase separation into dilute and dense phases. The dense phase is considered to constitute bulk droplike aggregates. This phase transition occurs when the total number of magnetic particles exceeds a threshold value which varies between hundreds and thousands depending on the applied magnetic field, volume concentration of particles and ε'. Usually in computer simulation studies the appearance of such bulk dense drops is not observed since the number of particles used in the simulations are far lesser than the ones that appear in real ferrofluids. The influence of droplike and chainlike aggregates on the rheology of ferrofluids was theoretically studied by Zubarev et al.[94] who showed that droplike aggregates were formed in magnetic fluids when the magnetic field exceeded a threshold value. As the field increased, the individual particles formed linear chains. Above the threshold field, the longest chains transformed into compact dense globules which acted as nuclei for a new dense phase. The shape and volume fraction of the drops influence the macroscopic rheology of the ferrofluid. The drop shape is determined by the balance between surface tension and demagnetizing field. The surface tension tries to transform the drop to a ball like aggregate while the demagnetizing field tries to make it into a long thin needle. The appearance of drops that span the gap between the rheometer plates induces elastic and yield stress effects in ferrofluids. The bridging of the gap between the plates leads to quasielastic behavior.

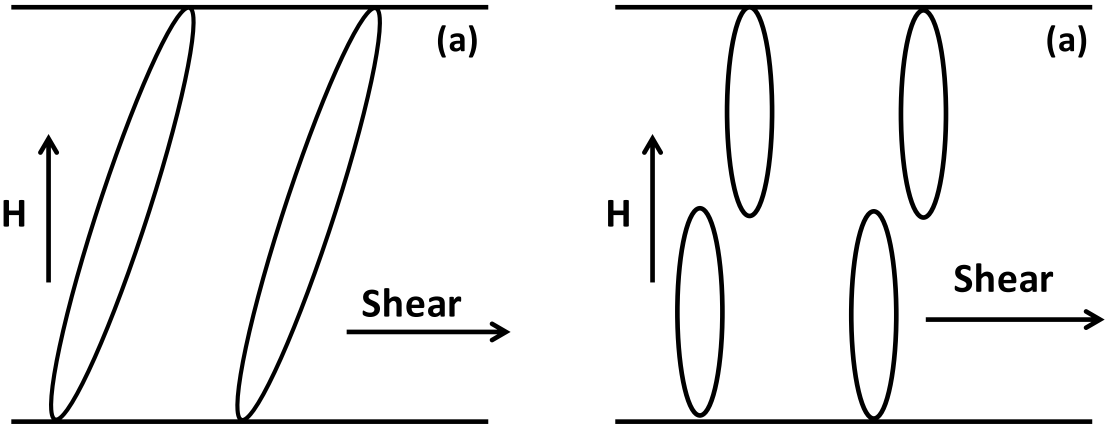

Figure 1.12: Schematic of (a) gap-spanning and (b) non gap-spanning drops in a ferrofluid in presence of magnetic field.

When the applied deformation exceeds a certain magnitude, the bridges are destroyed and form smaller drops that are non gap-spanning (**Fig. 1.12**) and hence the behavior changes from quasielastic to fluid regime. The destruction of the larger gap-spanning drops into small drops is thermodynamically favored as the smaller drops align along the direction of the magnetic field while the larger drops are slopped with respect to the field direction. The destruction is associated with a minimum stress thus giving rise to an yield stress effect.

The effect of droplike aggregates on the macroscopic rheological properties of ferrofluids was studied by Zubarev et al.[141] Their study showed that the presence of drops leads to an increase in viscosity when the magnetic field is parallel to the gradient of flow. In a shear flow the shape of the drop is determined by the competition between the magnetic force which causes particles to adsorb on the drop and the hydrodynamic force which tends to destroy the drop. When a balance is reached between the two forces the drop attains a critical volume. Drops larger than the critical volume are destroyed. They also studied the influence of polydispersity on the observed magnetoviscous effect by neglecting the interdrop interaction and found that the polydisperse ferrofluids with larger particles in the fluid form drops even at weak field. With increasing field, the magnetoviscous effect due to such large particles tends to saturate. On the other hand, at high magnetic fields, the smaller particles begin to participate in the drop formation. The combined effect due to both small and large particles leads to an increase in the viscosity of the system.

1.4 Factors Affecting the Magnetorheology of Ferrofluids

The magnetorheological properties of ferrofluid are affected by several factors such as the shear rate, magnetic field, particle morphology, volume concentration of nanoparticles and presence of additives.

1.4.1 Effect of Shear Rate

Odenbach et al.[116] observed a decrease in magnetoviscosity of the ferrofluid subjected to increasing shear rates. The breaking down of field induced aggregates under shear was found to be the reason for the observed shear thinning behavior. The magnetic force between two aligned magnetic dipoles at a distance of $d+2b$ is given by

$$F_m = \frac{\mu_0 M_0^2 \pi d^6}{24(d+2b)^4} \tag{1. 13}$$

where b is the thickness of the surfactant layer covering the particle and M_0 is the spontaneous magnetization of the magnetic material of the particle. The field induced structures are disrupted by the viscous force given by

$$F_v = 6\pi\eta_c\dot{\gamma}\frac{1}{2}\left[\frac{N(d+2b)}{2}\right]^2 \tag{1. 14}$$

where N is the number of particles in the chain and $\dot{\gamma}$ is the shear rate. The number of particles in a chain is computed from the balance between the magnetic and viscous forces. For a ferrofluid of $\varphi = 0.067$ containing magnetite nanoparticles of mean diameter 10 nm, the typical values for the number of particles in a chain in presence of magnetic field were found to be 130, 80 and 60 for shear rates of 1, 2.6 and 5.2 s^{-1}, respectively.[116] Thus, the number of particles in a chain decreases as the shear rate increases. In addition to shear and magnetic forces, the number of particles in a chain also depends on the thermal energy and hence the expression for chain length must also contain a k_BT dependence. Chirikov et al.[142] arrived at an expression for the maximal number (N_{max}) of particles in a chain under a shear rate $\dot{\gamma}$ as

$$N_{\max} = \sqrt{\varepsilon\frac{D}{\dot{\gamma}}} \tag{1. 15}$$

where ε is defined in **Section 1.3.5** and D is given by **Eqn. (1.5)**. Shear thinning arises when the microstructure of the system is disturbed by the shear forces and is unable to restore back to equilibrium. Most ferrofluids show decrease in viscosity (shear thinning) owing to the disruption of the field induced structures by the shear forces. The alignment of the field induced structures along the shear flow direction also reduces the suspension viscosity.[143]

This has been confirmed through Small Angle Neutron Scattering (SANS)[144] in which the scattering from a single particle system at a shear rate of 200 s^{-1} was considered as the reference from which the scattered patterns at different shear rates and magnetic fields were subtracted to get the difference pattern which contains information about the microstructure of the ferrofluid. At high magnetic field and low shear rates, all the chains are aligned along the direction of the magnetic field. The cross-sections of the chains have the same size as that of single particles and hence the difference between the reference and the scattered pattern is almost zero. As the shear rate increases the deviation of the chains from the field direction becomes more pronounced and their projection as seen by the neutrons also increases. This results in a significant change in the difference pattern where the difference was more evident at higher shear rate. For a low magnetic field and low shear rate, the effect of the magnetic torque on the chains is weaker as compared to the high field resulting in shorter chains. Depending on the ratio between the magnetic and mechanical torques, the former acting to orient the chains along the magnetic field direction and the latter causing the chains to deviate from the field direction, the microstructure will give rise to a non-zero difference pattern. As the shear rate is increased, keeping the field fixed at a low value, the chains deviate significantly from the field direction showing a difference pattern. At very high shear rates, the chains are broken down to individual particles that are homogenously distributed in the carrier fluid resulting in the absence of a difference pattern. Shear thinning in ferrofluids under magnetic field has been reported by many groups.[72, 145-147] The degree of shear thinning increases as the magnetic field increases.[72, 145]

In a ferrofluid containing γ-Fe_2O_3 particles of size < 50 nm dispersed in paraffin at a concentration of 30 wt%, Masoud et al.[143] found that at low shear rates (1 and 10 s^{-1}), the viscosity increased up to a certain magnetic field beyond which it decreased. However, at high shear rate (100 s^{-1}) the viscosity increase with magnetic field was monotonic. The decrease in viscosity beyond a certain field at low shear rates is attributed to the phase separation occurring in such ferrofluids. The particles in the fluid get concentrated at a particular region which grows in size as the field increases resulting in their restricted movement in the suspension medium while the flow of the separated liquid between the concentrated regions becomes easier. This process in turn leads to a decrease in the viscosity of the ferrofluid. However, at high shear rates, the concentrated regions are prevented from being still and hence the viscosity increases continuously. From application point of view, in particular biomedical applications like magnetic drug targeting, the ferrofluids are often subjected to a high shear and magnetic field. Johannes et al.[148] studied biocompatible ferrofluid containing 25 mg/mL of magnetite nanoparticles stabilized with starch in the shear rate range of 100 to 1000 s^{-1} and magnetic fields up to 650 kA/m. The particles were superparamagnetic with a mean diameter of about 200 nm. Almost 2000 % increase in the viscosity of the ferrofluid when subject to magnetic field of 280 kA/m was observed. The ferrofluid showed a shear thinning behavior with increasing shear rate with an apparent yield stress.

1.4.2 Effect of Magnetic Field

The magnetoviscous effect in ferrofluids is also associated with the presence of yield stress which is the minimum stress required to cause the suspension to flow. In ferrofluid containing magnetite particles of diameter 18 nm embedded in nanoscale silica and dispersed in silicone oil at 1.3 vol% of magnetic material in 4.1 vol% of nanocomposite, the application of magnetic field leads to an increase in yield stress of the suspension.[149] The yield stress increases from 0.19 to 2.5 Pa as the field increases from 0 to 35 kA/m. In oscillatory measurements at low magnetic fields, the imaginary part of the complex viscosity (η'') of the above ferrofluid was independent of the oscillating frequency while at higher fields the η'' increased with ω and showed a maximum, followed by a decrease. In a study on the magnetorheological response of hydrophobic and hydrophilic silica-coated magnetite particles suspended in silicone oil, suspensions containing hydrophilic silica-coated magnetite nanoparticles showed an increase in the yield stress and a shear thinning response with increase in magnetic field due to the van der Waals and polar interactions between silica, while hydrophobic silica-coated nanoparticles showed a weak magnetorheological response with negligible yield stress.[150] Yield stress effect was observed in ferrofluids when the particle size exceeded a critical value.[130] Ferrofluid containing magnetite particles with size ~ 10 nm showed no yield stress while those containing a mixture of 10 and 16 nm sized particles showed an yield stress due to the formation of chains.[130] The yield stress was also found to depend on the concentration of the large particles that are capable of forming chainlike structures which implied that the yield stress depends strongly on the interparticle interaction. The yield stress decreased as the gap height increases. The decrease in yield stress was about 3.3 times as the gap height was reduced from 2.5 to 0.2 mm.

An increase in yield stress with magnetic field and volume fraction was reported in water based ferrofluids containing Tetramethylammonium hydroxide (TMAOH) coated magnetite particles of diameter 13 nm and saturation magnetization of 46 emu g^{-1}.[151] In the presence of magnetic field, frequency sweep measurements showed a frequency independent plateau for G' and a dominant elastic behavior due to the formation of gap spanning chains. The G' scales with the volume fraction as $G' \alpha \varphi^{4.62}$. At a constant magnetic field the linear viscoelastic region was found to decrease with increase in φ due to the brittle nature of the structures.

A study showed that the capillary diameter as well as the angle between the magnetic field and vorticity influences the rotational viscosity of water based and kerosene based ferrofluids.[128] The percentage contribution of rotational viscosity for water and kerosene based ferrofluids were found to be 32, 28, 16 % and 16.3, 13, 8.3 %, respectively for 0.5, 1.0 and 2.0 mm diameter capillary, respectively which implies that the rotational viscosity varies inversely with the capillary diameter. The rotational viscosity also decreased exponentially with the angle between field and vorticity. The viscosity increase was minimum when the angle was 0^o and maximum when it was 90^o.

In contrast to the regular shear thinning response of ferrofluids, shear thickening behavior was observed in a ferrofluid when the yield stress was sufficiently small.[152] Magnetite nanoparticles doped Polyethylene glycol (PEG) rods suspended in PEG at φ = 0.2 showed shear thickening which was masked by the presence of yield stress. Yield stress resulted in a smaller range of applied stresses over which shear thickening was observed. When the yield stress was large enough to encroach the upper limit of shear thickening, then the thickening effect was fully eliminated.

1.4.3 Effect of Particle Morphology

Particle morphology plays a significant role in controlling the rheology of ferrofluids. Anisotropic particles can lead to an enhanced magnetoviscous effect compared to suspensions of isotropic magnetic particles. Such a study on the rheology of ferrofluid containing cobalt nanodiscs was reported by Shahnazian et al.[153] The interparticle interaction for spherical particles quantified by the coupling constant is given by $\lambda = \dfrac{\mu_0 {M_0}^2 V^2}{2\pi (d+2b)^3 k_B T}$.

In case of non-spherical particles the particle diameter *d* in the above expression is replaced by the characteristic distance *L* between the centres of the particles. It was observed that the interaction parameter for ferrofluid with nanospheres and nanodiscs were 2 and 178, respectively. Such a large value for λ for non-spherical particles strongly modifies the rheological quantities such as yield stress and viscosity. The nanodiscs containing ferrofluid showed an enhanced yield stress than its spherical counterpart. The yield stress increase with magnetic field was attributed to the enhanced interaction parameter.

Lopez et al.[72] studied ferrofluids containing cobalt particles of two different morphologies, spheres and nanofibers. The nanofiber based ferrofluid showed a larger yield stress and magnetoviscous effect than that of conventional ferrofluid with nanospheres. The magnetic field dependence of the yield stress for fiber based ferrofluid showed a positive curvature indicating a faster increase of yield stress with magnetic field while that of nanosphere suspensions showed saturation at high fields with a negative curvature. The domination of magnetostatic forces over the Brownian motion was more in the case of nanofiber suspension. The interparticle dry friction between the nanofibers was found to be the cause for the enhanced magnetorheological effects in the nanofiber nanofluids.

1.4.4 Effect of Additives

With the aim of achieving better enhancement in the magnetorheological properties, researchers have attempted to couple the spherical magnetic nanoparticles to anisotropic structures. For this purpose magnetic particles were attached to the surface of the carbon nanotubes (CNTs) and the resulting CNTs decorated with magnetic nanoparticles were manipulated by an external magnetic field.[154-156] CNTs were also filled with ferrofluid to produce magnetic nanotubes[157] but their rheological behavior is not studied. Biological nanotubes introduced into ferrofluid were shown to enhance the magnetoviscosity of the ferrofluid.[158, 159]

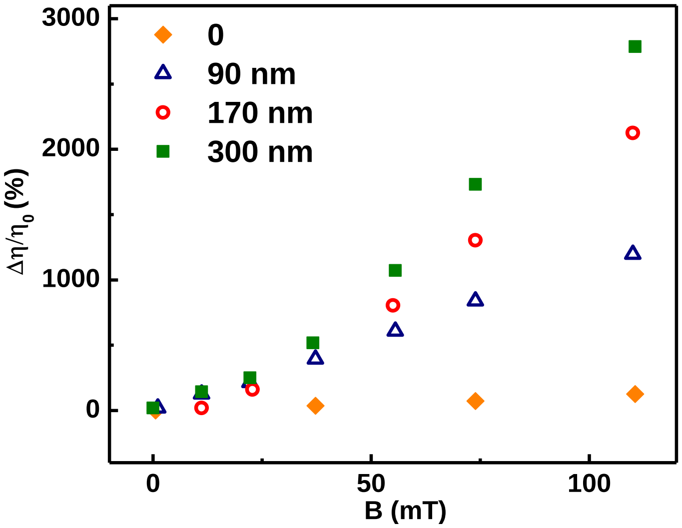

Figure 1.13: Variation of relative viscosity as a function of magnetic field for ferrofluid containing Tobacco Mosaic Virus of different lengths at a concentration of 0.033 mg/mL.[158]

A small amount of Tobacco Mosaic Virus (TMV) added in ferrofluid leads to more than one order of magnitude enhancement in the magnetoviscosity of cobalt-ferrite ($CoFe_2O_4$) based ferrofluid.[158] The $CoFe_2O_4$ particles which were electrostatically bound to the surface functional groups on TMV formed quasi-linear aggregates of magnetic nanoparticles. Application of a magnetic field led to the alignment of these rod shaped structures which caused the observed viscosity enhancement. The longer TMV-based structures were mechanically stable and hence less susceptible to shear thinning. The viscosity enhancement increased with magnetic field, the length and concentration of the TMV. The maximum viscosity enhancement reached 2800 % at a magnetic field of 110 mT for the ferrofluid containing 300 nm long virus particles as seen in **Fig. 1.13**.

Table 1.4: Summary of the studies on the factors affecting the magnetorheological properties of ferrofluids.

Effect of shear rate				
Particle/base fluid	**Size (nm)**	**Concentration**	**Key findings**	**Ref**
Fe_3O_4/ di-ester	10	6.7 vol%	Shear thinning	116
Fe_3O_4 / di-ester	8.3 – 10.1	7.2 vol%	Reorientation of chains along shear flow	144
γ- Fe_2O_3 / paraffin	50	30 wt%	• Low $\dot{\gamma}$ - η decreases beyond critical H. • High $\dot{\gamma}$ - monotonic increase in η with H.	143
Iron oxide	200	0.025 wt%	Shear thinning with yield stress	148
Fe_3O_4 @SiO_2 /PEG/water	35	7.12 - 17. 81 vol%	Degree of shear thinning increases with B	145
CoNi / mineral viscosity	56× 6.6 (L×W)	5 vol%	Degree of shear thinning increases with B	72
Tb-doped Gd_2O_3 / Ethanol	~ 8	0.0158 wt%	Degree of shear thinning increases with γ-irradiation dose	147
Fe_3O_4/ Silicone oil	~ 8	-	Shear thinning	146
Effect of Magnetic Field				
Iron oxide embedded in silica/ oily medium	18	1.3 vol%	η and yield stress increases with B	149
Hydrophobic Silica-coated magnetite/silicone oil	35 ± 12	11.5 vol%	Strong chain formation and yield stress with B	150
Hydrophilic Silica-coated magnetite/ silicone oil	32 ± 11	40 vol%	• Weak chains with B • No yield stress	150
Fe_3O_4 / Synthetic ester	10-16	7.2 vol%	• Yield stress α B^2 • Yield stress α 1/gap between plates	130
Cobalt/ L9	8	2.83 vol%		
Magnetite filled PEG / PEG	254x 32x25 μm)	20 vol%	Shear thickening suppressed by yield stress	152

Magnetite filled PEG / PEG	254x 32x25 µm)	20 vol%	Shear thickening suppressed by yield stress	152
Fe_3O_4 / water	13	4 – 14 vol%	• Increase in yield stress with B & φ • Viscoelastic behavior with B under oscillatory shear • LVE range deceases with increase in φ • G' constant with ω. • $G'_p \alpha \varphi^{4.62}$	151
Effect of Particle Morphology				
Cobalt nanodiscs/ n-cetyl added oleic acid	20 × 5 (diameter × height)	0.1 vol%	Enhanced η and yield stress for disc shaped particles	153
Cobalt nanospheres/ L9 oil	8	2.83 vol%	Large η and yield stress for Co fibers than Co spheres	72
Effect of volume fraction				
Fe_3O_4 / Transformer oil	8.6	1.8-6.4vol%	η increases with φ	160
PEG coated Fe_3O_4	48.5	0.78-11.66 vol%	Newtonian to shear thinning at high φ	161
Fe_3O_4 / water	10	0.17 - 0.366 wt%	Shear thinning at high φ	162
α-Fe_2O_3 / Ethylene glycol	29±18	6.6 vol%	• Shear thinning • $G' > G''$ • Damping decreases at high φ • $G' \alpha \varphi^{4.6}$	163

1.4.5 Effect of Volume Fraction

The particle content in ferrofluid influences its magnetorheological properties. An increase in the capillary viscosity of ferrofluid with volume fraction was reported which is attributed to the formation of larger aggregates.[160] Polyethylene coated magnetite nanoparticles showed an increase in viscosity with particle concentration. As the concentration is increased from 1 to 15 wt%, the behavior of the ferrofluid changed from Newtonian to shear thinning.[161] Shear thinning and viscoelastic behavior were observed in 6.6 vol% of ethylene glycol based nanofluids containing α-Fe_2O_3 nanoparticles of size ~ 29 nm. With increasing φ, the damping factor of the ferrofluid decreased, indicating the evolution from fluid to elastic behavior.[163] The studies on the factors influencing the magnetorheology of ferrofluids are summarized in **Table 1.4**.

1.5 Motivation

Ferrofluids have emerged as reliable materials in solving several complex engineering problems.[164] Applications demand ferrofluids with varying rheological properties. For efficient use of ferrofluids in applications such as sealants, coolants and dampers, a knowledge of the quantities such as viscosity, yield stress and hysteresis is essential to optimize the magnetorheogical behavior of ferrofluids. Irrespective of several theoretical and experimental studies, a systematic study of the magnetorheological properties of ferrofluids does not exist in literature probably due to issues such as high polydispersity of the ferrofluid and difficulty in preparing stable ferrofluids with reproducible properties. A model system of ferrofluid should have minimum polydispersity and particles be protected against destabilization mechanism by proper surface capping. A proper understanding of the microstructure in ferrofluid under an external magnetic field and shear and their influence on magnetorheological properties is still incomplete. Further, the effect of magnetic field on the dynamic rheological properties of ferrofluids has not been studied, which is also a motivation to take up this study. In addition, the effect of uncoupled nonmagnetic additives on the magnetorheological behavior of ferrofluids is also not explored. This thesis attempts to provide a systematic study of the magnetorheological properties of model ferrofluids synthesized and characterized in our laboratory.

1.6 Objectives

The main objectives of the thesis are as follows:

- To study the magnetorheological properties of oil based ferrofluid containing Fe_3O_4 nanoparticles stabilized by a protective coating, especially to probe the effect of shear force and applied magnetic field on the formed internal structures, viscoelastic properties and the static and dynamic yield stresses of the ferrofluid.
- To design and build a custom-made opto-rheological setup to gain insight into the formation of field induced structures in ferrofluid and their rheological behavior and to establish the relationship between the sizes of the field induced structures, the applied field strength and concentration of the ferrofluid.
- To probe the lateral interaction mechanisms and their consequences on long-time coarsening of structure using a rheomicroscope.
- To investigate the relaxation dynamics in ferrofluids using strain-rate frequency superposition (SRFS) principle.
- To probe the effect of nonmagnetic additives such as silica nanoparticles and carbon nanotubes on the rheological properties of ferrofluid.

1.7 Overview of the Thesis

The thesis consists of eight chapters. **Chapter 1** gives an introduction to ferrofluids with a focus on the initial studies on viscosity measurements of ferrofluids in the presence of an external magnetic field. The concepts of rotational viscosity, magnetoviscosity, negative viscosity and the relaxation mechanisms involved are discussed. The factors affecting the magnetorheological properties of ferrofluids such as shear rate, applied external magnetic field, concentration of the magnetic particles, presence of additives, and particle morphology are also described. **Chapter 2** describes the methods of preparation of ferrofluids and the experimental techniques used for their characterization. **Chapter 3** discusses the magnetorheological properties of the ferrofluid containing Fe_3O_4 nanoparticles of size ~12 nm coated with oleic acid and dispersed in kerosene at a volume fraction of 0.038. The results on the steady shear rheology of the ferrofluid, the yield stress, Mason number scaling, the hysteresis behavior and the dynamic response under magnetic field are described in detail. **Chapter 4** discusses the results on the study of magnetic field induced structures in dilute ferrofluids (φ = 0.00078 to 0.0063) using a rheomicroscope with custom-made solenoid set up. This chapter provides the correlation between the microstructure of the ferrofluid and its macroscopic rheological properties. **Chapter 5** presents the results of field induced structures and their dynamics in ferrofluid (φ = 0.046) using oscillatory rheology. These studies show that the ferrofluid exhibits a soft solidlike behavior whose relaxation is governed by the imposed strain-rate and the magnetic field. **Chapter 6** describes the effect of multiwalled carbon nanotubes on the magnetorheological properties of an oil based ferrofluid of volume fraction 0.087. **Chapter 7** discusses the effect of network forming hydrophilic silica nanoparticles on the rheology of a nonpolar oil based ferrofluid under varying magnetic field using magnetorheometer and rheomicroscope. **Chapter 8** summarizes the results obtained, conclusions drawn and the recommendations for future work.

Chapter 2 Materials and Experimental Techniques

2.1 Materials

The iron salts $FeCl_2.4H_2O$ and $FeCl_3.6H_2O$ and chemicals 25% Ammonium hydroxide (NH_4OH), oleic acid, 35% Hydrochloric acid (HCl), hexane and acetone used for the synthesis of magnetite (Fe_3O_4) nanoparticles were procured from E-Merck. All the chemicals were of GR grade and used without further purification. Elga water with resistivity of 15 MΩ cm was used for all synthesis. Multiwalled carbon nanotubes were purchased from Nanostructured & Amorphous Materials, Inc. USA. The CNT has a length of 10-30 μm and an outer diameter less than 8 nm with a specific surface area of 350-420 m^2/g. About 0.5 wt% of CNTs was added to the ferrofluid of volume fraction 0.087 (38 wt%) and sonicated for 30 minutes using a Sonics Vibracell horn sonicator (USA) to obtain a stable dispersion. The suspension was homogenized using a vortex mixer prior to experiments. Hydrophilic fumed silica nanoparticles were purchased from Sigma Aldrich. The primary particles were about 7 nm in diameter with surface area of 395 ± 25 m^2/g. About 0.5 wt% of fumed silica was added to the ferrofluid of $\varphi = 0.087$ and sonicated for 20 minutes using a Sonics Vibracell horn sonicator.

2.2 Preparation of Ferrofluid

The ferrofluids used in this thesis work were prepared by dispersing surfactant capped magnetite nanoparticles in kerosene. The nanoparticles were synthesized by co-precipitation technique.[165, 166] A 1:1 ratio of freshly prepared iron salt solutions of 0.2M $FeCl_2.4H_2O$ and 0.4M $FeCl_3.6H_2O$ were mixed at a stirring speed of 1000 rpm. Ammonia was added until the solution pH reached a value of 10. This was followed by the addition of 20 mL oleic acid and adjusting the pH to 9.5 while the temperature was increased to 70 °C. At the same pH, temperature and stirring speed, the solution was kept for 30 minutes to finish the coating process. The elimination of excess ammonia and the protonation of adsorbed and un-adsorbed ammonium oleate as oleic acid was achieved by increasing the temperature to 79 °C. The oleic acid coated magnetite nanoparticles were washed with triply distilled water at 60 °C, until the pH became 7 to remove the ionic impurities and later dispersed in hexane. Aggregation of the particles was induced by treating the hexane dispersion with acetone followed by centrifugation of aggregated particles at 2500 rpm for 30 minutes. The hexane-acetone washing procedure was repeated to remove excess surfactant. The surfactant-coated magnetite nanoparticles were finally vacuum dried at 35 °C for 48 hours and the dried particles were dispersed in kerosene at the required volume fraction.

The oleic acid coating on the nanoparticles provides steric repulsion between the particles and thus prevents their agglomeration under van der Waals attraction while the small size of the particles ensures that the Brownian energy is sufficient to keep them apart against settling. A schematic representation of oleic acid coated magnetite nanoparticles and the net repulsive interaction as a function of interparticle spacing are shown in **Fig. 2.1**.

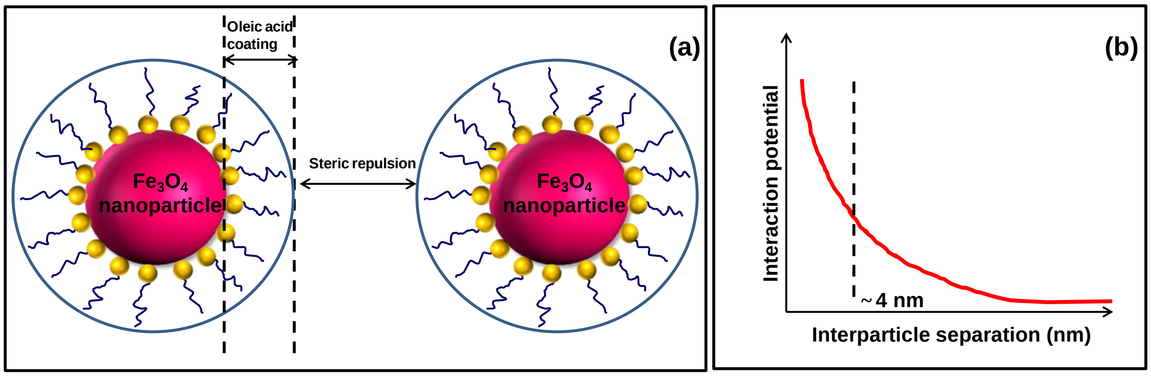

Figure 2.1: Schematic of (a) oleic acid coated Fe_3O_4 nanoparticles and (b) the net repulsive interaction as a function of interparticle spacing.

2.3 Rheology - Basics

Rheology is the science of *deformation and flow* of matter[96] whose behavior does not fall under the classical extremes of Hookean elastic solids or Newtonian viscous liquids. The behavior of the extreme case of elastic solids is best described in the words of Robert Hooke as “the power of any spring is in the same proportion with the tension thereof.”[96] In a similar manner the behavior of liquids is described by Isaac Newton as “The resistance which arises from the lack of slipperiness of the parts of the liquid, other things being equal, is proportional to the velocity with which the parts of the liquid are separated from one another.”[96, 167] Ideal solids subject to a force deform elastically while ideal liquids deform irreversibly (i.e., they flow). However, real bodies are neither ideal solids nor ideal liquids. As an example, from his experiments on silk thread, Wilhelm Weber[96, 168] observed that application of a longitudinal load resulted in the immediate extension of the thread which was then followed by further lengthening with time. Similarly on removal of the load, there was an immediate contraction followed by a gradual decrease in length of the thread until its original length was restored. Thus the behavior of the silk thread could not be described by Hooke’s law alone as there are also elements resembling a liquidlike response. Such materials exhibiting a behavior intermediate between the Hookean solids and Newtonian liquids are termed as viscoelastic materials.

2.3.1 Rheological Parameters

Consider a set up with two parallel plates separated by a gap h and filled with the viscoelastic material to be studied as shown in **Fig. 2.2**.

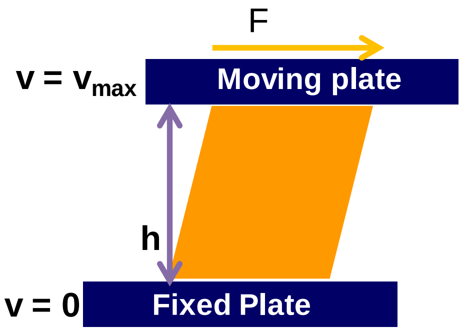

Figure 2.2: Schematic showing a viscoelastic material confined between a bottom fixed plate and a top moving plate separated by a gap *h*. The top plate moves with a velocity v_{max} when subjected to a tangential force *F*.

A tangential force (*F*) is applied to the top plate which causes the liquid layer adjacent to the top plate to move with a certain velocity v_{max}. The velocity of the fluid layers decreases down the gap to the bottom plate which is at rest resulting in a velocity gradient across the sample. The tangential force per unit area is called the shear stress, σ (= F/A). The shear rate is defined as

$$\dot{\gamma} = \frac{dv}{dh} \tag{2. 1}$$

where *dv* is the differential velocity and *dh* is the differential thickness of the flow layers. In laminar flow, the velocity differential between adjacent velocity layers of like thickness is constant. Hence the shear rate is given by

$$\dot{\gamma} = \frac{v}{h} \tag{2. 2}$$

Viscosity (η) is a measure of the 'resistance to flow' of the liquid. It is defined as the ratio of the shear stress to the shear rate.

$$\eta = \frac{\sigma}{\dot{\gamma}} \tag{2. 3}$$

2.3.2 Rheological Response of Materials

For some fluids, the stress exhibits a linear relationship with shear rate and their viscosity is independent of the shear rate. Such materials are called Newtonian fluids. The viscosity of Newtonian fluids is constant with the time of shearing and the stress in the liquid falls to zero immediately after the shearing is stopped. For most other materials such as dispersions, polymer solutions and emulsions, the viscosities are functions of shear rate. Such materials are called non-Newtonian whose viscosity either decreases or increases with increasing shear rate. The decrease in viscosity with increasing shear rate is termed as ‘shear thinning’ or ‘pseudoplasticity’ while increase in viscosity with shear rate is termed as ‘shear thickening’ or ‘dilatancy’. The stress-shear rate and viscosity-shear rate responses of Newtonian and non-Newtonian fluids are shown in **Fig. 2.3.**

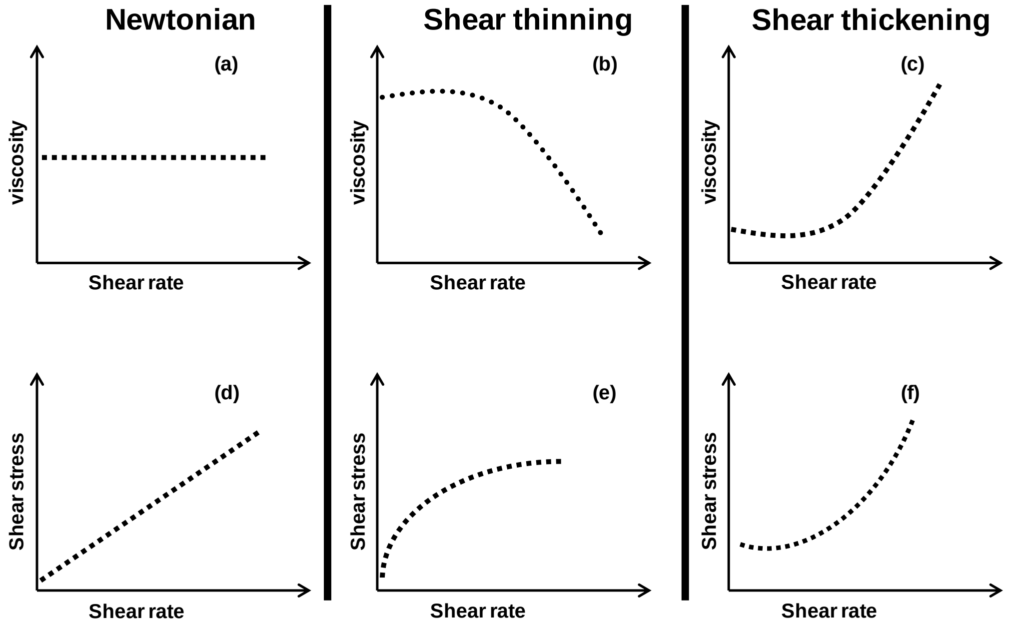

Figure 2.3: Viscosity and shear stress as functions of shear rate for (a,d) Newtonian (b,e) shear thinning and (c,f) shear thickening materials.

Systems like emulsions, suspensions and polymer solutions maintain an irregular internal order and hence have a considerable resistance to flow meaning they have high viscosity. When subjected to increasing shear rates, anisotropic particles in suspensions orient along the direction of flow, polymer chains disentangle and stretch to orient along the shear flow, elastically deformable materials like blood cells reshape themselves to structures with reduced diameters, particle clusters break up leading to the flow of entrapped solvent and particle alignments favor their easy slip past each other as shown in **Fig. 2.4**.[169]

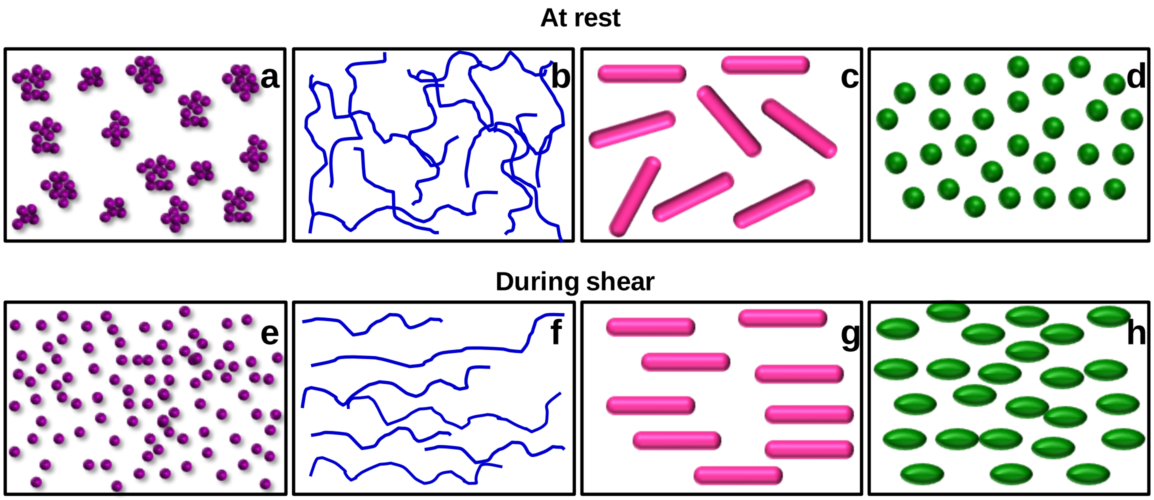

Figure 2.4: Schematics showing the microstructure at rest (top) and during shear (bottom) of (a,e) suspensions containing particles (b,f) polymer chains (c,g) anisotropic particles and (d,h) elastically deformable particles.

In most cases at low shear rates, the materials behave as Newtonian with a shear rate independent viscosity since the Brownian motion keeps the particles at random despite the effect of shear orientation. However when the effect of shear exceeds the randomizing effect of the Brownian motion, the viscosity of the system decreases. A dimensionless number used to represent the relative dominance of the Brownian and shear forces is the Peclet number given by,

$$Pe = \frac{6\pi\eta_c \dot{\gamma} a^3}{k_B T} \tag{2. 4}$$

where a is the radius of the particle dispersed in a medium of viscosity η_c. Shear thinning is caused by the decrease of the Brownian contribution to the viscosity. As the strength of the flow increases, the relative time scale available for the Brownian movement to achieve the structural relaxation progressively decreases.[170] As Pe increases with shear rate, the restoring effect of the Brownian motion reduces and the response becomes shear thinning.

Shear thickening occurs in suspensions containing large volume fraction of solid particles. At high shear rates, as the particles approach each other closely, the lubrication hydrodynamics strongly couples the relative motion between particles.[171] This coupling leads to the formation of hydroclusters as shown in **Fig. 2.5** which are driven and sustained by the applied shear field.

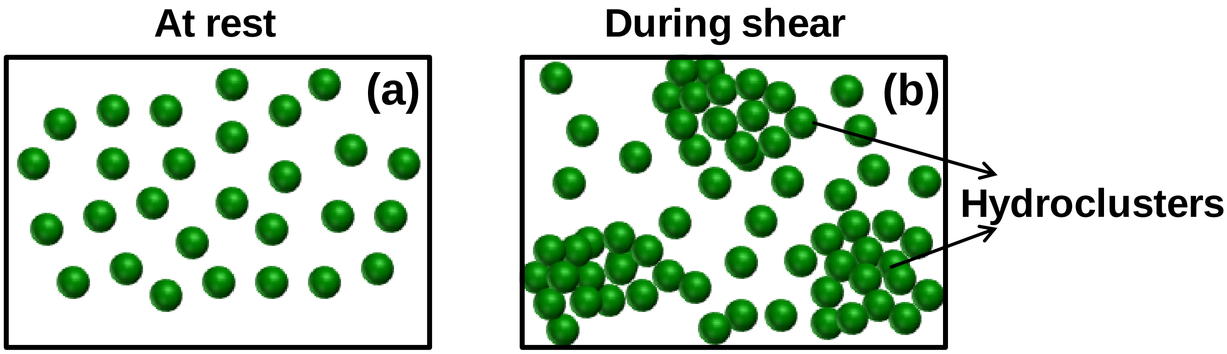

Figure 2.5: Schematics showing the microstructures (a) at rest and (b) during shear of a shear thickening suspension.

The higher particle concentration in these transient clusters causes greater stress in the fluid leading to energy dissipation and consequently a higher viscosity.[171] The formation of hydroclusters is mostly reversible implying that reducing the shear rate brings the suspension viscosity back to its low value. Shear thickening depends on the phase volume, particle size, their distribution and particle morphology.[96]

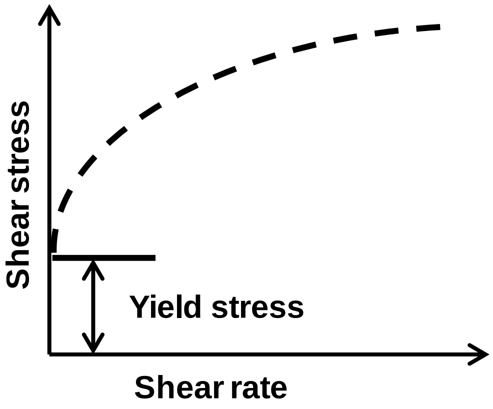

Figure 2.6: Stress-shear rate curve for Bingham plastics showing the yield stress.

Certain materials such as clay suspensions, drilling mud, toothpaste, mayonnaise, chocolate, and mustard have flow behavior similar to Pseudoplastic liquids but with a yield point. Such materials are called ‘Bingham plastics’. No flow is observed in Bingham plastics until the stress reaches a critical value called the yield stress (τ_y). Beyond the yield stress, the Bingham plastics exhibit shear thinning response. The stress-shear rate curve of Bingham plastics is shown in **Fig. 2.6**.

Apart from viscosity changes under varying shear, the viscosity can also change with the time of shearing. A description of the time dependence of viscosity under shearing is given below. A decrease in the viscosity with the time of shearing followed by recovery of the structure on removal of the shear is termed ‘Thixotropy’. Liquid crystals, micellar structures, greases, biological systems, clay dispersions, emulsions, molten salts, etc. exhibit thixotropic behavior. The microstructure of thixotropic systems consists of flocculated particles, entangled polymer chains, randomly oriented particles and fibers leading to a high viscosity. Application of shear leads to alignment of fibres along flow, asymmetrical spatial distribution of particles and minimum polymer entanglement resulting in lower viscosity.[172, 173] On removal of the shear, the microstructure begins to recover to its initial state. The typical viscosity response of a thixotropic system is shown in **Fig. 2.7 (a)**. Thus shearing induces loss of the initial order, while resting leads to rebuilding of the lost order. The timescales for the breakdown of the structure and its rebuilding are different, with the breakdown time being typically in the range of a few milli-seconds to few minutes and the rebuilding time in the order of hours to days. Thixotropy is a reversible process.

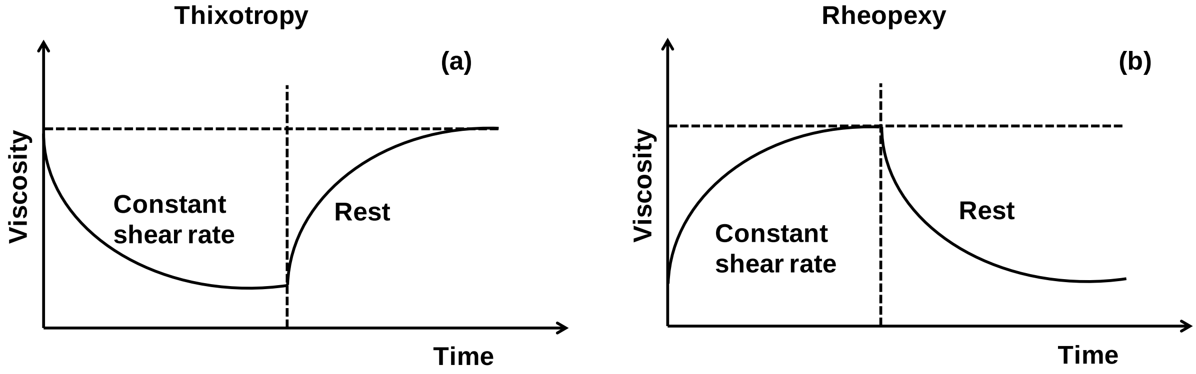

Figure 2.7: Viscosity as a function of time for (a) thixotropic and (b) rheopetic materials.

‘Rheopexy’ (or anti-thixotropy) is the opposite behavior of thixotropy where the viscosity increases with shearing time and recovers back to its lower value on cessation of shear. In systems where the right kind of attraction between particles exists, shearing promotes temporary aggregation rather than their breakdown as a result of the collision between the attractive particles.[173] When the shear is removed, the change in configuration, orientation or interaction field are sufficient to restore the rest condition which has a less structured microstructure. An example of rheopetic material is the suspension of ferric-oxide in mineral oil which is found to flocculate.[174] Under shear the flocs become looser and occupy a higher effective phase volume causing an increase in viscosity. The typical viscosity response of a rheopetic system is shown in **Fig. 2.7 (b)**. In comparison to thixotropy, rheopexy occurs less frequently and is an irreversible process.

2.3.3 Linear Viscoelasticity

All real materials have both elastic as well as viscous properties. The type of response exhibited by materials depends on the time scale of the measurement relative to the natural time of the material. At a faster time scale the material may respond as elastic while at slower time scales it may appear as viscous. At intermediate times the behavior is viscoelastic.

Linear viscoelasticity is based on the superposition principle which means that the response (e.g. strain (γ)) at any time is directly proportional to the value of the initiating signal (e.g. stress). The linear viscoelastic behavior is represented by the following equation.

$$\left(1+\alpha_1\frac{\partial}{\partial t}+\alpha_2\frac{\partial^2}{\partial t^2}+.......+\alpha_n\frac{\partial^n}{\partial t^n}\right)\sigma=\left(\beta_0+\beta_1\frac{\partial}{\partial t}+\beta_2\frac{\partial^2}{\partial t^2}+.......+\beta_n\frac{\partial^n}{\partial t^n}\right)\gamma \tag{2. 5}$$

In the above equation if β_0 is the only nonzero coefficient, the behavior is termed elastic and the resultant **Eqn. (2.6)** represents the Hooke's law of elasticity where β_0 = G is the rigidity modulus.

$$\sigma=\beta_0\gamma \tag{2. 6}$$

If β_1 is the only non-zero parameter then **Eqn. (2.7)** represents a Newtonian behavior with β_1 = η being the coefficient of viscosity.

$$\sigma = \beta_1 \frac{\partial \gamma}{\partial t} = \beta_1 \dot{\gamma} = \eta \dot{\gamma} \tag{2. 7}$$

If β_0 and β_1 are non-zero while all other constants are zero then **Eqn. (2.5)** leads to **Eqn. (2.8)** which represents a viscoelastic behavior. **Eqn. (2.8)** is the representation of the Kelvin Voigt model that combines both the elastic and viscous responses of a viscoelastic material.

$$\sigma = G\gamma + \eta \dot{\gamma} \tag{2. 8}$$

If a stress ($\bar{\sigma}$) is suddenly applied to a viscoelastic material at time, $t = 0$ and held constant thereafter, the strain is given by

$$\gamma = (\bar{\sigma} / G)[1 - \exp(-t / \tau_K)] \tag{2. 9}$$

The strain does not reach its final value instantaneously but does so with a time constant τ_k, which controls the rate at which the strain grows on imposition of the stress. τ_k is called the retardation time. The growth of strain on application of a stress at time $t = 0$ is shown in **Fig. 2.8 (a)**.

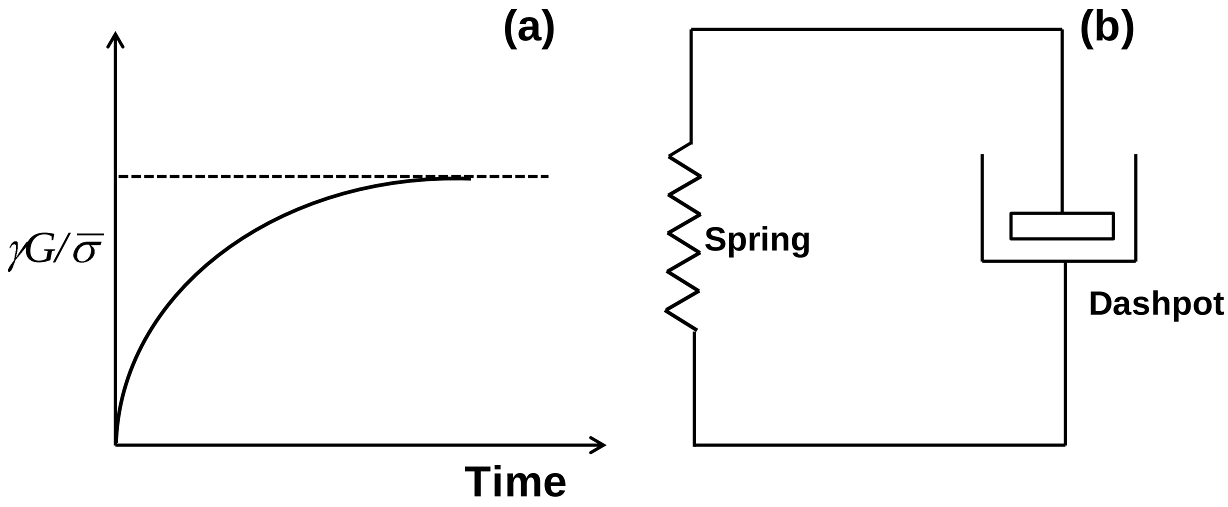

Figure 2.8: (a) Growth of strain following the application of stress at time t = 0. (b) Mechanical representation of the Kelvin Voigt model showing the spring and dashpot connected in parallel.

Mechanical models are often employed to describe viscoelastic behavior. The Kelvin model[96] is physically visualized using a spring and dashpot connected in parallel as shown in **Fig. 2.8 (b)**, in which the spring represents Hookean deformation and the dashpot represents Newtonian flow. On sudden application of stress, the spring will reach the strain but the dashpot will retard the growth of the strain.

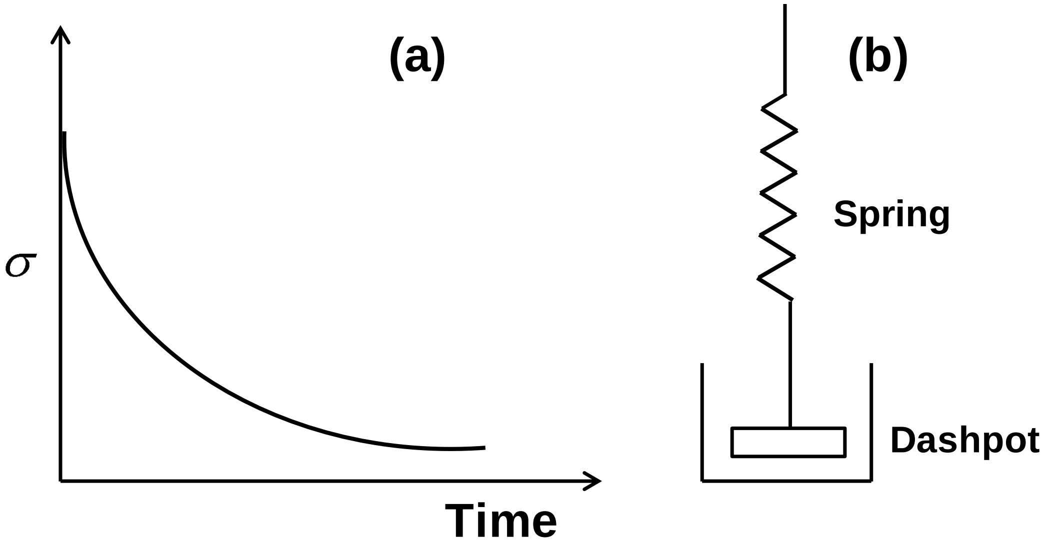

Figure 2.9: (a) Decay of stress following the removal of the steady shear at time *t* = 0 for Maxwell model. (b) Mechanical representation of the Maxwell model showing the spring and dashpot connected in series.

Another model used to describe linear viscoelasticity is the Maxwell model. In **Eqn. (2.5)** if α_1 and β_1 are the only nonzero parameters, then

$$\sigma + \tau_M \dot{\sigma} = \eta \dot{\gamma} \qquad (2.\ 10)$$

where $\alpha_1 = \tau_M$ and $\beta_1 = \eta$. On application of strain at a particular rate ($\bar{\gamma}$), at time *t* = 0 which is held constant thereafter, the stress is given by

$$\sigma = \eta\bar{\gamma}[1 - \exp(-t / \tau_M)] \tag{2. 11}$$

This implies that on start up of shear, the growth of stress is delayed by a time constant τ_M. Similarly, if the strain rate which had a certain value for $t < 0$ is removed at $t = 0$, the stress is given by

$$\sigma = \eta\bar{\gamma}\exp(-t / \tau_M) \tag{2. 12}$$

The stress relaxes exponentially from its equilibrium value to zero with a relaxation time τ_M as shown in **Fig. 2.9 (a)**. Mechanically this is modeled using a spring and a dashpot in series as shown in **Fig. 2.9 (b)**.

The linear viscoelastic behavior is investigated using two methods namely the static and the dynamic methods. The static method employs either creep test at constant stress or relaxation tests at constant strain.[96] In dynamic method, an oscillatory strain is imposed on the material and the resulting stress response is measured. The strain and the stress are mathematically expressed by **Eqn. (2.13)** and **(2.14)** as

$$\gamma = \gamma_0 \sin \omega t \tag{2. 13}$$

$$\sigma = \sigma_0 \sin(\omega t + \delta) \tag{2. 14}$$

where γ_0 and σ_0 are the amplitudes of the strain and stress, respectively, ω is the angular frequency of oscillation and δ is the phase lag between the imposed strain and measured stress. The total resistance of a substance against the applied strain is called the complex modulus (G^*) and is given by the ratio of the stress to strain

$$G^* = \frac{\sigma}{\gamma} \tag{2. 15}$$

$$G^* = G' + iG'' \tag{2. 16}$$

G' is the elastic/storage modulus which is a measure of the energy that is stored during the test which can be recovered back and *G''* is the viscous/loss modulus which is a measure of the energy that is lost as heat during the flow. The phase lag also called the damping factor is given by $\delta = \frac{G''}{G'}$. Purely elastic materials have $\delta = 0$ while pure viscous materials have $\delta = 90^0$. The waveforms of the oscillatory strain input and the stress output for different materials are shown in **Fig. 2.10**.

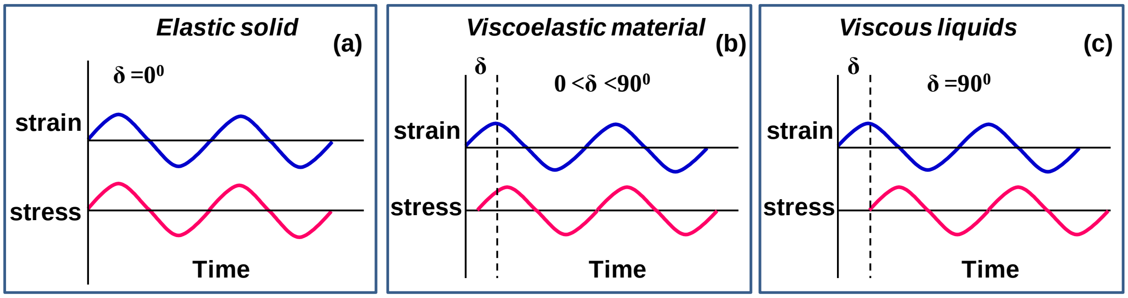

Figure 2.10: Schematic representation of the input strain and measured stress as functions of time for (a) elastic solid (b) viscoelastic material and (c) viscous liquids.

In general the rheological properties of viscoelastic materials are independent of the applied strain up to a critical strain (γ_c) where the behavior is termed as linear. As the strain exceeds γ_c, behavior of the material becomes non-linear. The linear viscoelastic range (LVE) is limited to that amplitude range for which *G** is ~ 0.9*G**.

2.4 Experimental Techniques

2.4.1 Rheometer

Instruments which measure the viscoelastic properties of solids, semi-solids and fluids are called rheometers. Rheometers are broadly classified as rotational rheometers, capillary viscometers and falling ball viscometers. The rotational rheometer which is used for the present study is discussed in detail. In rotational rheometers the fluid is sheared in a narrow gap between two surfaces. Rotational rheometers have numerous experimental modes for controlling shear rate, shear deformation or shear stress. Rotational rheometers are classified into two, namely controlled stress and controlled strain, based on the preset and measured quantities.[169] In controlled stress (CS) rheometers, the measuring system is driven by a motor whose torque values are preset. An electrical power supply results in a linearly related torque values on the motor shaft. The resistance offered by the sample against the applied torque allows the measuring system to rotate at a speed that is inversely related to the viscosity of the sample. Thus in CS rheometers the torque is preset and the angular velocity is measured. In controlled strain (CR) rheometers the velocity is preset and the torque is measured. The CR measuring system is driven by the motor at a controlled speed which forces the sample to flow. The resistance of the sample to flow results in a viscosity related torque which counteracts the torque provided by the motor. A spring that twists as a result of the applied torque is used as a torque detector. The twist angle of the spring is a measure of the sample viscosity. The measuring geometries in rotational rheometers include cone- plate, parallel plates and concentric cylinders. A schematic representation of the geometries is shown in **Fig. 2.11**.

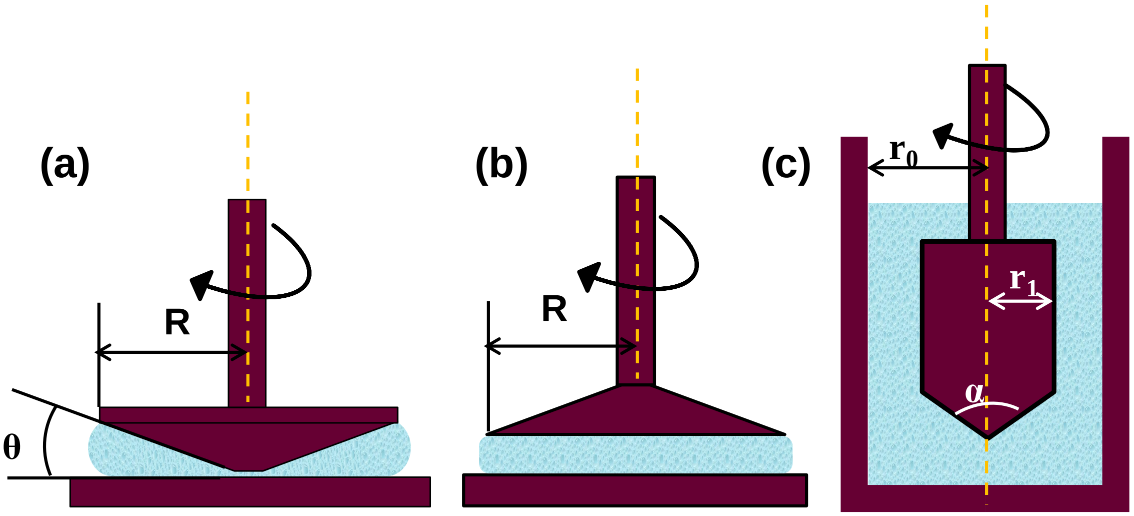

Figure 2.11: Schematics representation of (a) cone-plate (b) parallel plate and (c) concentric cylinder geometries used in rotational rheometers.

Cone-plate: A cone of radius *R* and angle θ_{cp} has its axis perpendicular to the plate, the vertex of the cone being in the plane of the surface of the plate as shown in **Fig. 2.11 (a).**[175] The cone rotates relative to the plate with an angular velocity Ω'. The cone angle is chosen such that for any point of the cone surface the ratio of the angular speed and distance to the plate is constant, i.e. the shear rate is constant from the cone tip to the outer radius. In order to avoid wear of the tip and indentation of the plate, the cone tip is usually truncated. Cone-plate geometry is used for suspensions with smaller particle size (< 50 μm) and it requires only a small sample volume of ~700-800 μL.

Parallel plate: The sample is sheared between two parallel plates separated by a distance *h* as in **Fig. 2.11 (b)**. The top plate rotates about an axis trough its centre with an angular velocity Ω'. If the plate radius is *R*, the shear rate is given by

$$\dot{\gamma} = \frac{R\Omega'}{h} \tag{2. 17}$$

Parallel plate is ideal for samples of high viscosity such as gels and pastes and for suspensions with larger particles (micron sized).

Concentric cylinder: In this geometry, the sample is sheared between two concentric cylinders which are in relative motion as shown in **Fig. 2.11 (c)**. The shear rate throughout the tested region is almost constant. If r_0 and r_1 are the radii of the outer and inner cylinders, respectively and Ω' is the angular velocity of the inner cylinder (outer is stationary) then the shear rate is given by

$$\dot{\gamma} = \frac{r_0\Omega'}{r_0 - r_1} \tag{2. 18}$$

This approximation is valid when the ratio of r_0 to r_1 is greater than 0.97. The concentric cylinder geometry is suitable for low viscosity samples.

2.4.2 Construction of Rheometer

The rheometer used in this work (Anton Paar, MCR series, Germany) is a CR type rheometer that has an air-bearing-supported synchronous Electrically Commutated (EC) motor which is accurate over a wide range of viscosities. The rotor of the EC motor drive is equipped with permanent magnets. Magnetic poles are produced in the stator which has coils of opposite polarity. A rotating flux of current in the coil windings produces a frictionless synchronous movement of the rotor due to the attraction of magnets in the rotor and stator coils. The torque of the motor is set and measured via the input current to the stator coils. From the measured torque, the sensor system calculates the rheologically relevant quantities such as shear rate (**Eqn. (2.2)**), viscosity (**Eqn. (2.3)**), complex modulus (**Eqn. (2.15)**), etc. The EC motor is supported by radial and axial air bearings which are used to center and stabilize the shaft and hold the weight of the rotating parts, respectively. In the rotational mode the rheometer can measure torque in the range of 0.05 μNm - 200 mNm, with a resolution of 0.1 nNm. In the oscillatory mode the minimum measurable torque is 0.01 μNm. The speed of rotation can vary between 10^{-7} and 3000 min^{-1} while the angular frequency range lies between 10^{-5} and 628 rad/s. The temperature of the samples is controlled using a Peltier controller (P-PTD200/56) and water circulator (Anton Paar Viscotherm VT2).

2.4.3 Magnetorheometer

The magnetorheological measurements were performed using strain controlled rotational rheometer Anton Paar Physica MCR 301 equipped with a magnetorheological device (MRD 180). The measuring system is a parallel plate with a diameter of 20 mm made up of non-magnetized metal to prevent radial magnetic forces acting on the measuring shaft. The magnetic field is generated by coils and is directed perpendicular to the plane of shear as shown in the schematic in **Fig. 2.12 (a)**.

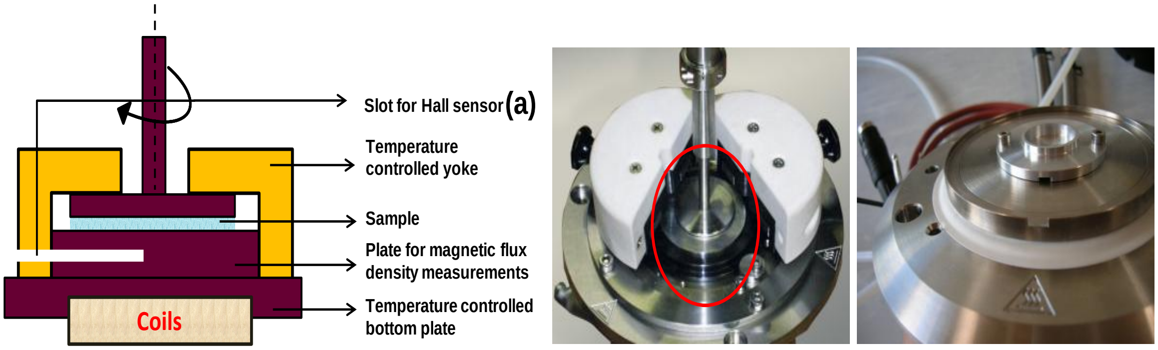

Figure 2.12: (a) Schematic of the magnetorheological device with parallel plate geometry (b) photograph of magnetorheological device with the temperature controlled yoke and (c) magnified view of the encircled region in (b) showing the sample holder.

The photograph of the MRD and its magnified view showing the sample stage is shown in **Fig. 2.12 (b)** and **(c)**. The current in the coil and the magnetic flux density are controlled using a separate power supply by the Rheoplus software. The magnetic flux density in the air gap can reach a maximum of 1 tesla corresponding to a current of 5A. The magnetic field is homogenous within the shear-rate-sensitive region of the geometry. The rheometer is also equipped with a demagnetizer to remove the residual magnetic field.

2.4.4 Rheomicroscope

Rheomicroscopic studies were performed using strain controlled rotational rheometer Anton Paar Physica MCR 102. The rheomicroscope consists of a microscope tube, long distance working objective and a charge-coupled device (CCD) camera as shown in the schematic in **Fig. 2.13**. The photographs of the rheomicroscope with the solenoid coil and power supply are shown in **Fig. 2.14**.

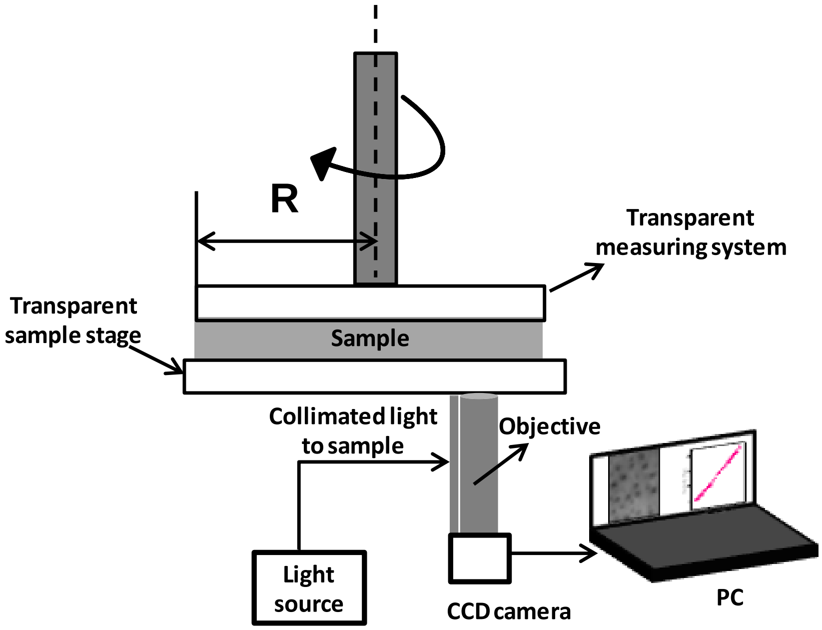

Figure 2.13: Schematic of the rheomicroscope set up showing the sample stage, light source, objective and CCD camera.

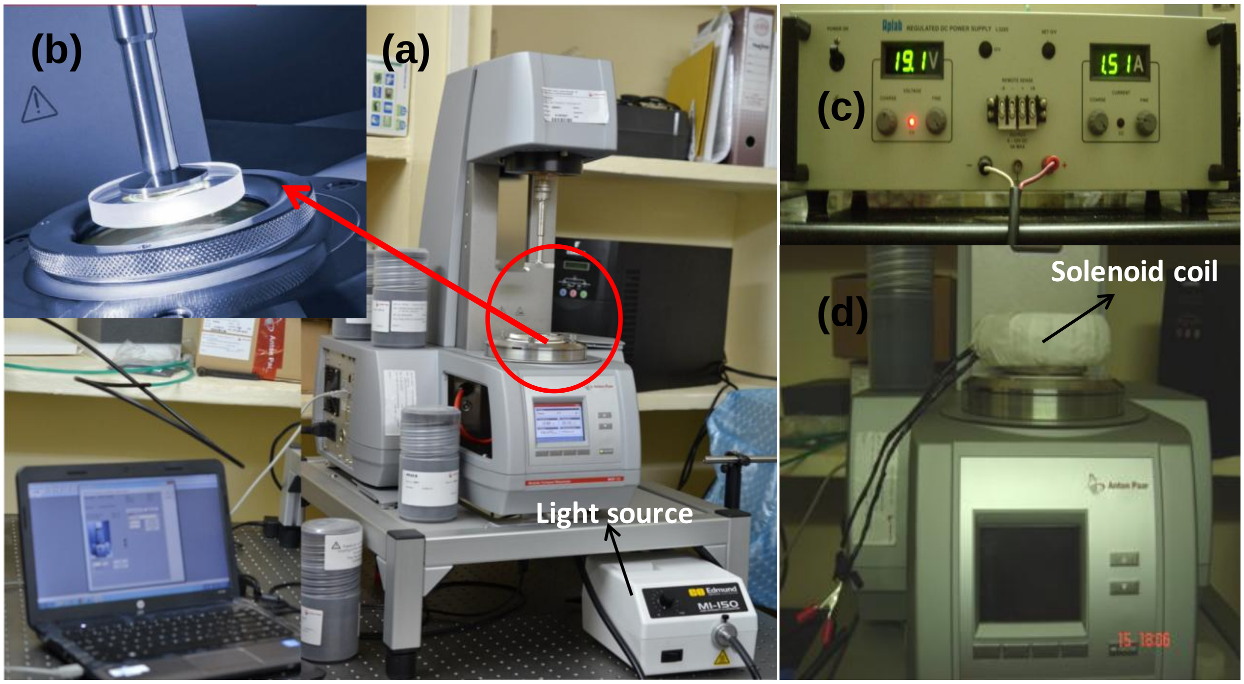

Figure 2.14: Photographs of (a) rheomicroscope set up (b) magnified view of the sample stage (c) DC power supply (d) solenoid coil surrounding the sample stage.

The sample stage (Peltier Universal Optical Device (P-PTD 200/GL) is made of transparent glass and is illuminated by a light source (MI-150 high intensity illuminator, Edmund Optics Worldwide) from below. The microscope can be moved in the x and z directions for choosing areas of interest and focusing, respectively. The magnetic field is applied to the sample by a custom-made solenoid coil powered by a DC power supply, enclosing the sample stage. The image of the sample during rheological measurements is captured automatically by the CCD (Lumen*era* LM165C) camera using the Rheoplus software.

2.4.5 Magnetorheological Measurements

For steady state measurements, the sample was placed in the measuring system of the rheometer. The sample was presheared at a rate of 100 s^{-1} for 2 minutes and then subjected to a magnetic field for 2 minutes for the equilibrium structure to be established. Following this the viscosity and shear stress of the sample were measured as functions of shear rate at a particular magnetic field. The procedure was repeated for different magnetic field strengths by changing the coil current. In magnetic sweep experiments, the shear rate was held constant at different values (0.001, 0.01, 0.1, 1, 10 and 100 s^{-1}) and the viscosity of the ferrofluid was measured by varying the magnetic field from 0 to 350 mT and back to 0 mT. The oscillatory measurements in the ferrofluid samples were done by amplitude sweep and frequency sweep measurements. In the amplitude sweep measurements, the ferrofluid was subject to a magnetic field for 2 minutes following which an oscillatory strain of increasing amplitude ranging from 0.01 to 100 % was imposed on the sample at a fixed frequency of 10 rad/s and the storage and loss moduli were measured. For the frequency sweep measurements, the strain amplitude was held fixed at a value within the LVE region and the frequency varied between 10^{-2} and 10^{2} rad/s. The Strain-rate Frequency Superposition[176] (SRFS) measurements were performed by simultaneously varying both the strain amplitude and frequency such that the product of the two is a constant. For the rheomicroscopic studies under magnetic field, a custom made solenoid coil enclosing the sample stage as shown in **Fig. 2.14** was used. The current in the coil was varied from 0 to 2.34 A using a DC power supply. The rheomicroscopic images were acquired perpendicular to the plane of shear from the bottom of the sample stage using a 20X objective. For the experiments in **Section 4.3.1**, the shear rate was held fixed at 10^{-3} s^{-1}. For the experiments in **Section 4.3.2**, the magnetic field was kept at a constant value of 176 gauss.

2.4.6 Phase Contrast Optical Microscopy

Phase contrast optical microscopy is a technique used to visualize transparent specimens, such as living cells, microorganisms, thin tissue slices, lithographic patterns, fibers, dispersions containing micron sized particles, glass fragments, subcellular particles etc. with better contrast. It converts the change in phase of the light passing through the sample specimen into change in the intensities that can be perceived by the human eye. When passing through a sample specimen the light waves are shifted by a small degree due to the difference in refractive indices between the sample and the background slide. The light wave that passes through the sample lags behind the light wave that passes through the slide alone. The amount of lag called the phase shift depends on the refractive index of the sample. Phase contrast microscope converts differences in refractive indices between the specimen and background to differences in image brightness.

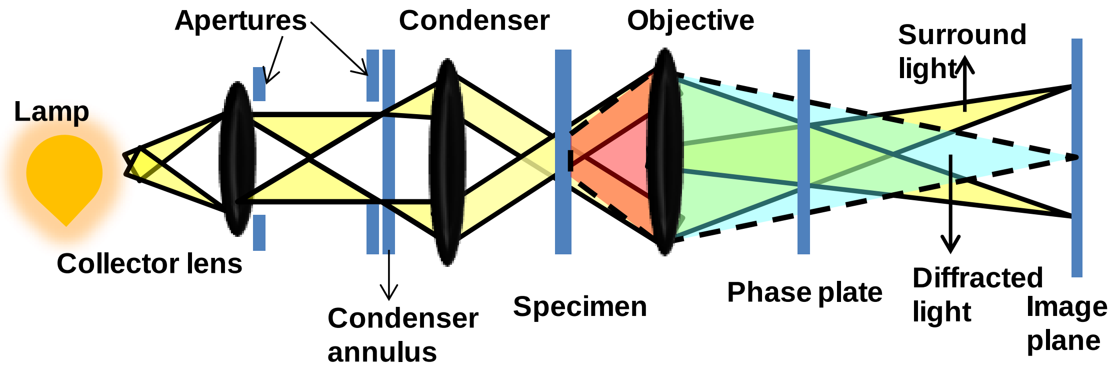

Figure 2.15: Schematic representation of phase contrast optical microscope showing the arrangement of light source, lenses, specimen, phase plate and image plane.

In a phase contrast microscope, light from the source, usually a tungsten halogen lamp is directed through a collector lens and focused on a condenser annulus as shown in **Fig. 2.15**. The light wave passing through the annulus illuminate the specimen and is divided into two components. The undeviated component of the wavefront passes through and around the specimen without interacting with it and is termed the surround wave (*S*). The other component is diffracted by the specimen and is called the diffracted wave (*D*). Both the surround and the diffracted wavefronts enter the objective front lens and are subsequently focused at the intermediate image plane where they interfere to produce the resultant particle wave (P).

In order to maximize the differences in intensity between the specimen and the background in the image plane, the phase difference between the surround wave and the diffracted wave must be larger. The phase difference is generated using a two step process. Firstly, the diffracted waves are retarded in phase by a quarter wavelength at the specimen. The presence of the specimen retards the optical path of the portion of the incident light wavefront that passes through it. The velocity of light when it passes from one medium to another is altered proportional to the difference in refractive indices between the two media. When light passes through a specimen having a thickness t', the wave is either increased or decreased in velocity. This in turn leads to a subsequent advancement or retardation of the phase of the wave in comparison to the surrounding medium. The phase shift (δ') between the waves emerging from the specimen and surrounding medium is given by $\delta' = 2\pi\Delta/\lambda'$, where Δ is the optical path difference given by $\Delta = (n_2 - n_1) \times t'$. Here, n_1 and n_2 are the refractive indices of the surrounding medium and specimen, respectively. Secondly the surround waves are advanced or retarded in phase by a phase plate that is positioned in or very near the objective rear focal plane as shown in **Fig. 2.15**. The phase and amplitude of the surround light wave is selectively altered by the phase plate that can give either positive or negative phase contrast. In positive phase contrast systems, the phase of the surround wavefront is advanced relative to the diffracted wavefront from the specimen while in negative phase contrast, the surround wavefront is retarded with respect to the diffracted wavefront. For the present work the microscopic pictures were obtained using phase contrast microscopes from M/s Leica, Germany and M/s Carl Zeiss, Germany, using 40X objective.

2.4.7 Vibrating Sample Magnetometer

Vibrating sample magnetometer (VSM) is used to the measure the magnetization of the sample. It operates on Faraday's law of induction. VSM consists of a sample rod driven by a mechanical vibrator and positioned between the pole pieces of an electromagnet. The sample is vibrated perpendicular to the field produced by the electromagnet. The oscillating magnetic field produced by the vibrating sample induces a voltage in the stationary detection coils. A small permanent magnet or electromagnet is used as reference in which is induced a second voltage. Both the sample and the reference are driven synchronously and a known portion of voltage from the reference coils which is phased to balance the voltage from the sample coil is proportional to the magnetic moment of the sample.[177] The measurements are insensitive to the vibration amplitude, frequency, small magnetic field instabilities, magnetic field non-uniformity, amplifier gain, or amplifier linearity. The measurements are also made insensitive to the exact sample position by employing suitable pairs of coils. For the present study, the magnetic properties of the ferrofluid were determined using cryogen free mini VSM (M/s Cryogenics, UK) for applied fields between -1.5 and 1.5 tesla.

2.4.8 Dynamic Light Scattering

Dynamic Light Scattering (also called Photon Correlation Spectroscopy or Quasi elastic light scattering) determines the size of the particle by measuring the time dependence of the fluctuations in intensity of the light scattered by particles in a suspension. The particles which are in constant Brownian motion due to the room temperature thermal energy are illuminated by a laser light. Scattering of the laser light by the moving particles produces intensity fluctuations whose rate varies with the speed of the particle. Smaller particles move faster than larger ones. The measured intensity fluctuations are send to a correlator which measures the degree of similarity between the intensities over a period of time. The scattered intensity at time t and that at a short time $t+\delta t$ afterward will be strongly correlated. However as δt becomes larger, the correlation between the intensities will decrease due to the random Brownian motion of the particles and finally fall to zero at longer time. Perfect correlation between the intensities is represented by unity and no correlation by zero. The correlation function depends on the size of the particle scattering light. The correlation of larger particles decays slowly when compared to that of smaller particles due to their rapid motion. The software then constructs the intensity-intensity auto correlation function $g^{(2)}(q,t)$ given by

$$g^{(2)}(q,t) = \frac{\langle I(q,0)I(q,t)\rangle}{\langle I(q)\rangle^2} \tag{2. 19}$$

where q is the scattering vector. The intensity auto correlation function is converted to the electric field auto correlation function $g^{(1)}(q,t)$ using the Siegert's relation

$$g^{(2)}(q,t) = 1 + \beta\left|g^{(1)}(q,t)\right|^2 \tag{2. 20}$$

For monodisperse particles $g^{(1)}(q,t)$ is a single exponential function given by

$$g^{(1)}(q,t) = \exp(-\Gamma t) \tag{2. 21}$$

where $\Gamma = Dq^2$ is the relaxation rate and D is the translation diffusion coefficient of the particles. The diameter of the particle is then deduced from Stokes-Einstein equation given by

$$d = \frac{k_B T}{3\pi\eta_c D} \tag{2. 22}$$

In the present study, the hydrodynamic size of the particles was determined by dynamic light scattering using Zetasizer Nano ZS (Malvern Instrument, UK).

2.4.9 Thermogravimetry

In thermogravimetry the mass of the substance is monitored as a function of temperature or time under controlled atmosphere. Thermogravimetric analysis (TGA) is used to characterize samples with regard to their composition and thermal stability. The TGA instrument includes a high precision analytical balance with a sample pan attached to it and a furnace programmed for a linear rise of temperature with time.[178] In the present study the thermogravimetric analysis of the ferrofluid was carried out using a Mettler Toledo TGA-DSC-1, 1100LF system (Switzerland) under an inert atmosphere from 35-600 °C at a heating rate of 10 °C min^{-1}.

Chapter 3

Probing of Field Induced Structures and Tunable Rheological Properties of Ferrofluid

3.1 Introduction

The study of the magnetorheological properties of ferrofluids is important for both fundamental understanding and applications. Because of agglomeration and settling of nanoparticles in ferrofluids and lack of model dispersions (minimum polydispersity and particle size within single domain and superparamagnetic limit, long term stability, etc.), many of the results reported in the literature are often non reproducible. The metastable nature of such dispersions adds yet another complexity that results in a continuous evolution of nanostructures in ferrofluids. Literature reports are mainly on studies in dilute ferrofluids wherein interparticle or interchain interactions are neglected. However in most applications involving ferrofluids the concentration of the nanoparticles is higher and hence these interactions cannot be ignored. The objective of the present work was to undertake a systematic study of the magnetorheological properties of model ferrofluids. The questions addressed in this study are: (1) What is the role of the external field on the microstructural formation inside the fluid and the consequence of the formed structures on the magnetoviscous effect of the fluid? (2) What is the effect of shear force and applied magnetic field on the formed internal structures, viscoelastic properties and the static and dynamic yield stresses of the suspension? (3) Can the specific viscosity data against Mason number for different magnetic field strengths collapse on to a single master curve? To realize the above objectives, the steady state and dynamic magnetorheological properties of stable ferrofluids of two different volume fractions for a large number of applied magnetic field strengths were probed.

3.2 Experimental Details

Magnetite nanoparticles dispersed in kerosene at volume fractions of 0.038 and 0.05 were used for the present study. These concentrations were chosen because the interparticle separations at these concentrations are significant. The particles were synthesized by co-precipitation technique as discussed in **Chapter 2**. The magnetorheological measurements for samples of $\varphi = 0.038$ and 0.05 were performed as described in **Chapter 2**. The results for $\varphi = 0.038$ are shown in this chapter.

3.3 Results and Discussion

3.3.1 Properties of the Ferrofluid

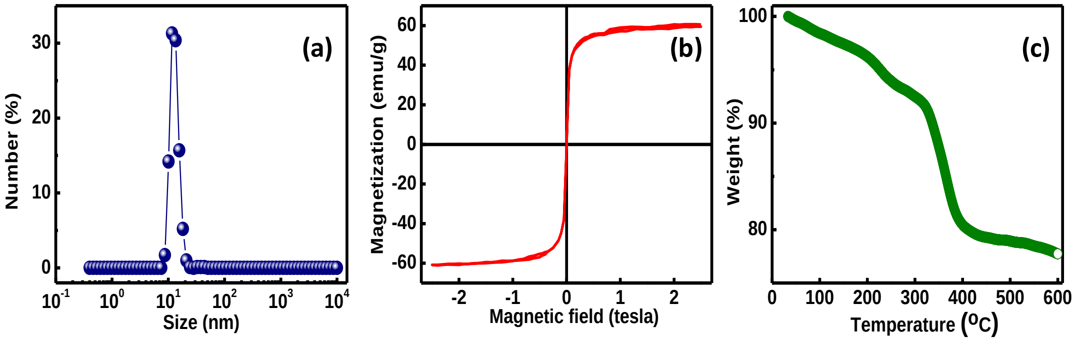

Figure 3.1: (a) Hydrodynamic size distribution (b) magnetization curve and (c) thermogravimetric curve of Fe_3O_4 nanoparticles.

The hydrodynamic size of the nanoparticles was obtained using dynamic light scattering measurements. From the size distribution shown in **Fig. 3.1 (a)**, the average diameter of the particles was found to be ~12.5 nm. The magnetization curve for the iron oxide nanoparticles in **Fig. 3.1 (b)** shows that the particles are superparamagnetic in nature with a saturation magnetization of 59 emu g^{-1}. The thermogravimetric curve for the magnetite nanoparticles in **Fig. 3.1 (c)** shows a two-step weight loss at ≈199 and ≈320 °C. The first step is due to the removal of loosely bound or free surfactant (oleic acid) and the second step is due to the removal of strongly bound surfactant molecules. The carboxylic acid group of oleic acid binds to the magnetite while the aliphatic chain extends out into the non-polar solvent thus providing steric hindrance between the particles. The charges at the carboxylate ion of oleic acid, de-localizes in between two oxygen atoms because of the resonance effect. The surfactant coating thus prevents the agglomeration of particles against van der Waals and magnetic attractive interactions. Besides, it passivates the nanocrystals against further oxidation. A simple calculation shows that the surfactant present in the system is slightly more than the amount required to form a close-packed monolayer on the surface of the spherical nanoparticles. For a monolayer coating, the amount of surfactant required for a particle of size 12.0 nm is ~13 wt%.

3.3.2 Steady Shear Rheology

Fig. 3.2 shows the viscosity curves for the ferrofluid of $\varphi = 0.038$ at different magnetic fields. In general, the addition of nanoparticles to a Newtonian carrier fluid increases the viscosity of the suspension, due to occlusion of the solvent within the temporary nanoparticle clusters. As the liquid occluded within the clusters does not participate in the flow, the effective solid phase concentration increases leading to an increase in viscosity.[179-182] With increasing shear rates the clusters are broken down by the hydrodynamic forces allowing the entrapped solvent to flow thus reducing the viscosity. Hence the sample exhibits a shear thinning behavior.[179] Weak attraction between the particles leads to the formation of dense aggregates (reversible) with a significant number of nearest neighbors. Such aggregates exhibit complex responses to applied flows and osmotic stresses. In such cases, the hydration layer between the particles of the aggregates provides a slippery bond that is not shear resistant.[183]

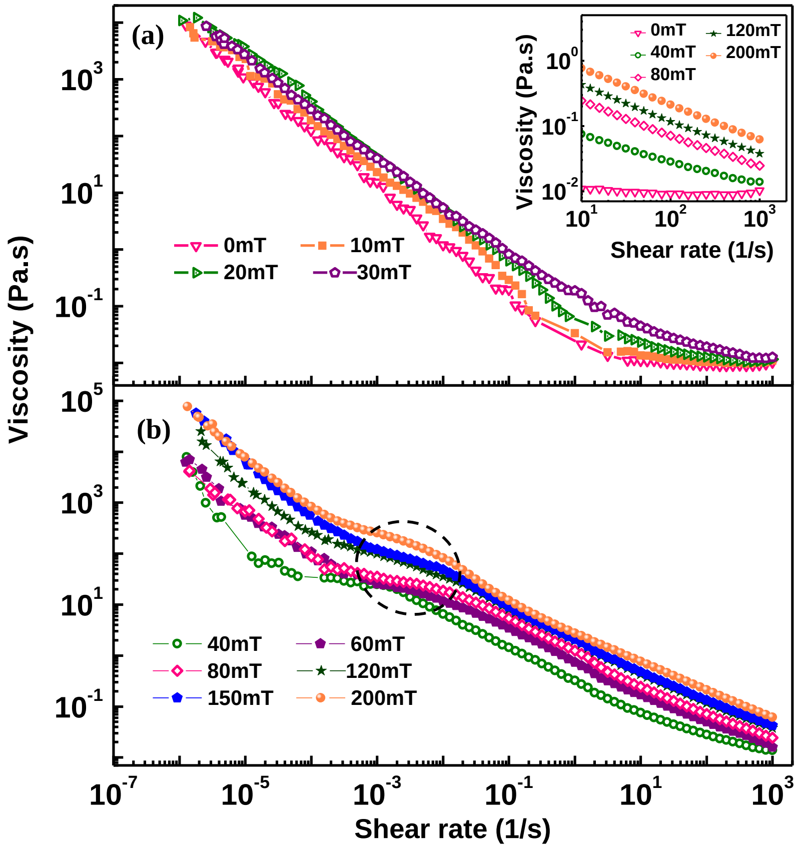

Figure 3.2: Viscosity as a function of shear rate for ferrofluid of volume fraction 0.038 at magnetic fields of (a) 0, 10, 20 and 30 mT and (b) 40, 60, 80, 120, 150 and 200 mT. The plateau region is shown by the encircled region. Inset (a) Magnified view of the viscosity curves for magnetic fields of 0, 40, 80, 120 and 200 mT at higher shear rates (> 10 s^{-1}).

The shear thinning behavior in the absence of magnetic field is observed up to a shear rate of 10 s^{-1} followed by a Newtonian region. The Newtonian regime at higher shear rate is attributed to the breaking down of clusters into primary particles. For the studied volume fractions of 0.038 and 0.05, the corresponding particle number densities are 3.7×10^{22} and 4.9×10^{22} m^{-3}, respectively. For a well dispersed nanoparticle dispersion, the interparticle spacing for φ = 0.038 and 0.05 corresponds to 19.5 and 16.7 nm, respectively. Under such a scenario, the interaction between colloidal particles can be significant. Besides, the local packing of the solvent around the nanoparticles can modify the effective interactions between nanoparticles strongly, thereby affecting both the structure and dynamics of the ferrofluid. Using a computationally tractable model, it was shown that the interparticle interaction and the solvent has important effects on both the structure and dynamics of nanofluids.[182] The stronger interaction leads to an enhanced viscosity and a shear thinning behavior.

When the sample was subjected to a magnetic field of 10 mT, the viscosity increased as compared to that in the absence of a field. For systems with non-interacting particles, the increase in viscosity in the presence of magnetic field is due to the rotational viscosity contribution as described in **Chapter 1**.[104] For systems with interacting particles, the formation of chainlike structures that are aligned along the field direction results in a very large increase in viscosity (MVE).[184] As described in **Chapter 1**, when the coupling constant is much greater than unity, magnetostatic particle interaction dominates the thermal motion leading to the formation of chains that are aligned along the direction of the magnetic field.[185] The aspect ratio of the chains depends on several factors such as size distribution of magnetic particles, applied field strength, the saturation magnetization of the particles and volume fraction of nanoparticles. Therefore, there is a distribution of chain lengths for a particular value of the magnetic field.[186, 187] As the magnetic fields strengths used in our study are modest, the structures formed are mostly linear chains as against the bulk dense drops that are predicted to form at higher magnetic fields.[72, 140, 186, 188] With increasing magnetic field, the linear chains grow with increasing aspect ratio.[189] At sufficient field strength they span the gap between the rheometer plates. With further increase in field, zippering [120, 190] occurs leading to the formation of thick columns. These columns resist flow leading to very high values of viscosity. The chain with a dipole moment per unit length $m/a \sim \mu_0 \chi a^2 H$ interacts with the mean squared lateral field induced by chain fluctuations and the interaction energy (U) per unit length a is given by[3, 191]

$$U \approx (m/a)\langle H^2 \rangle^{1/2} \approx \frac{\chi H(\mu_0 k_B T)^{1/2} a^{5/2}}{\rho^2} \qquad (3.\,1)$$

The time scale for chain coalescence is found by balancing the fluctuation force experienced by a chain segment and the viscous drag on the segment.[120] For moderate and highly concentrated dispersions, the coalescence time scale is much smaller than the characteristic relaxation time of the fluctuations; that is the fluctuations persist long enough to drive the coarsening process. We observe such zippering transition in our dispersions that lead to the formation of interconnected fibrous structure (**Fig. 3.3**). Such lateral coalescence of dipolar chains using micron sized superparamagnetic latex particles was first demonstrated with microscopy by Fermigier and Gast.[190] The modified Halsey-Toor (MHT) theory also predicts lateral aggregation of two chains under a large-amplitude fluctuation.[191]

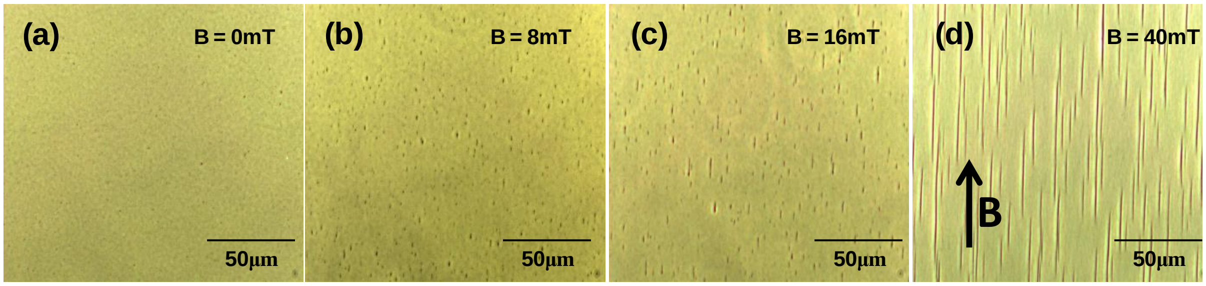

Figure 3.3: The phase contrast microscopic images of ferrofluid (a) without magnetic field and at magnetic fields of (b) 8 mT (c) 16 mT and (d) 40 mT. Particles are not seen in (a) as the size of the primary particles is beyond the resolution of the microscope. In (b) relatively small chains with large inter-chain spacing is seen. In (c) longer chains are seen. In (d) fibrous structure due to zippering of large number of chains are visible. The direction of the magnetic field is shown by the arrow in (d).

When the sample under magnetic field is subjected to increasing shear rates, the field induced structures start breaking and the viscosity decreases[105, 116] leading to shear thinning as shown in **Fig. 3.2**. In electrorheological fluids, Martin and Anderson[192] showed that the fragmentation spontaneously occurs when the applied force is such that the pair potential reaches an inflection point and the lifetime of an electric field induced chain decreases with an increase in the applied force. Further, it was shown that the chains under confinements can behave very differently than unconfined chains.

The shear thinning behavior persists even up to the highest shear rates indicating that the structures formed are not completely destroyed (inset of **Fig. 3.2 (a)**) by the hydrodynamic forces. For values of the magnetic field less than 40 mT, the suspension shows a strong shear thinning behavior for the entire range of shear rates studied. Above 40 mT, the suspension viscosity decreases drastically up to certain shear rate above which the rate of decrease slows down. This decrease of slope or slowing down of shear thinning (encircled region in **Fig. 3.2 (b)**) can be explained as follows. The maximum number of particles ($N_{\max}$) in a chain and the maximum chain length ($L_{\max}$) for different field strengths are given by the relation[192]

$$2N_{\max} = (\sqrt{6}Mn)^{-1/2} \text{ and } \qquad L_{\max} = 4aN_{\max}\sqrt{3/5} \tag{3. 2}$$

Mn is the Mason number defined as the ratio of the shear (hydrodynamic) force to the magnetic force.[192-194]

$$Mn = \frac{\eta_c \dot{\gamma}}{2\mu_o \mu_c \beta^2 H^2} \tag{3. 3}$$

where μ_c is the relative permeability of the carrier fluid and β is the contrast factor defined as

$$\beta = \frac{\mu_p - \mu_c}{\mu_p + 2\mu_c} \tag{3. 4}$$

with μ_p being the relative permeability of the particle which is taken as 2.7 for Fe_3O_4 particles.[195]

From the theoretical work by Martin and Anderson[192], the maximum number of particles allowed for a just gap spanning chain is given by

$$N^* = \frac{h}{4d\sqrt{3/5}} \tag{3. 5}$$

This occurs at a critical Mason number

$$Mn^* = \frac{2\sqrt{6}}{5}\left(\frac{d}{h}\right)^2 \tag{3. 6}$$

where h and d are the gap between the rheometer plates and the particle diameter, respectively. For smaller Mason numbers, the chains will span the gap and align more closely with the field. As the Mason number increases, the chain will increase from zero angle to a maximum of θ_c where $\tan\theta_c = \sqrt{2/3}$, above which the chains part from the rheometer plates and maintain a constant orientation. A chain length distribution will result in a much broader chain angle distribution. The variation of maximum chain length (L_{max}) with field is shown in **Fig. 3.4 (a)**. It shows that the maximum chain length up to 180 mT is less than the gap between the plates of the rheometer. Thus at a critical shear rate, the chains are oriented at an angle $\theta \le \theta_c$ accounting for the polydispersity in the chain lengths as well.

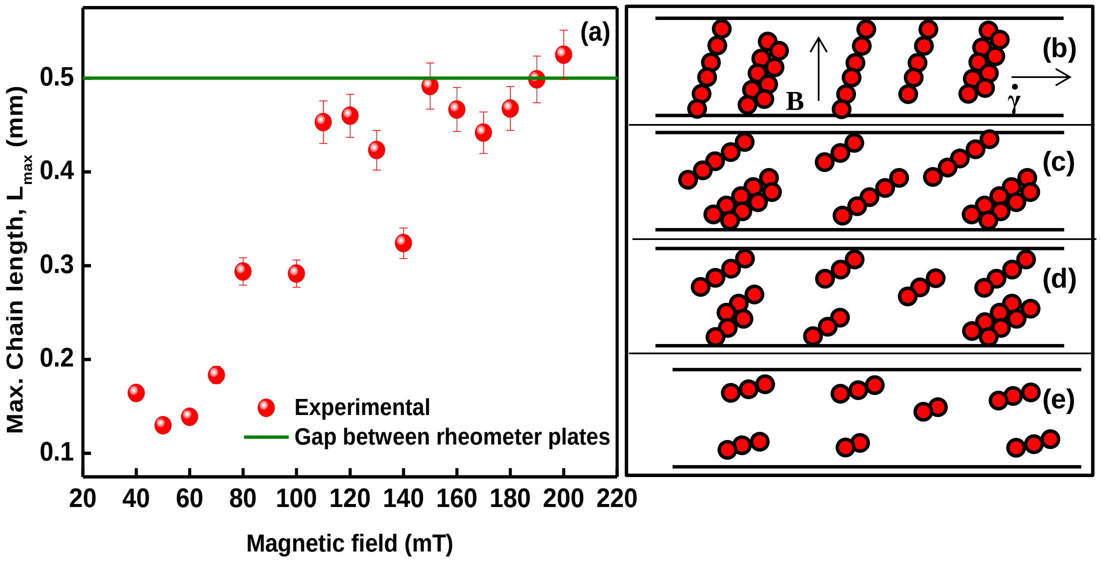

Figure 3.4: (a) Maximum chain length as a function of magnetic field for ferrofluid of volume fraction 0.038 (calculated using **Eqn. (3.2)**). The solid green line indicates the gap between the rheometer plates. Schematics showing the suspension microstructures (b) below the critical shear rate (c) at the critical shear rate (d) above the critical shear rate (e) at very large shear rates. The directions of the shear rate $\dot{\gamma}$ and magnetic field *B* are shown by arrows.

The microstructural arrangement of suspended particles greatly influences the suspension viscosity. The schematic representation of the microstructure of the system at very low shear rates is shown in **Fig. 3.4 (b)**. Here the chains are long enough to span the gap between the plates and are more closely aligned with the magnetic field *B*. The microstructure of the system at the critical shear rate is shown in **Fig. 3.4 (c)** where the chains are oriented along $\theta \leq \theta_c$. When the shear rate is further increased, the inclined chains are broken down and they again tend to orient along $\theta \leq \theta_c$ which will create a microstructure as shown in **Fig. 3.4 (d)**. The viscosity change with shear rate is slow beyond the critical shear rate due this process where the chains continuously orient along θ_c. This process continues until the shear forces become very large, where the chains are more aligned along the shear direction than along *B*, which leads to a faster decrease in viscosity. The microstructure in this case is shown in **Fig. 3.4 (e)**. At low fields (< 40 mT), the chains are too short (similar to **Fig. 3.4 (e)**) that they are easily aligned along the shear flow and hence the plateau was not observed. Similar observations were made in systems of nanoemulsion gels under shear where the plateau region between two shear thinning regimes was attributed to the continuous breaking and reforming of the clusters.[183] The shear thinning behavior observed in this system resembles those predicted for interacting nanoparticle dispersion using molecular dynamics simulations.[182] In the simulations, the Hamaker constant was varied to tune the interaction whereas the magnetic field is varied to achieve the same in the present study. This shows the wonderful applications of magnetically polarizable dispersions for fundamental understanding of colloidal interparticle interactions.

3.3.3 Yield Stress Measurements

Yield stress is an important parameter that determines the flow behavior of a material. In magnetic fluids two types of yield stresses namely the static and the dynamic yield stress are present. The static (or frictional) yield stress is the minimum stress required to cause the suspension to flow. This yield stress is frequently associated with the slip of the aggregates on the plates rather than the structure collapse under shear and is obtained from the double logarithmic representation of stress versus shear rate curve (flow curve). The dynamic yield stress corresponds to the stress needed to continuously break the aggregates which have a tendency to reform in the presence of the magnetostatic forces once the stress exceeds the static yield stress. In general, the yield stress is obtained by fitting a constitutive model, such as the Bingham, Herschel–Bulkley or Casson equations, to the experimental data.[196-198]

In the present study the static and dynamic yield stresses were determined from the flow curves at different magnetic fields shown in **Fig. 3.5** using the Herschel–Bulkley model given by

$$\tau = \tau_y + k\dot{\gamma}^n \tag{3. 7}$$

where τ_y is the yield stress and k and n are the consistency factor and power law index, respectively.

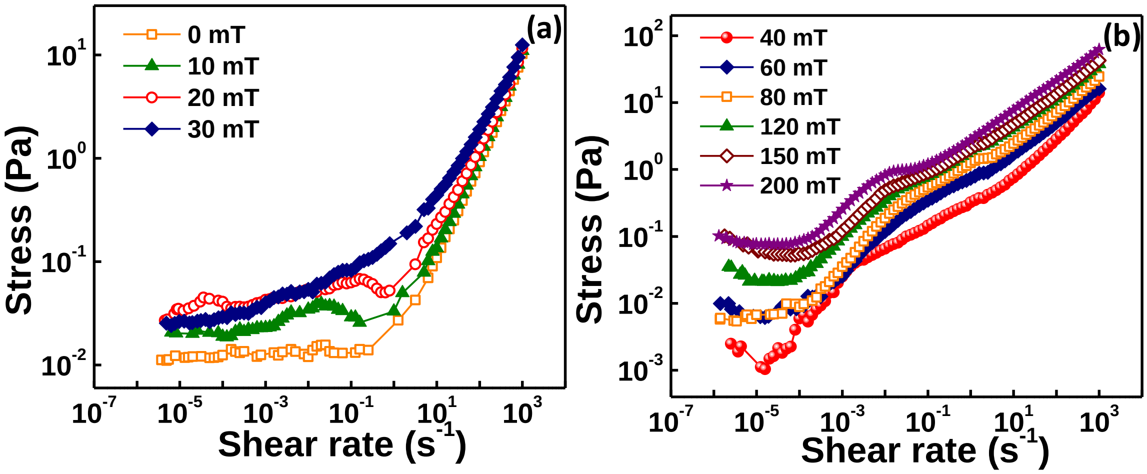

Figure 3.5: Flow curves for ferrofluid of volume fraction 0.038 (a) at magnetic fields of 0, 10, 20 and 30 mT (b) at magnetic fields of 40, 60, 80, 120, 150 and 200 mT.

The yield stresses are plotted as functions of H^2 in **Fig. 3.6 (a)**. According to the work of Ginder et al.[199], the yield stress variation with magnetic field strength is dependent on the magnetization of the particle. They showed that in the linear regime of magnetization, the yield stress increases quadratically with magnetic field strength as given by

$$\tau_y \propto \mu_0 \mu_c \beta^2 H^2 \tag{3. 8}$$

In the intermediate region, the yield stress increases subquadratically with the external field strength and it becomes independent of the field at large field strengths when the particle magnetization saturates. The yield stress for the intermediate and saturation regimes are given by **Eqn. (3.9)** and **(3.10)**, respectively.

$$\tau_y = \sqrt{6}\mu_0 M_S^{1/2} H^{3/2} \qquad (3.\ 9)$$

$$\tau_y = 0.086\varphi\mu_0 M_S^2 \qquad (3.\ 10)$$

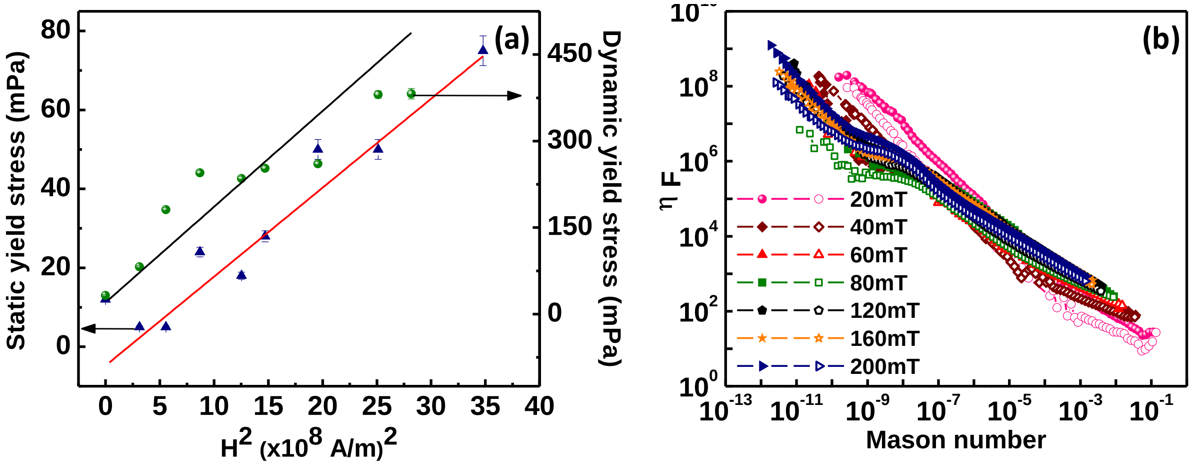

Figure 3.6: (a) Static yield stress (triangles) and Dynamic yield stress (solid circles) as a function of H^2 for ferrofluid of volume fraction 0.038. Solid lines represent fit using **Eqn. (3.8)** with μ_c = 1 and β = 0.3617 (b) Field specific viscosity vs. Mason number for ferrofluid of volume fraction 0.038 and 0.05 at magnetic fields 20, 40, 60, 80, 120, 160 and 200 mT.

As the field strengths used in our studies lie within the linear magnetization regime, the experimental yield stress values were fitted with **Eqn. (3.8)** (see **Fig. 3.6 (a)**) using the values μ_c = 1 and β = 0.3617. Such dependence of yield stress on magnetic field strength has been reported on MR fluids and inverse ferrofluids.[198, 200, 201] In the present study it was observed that both yield stresses increased linearly with H^2, with the dynamic yield stress being larger than the static yield stress. The increase in static yield stress with magnetic field indicates that it becomes harder for the suspension to flow with increasing field strength.

3.3.4 Mason Number Scaling

Mason number is an important quantity in magnetorheological analysis. It is defined as the ratio of the hydrodynamic force to the magnetic force (**Eqn. (3.3)**).[192-194] The utility of this dimensionless number is that the shear rate and field strength dependence of the suspension viscosity can be described in terms of the single independent variable *Mn*.[194] The forces governing the rheology of ferrofluids can be understood by representing the magnetic field strength and shear rate dependence of the viscosity using the Mason number. The Mason number scaling was obtained by plotting the field specific viscosity (η_F) [192, 193] defined below against the Mason number.

$$\eta_F = \frac{\eta - \eta_\infty}{\varphi \eta_c} \tag{3. 11}$$

where η_∞ is the viscosity of the suspension at infinite shear rate in the absence of field. It is observed that the Mason number produces a collapse of the viscosity curves at different magnetic field strengths and volume fractions onto a single master curve for magnetic fields of 60 mT and above as shown in **Fig. 3.6 (b)**. Below 60 mT, deviation from the master curve is noticed which indicates the fact that at low magnetic fields, in addition to the magnetic and hydrodynamic forces, the rheology is also influenced by thermal energy contribution. However at high magnetic fields, hydrodynamic and magnetic forces are dominant over thermal forces. Mason number scaling has been reported for electro and magnetorheological fluids.[193, 194, 202] This is the first time that Mason number scaling has been employed to analyze the behavior of ferrofluids except one simulation study in dilute ferrofluid.[203]

3.3.5 Magnetic Field Sweep

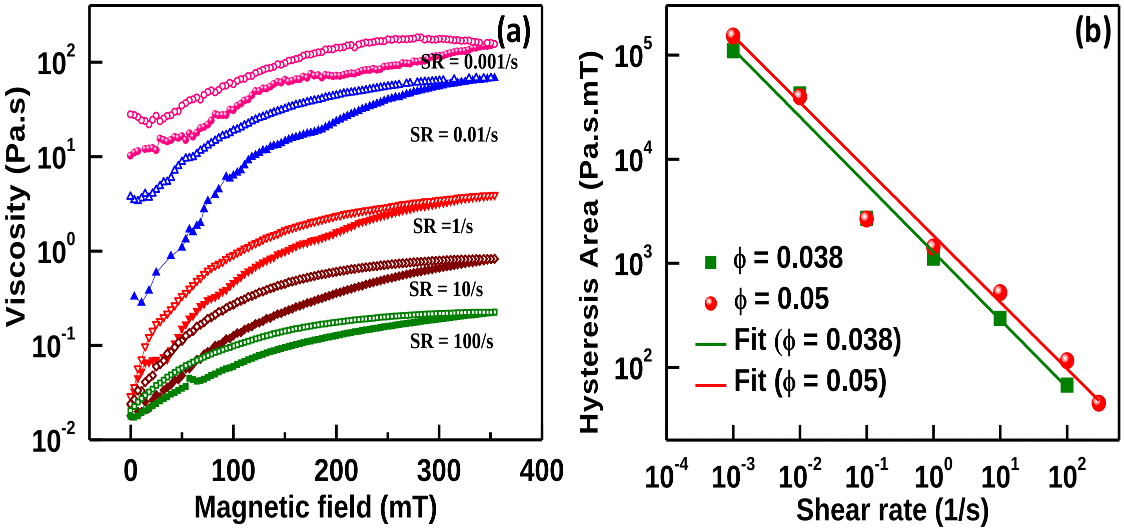

Figure 3.7: (a) Viscosity as a function of magnetic field for ferrofluid of volume fraction 0.038 at shear rates of 0.01, 0.1, 1, 10 and 100 s^{-1}. Closed and open symbols represent increasing and decreasing magnetic field, respectively. (b) Hysteresis area as a function of shear rate for ferrofluids of volume fraction 0.038 and 0.05. The symbols represent the hysteresis area obtained from (a). Solid lines represent power law fit ($A = p\dot{\gamma}^q$) to the data where the exponents for volume fractions 0.038 and 0.05 are found to be -0.64 and -0.65, respectively.

Fig. 3.7 (a) shows the magnetic sweep for ferrofluid of φ = 0.038 at different shear rates wherein the viscosity of the ferrofluid as a function of increasing and decreasing magnetic fields was studied. It is seen that the viscosity of the ferrofluid increases with increase in magnetic field and tends to saturate at higher fields for all the shear rates which indicates the evolving nature of the ferrofluid microstructure. The viscosity increase is attributed to the formation of chain-like structures and their growth with increasing magnetic field. At higher magnetic fields zippering of chains that are off registry or of different lengths takes place resulting in the formation of thick columns. When the entire particles assemble into space filling columns within the gap between the plates, saturation in the viscosity is observed. The viscosity is lower at higher shear rates.

On removal of the magnetic field, however, the viscosity values do not trace those during the increase of the field. In other words, the sample shows hysteresis upon application and removal of magnetic field. The higher viscosity values during the reversal of the field indicate that field induced structures do not relax back to their initial configuration. The field induced structures require a larger time than the measurement time (which is about 10 s) to relax.[204] As described in **Chapter 1** the magnetic moment relaxation can occur by either the Neel or the Brownian mechanism[118, 137] with timescales given by **Eqn. (1.10)** and **(1.11)**. The typical values of τ_B and τ_N for the nanoparticle used in the present study are 1.23×10^{-6} and 2.56×10^{-9} s, respectively. However larger field induced structures formed in the presence of magnetic field can have quite larger relaxation times than a single particle depending on their aspect ratio. For example, the Brownian relaxation time for a particle of diameter 2 μm is about 5 s. When the measurement time is smaller than the actual relaxation time of these chains, they do not relax and hence the viscosity during the backward magnetic field sweep is higher than that during the forward sweep leading to the observed hysteresis. The area between the forward and reverse magnetic field sweeps termed as the hysteresis area gives a quantitative expression of the hysteresis behavior. It is found that the hysteresis area reduces with increasing shear rate as a power law $A = p\dot{\gamma}^q$ with exponents q = -0.64 and -0.65 for the volume fractions 0.038 and 0.05, respectively as shown in **Fig. 3.7 (b)**. The shear force breaks down the larger field induced structures and the resulting smaller structures have lower relaxation times. Therefore, larger the shear force, smaller will be size of the field induced structures resulting in smaller relaxation times. The observed decrease in hysteresis area with increase in shear rate suggests that the shear forces drive the relaxation of the field induced structures.

3.3.6 Dynamic Rheology

Dynamic or oscillatory rheology is a valuable tool for studying the mechanical behavior of soft materials wherein a sinusoidal strain is imposed on the material and the stress response is measured.[205] The relative contribution of the viscous and the elastic response of the material is obtained from the measured stress. The frequency of oscillation sets the timescale of the test. By varying the frequency of oscillation, the materials are probed at different timescales. This observation of material response at different frequencies is also referred to as mechanical spectroscopy. The oscillatory studies on ferrofluid under magnetic field provide valuable information on their microstructure. In the present study, the linear and nonlinear viscoelastic measurements were carried out in the ferrofluid at constant magnetic fields.

The results of the amplitude sweep measurements in the ferrofluid of $\varphi = 0.038$ at different magnetic fields are shown in **Fig. 3.8**. In the absence of magnetic field, the storage and loss moduli show a decrease with increase in strain amplitude. The suspension is predominantly viscous without linear viscoelastic region at the measured strain amplitudes. In the presence of magnetic field, the storage modulus is greater than the loss modulus and both the moduli remain constant up to a certain value of strain indicating a predominant solidlike behavior of the ferrofluid. The elastic nature is imparted by the magnetic field, which induces the formation of gap-spanning chains and thick columns which undergo affine deformation. When the strain exceeds a critical value, the motion of the field induced structures is no longer affine leading to particle rearrangements within these structures. The larger strain also leads to destruction of the field induced structures. As a result beyond γ_c, *G'* decreases and falls off as power law. At the critical strain, the loss modulus shows a distinct maximum and then decreases as a power law - a typical characteristic of soft glassy materials. The peak in loss modulus (shown by arrow in **Fig. 3.8 (b)**) at the critical strain is due to the maximum dissipation of energy during the onset of destruction of chains (de-aggregation of particles). The critical strain is found to be about 2.5 and 3.9 % for φ = 0.038 and 0.05, respectively for almost all field strengths. Above the critical strain, *G"* dominates over *G'*, due to the viscous nature of the samples.

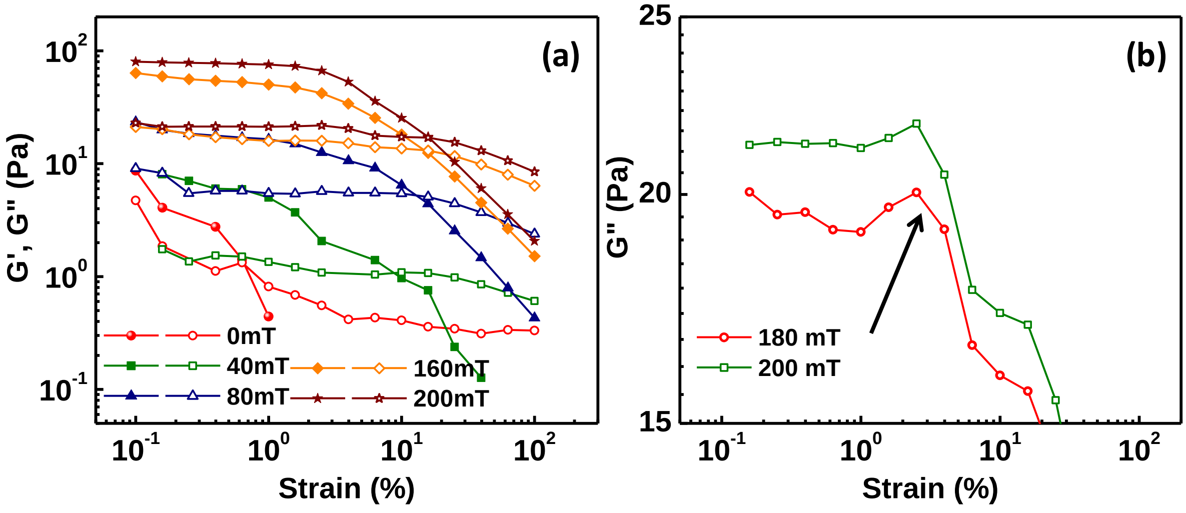

Figure 3.8: (a) Storage (closed symbols) and loss (open symbols) moduli as function of strain amplitude for ferrofluid of volume fraction 0.038 at magnetic fields of 0, 40, 80, 160 and 200 mT. (b) Loss modulus at magnetic fields 180 and 200 mT showing maximum energy dissipation at the critical strain indicated by the arrow.

The observed increase in the magnitudes of both *G'* and *G"* and a clearly distinct LVE region with increase in field (**Fig. 3.8 (a)**) suggests the continuous evolution of chains, which grow with field and span the gap between the rheometer plates. The storage modulus increases from about 1.41 Pa at zero field to 75.6 Pa at 200 mT for a strain of 1 %. This is due to lateral coalescence (zippering) of gap-spanning chains into thick columns giving rise to a large increase in storage modulus. Interestingly, the loss modulus also increases with magnetic field from 1.33 to 21.2 Pa when the field is varied from 0 to 200 mT. As discussed earlier, a broad distribution of chains with different lengths (aspect ratios) is formed between the plates.[186, 187] The unpinned or non gap-spanning chains align along the magnetic field in the absence of a shear. The application of a rapid shear deforms these structures but they relax back to their initial state on rheological time scales resulting in a viscous response.[98, 103, 206]

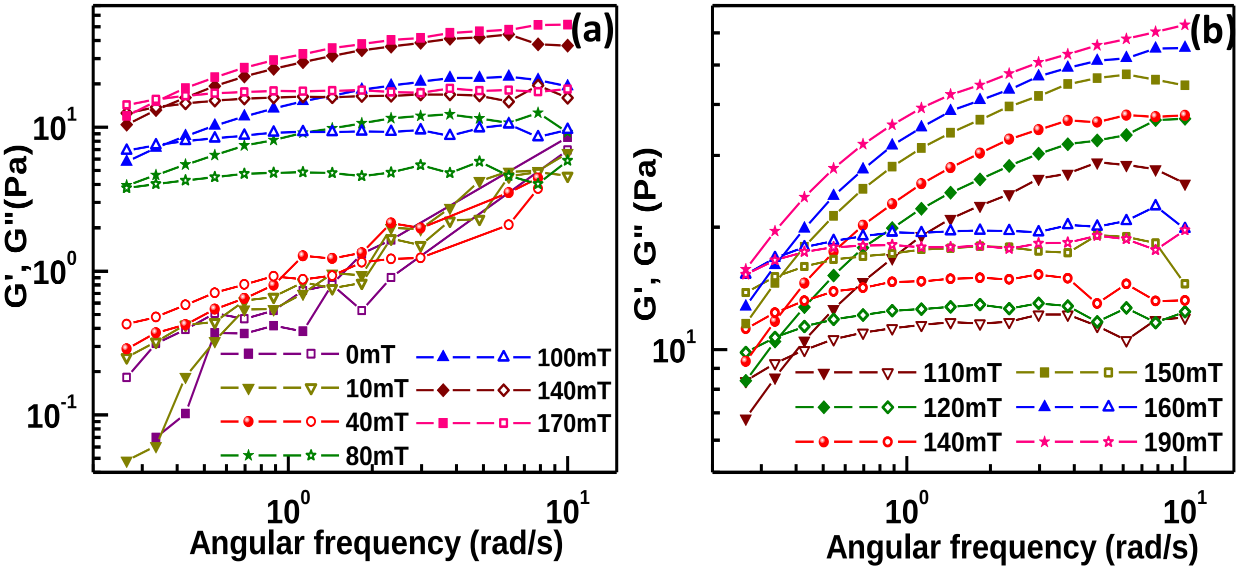

Figure 3.9: Storage (closed symbols) and loss (open symbols) moduli as function of angular frequency for ferrofluid of volume fraction 0.038 at magnetic fields of (a) 0, 10, 40, 80, 100, 140 and 170 mT and (b) 110, 120, 140, 150, 160 and 190 mT.

To obtain insight into the structural (rheological) relaxation occurring in the ferrofluid, frequency sweep measurements were carried out and the results are shown in **Fig. 3.9**. In the absence of magnetic field, both *G’* and *G”* steadily increase with frequency. At low frequencies, the loss modulus is higher than the storage modulus indicating viscous like behavior of the sample, while at higher frequencies the system behaves like elastic solid with the storage modulus greater than the loss modulus. The cross-over from viscous behavior to elastic behavior occurs at a cross-over frequency ω_c, where stresses in the system relax within a finite time. The viscous and elastic response of the system is explained in terms of the time scale of observation (experimental time) which is inversely proportional to the frequency of deformation. If the time of observation t_e is greater than the relaxation time t_r of the system, then the structures will have sufficient time to relax and the suspension behaves as a viscous liquid. For experimental time scale smaller than the relaxation time, the structure is unable to relax and hence it stores most of the energy. When both the times are equal, the system is viscoelastic with dissipation and storing of energy happening equally.[180]

As the magnetic field increases, the magnitudes of both the storage and the loss moduli increase. The cross-over frequency is found to decrease with increase in magnetic field. The relaxation times for two different volume fractions of nanoparticles φ = 0.038 and 0.05, calculated from the cross-over frequencies, plotted as functions of magnetic field, are shown in **Fig. 3.10**. The relaxation times increase with magnetic field and saturate at high fields. This observation can be explained on the basis of the heterogeneous structure formation in the presence of magnetic field. The aggregation of particles into linear chains starts at low fields. At sufficient field strength the chains begin to span the gap between the rheometer plates. And finally at high fields lateral coalescence of these chains into thick columns occurs.

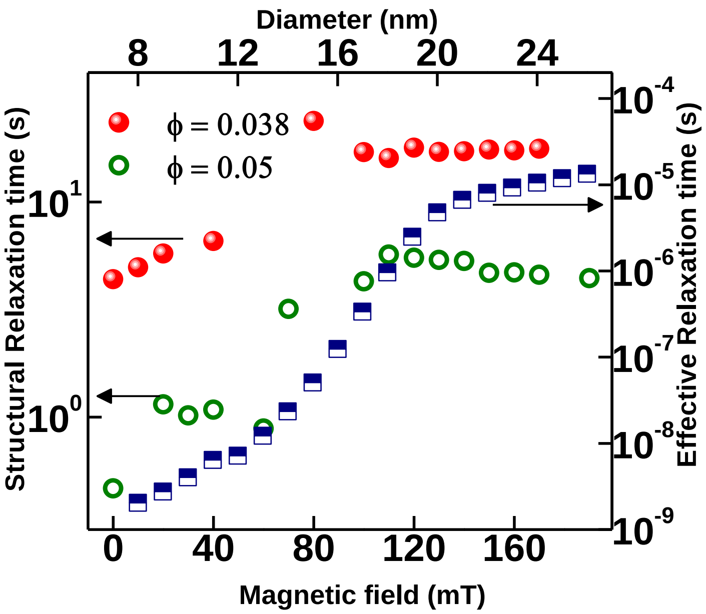

Figure 3.10: Left-bottom axes: Variation of structural relaxation time as a function of magnetic field for volume fractions of 0.038 and 0.05. Strain-rate amplitudes are 0.01 and 0.1 s^{-1} for volume fractions 0.038 and 0.05 respectively. Right-top axes: Effective single particle relaxation time as a function of the particle diameter.

It has been reported that single-sphere-width chains possess frequency independent storage modulus, while thick columnar structures show a significant relaxation time.[207] This is yet another evidence for the existence of thick columns in our system at high fields. With no further coalescence, the relaxation time saturates. The magnetic field dependence of the structural relaxation time of the chains can be compared to the size dependence of the effective magnetization (magnetic moment) relaxation time (τ_{eff}) of a single particle as shown in **Fig. 3.10** (right-top axes). The effective relaxation time is given by **Eqn. (1.12)**. Interestingly, both the effective single particle relaxation time and the structural relaxation times of the chains continue to increase with particle size and magnetic field, respectively. The saturation of structural relaxation time depends on factors like volume fraction of the sample, saturation magnetization, applied magnetic field, confinement of fluid etc. This result shows that the aspect ratio of the formed structures increases with applied magnetic field and reaches saturation above certain magnetic field strength where the length of these structures equals the gap separation.

3.4 Conclusions

The magnetorheological properties of oil based ferrofluid containing magnetite nanoparticles of average particle size ~12 nm stabilized with a monolayer of surfactant for two different volume fractions 0.038 and 0.05 were studied. The formation of heterogeneous internal structures, of linear chains at moderate magnetic field and dense columns at larger fields, due to magnetic dipolar interactions between the particles results in a significant increase in the viscosity. The system, containing internal structures, exhibits a shear thinning behavior followed by a plateau region, where the 'space filling microstructure' is able to resist the shear due to a peculiar alignment of the chains with respect to the applied field direction (i.e. $\theta \leq \theta_c$). At larger shear rates, the system exhibits further shear thinning due to the dominant shear force that is strong enough to disrupt the alignment. The collapse of specific viscosity data against Mason number for different magnetic field strengths and volume fractions onto a single master curve clearly shows the dominance of hydrodynamic and magnetic forces over thermal force. The increase in yield stress with magnetic field confirms that the field induced structures hinder the flow behavior of the suspension. The hysteresis observed in the magnetic sweep experiments confirms the inability of chains and columnar structures to relax within the measurement time. The decrease in hysteresis area with shear rate suggests that shear forces augment the relaxation phenomenon. The dynamic measurements also confirm the evolution of field induced structures upon increasing magnetic field that provide elastic nature to the dispersion.

This study gives several new insight into magnetorheological properties of oil based ferrofluids that are useful for better utilization of ferrofluids in static and dynamic applications such as electronic cooling for micro and nanomechaical devices (MEMS and NEMS), smart dampers, dynamic liquid seals etc. For example, in cooling applications, the fast switching of Brownian particles to linear structures and their retention under flow conditions is essential when the temperature of the gadgets becomes abnormally high. Further, on reducing the temperature to the desired level the system should undergo a reversible transition to Brownian particles. Both the above conditions are found to be satisfied in the investigated samples. Similarly for dynamic sealing conditions, the 1-dimenional structures in the region of interest (radial gap for a shaft assembly) should remain intact under operation (shear forces), which is again found to be good for the samples studied.

Chapter 4 Study of Field Induced Structures in Ferrofluid using Rheomicroscope

4.1 Introduction

The magnetic field dependent viscosity increase in ferrofluid is attributed to the formation of field induced chains and their evolution under magnetic field which restricts the flow of the fluid. The evolution of the field induced structures in ferrofluids has been investigated using techniques such as light scattering,[36] thermal conductivity measurements,[71] rheology,[94, 142] Brownian dynamics[95] and small angle neutron scattering.[144, 208] While light scattering and thermal conductivity measurements provide qualitative information about the microstructure evolution under magnetic field from the scattered pattern and thermal conductivity values, they do not provide quantitative information about the size or spatial distribution of the field induced structures. In SANS experiments, the formation and evolution of heterogeneous structures under magnetic field is obtained from the scattered pattern produced by neutrons from these structures. The orientation of the field induced structures under simultaneous shear and magnetic field is deduced from the scattered neutron pattern. All the above techniques provide information about the ferrofluid microstructure through indirect means under static conditions i. e., in the absence of shear or flow. There are no experimental studies on the evolution of the ferrofluid microstructure from a rheological perspective except few neutron scattering studies.[144, 208] Techniques that provide direct or visual observation of the microstructure of the ferrofluid during magnetorheological measurements have not been reported so far. Such a technique will not only provide first hand information of the formed microstructure in the ferrofluid but also provide insight into the field induced microstructure evolution during rheological measurements which is crucial to the understanding of rheological properties of ferrofluid. In this work, attempts are made to provide direct experimental evidence for the microstructure evolution under simultaneous shear and magnetic field in dilute ferrofluids using a rheomicroscope.

4.2 Experimental Details

Magnetite nanoparticles of size 10 nm coated with oleic acid, dispersed in kerosene at volume fractions of 0.00078, 0.0012, 0.0031, 0.0046 and 0.0063 were used in the present study. The particles were monodisperse with a saturation magnetization of 70 emu g^{-1}. The detailed characterization of the sample can be found in **Chapter 6**. For the rheomicroscopic studies under magnetic field, a custom made solenoid coil enclosing the sample stage as shown in **Fig. 2.14** was used. The current in the coil was varied from 0 to 2.34 A using a DC power supply. The rheomicroscopic images were acquired perpendicular to the plane of shear from the bottom of the sample stage using a 20X objective. For the experiments in **Section 4.3.1**, the shear rate was held fixed at 10^{-3} s^{-1}. For the experiments in **Section 4.3.2**, the magnetic field was kept at a constant value of 176 gauss.

4.3 Results and Discussion

4.3.1 Magnetic Field Dependent Evolution of Ferrofluid Microstructure

The application of magnetic field induces heterogeneous structures in the ferrofluid which evolve with increasing field. In order to gain insight into the evolution of the microstructure of the ferrofluid under magnetic field, magnetorheological measurements were performed in dilute ferrofluids with the simultaneous acquisition of the microscopic images.

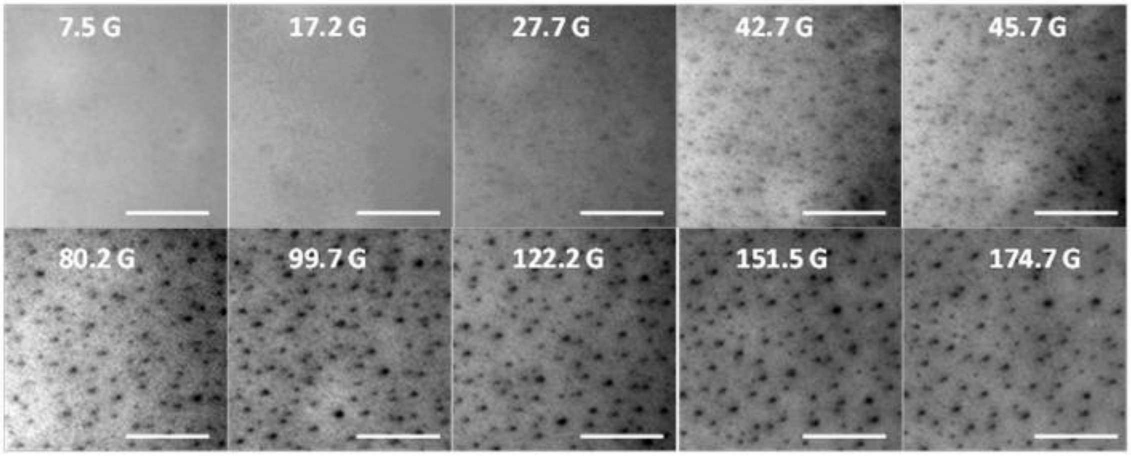

Figure 4.1: Rheomicroscopic images of the ferrofluid of volume fraction 0.0063 under increasing magnetic field at a constant shear rate of 10^{-3} s^{-1}. The scale bar corresponds to 100 μm.

Fig. 4.1 shows the microscopic images of the ferrofluid of φ = 0.0063 at different magnetic fields at a constant shear rate of 10^{-3} s^{-1}. It is observed that up to a magnetic field of 17.2 gauss, the field induced structures could not be resolved from the microscopic pictures probably, due their large number density. At 27.7 gauss, the image shows the presence of nearly circular objects which represent one end of the field induced columnar structures. As the magnetic field is increased to 42.7 gauss, the diameter of the columns increase. With further increase in the magnetic field, the diameter of the columns undergoes a drastic increase. The diameter increases from 15.63 μm at 42.7 gauss to 41.76 μm at 174.7 gauss as seen from **Fig. 4.7 (a)**. On the other hand, the number density of the columns (number of columns per unit area) decreases from 0.0018 to 0.0011 μm^{-2} for change in magnetic field from 80.2 to 174.7 gauss as shown in **Fig. 4.7 (b)**. The increase in diameter of the columns and decrease in their number density indicates that the columns grow in size due to the lateral coalescence leading to the formation of structures with larger diameter. As zippering proceeds, the number of individual columns decreases resulting in a reduction in their number density. As the shear rate used is very small, the columns remain intact without undergoing destruction. The fact that field induced structures are observable at such a low ferrofluid concentration indicates that though the long-range dipole-dipole interaction is responsible for particle aggregation into columns, the thermal stability of such columnar aggregates is not possible without an additional attractive contribution. Tobias et al.[209] have shown that the additional contribution arises from van der Waals interaction. In their study on ferrofluids, the coupling constant was found to be 0.37 while the thermal stability requires $\lambda \geq 1$. By incorporating the van der Waals energy contribution to the formation of field induced clusters, the total coupling constant λ_{total} was found to be ≈ 1, which ensures the presence of thermally stable clusters. In the present study, van der Waals contribution is considered responsible for the thermal stability of the field induced structures.

The changes observed in the microstructure of the ferrofluid influences its macroscopic rheology. From **Fig. 4.2** it is seen that increase in the magnetic field leads to an increase in the viscosity of the ferrofluid. Thus it can be concluded that the growth of the field induced structures under magnetic field is responsible for the increase in the macroscopic viscosity of the ferrofluid.

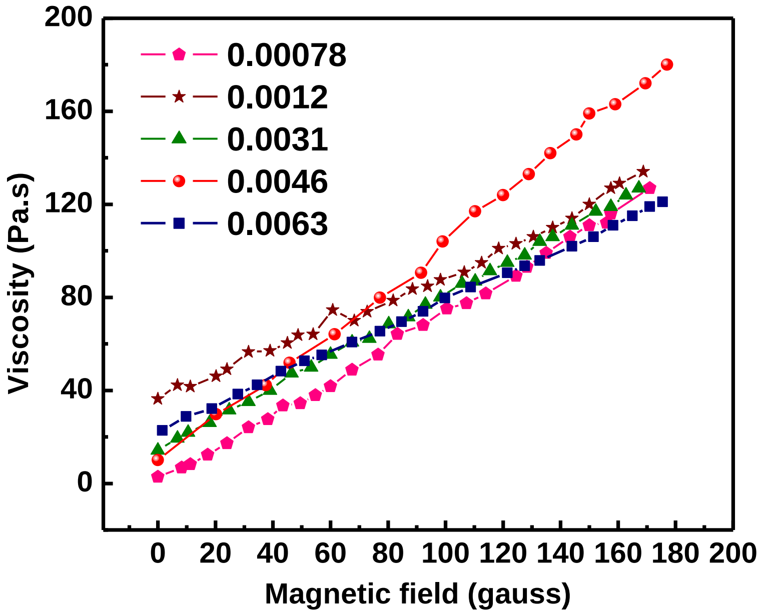

Figure 4.2: Viscosity as a function of magnetic field for ferrofluids of different concentrations at a shear rate of 10^{-3} s^{-1}.

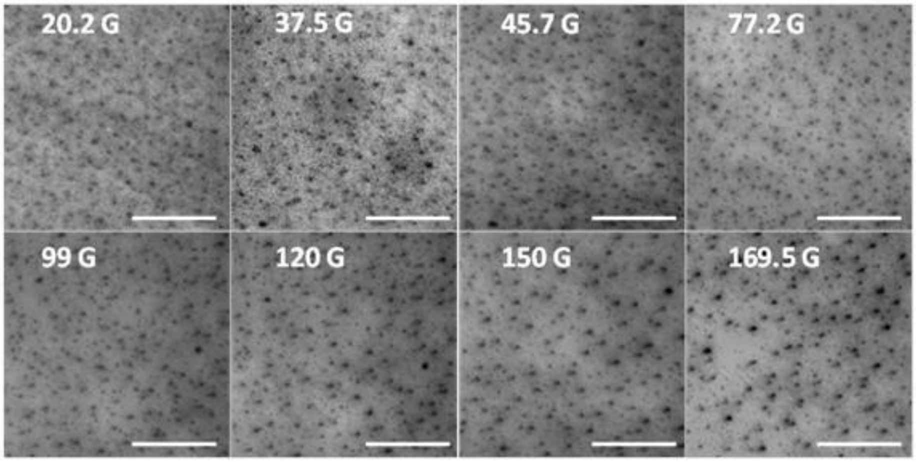

Figure 4.3: Rheomicroscopic images of the ferrofluid of volume fraction 0.0046 under increasing magnetic field at a constant shear rate of 10^{-3} s^{-1}. The scale bar corresponds to 100 µm.

The results of the rheomicroscopic studies under increasing magnetic field at a fixed shear rate for a ferrofluid concentration of $\varphi = 0.0046$ is shown in **Fig. 4.3**. The columnar structures formed in the presence of magnetic field are well resolved at this concentration. The microstructure evolves from columns of diameter 11.4 μm at 20 gauss to those of diameter 34.7 μm at 176 gauss, while the number density decrease from 0.0039 to 0.001 μm^{-2}, as the field increases from 20 to 176 gauss.

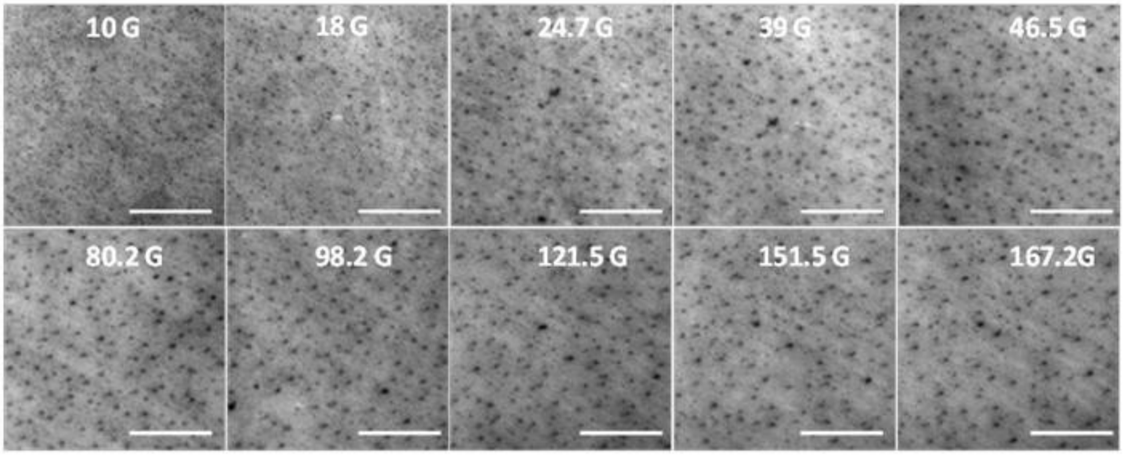

Figure 4.4: Rheomicroscopic images of the ferrofluid of volume fraction 0.0031 under increasing magnetic field at a constant shear rate of 10^{-3} s^{-1}. The scale bar corresponds to 100 μm.

As the concentration of the ferrofluid is further decreased to φ = 0.0031, it is observed that the columns are slightly smaller in diameter than the one at higher concentrations. The diameter of the columns at 10 gauss is found to be 7.1 μm. As the field increases, the columns grow in size, which is clearly seen in the microscopic pictures in **Fig. 4.4**. The columnar size increases from 7.1 μm at a field of 10 gauss to 26 μm at 167 gauss. On the other hand the number density of the columns decreases from 0.0046 to 0.0015 μm^{-2} as the field increases from 10 to 167 gauss.

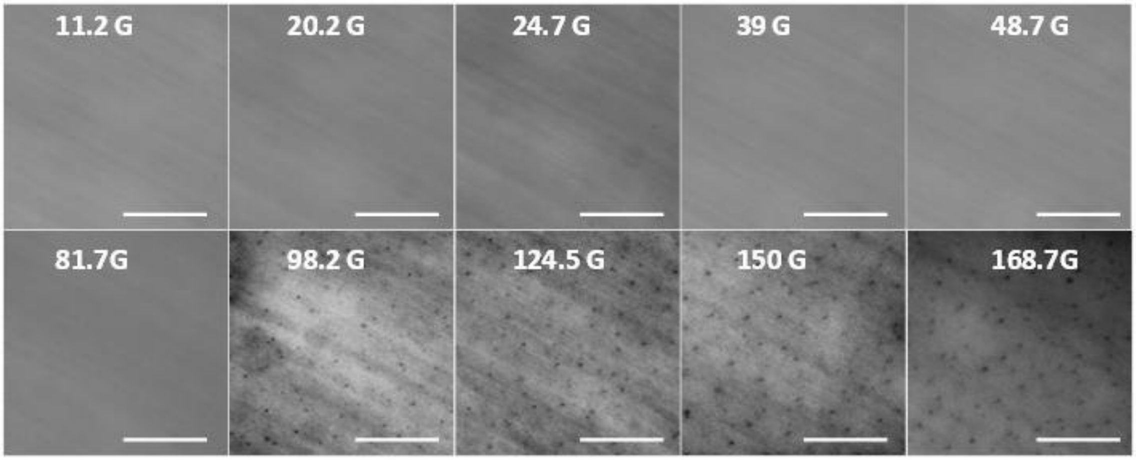

Figure 4.5: Rheomicroscopic images of the ferrofluid of volume fraction 0.0012 under increasing magnetic field at a constant shear rate of 10^{-3} s^{-1}. The scale bar corresponds to 100 μm.

Fig. 4.5 shows the microscopic images of the ferrofluid of φ = 0.0012. It is observed that up to a magnetic field of 80 gauss, the field induced structures formed in the ferrofluid are smaller and hence are not observable using a microscope. As the magnetic field is increased to 98 gauss, the columns with an average diameter of 16.5 μm are observed. With increase in magnetic field the columns grow in size, reaching a diameter of 22.5 μm at 168 gauss. The columnar number density here varies between 9.89×10^{-4} and 10^{-3} μm^{-2}.

For the lowest concentration of φ = 0.00078, the size of the columns are still smaller as seen in **Fig. 4.6**. The column diameter shows a weak increase from 17.5 to 21.4 μm while the number density decreases from 6.82×10^{-4} to 5×10^{-4} μm^{-2} as the magnetic field increases from 75 to 167 gauss. At the concentrations of φ = 0.00078 and 0.0012, the size of the columns do not change much due to the lower column number density in the ferrofluid.

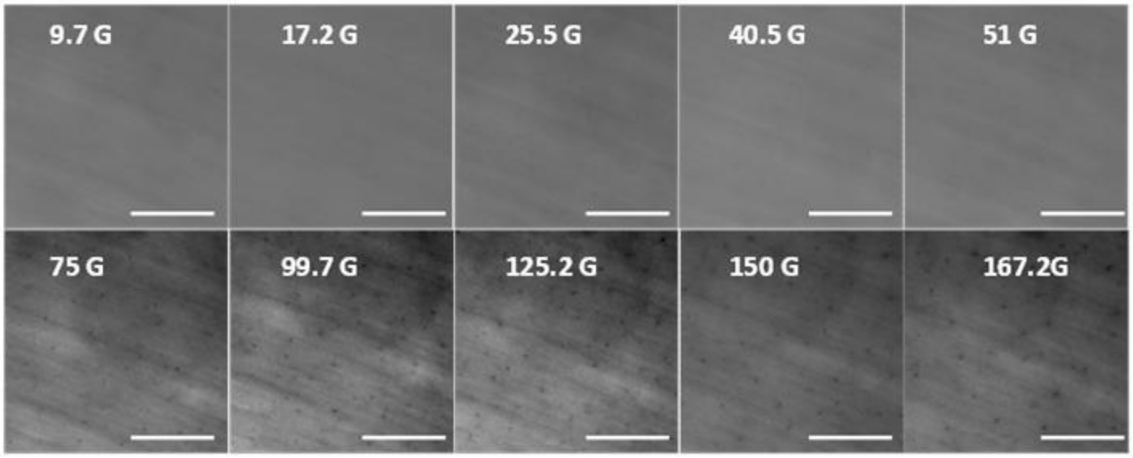

Figure 4.6: Rheomicroscopic images of the ferrofluid of volume fraction 0.00078 under increasing magnetic field at a constant shear rate of 10^{-3} s^{-1}. The scale bar corresponds to 100 μm.

The macroscopic rheological measurements (**Fig. 4.2**) show that the viscosity for all the concentrations of the ferrofluid increases with magnetic field. However, as the studied concentration range is small (0.00078-0.0063) the viscosity values do not show much variation with ferrofluid concentration. The above results show that the microstructure of the ferrofluid undergoes evolution in the presence of magnetic field, which is reflected as an increase in its macroscopic viscosity. The concentrations above φ = 0.0063 could not be probed using rheomicroscopy as the samples became too dark.

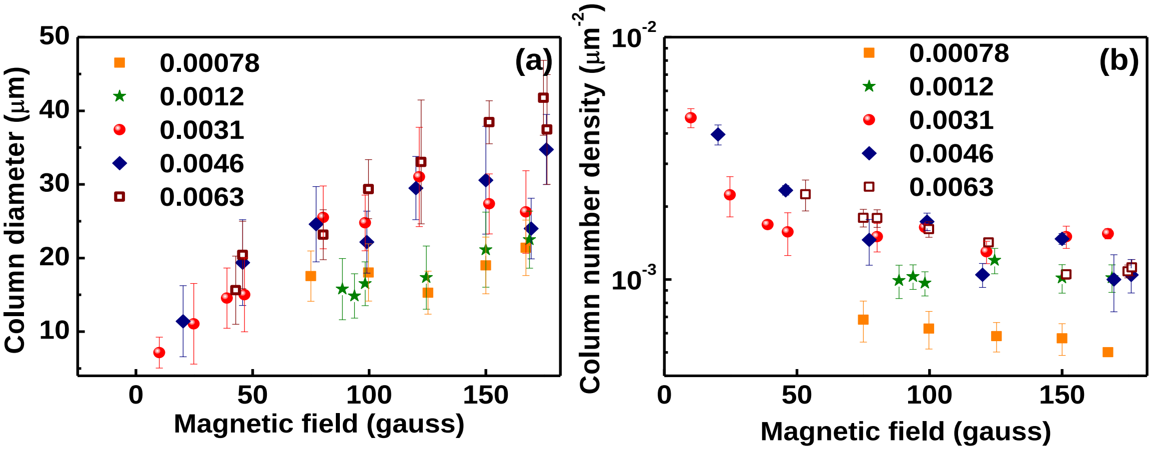

Figure 4.7: Variation of (a) column diameter and (b) column number density with magnetic field for ferrofluids of different concentration.

4.3.2 Shear Rate Dependent Evolution of Ferrofluid Microstructure

Fig. 4.8 shows the rheomicroscopic images of ferrofluid of volume fraction 0.0063 under a constant magnetic field of 176 gauss at different shear rates. At the lowest shear rate of 10^{-3} s^{-1}, the columns are undisturbed and aligned along the direction of the magnetic field. As the shear rate is increased to 10^{-2} s^{-1}, the columns are slightly disturbed and their number density decreases. As the shear rate is further increased, the columns are broken as seen from the decrease in their number density at 0.1 s^{-1}. The columnar aggregates also begin to deviate from their perpendicular orientation. With further increase in shear rate, the columns become aligned along the shear and at the highest shear rate of 10 s^{-1} they are fully aligned along the shear direction. The breaking up of the field induced structures and their subsequent rearrangement under shear force influences the macroscopic rheology of the ferrofluid. It is seen from **Fig. 4.9** that the ferrofluid exhibits shear thinning with increasing shear rate, which is attributed to the reduced resistance to flow owing to the destruction and reorientation of the field induced structures as observed from the rheomicroscopic images. The ferrofluids of other concentrations also showed similar changes in their microstructure and a consequent shear thinning behavior.

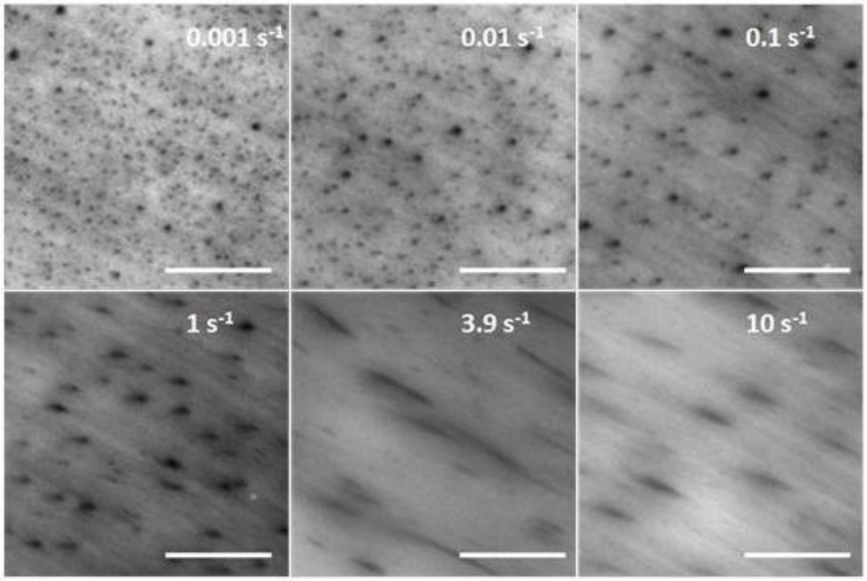

Figure 4.8: Rheomicroscopic images of the ferrofluid of volume fraction 0.0063 under increasing shear rates at a constant magnetic field of 176 gauss. The scale bar corresponds to 100 μm.

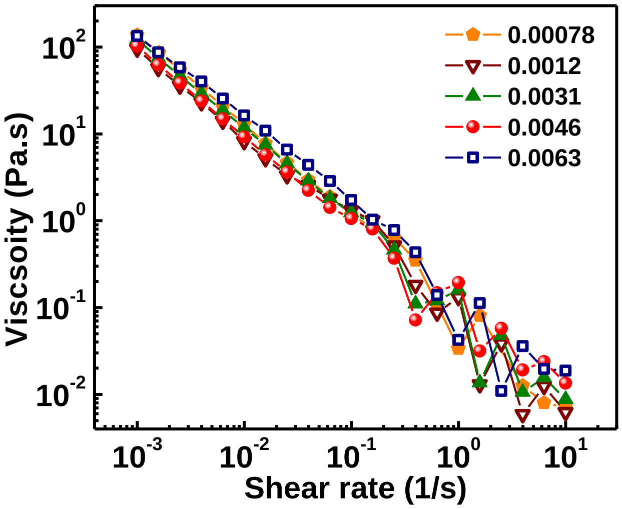

Figure 4.9: Viscosity as a function of shear rate for ferrofluids of different concentrations at a fixed magnetic field of 176 gauss.

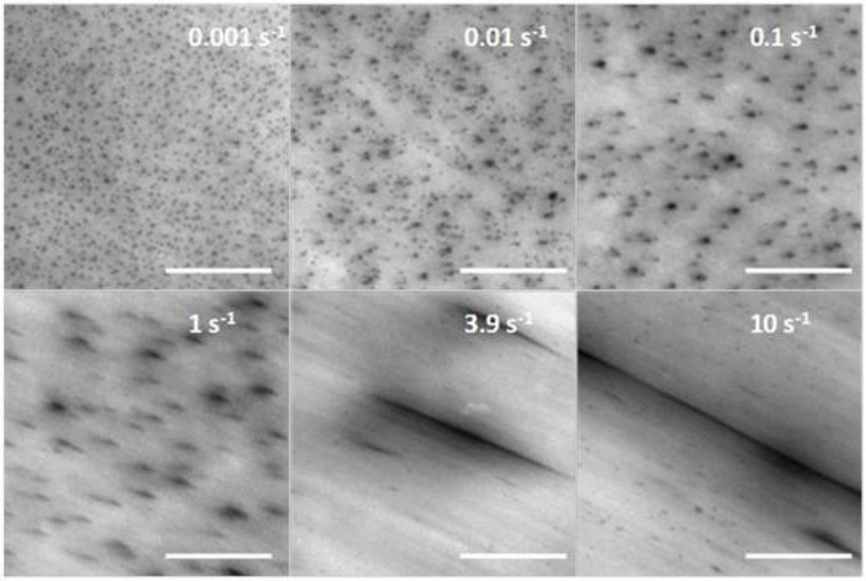

Figure 4.10: Rheomicroscopic images of the ferrofluid of volume fraction 0.0046 under increasing shear rates at a constant magnetic field of 176 gauss. The scale bar corresponds to 100 μm.

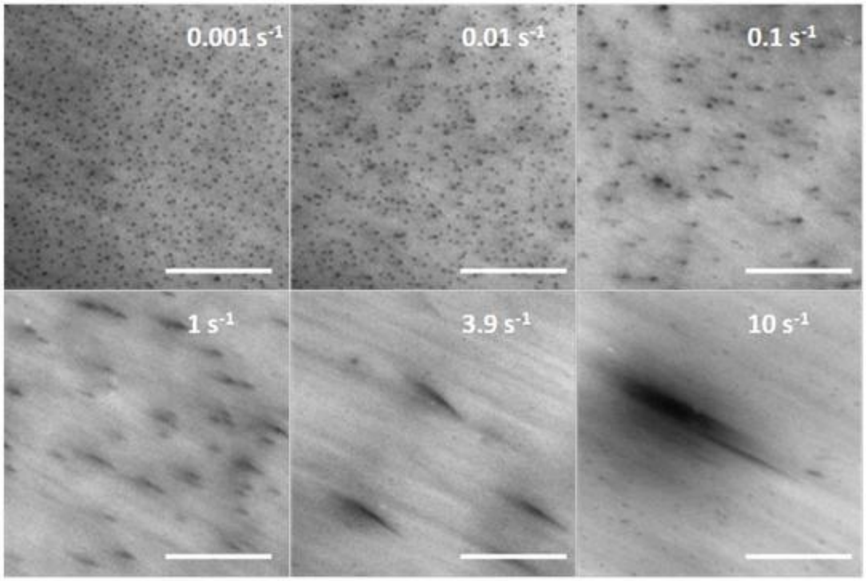

Figure 4.11: Rheomicroscopic images of the ferrofluid of volume fraction 0.0031 under increasing shear rates at a constant magnetic field of 176 gauss. The scale bar corresponds to 100 μm.

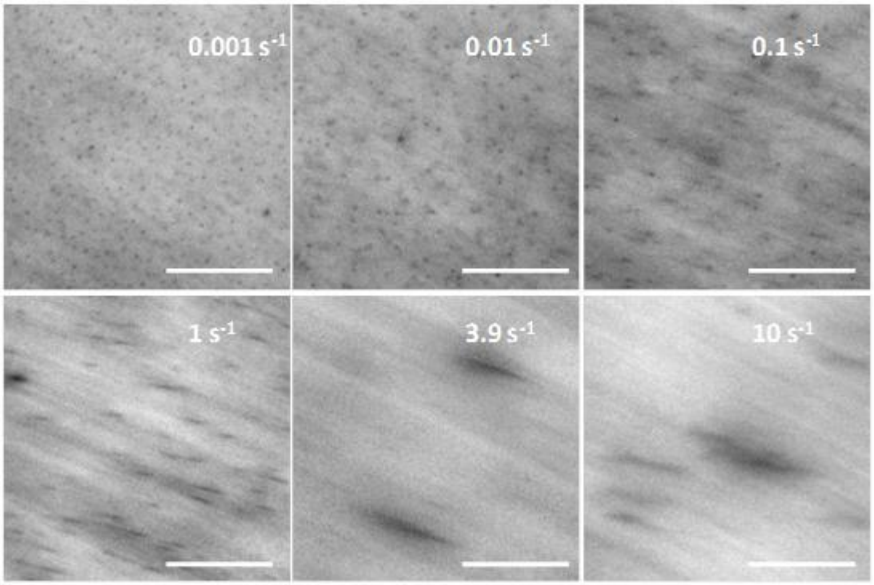

Figure 4.12: Rheomicroscopic images of the ferrofluid of volume fraction 0.0012 under increasing shear rates at a constant magnetic field of 176 gauss. The scale bar corresponds to 100 μm.

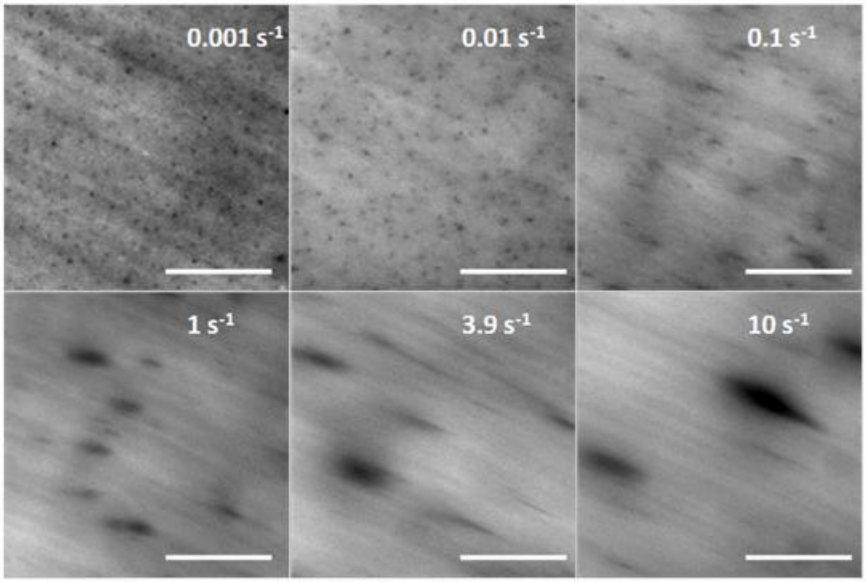

Figure 4.13: Rheomicroscopic images of the ferrofluid of volume fraction 0.00078 under increasing shear rates at a constant magnetic field of 176 gauss. The scale bar corresponds to 100 μm.

The rheomicroscopic images for other concentrations of the ferrofluid (φ = 0.0046, 0.0031, 0.0012 and 0.00078) are shown in **Fig. 4.10** to **4.13**. The images show a clear change in the ferrofluid microstructure when subjected to increasing shear rates with the columns aligned along the magnetic field at low shear rate and column alignment along the shear flow direction at high shear rate. The macroscopic rheology shows a shear thinning response for all concentrations of the ferrofluid as shown in **Fig. 4.9**. However viscosity curves for different ferrofluid concentrations do not show much difference due to the small range of concentrations studied.

4.4 Conclusions

The microstructure of the ferrofluid under magnetic field and shear rate and its influence on the macroscopic rheological properties of ferrofluids are studied for the first time using rheomicroscope. This study provides insight into the evolution of the microstructure under simultaneous application of shear and magnetic field. The rheomicroscopic images show that the formation and growth of the field induced columns under increasing magnetic field is the cause for the increase in the macroscopic viscosity of the ferrofluids. The images also confirm that the disruption of columnar aggregates and their subsequent reorientation along the direction of shear at high shear rate gives rise to shear thinning response.

Chapter 5 | Probing the Dynamics in Ferrofluid using Oscillatory Rheology

5.1 Introduction

Ferrofluid is a metastable colloidal system that exhibits soft glassy behavior and interesting rheological response.[210] In contrast to other soft systems,[211] ferrofluids offer easy maneuvering by external stimuli, which makes them suitable for stimuli responsive applications where their properties can be tuned by varying an external magnetic field.[92] Ferrofluid undergoes reversible phase transformation from a fluid to a viscoelastic solid under the influence of an external magnetic field. Most of the studies on the magnetorheological properties of ferrofluids report the steady shear behavior of the ferrofluids[118, 143, 153, 208, 212, 213] while only a few studies concentrate on their oscillatory behavior.[214, 215] Even in these studies the particle concentrations are so small that the particles are considered to be non-interacting and hence the results do not represent the true behavior of the ferrofluids used in applications. The objective of the present work is to gain insight into the dynamic rheology of a concentrated ferrofluid where the relaxation dynamics under magnetic field is probed using oscillatory rheology.

5.2 Experimental Details

Magnetite nanoparticles dispersed in kerosene at $\varphi = 0.046$ was used in the present study. The particles were synthesized by co-precipitation technique as discussed in **Chapter 2**. The magnetorheological measurements were performed as described in **Chapter 2**.

5.3 Results and Discussion

5.3.1 Properties of the Ferrofluid

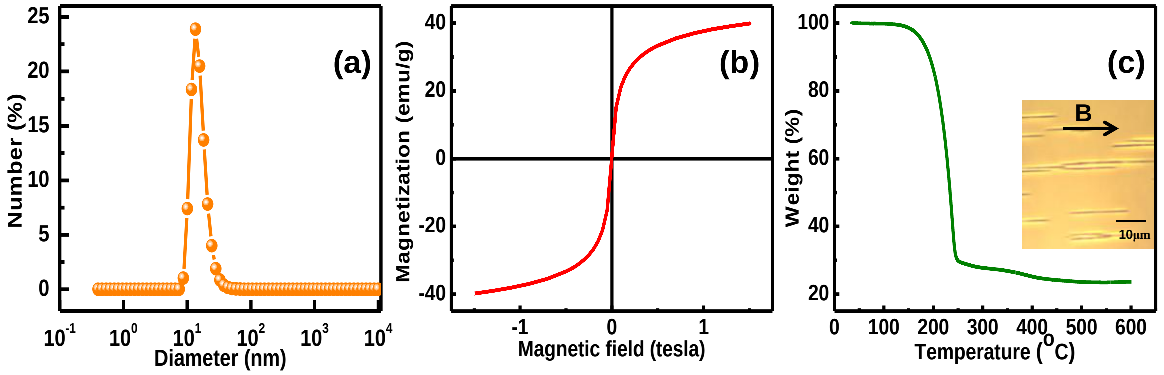

Figure 5.1: (a) Hydrodynamic size distribution (b) magnetization curve of the Fe_3O_4 nanoparticle and (c) thermogravimetric curve of ferrofluid Inset of (c) phase contrast optical microscopic picture (in the presence of magnetic field) of ferrofluid.

From the size distribution curve (**Fig. 5.1 (a)**), the average hydrodynamic diameter of the particles was found to be 13.5 nm. **Fig. 5.1 (b)** shows the magnetization curve of the particles used in the ferrofluid. The particles were superparamagnetic with a saturation magnetization of ~40 emu g^{-1}. **Fig. 5.1 (c)** shows the thermogravimetric curve of the ferrofluid indicating three step weight losses at 143, 250 and 493 °C. The weight loss at 143 °C corresponds to the evaporation of the base fluid. The second and third step weight losses correspond to the removal of the weakly and strongly bound surfactant molecules, respectively. The optical microscopic image of the ferrofluid under magnetic field is shown in the inset **Fig. 5.1 (c)**. The particles form linear chains and zippered structures aligned that are along the field direction.

5.3.2 Non-Linear Viscoelastic Measurements

Non-linear oscillatory studies (**Fig. 5.2 (a)**) in the presence of magnetic field (40 to 530 mT) show that at a constant angular frequency, up to a critical strain (shown by the green arrows), the ferrofluid exhibits a strain-independent storage modulus where G' is larger than the loss modulus. Above the critical strain, the storage modulus decays as a power law with strain amplitude i.e., $G'(\gamma_0)$ α $\gamma_0^{-\upsilon'}$. The loss modulus exhibits a peak above the critical strain and then falls off as a power law $G''(\gamma_0)$ α $\gamma_0^{-\upsilon''}$.

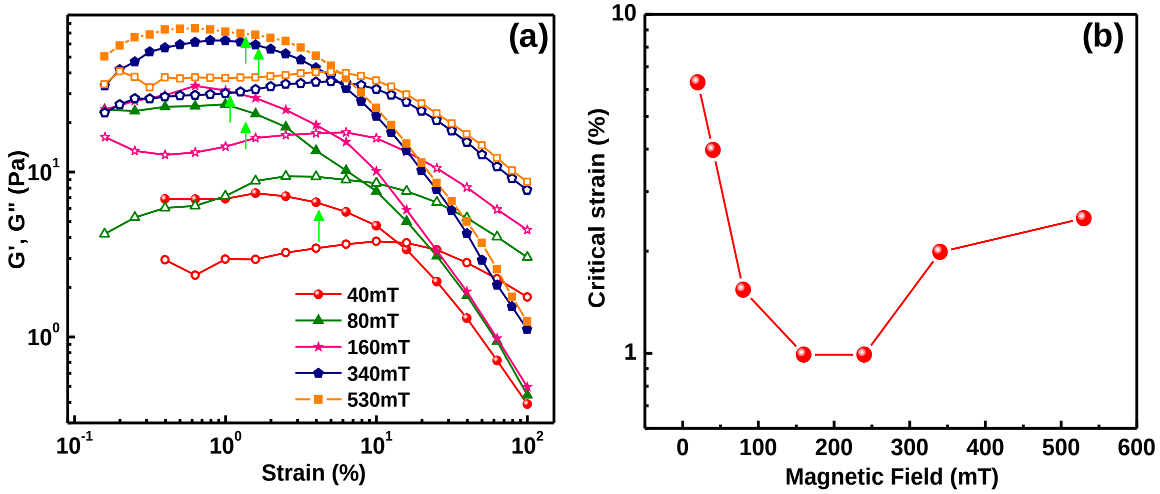

Figure 5.2: (a) Variation of storage (closed symbols) and loss (open symbols) moduli with strain amplitude at magnetic fields of 40, 80, 160, 340 and 530 mT. (b) Variation of the critical strain with magnetic field.

The ratio of the exponents, υ'/υ'' is close to 2 for all the magnetic fields. It is observed from Fig. 5.2 (b) that the critical strain marking the onset of nonlinearity decreases with magnetic field up to 160 mT and slightly increases thereafter. The response of ferrofluid to an oscillatory shear studied by Pinho et al.[214] revealed that the viscosity of the ferrofluid increased with magnetic field and monotonically decreased with oscillation frequency. A similar observation was recorded for the viscous damping force on an oscillating plate in contact with the ferrofluid subjected to a constant magnetic field. The video microscopic studies in electrorheological fluids showed that during the transition from linear to the nonlinear regime of oscillatory shear flow, the particulate columns do not break but are structurally rearranged.[216] Further simulation studies showed that the onset of nonlinearity is due to the slight rearrangements of particle clusters when the structures are sheared into unstable configurations.[217]

5.3.3 Linear Viscoelastic Measurements

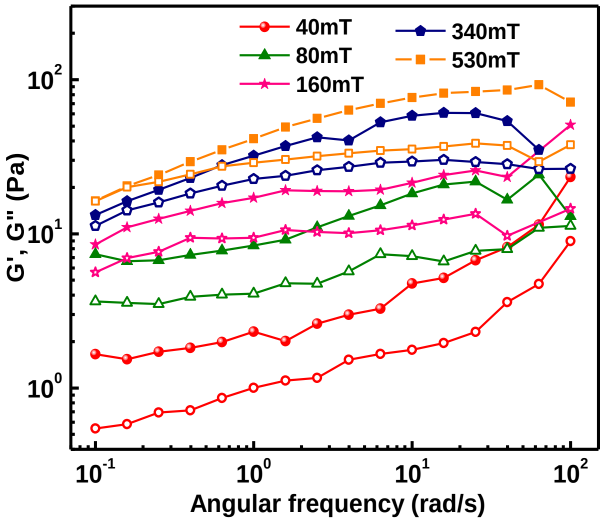

Figure 5.3: Variation of storage (closed symbols) and loss (open symbols) moduli with angular frequency at magnetic fields of 40, 80, 160, 340 and 530 mT.

The linear viscoelastic measurements in **Fig. 5.3** show that the storage modulus increases with increase in the magnetic field from 40 to 530 mT. The storage and loss moduli are weakly dependent on frequency for magnetic fields up to 160 mT. Above 160 mT, the moduli increase with increasing frequency and the storage modulus exhibits a plateau at higher frequencies. For all the magnetic fields, the storage modulus is greater than the loss modulus over the entire frequency range. However for magnetic fields above 160 mT, a tendency for the moduli to cross-over is observed at the low frequency end. These observations indicate that above 160 mT the ferrofluid exhibits short-time structural relaxation while at lower fields the system is dominated by long-time relaxation.

The field induced microstructural changes are reflected in the rheological properties of the ferrofluid. The increase in storage modulus with magnetic field observed in **Fig. 5.2** and **Fig. 5.3** is attributed to the field induced aggregation of particles into chains when λ exceeds unity. With the number of chains increasing with field strength, the storage modulus increases. Under a strong magnetic field, the ferrofluid holds its weight on an inverted vial, which is a confirmation of the solidlike behavior. Interestingly the loss modulus also increases with magnetic field, which is attributed to the unpinning of chains from one or both ends of the rheometer plates.[103, 206] These unpinned chains have equilibrium configurations when aligned along the magnetic field. On application of rapid step shear, they may deform affinely but will relax to alignment on rheological time scales.[103, 206]

In conventional frequency sweep experiments (**Fig. 5.3**), *G'* is weakly dependent on the frequency up to 160 mT. In the molecular dynamics simulation studies on ER fluids, consisting of purely single-sphere-width chains spanning the electrode gap, *G'* was found to be independent of frequency and was always greater than *G"*.[218] The ER suspensions were modeled as monodisperse, neutrally buoyant, hard spheres, suspended in a Newtonian fluid held between parallel-plate electrodes. The frequency independent *G'* was attributed to the zero lag between the motion of the particles in the chain and the imposed shear, where near zero hydrodynamic resistance leads to a non relaxation mechanism.[218, 219] On the contrary such suspensions display a significant relaxation due to competition between hydrodynamic and electrostatic forces on spheres within the thick clusters leading to frequency-dependent moduli. The frequency-dependent moduli observed in the present study suggest that the microstructure of the ferrofluid is not composed entirely of single-sphere-width chains. The probable configuration is that small side chains are attached to the gap spanning single chains. The motion of particles in the side chain, perpendicular to the shear flow during oscillation gives rise to a weak hydrodynamic resistance leading to a relaxation mechanism and hence a weak frequency dependence of *G'*. But since the strain is less than the critical strain, the transition to nonlinearity is not witnessed and the relaxation time falls below the accessible frequency window. Above 160 mT, there is a tendency for the system to relax within the accessible frequency window, which is more pronounced at the highest applied field of 530 mT where the storage modulus decreases from a high frequency plateau and becomes almost close to the loss modulus value at the lowest frequency. Parthasarathy et al.[218] reported that the thick columns of particles in ER fluids exhibit frequency dependent moduli. The loss modulus of the ER fluid increases with frequency at low frequencies, passes through a maximum and then decreases with further increase in ω. Near the loss modulus maximum, the storage modulus increases from a low frequency plateau value to a high frequency plateau value. Such a low frequency relaxation results from the large number of side chains laterally attached to the gap spanning center chain. The competition between the hydrodynamic and magnetic forces causes the perpendicular motion of particles in the outer most chain. In the present study the observation of a decrease in the *G'* with decreasing frequency and the tendency to approach the *G''* (above a field of 160 mT) is an indication of the fact that the structures formed above 160 mT are composed of thick zippered clusters. These clusters show a tendency to relax even under linear deformation. The above results show that the magnetic field regime can be divided into two regions, based on the types of microstructures between the parallel plates and their frequency responses. In the region 1 (magnetic field range of 40-160 mT), the single-sphere-width linear chains with small side chains attached to them exist while in the region 2 (fields ≥ 160 mT) the microstructure is dominated by thick clusters containing more number of side chains. Simulation studies show that the chain-chain interaction depends on the relative shift along the chain direction.[220] There are reports by Modesto et al.[72] and Zubarev et al.[141], on the formation of dense drop-like aggregates in ferrofluids, due to condensation phase transition where the possibility of linear chain formation is neglected because the gap between the plates (350 μm) is much larger than the primary particle size (~10 nm). These droplike aggregates span the gap between the rheometer plates and the breaking of drops into non-spanning smaller drops occurs above a critical strain. However, in the present study, as the gap separation is much smaller (about 100 μm) compared to earlier studies, gap-spanning nanoparticle chain formation is very much possible. Such gap-spanning structures are indeed evidenced in light scattering[124] and microscopic[221] studies.

In order to study the low frequency structural relaxation in ferrofluids the strain-rate frequency superposition was used as the oscillatory behavior of the ferrofluid under magnetic field resembled that of soft materials. In soft materials such as hard sphere suspensions, emulsions, foams, etc, the strain-dependent viscoelastic measurements show that beyond a critical yield strain, the storage modulus decays as a power-law while the loss modulus exhibits a peak and decays as a power law. The ratio (υ'/υ'') of the exponents of G' to G'' is 2.[222, 223] Frequency sweep measurements show that both the storage and loss moduli are weakly dependent on frequency. A shallow minimum in the G'' near the lowest experimentally accessible frequencies followed by a pronounced maximum is considered as an indicator for a cross-over from solidlike to liquidlike behavior. The frequency independent modulus indicates that the structural relaxation occurs at a longer time scale or at a very low frequency. The cross-over from solidlike to liquidlike behavior due to low frequency structural relaxation is difficult to detect because such relaxation frequencies are below the accessible range of rheometers. This problem was circumvent by Wyss et al.[176] by forcing the relaxation into an accessible frequency region using SRFS which has been applied to a broad variety of soft materials like suspensions,[176, 224] emulsions,[224] foams,[176] polymers,[225, 226] soft tissues[227] and interfacial particle monolayers[228].

The structural relaxation time (t_r) is related to the applied strain-rate amplitude ($\dot{\gamma}_0$) as [176]

$$\frac{1}{t_r} = \frac{1}{t_0} + K'\dot{\gamma}_0^{\nu} \tag{5. 1}$$

To isolate the frequency response due to structural relaxation of the soft matter system, the strain-rate is maintained constant by simultaneously varying both the strain amplitude and the angular frequency. Wyss et al.[176] observed that the response of hydrogel spheres dispersed in water was shifted to higher frequencies with increasing strain-rate amplitude while the general shape of the curves remains unaltered by $\dot{\gamma}_0$. The low frequency response was liquidlike with the *G” > G’* where both the moduli scaled with frequency as a power law, with a ratio of 2 between the exponents of *G’* and *G”*. In the high frequency region, *G’* was greater than *G”* and the storage modulus reached a plateau while the loss modulus showed a peak followed by a shallow minimum. Using this approach, the rescaled moduli in both magnitude and frequency were superimposed onto a single master curve. The underlying concept of this method is that factors other than the probe frequency can drive the relaxation in materials. The first ever such technique was employed in polymer melts where the equivalence between probe frequency and temperature was used to study the dynamics of the system.[229] In this method, termed as time-temperature superposition (TTS), the response of polymeric systems shifts to higher frequency by increasing the temperature. In electrostatic complexes time-salt superposition was demonstrated by Spruijt et al.[230], where the salt concentration was the deciding factor in enhancing the process. Cramer et al.[231] demonstrated time-humidity superposition where hydration played the role similar to temperature in TTS. These superposition experiments revealed that probing the dynamics of the system at very low frequencies is equivalent to probing the dynamics at higher strain-rate, temperature, salt concentration or humidity depending on the system under consideration. The observed similarity between viscoelastic responses of the ferrofluid and soft materials suggest that the low frequency response or the structural relaxation in ferrofluid can be probed by the SRFS method.

5.3.4 Strain-Rate Frequency Superposition

The SRFS experiments were performed in the ferrofluid under constant values of the magnetic field at different strain-rates between 0.02 to 1 s^{-1}. The results are shown in **Fig. 5.4**. At a field of 160 mT (**Fig. 5.4 (a)**), for a strain-rate of 0.02 s^{-1}, the high frequency storage modulus is larger than the loss modulus and exhibits a plateau. This indicates that the suspension exhibits a solidlike nature at higher frequencies.

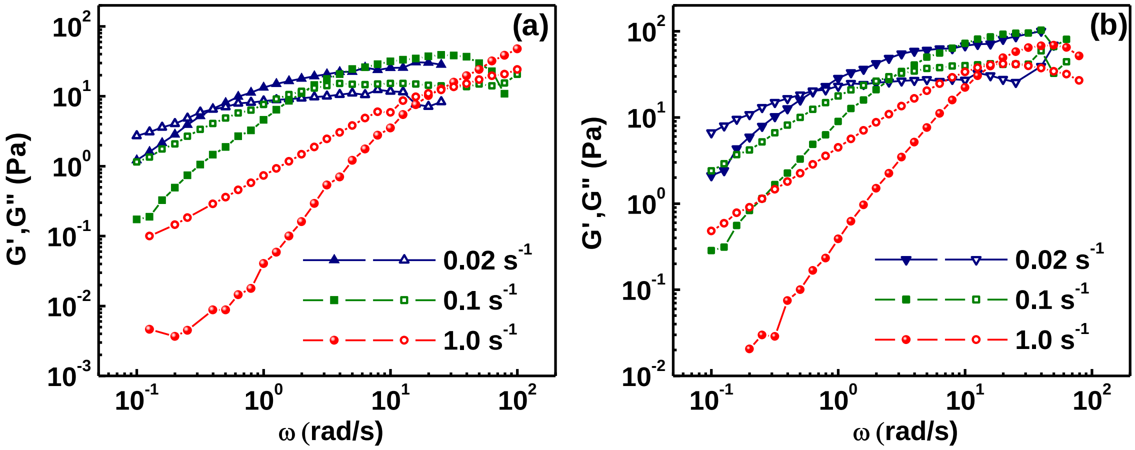

Figure 5.4: Frequency dependent storage (closed symbols) and loss (open symbols) moduli measured at constant strain-rates of 0.02, 0.1 and 1.0 s^{-1} at (a) 160 mT and (b) 340 mT.

With decrease in frequency, both *G*’ and *G”* decrease and the response becomes liquidlike beyond a frequency of 0.38 rad/s (*G” > G’*). This behavior is reminiscent of soft materials. As the strain-rate increases, the cross-over point shifts to a higher frequency. Thus the previously non-observable solidlike (elastic) to liquidlike (viscous) transition (**Fig. 5.3**) has been observed within an accessible frequency window. Similar results are observed at 340 mT as shown in **Fig. 5.3 (b)**. The experiments performed at other magnetic fields (40 and 530 mT) also showed that the transition occurs within the accessible frequency range under constant strain-rate. In the frequency region between the cross-over point and the storage modulus plateau, it is seen that *G’* decreases with decreasing frequency and becomes almost close to *G”*. In this region, the ferrofluid exhibits a weak solidlike or gellike behavior due to a weakened microstructure. The low frequency moduli at different strain-rates and magnetic field strengths are found to vary as a power law ($G'(\omega)$ α $\omega^{-\upsilon'}$ and $G''(\omega)$ α $\omega^{-\upsilon''}$). The exponents υ' and υ'' and their ratio (υ'/υ'') at different magnetic fields and strain-rates are summarized in **Table 5.1**. It is observed that at magnetic fields above 40 mT, the ratio is almost close to 2 as in the case of soft materials.

Table 5.1: The exponents υ' and υ'' and their ratio (υ'/υ'') at different magnetic fields and strain-rates.

Magnetic field (mT)	Strain-rate (s^{-1})	υ'	υ''	υ'/υ''
40	0.02	0.86	0.69	1.25
	0.05	1.06	0.71	1.49
	0.1	1.29	0.74	1.74
	0.5	1.49	0.86	1.73
	1.0	1.64	0.89	1.84
160	0.02	1.25	0.67	1.86
	0.05	1.39	0.71	1.96
	0.1	1.52	0.83	1.83
	0.5	1.49	0.92	1.62
	1.0	2.07	0.99	2.1
340	0.02	1.31	0.68	1.93
	0.05	1.44	0.78	1.85
	0.1	1.47	0.85	1.73
	0.5	1.62	0.90	1.8
	1.0	1.80	0.96	1.9
530	0.02	1.18	0.55	2.14
	0.05	1.45	0.74	1.96
	0.1	1.58	0.81	1.95
	0.5	1.66	0.91	1.82
	1.0	1.74	0.92	1.89

On application of SRFS at a given strain-rate and magnetic field, a clear transition from a low frequency viscous response to a high frequency elastic response (**Fig. 5.4**) was observed. Here, the relaxation from the elastic behavior at high frequency to the viscous behavior at low frequency is induced by the applied strain. Parthasarathy et al.[216] reported that in ER fluids nonlinearity due to the rearrangement of clusters is induced by decreasing the deformation frequency by maintaining a strain greater than the critical strain. In SRFS, for a particular magnetic field, the strain amplitude exceeds the critical strain in the low frequency region. In this region, the hydrodynamic forces appear to be negligible while the magnetostatic force drives the particles into positions where the net force on the particle is zero at every instant. This results in the rearrangement of particles in the side chain leading to a viscous response. The rearrangement occurs due to the motion of particles in the side chains during an oscillation when the competing magnetostatic and hydrodynamic forces cause the particle to move a fraction of its diameter in the direction perpendicular to the shear flow.[216, 218] In monodisperse ER fluids, this relaxation mechanism is characterized by the time which is independent of the size of the particle.[218] As the frequency increases, hydrodynamic forces begin to dictate the particle motion. Though magnetic force influences the particle motion in the direction perpendicular to the applied shear, the time available for the structures to rearrange is not sufficient during the oscillation at such high frequencies.[218] Hence due to non rearrangement of particles at high frequencies, the response is linear (i.e. elastic). This explains the observed transition from a low frequency viscous behavior to a high frequency elastic behavior.

For each magnetic field, the SRFS responses at different strain-rates were rescaled in moduli and frequency as $G_{scaled} = G/G_c$ and $\omega_{scaled} = \omega/\omega_c$ using the method of Spruijt et al.[230] The scaling factors ω_c and G_c are the values of the frequency and modulus at the cross-over point. It is observed that on rescaling, the data at different strain-rates can be superimposed onto a master curve. **Fig. 5.5** shows the master curve obtained for magnetic fields of 160 and 340 mT. The master curve at 530 mT is shown in **Fig. 5.6 (a)**. Indeed the curves at all magnetic fields can be collapsed onto one single master curve as shown in **Fig. 5.6 (b)**. This collapse suggests that the cross-over modulus, G_c should scale with the magnetic field or in turn the coupling constant. The plot of G_c with λ is shown in the inset of **Fig. 5.6 (b)**. It is seen that G_c

varies with λ as a power law with exponent of 0.7, 0.58, 0.54, 0.45 and 0.5 for the strain-rates of 0.02, 0.5, 0.1, 0.5 and 1 s^{-1}, respectively.

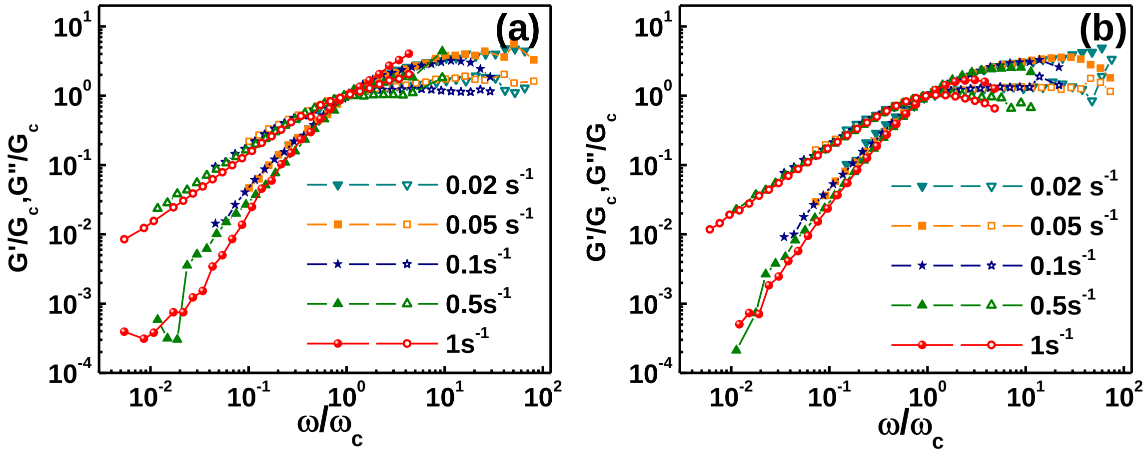

Figure 5.5: Constant strain-rate frequency sweep measurements shifted onto master curves at magnetic fields of (a) 160 mT and (b) 340 mT. Solid symbols represent storage modulus and open symbols represent loss modulus.

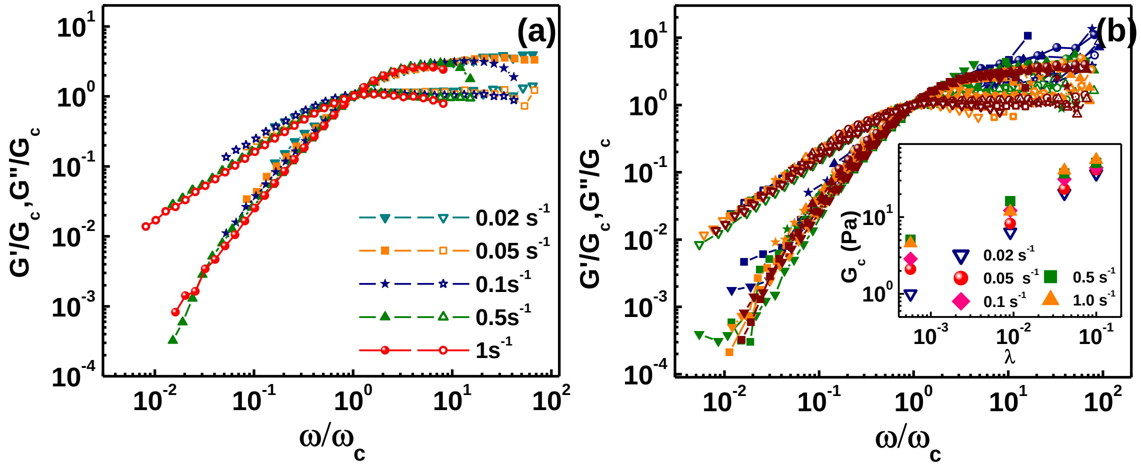

Figure 5.6: (a) Constant strain-rate frequency sweep measurements shifted onto master curve at magnetic field of 530 mT (b) Constant strain-rate frequency sweep measurements shifted onto one single master curve at magnetic fields of 40, 160, 340 and 530 mT. Solid symbols represent storage modulus and open symbols represent loss modulus. The colors blue, green, orange and brown represent data at magnetic fields of 40, 160, 340 and 530 mT, respectively.

Inset of (b) shows the cross-over modulus as a function of coupling constant for different strain-rates.

5.3.4.1 Effect of Strain-Rate

The variation of the scaling factors ω_c and G_c with strain-rate for different magnetic fields is shown in **Fig. 5.7**. The frequency scaling factor (ω_c) increases with the strain-rate as a power law. The exponents for the power law dependence of ω_c on strain-rate are 0.9, 1.0, 0.8 and 0.8 for magnetic fields of 40, 160, 340 and 530 mT, respectively. These values are almost close to unity and are in agreement with that observed in soft materials (~1).[176]

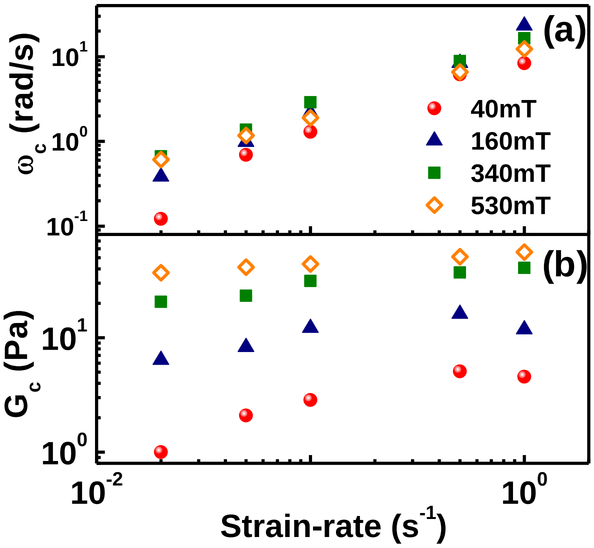

Figure 5.7: (a) Cross-over frequency and (b) cross-over modulus as functions of strain-rate for magnetic fields of 40, 160, 340 and 530 mT.

The increase in ω_c is about two orders of magnitude as the strain-rate is increased from 0.02 to 1 s^{-1}. The amplitude scaling factor (G_c), on the other hand, varies weakly with the strain-rate. The increase in the G_c is about half an order of magnitude for the lowest magnetic field (40 mT). As the field strength increases, G_c becomes almost strain-rate independent. The increase in ω_c with strain-rate is attributed to the fact that the rearrangement of structures happens quickly in the presence of a larger strain-rate as the strain amplitude is higher in this case. Hence the relaxation observed from such rearrangements is shifted to a higher frequency.

5.3.4.2 Effect of Magnetic Field

Having studied the structural relaxation process in ferrofluid and the effect of strain-rate on such relaxation the next objective was to probe the role of magnetic field on the relaxation phenomenon.

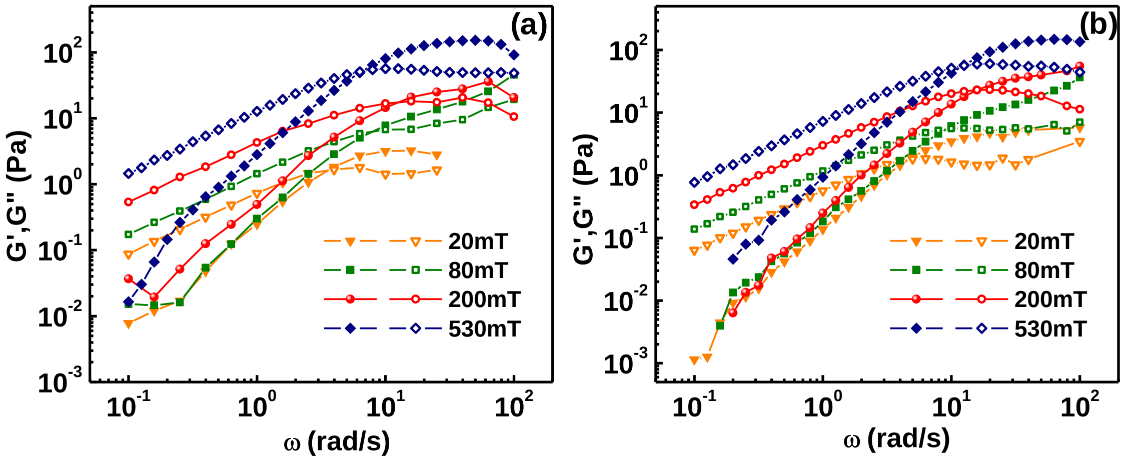

Figure 5.8: SRFS data under constant strain-rate of (a) 0.5 s^{-1} and (b) 1 s^{-1} at magnetic fields of 20, 80, 200 and 530 mT. Solid symbols represent storage modulus and open symbols represent loss modulus.

The magnetic field dependence of the relaxation time and G_c were analyzed by performing the SRFS experiments at a fixed strain-rate by varying the magnetic field as shown in **Fig. 5.8**. It was observed that at a strain-rate of 0.5 s^{-1} (**Fig. 5.8 (a)**), as the magnetic field is increased up to 200 mT, the transition from the linear to nonlinear behavior is shifted to higher frequencies. Above 200 mT, a decrease in the cross-over frequency is noticed. Similar results were observed for SRFS experiments performed at a strain-rate of 1 s^{-1} (**Fig. 5.8 (b)**).

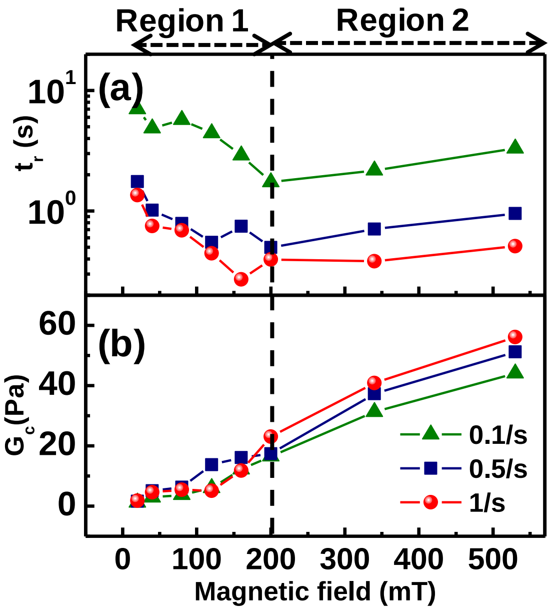

Figure 5.9: (a) Relaxation time and (b) cross-over modulus as functions of magnetic field at three different strain rates - 0.1, 0.5 and 1 s^{-1}.

The cross-over parameters were plotted as a function of magnetic field in **Fig. 5.9**. In terms of the structural relaxation time, t_r ($=2\pi/\omega_c$), we see that the t_r decreases with increase in magnetic field up to ~ 200 mT and increases beyond this, as seen in **Fig. 5.9 (a)**. For instance at a strain-rate of 0.1 s^{-1} the relaxation time decreased from 4.8 to 1.7 s as the field was varied from 40 to 200 mT and the relaxation time increased to 3.3 s at 530 mT. Similar observations were recorded at other strain-rates. This shows a striking similarity with the earlier observation that the field induced structures are different in the two magnetic field regimes; region 1(40-160 mT) and region 2 (≥ 160 mT). The variation of t_r with magnetic field can be explained as follows. In region 1, the microstructure of the ferrofluid mainly consists of gap spanning chains with or without small side chains laterally attached (zippered chains)[232] to them as shown in schematic **Fig. 5.10 (a)**. The controlling factors for the relaxation of the structures here are the applied strain-rate and magnetic field. The magnetic field defines the critical strain for transition from linear to a nonlinear behavior. From **Fig. 5.2 (b)** it is observed that the critical strain decreases as the magnetic field increases up to 160 mT and increases slightly thereafter. A decrease in critical strain with increasing electric field was also observed in ER fluids.[216] As the critical strain decreases, the domination of the hydrodynamic forces on the microstructure begins at higher frequencies, which in turn leads to a reduction in the relaxation time. In region 2, it is observed that t_r increases with increase in magnetic field for all the strain-rates. This sudden change in the dependence of t_r on magnetic field indicates that the nature of the field induced structures in this region is different from that of region 1. Clusters with larger sizes are known to exhibit relaxation at lower frequencies than those with smaller sizes as particles in the outer chains of the clusters

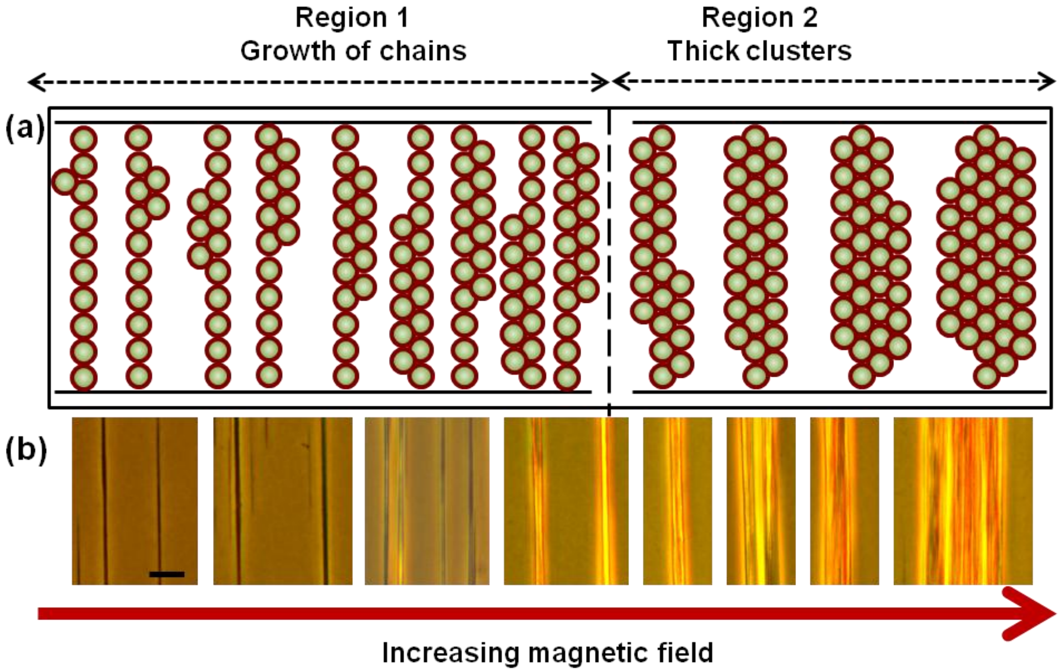

Figure 5.10: (a) Schematic picture of the microstructure of the ferrofluid and (b) optical phase contrast microscopic images of the ferrofluid under increasing magnetic field. The scale bar in microscopic image corresponds to 10 μm.

undergo large excursions perpendicular to the shear flow (z direction) during oscillation.[218] The hydrodynamic resistance on these outer spheres is larger than that on spheres in the side chains in region 1 resulting in a restricted motion at smaller frequencies.[218] Hence the relaxation time increases for clusters with larger thickness. This coincides with our observation of increase in relaxation time with field in region 2 suggesting that in this region, the thickness of the field induced structures is larger than those of region 1. The evolution of the field induced structures is supported by microscopic images showing few chains and their subsequent growth into thick bundles comprising large number of chains under increasing magnetic field as shown in **Fig. 5.10 (b)**.

Chirikov et al.[142] showed that relaxation time in ferrofluids continuously increases with magnetic field with time less than 10 s which is almost similar to those observed in our study. Kroell et al.[149] demonstrated in ferrofluid containing silica-coated magnetic nanoparticles that the relaxation time is approximately 15 s as obtained from the maximum of the imaginary part of the complex viscosity although the dependence of relaxation time on the magnetic field was not clear from their study. Simulation studies on ER fluids[218] also show that the time scales are almost similar to those observed in the present study. In the simulation studies by Soto-Aquino et al.[215] it was observed that despite the particles being considered to be non-interacting an elastic response was obtained under oscillating shear. The cross-over frequency denoting the transition from elastic to viscous response monotonically increased with increase in magnetic field indicating a decrease of the ferrofluid relaxation time with increasing magnetic field.

The variation of G_c with magnetic field further supports the claim about the nature of field induced structures in the two regions. **Fig. 5.9 (b)** shows that for all strain-rates, G_c increases weakly with magnetic field in region 1 and drastically in region 2. The microstructure in region 1 as described involves the growth process where the length of the side chains attached to the gap spanning chain as well as the number of such structures increases. In region 2, the process of zippering involving the lateral coalescence of large number of side chains occurs. This leads to the formation of clusters with greater thickness than those in region 1 giving rise to a dramatic increase in G_c with magnetic field. ER fluids also exhibit similar increase in storage modulus with increasing electric field.[216] Thus, the SRFS experiments give new insights into the nature and the evolution of field induced structures. Under sufficiently strong magnetic field, the Brownian and repulsive forces become negligible where the magnetic and hydrodynamic forces dictate the rheological behavior of the ferrofluid system. The competition between these forces decides the system response. In oscillatory measurements this competition is revealed in both the linear and nonlinear deformations. At low strain amplitudes and low frequency the magnetic force dominates and the response becomes linear. At higher strain or frequency, the hydrodynamic force begins to compete with the magnetic force leading to an effective motion of the particles through rearrangements and hence the behavior becomes nonlinear.

5.4 Conclusions

The field induced structural relaxation in ferrofluid is studied using oscillatory rheology. Using the scaling factors obtained from the frequency and modulus at the cross-over point in oscillatory rheological measurements, the constant strain-rate frequency sweep data are superimposed onto a single master curve. The frequency scaling factor (ω_c) increased with the strain-rate as a power law with an exponent value close to unity whereas the amplitude scaling factor (G_c) is almost strain-rate independent at high magnetic field strengths**.** The structural relaxation resulting from rearrangement of particles occurred more easily as the strain-rate increases. These rearrangements occur when the particles in the side chains attached to the single-sphere-width gap spanning chain undergo motion perpendicular to the shear flow due the competition between the hydrodynamic and magnetostatic forces and are reflected as transition from solidlike to liquidlike rheological response. The relaxation time exhibited a decrease with magnetic field up to 200 mT and an increase thereafter. The G_c on the other hand shows an increase with the magnetic field. The magnetic field dependence of the relaxation time and cross-over modulus indicates two distinct regimes. Region 1 comprises of small and thin linear chains with a few particles attached to its side while the region 2 contains thick zippered structures. These results suggest that the ferrofluid microstructure under magnetic field is similar to a soft solid with relaxation governed by the imposed strain-rate and the magnetic field. The new insight into the relaxation behavior of field induced aggregates in ferrofluids may find use in applications ranging from medicine to opto-electronic devices.

Chapter 6 Effect of Multiwalled Carbon Nanotubes on the Magnetorheological Properties of Ferrofluid

6.1 Introduction

The tunable nature of the rheological properties of ferrofluids has been exploited in several applications such as in magnetofluidic seals,[73] lubricants,[74] density separation,[75] ink jet printers,[76] refrigeration,[77] clutches,[78] tunable dampers[79] and tunable heat transfer fluids.[80] Magnetic field is the main parameter controlling the rheological properties of ferrofluids by tuning the dipolar interactions between the magnetic particles. However the magnetorheological properties of ferrofluids can be significantly altered in the presence of nonmagnetic entities. These nonmagnetic additives can alter the effective dipolar interaction and hence the microstructure of the ferrofluid under magnetic fields. Because the magnetorheological properties of ferrofluids is being exploited in several applications such as static and dynamic seals, dampers, actuators etc, optimization of the properties such as yield stress, magnetic hysteresis, etc using additives that do not influence the inherent physical properties of the ferrofluid is very important. Although studies have been carried out to understand how additives such as carbon nanotubes influence the mechanical behavior of MR fluids[233, 234] such studies are scarce in ferrofluids. In MR fluids, multiwalled carbon nanotubes are mainly added to improve their sedimentation stability. Suspensions containing carbonyl iron coated MWCNT were found to show enhanced viscosity and stress in presence of magnetic field with better sedimentation stability and faster magnetic response.[233-236] However, the effect of such additives on the magnetorheological properties of ferrofluids has not been studied.

The aggregation, caused by the highly attractive van der Waals (vdW) forces which results in poor dispersibility of CNTs in base fluids, is a major obstacle for their potential use. Several dispersion techniques have been proposed to obtain stable dispersions of nanotubes. Mechanical methods such as ultrasonication produce CNT dispersions but are marred by the subsequent agglomeration of the dispersed CNTs. Chemical methods involve use of surfactants (non covalent) or functionalization (covalent) of CNTs that change their surface energy.[237] However, surface modification which involves acid treatments to attach carboxylic acid groups that impart electrostatic repulsion between CNTs may digest the nanotubes leading to severe change in their aspect ratio. On the other hand non-covalent methods such as the use of surfactant or polymer molecules that get adsorbed on the CNT surface providing either charge or steric stabilization have been employed to disperse carbon nanotubes in basefluids. Surfactants such as sodium dodecyl sulfate (SDS), Triton X-100, lithium dodecyl sulfate (LDS), Polysiloxane, etc, polymers, biomacromolecules like DNA or polypeptides, etc are commonly used.[238-240]

Studies on magnetic nanoparticles decorated CNTs showed that the CNTs can be manipulated by an external magnetic field.[154, 156] A study by Zhenyu et al.[158] showed that addition of biological nanotubes to ferrofluid resulted in an enhanced viscosity under a magnetic field. These studies revealed that coupling between magnetic nanoparticles and carbon nanotubes was responsible for the enhancement in magnetorheological property of ferrofluids. On the other hand when magnetic nanoparticles in a ferrofluid do not actually couple with the CNTs, a different result is expected. The CNTs instead of being manipulated by the field could alter the field induced properties which could lead to an opposite effect than the one observed with magnetic nanoparticles coupled to CNTs. Possible reduction in magnetorheological behavior could arise due to the hindrance to structure formation in the presence of CNT. This can be useful from the application point of view where ferrofluid is used as a heat transfer fluid.[241] Such applications require ferrofluid to flow easily, that is, to have lower yield stress so that heat is efficiently removed at low pumping power. Lowering the particle concentration will result in lower yield stress but with a compromise on the conductivity output. Under such circumstances, addition of pristine CNTs which have extraordinary mechanical and electronic properties could provide an optimal condition wherein the thermal conductivity is enhanced while the yield stress is reduced. Moreover pristine CNTs are preferred over surface modified CNTs, as the functional groups added to the surfaces of CNTs can distort the planar sp^2 geometry of the carbon atoms thereby reducing the electrical conductivity of the nanotubes.[242] The objective of the present study was to probe the role of pristine CNTs on the magnetorheological behavior of an oil based ferrofluid.

6.2 Experimental Details

Magnetite nanoparticles dispersed in kerosene at φ = 0.087 was used for the present study. The magnetite particles were synthesized by co-precipitation technique as discussed in **Chapter 2**. Multiwalled carbon nanotubes were dispersed in the ferrofluid as described by the method in **Chapter 2**. The pure ferrofluid and the ferrofluid containing CNT are henceforth referred as FF and CNT-FF, respectively. The CNT-FF was stable for a few days after which the CNTs showed a slight settling. The suspensions were homogenized using a vortex mixer prior to the experiments. The magnetorheological measurements were performed as described in **Chapter 2**.

6.3 Results and Discussion

6.3.1 Properties of the Ferrofluid

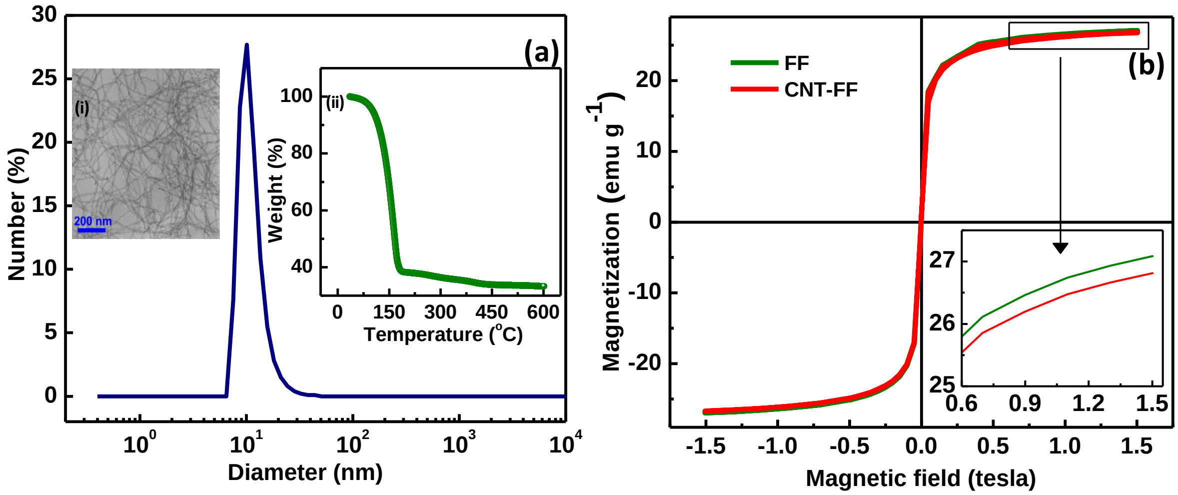

Figure 6.1: (a) Hydrodynamic size distribution of Fe_3O_4 nanoparticles and (b) magnetization curve of FF and CNT-FF. Inset (i) Transmission electron microscopy image of pristine carbon nanotubes (ii) thermogravimetric curve of Fe_3O_4 nanoparticles Inset of (b) Zoomed view of the saturation magnetization of FF and CNT-FF.

The average hydrodynamic diameter of the Fe_3O_4 nanoparticles obtained from dynamic light scattering measurements shown in **Fig. 6.1 (a)** was ~10 nm. The size distribution showed that the particles in the ferrofluid were monodisperse. The VSM measurements on the ferrofluid sample (**Fig. 6.1 (b)**) showed that the FF has a saturation magnetization of 27.1 emu g^{-1} and CNT-FF has a saturation magnetization of 26.8 emu g^{-1}. The bare magnetite nanoparticles used in the ferrofluid were superparamagnetic in nature with a saturation magnetization of ~70 emu g^{-1}. The transmission electron microscopy (TEM) image of the CNT is shown in inset (i) of **Fig. 6.1 (a)**. The TGA curve in inset (ii) of **Fig. 6.1 (a)** indicated three step weight losses at 90, 185 and 450 °C. The first loss which occurred at 90 °C was due to the removal of the base fluid. The second and third steps were due to the removal of the free and bound surfactant (oleic acid) molecules, respectively.

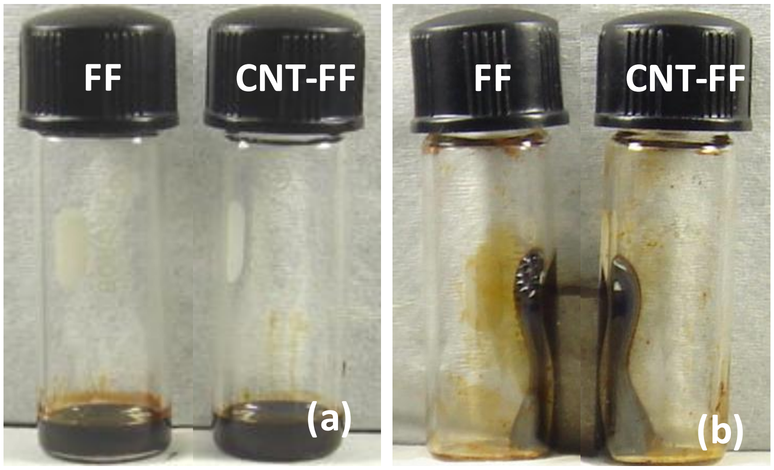

Figure 6.2: Photographs of FF and CNT-FF (a) without magnetic field and (b) under a magnetic field.

Figs. 6. 2 (a) and **(b)** show the photographs of FF and CNT-FF without magnetic field and with magnetic field, respectively. It can be seen that both the dispersions (FF and CNT-FF) are lifted by the magnetic field indicating that the CNTs in CNT-FF are uniformly distributed (otherwise the CNT would have been phase separated from the ferrofluid). In general, a ferrofluid under a normal magnetic field exhibits spikes on its surface (called Rosensweig instability) when the magnetic force dominates over the forces of surface tension and gravity.[68, 243] These spikes or distortions adopt a close-packed hexagonal pattern due to surface instability of suspended particles. The presence of CNTs reduces the net magnetization of the CNT-FF system (as seen from inset of **Fig. 6.1 (b)**) due to the non-magnetic CNT that leads to a lower magnetic response of the CNT-FF fluid. Saad et al.[244] observed that the surface tension increases with increasing concentrations of bare nanoparticle and CNT in basefluids. When the CNTs get closer to each other, the van der

Waals force increases which in turn increases the energy at the surface resulting in a higher surface tension. The combined effect of the reduction in magnetization and increase in surface tension probably leads to the absence of Rosensweig instability in CNT-FF.

6.3.2 Steady Shear Rheology

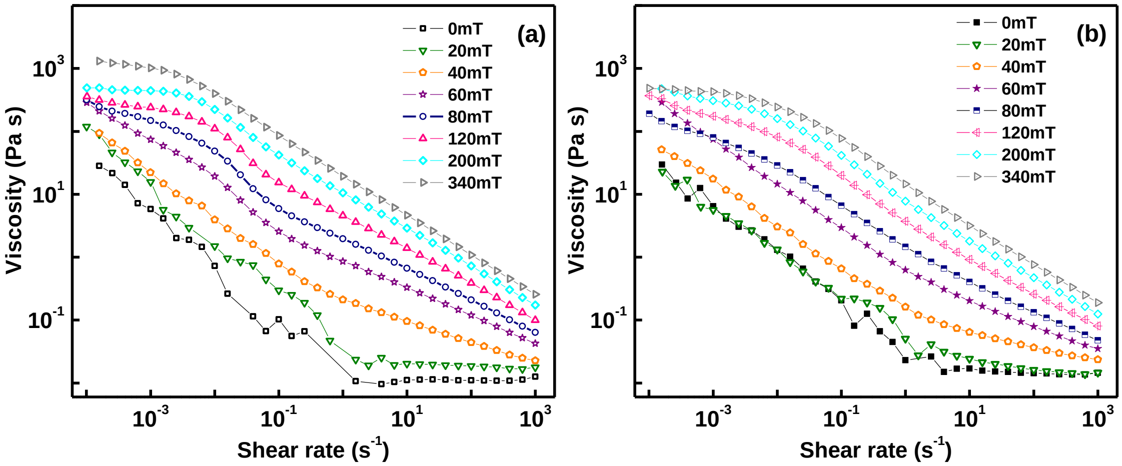

Figure 6.3: Viscosity curves of (a) FF and (b) CNT-FF at magnetic fields of 0, 20, 40, 60, 80, 120, 200 and 340 mT.

Fig. 6.3 (a) shows the viscosity curves for FF at different magnetic fields. In the absence of magnetic field, the nanoparticles are well dispersed in the fluid. On application of the magnetic field, the magnetic nanoparticles interact via dipolar interaction. When the $\lambda >> 1$, the individual particles aggregate to form chainlike structures aligned along the direction of the magnetic field with a distribution of chain lengths.[187, 245] Zippering occurs at higher fields producing thick columns of particles eventually leading to a decrease in the energy of the system.[33, 119, 120, 123] The field induced structures (chains and columns) hinder the flow of the ferrofluid resulting in an increase in the viscosity of the system. On application of shear, shear thinning of the ferrofluid is observed both in the absence and presence of magnetic field. In dilute suspensions, shear thinning is caused by the decrease of the Brownian contribution to the viscosity. Brownian motion tends to restore the equilibrium configuration, but, as the strength of the flow increases, the relative time scale available for the Brownian movement to achieve structural relaxation progressively decreases.[170] The ratio of Brownian to flow time is given by the Peclet number defined in **Eqn. (2.4)**. As *Pe* increases with shear rate, the restoring effect of the Brownian motion reduces. This explains the typical shear thinning behavior observed at 0 mT below a shear rate of 10 s^{-1}. Beyond 10 s^{-1}, Newtonian behavior is observed wherein the viscosity of the ferrofluid remains constant with shear rate indicating that no further rearrangement occurs. Under magnetic field, shear thinning is caused by the breaking down of the field induced structures by the shear forces.[116] The hindrance to flow of the ferrofluid is reduced and the viscosity decreases.

For small magnetic field (20 mT), the shear thinning is followed by a Newtonian behavior for shear rates above 10^{-2} s^{-1}. For magnetic fields lying between 20 and 80 mT, the suspension shows a strong shear thinning behavior for the entire range of shear rates studied. At 80 mT, a small hump like region is observed initially in the shear rate range of 10^{-4} to ~10^{-2} s^{-1} followed by shear thinning. As the field strength increases the hump develops into a plateau which becomes more prominent at higher magnetic fields. The plateau region arises due to the fact that the field induced chains, that are shorter than the gap between the rheometer plates, are oriented at an angle $\theta \leq \theta_c$ with respect to the magnetic field direction.[221] The microstructure of the ferrofluid under these conditions of magnetic field can sustain the shear force and hence the system exhibits Newtonian viscosity. The width of the plateau region increases as the magnetic field increases. This means that the magnetic field strengthens the microstructure of the ferrofluid so as to accommodate a larger shear force. As the shear force gains momentum with increasing shear rate, the microstructure collapses leading to a decrease in the viscosity. For fields greater than 20 mT, the shear thinning continues up to the highest shear rate (10^3 s^{-1}). This shows that the field induced structures are not fully broken down but persist even up to the highest shear rate.

The viscosity curves of the system under magnetic field are altered by the presence of carbon nanotubes. A comparison between the viscosity curves of FF and CNT-FF (**Fig. 6.3 (a)** and **(b)**) reveals that at 20 mT, the viscosity of FF is greater than that of CNT-FF. This shows that CNTs affect the field induced structure formation by weakening the dipolar interaction between the particles. With increase in magnetic field the viscosity of CNT-FF increases but it is still lower than that of FF. The CNTs make the field induced structures more susceptible to shear deformation. Another important observation is that the hump seen in FF at 80 mT is suppressed in CNT-FF. The shear resistant plateau seen in FF at 120 mT occurs in CNT-FF only at fields greater than 200 mT. This indicates that CNTs disrupt structure formation in ferrofluid under magnetic field by weakening the dipolar interaction between particles thus making the microstructure weaker and susceptible to breakage by shear forces.

6.3.3 Yield Stress Measurements

The weakening of the microstructure of the ferrofluid in the presence of nanotubes is further evident from the yield stress measurements. The flow curves at various magnetic fields for both FF and CNT-FF were fitted with the Herschel-Bulkley model and the yield stresses were determined. The static yield stress for both the systems plotted as a function of the magnetic field strength is shown in **Fig. 6.4 (a)**.

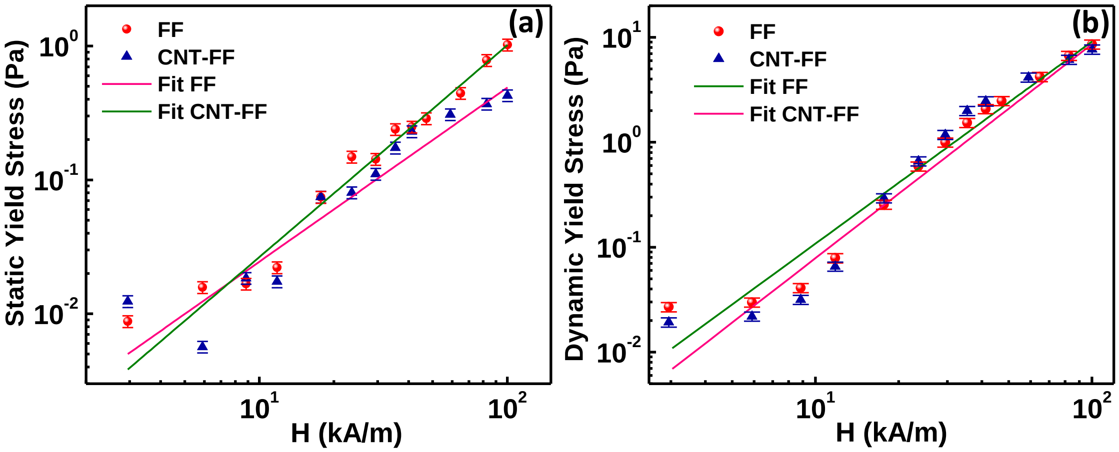

Figure 6.4: (a) Static yield stress and (b) dynamic yield stress of FF and CNT-FF as a function of magnetic field strength. The static yield stress varies as a power law with magnetic field strength with exponents of 1.6 ± 0.0018 and 1.3 ± 0.0048 for FF and CNT-FF, respectively. The dynamic yield stress varies as a power law with magnetic field strength with exponents of 1.92 ± 0.002 and 2.04 ± 0.005 for FF and CNT-FF, respectively.

It is observed that the static yield stress of FF scales with magnetic field strength as a power law with an exponent of 1.6 ± 0.0018. For CNT-FF, the static yield stress is lower than that of FF. Obviously, the CNTs embedded in between the field induced structures lead to weakening of these structures. Thus the system starts flowing at lower stresses than that needed to cause flow in FF where the dipolar interaction between the particles is strong. The dependence of static yield stress on H for CNT-FF is sub-quadratic with an exponent of 1.3 ± 0.0048 i. e., $\tau_y \propto H^{1.3}$. According to Ginder et al.[199] in the linear magnetization regime, the yield stress scales quadratically with magnetic field as given by **Eqn. (3.8)**. However, Lopez et al.[54] observed that the yield stress varies sub-quadratically with H if there are additional interactions other than hydrodynamic and magnetic in the system. For organo-clay added MR fluids, they found that the yield stress is given by $\tau_y \propto H^{1.4}$ suggesting that the colloidal interactions between the iron particles, clay-clay, and clay-iron interactions lead to deviation from the values reported by Ginder et al.[199] In the present study, the deviation observed in case of FF could be due to the contributions from thermal energy while in CNT-FF, it should be due to both the thermal energy contribution and CNT interactions.

The dynamic yield stress of both FF and the CNT-FF are almost similar as seen in **Fig. 6. 4 (b)**. The dynamic yield stress scales with magnetic field strength as a power law with exponents of 1.92 ± 0.002 and 2.04 ± 0.005 for FF and CNT-FF, respectively. The stress needed to break the aggregates that reform under magnetic forces at higher shear rates is expected to be almost the same for FF and CNT-FF as the influence of CNT on the ferrofluid microstructure at high shear rates is negligible. Hence the exponents are almost the same for both the systems.

6.3.4 Mason Number Scaling

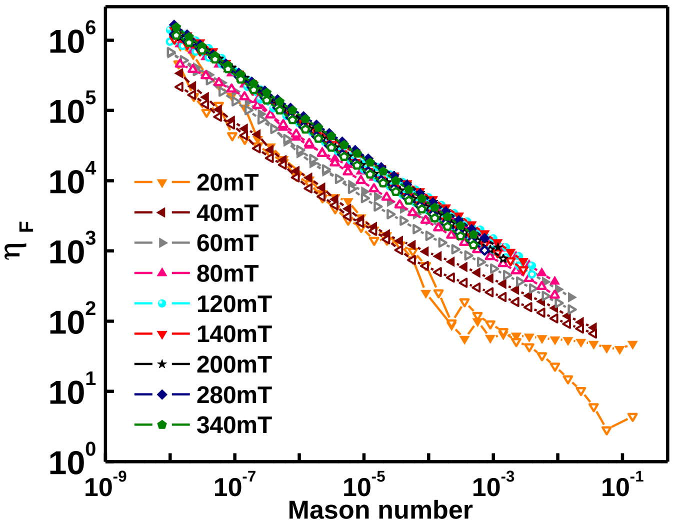

Figure 6.5: Field specific viscosity vs. Mason number for FF and CNT-FF at magnetic fields of 20, 40, 60, 80, 120, 140, 200, 280 and 340 mT. Closed symbols denote FF and open symbols denote CNT-FF.

In order to identify the interactions governing the rheology of pure ferrofluid and the CNT-ferrofluid composite, the field specific viscosity (**Eqn. (3.11)**)[192, 193] is plotted against the Mason number (**Eqn. (3.3)**) in **Fig. 6.5**. It is seen from **Fig. 6.5** that the field specific viscosity plotted against the Mason number gives a very good collapse of the experimental data at different field strengths onto a single master curve for both FF and CNT-FF, above 80 mT. It is expected that if interactions other than hydrodynamic and magnetic are present in the system, viscosity curves do not collapse onto a single master curve as observed by Lopez et al.[199] in a MR fluid containing additional interactions such as clay-clay, clay-iron etc. In the present study, the Mason number scaling is observed at higher magnetic fields (≥ 80 mT). At such high fields the effect of CNT is less pronounced or negligible. At lower magnetic fields, deviation from the master curve is observed as seen in **Fig. 6.5** because of interaction between CNT and magnetic particles as well as the thermal energy which are present in addition to the hydrodynamic and magnetic forces. It is also observed that the field specific viscosity scales as a power law with Mason number with exponents lying between 0.58 and 0.66 for the magnetic fields.

6.3.5 Magnetic Hysteresis

The viscosities of FF and CNT-FF under magnetic field sweep at different constant shear rates are shown in **Fig. 6.6 (a) – (f)**.

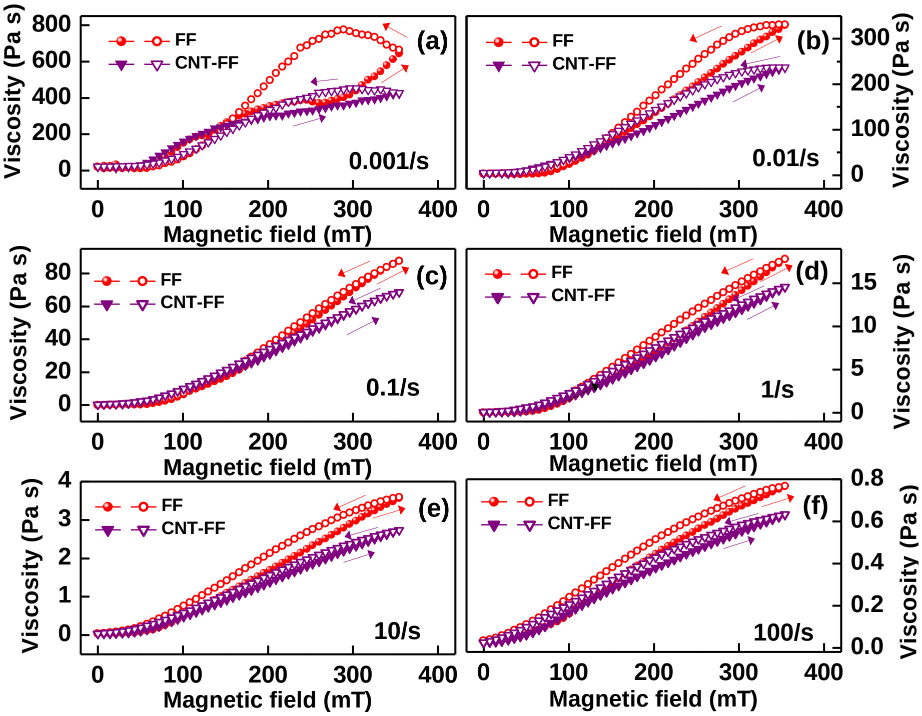

Figure 6.6: Viscosity as a function of magnetic field for FF and CNT-FF at shear rate of (a) 0.001 (b) 0.01 (c) 0.1 (d) 1 (e) 10 and (f) 100 s^{-1}.

At a shear rate of 10^{-3} s^{-1}, the viscosity of FF increases as the magnetic field is increased from zero to 350 mT. On decreasing the field, the viscosity decreases but is higher than the viscosity during the increase of the field thus exhibiting a hysteresis behavior. The hysteresis is attributed to the fact that the relaxation time of the field induced structures is larger than the measurement time (10 s).[71] Once the field is completely switched off the viscosity returns back to its initial value. On removal of the magnetic field, the magnetic moment of the particle relaxes by either the Neel or the Brownian mechanism[118, 137] with timescales given by **Eqn. (1.10)** and **Eqn. (1.11)**. The typical values of τ_B and τ_N for the particle of diameter ~10 nm used in this study are 6.27×10^{-7} and 2.46×10^{-9} s, respectively. However, as the field induced structures are of larger dimensions, they have quite larger relaxation times than that of a single particle. When the measurement time is smaller than the actual relaxation time of these structures, they do not relax that causes the viscosity during the backward magnetic field sweep to be higher than that during the forward sweep. The hysteresis effect is found to reduce with increasing shear rates. The hysteresis area as a function of shear rate for FF and CNT-FF is shown in **Fig. 6.7**.

For FF, the hysteresis area shows a power law decay $y = ax^q$ with shear rate with an exponent of q = -0.68 ± 0.0016. The shear force breaks down the larger field induced structures, resulting in smaller structures that have lower relaxation times. The observed decrease in hysteresis area with increase in shear rate suggests that the shear forces drive the relaxation of the field induced structures.

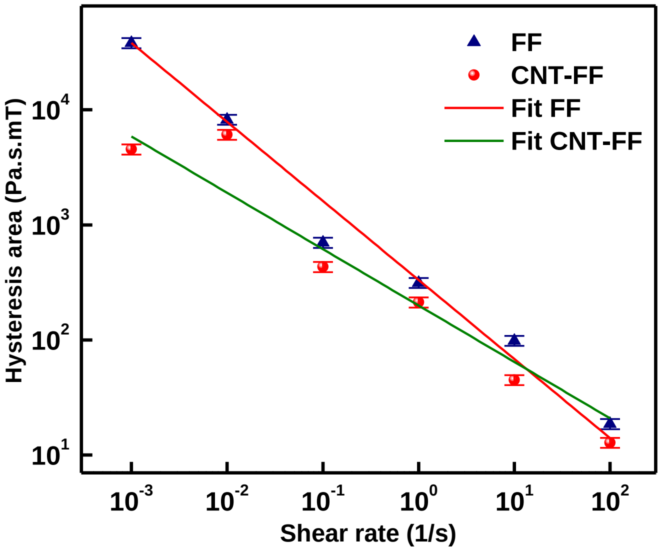

Figure 6.7: Hysteresis area as a function of shear rate for FF and CNT-FF. The exponents for FF and CNT-FF are -0.68 ± 0.0016 and -0.49 ± 0.051, respectively.

Similar measurements carried out on CNT-FF show that the viscosity increases with increasing magnetic field but the increase is lower when compared to that in FF. This can be explained on the basis of the weakening of microstructure of the ferrofluid due to the presence of CNT. As the field increases, the dipolar interaction energy increases leading to the formation of larger heterogeneous structures. When CNTs are present, they disturb the formation of these structures by decreasing the effective dipolar energy between two particles or two smaller chains. The effective interaction between individual particles or chains decreases thus resulting in smaller field induced structures. Hence at a given shear rate, the increase in viscosity of CNT-FF is lower than that of FF. The most important consequence of the presence of CNT is that the hysteresis effect is reduced. The hysteresis area of CNT-FF is lower than that of FF and its decay with shear rate follows a power law with an exponent of -0.49 ± 0.051. In many practical applications, hysteresis is an unwanted effect as it delays the switching behavior. Therefore, this finding may have important implications in practical applications as in ferrofluid sealants which require quick demagnetization of the ferrofluid on the removal of magnetic field.

6.3.6 Dynamic Rheology

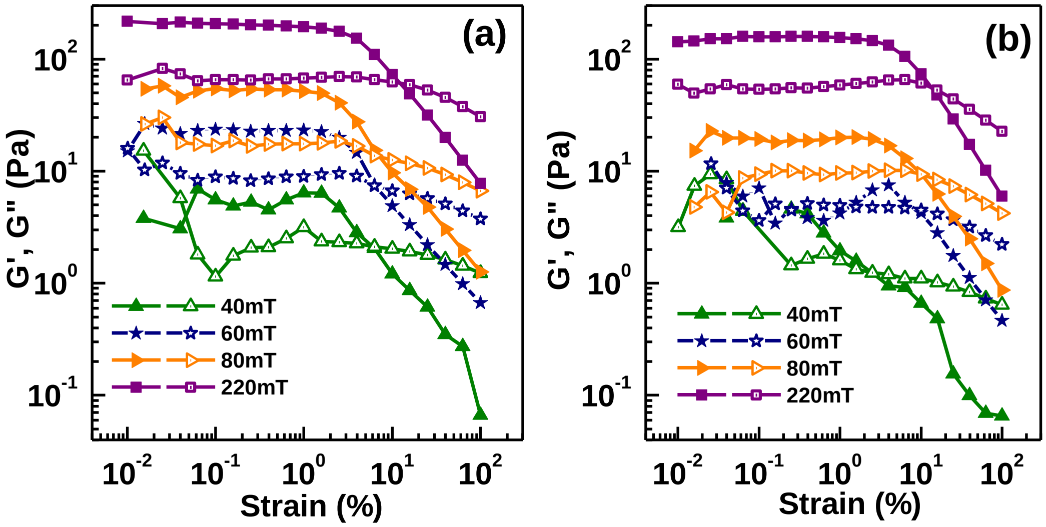

Figure 6.8: Storage (closed symbols) and loss (open symbols) moduli as function of strain amplitude at magnetic field of 40, 60, 80 and 220 mT for (a) FF and (b) for CNT-FF.

Oscillatory measurements were carried out to study the dynamic behavior of FF and CNT-FF. Amplitude sweep measurements were performed under a constant angular frequency of 10 rad/s under different constant values of the magnetic field. **Fig. 6.8 (a)** and **(b)** show that both the systems exhibit pure liquid like behavior in the absence of magnetic field. Even at 20 mT (not shown here), FF shows viscous behavior as the field induced structures are smaller to span the gap between the rheometer plates.

When the field is increased to 40 mT, the storage modulus becomes greater than the loss modulus and exhibits a strain independent LVE region. This elastic or solidlike behavior of the ferrofluid arises from the growth of chains and columns and the subsequent spanning of the gap between the rheometer plates by these field induced structures which impart a rigid nature to the ferrofluid. The LVE region extends up to a strain amplitude of 1.5 % beyond which, the structures breakdown under the action of the applied strain. The resulting microstructure dissipates most of the energy and hence the system exhibits a viscous behavior with *G" > G'*. As the magnetic field is further increased, the magnitude of the storage modulus as well as the length of the LVE region increases. At a strain amplitude of 1 %, the value of *G'* at 40 and 220 mT are 6.3 and 193 Pa, respectively. This show that under increasing magnetic fields, the microstructure continuously evolves from individual particles to chains to thick columns which are long enough to connect the rheometer plates and withstand a certain amount of strain. Yet another notable observation is that the loss modulus which is associated with the energy dissipation in the system also increases with magnetic field which is due to the presence of smaller non gap-spanning chains that do not move affinely with the applied deformation. The CNT-FF system on the other hand exhibits elastic behavior starting from 80 mT, below which the system is viscous with *G" > G'*. Comparison with FF shows that a higher magnetic field is required to produce strain sustainable microstructure in CNT-FF, because of the interpenetration of the CNT in the ferrofluid matrix and the subsequent weakening of the ferrofluid microstructure. Though the microstructure of CNT-FF at 80 mT is capable of withstanding strain, quantitatively it is weaker than that of FF which is evident from the lower G' at 80 mT for CNT-FF system (17 Pa compared to 51 Pa for FF).

The magnetite nanoparticles are stabilized with surfactant molecules which provide steric hindrance between particles, preventing aggregation of particles. Under an external magnetic field, the magnetic dipole moments of the nanoparticles interact through the potential energy $U(r, \theta)$ given by **Eqn. (1.2)**.[124] The dipolar energy tries to align the magnetic nanoparticles while the thermal energy randomizes them. When the coupling constant is much greater than one, the particles align to form chains. With increase in magnetic field the chains grow in length. The distribution of chain lengths favors energy minimization through the zippering phenomenon where the microstructure evolves from single chains to columns due to the lateral aggregation of single chains. The chains and columns can grow long enough to span the gap between the rheometer plates imparting solidlike nature to the ferrofluid under magnetic field. In CNT-FF, the unmodified CNTs are present as individual CNT and aggregates (owing to the large van der Waals interaction between them) interspersed between the magnetite nanoparticles. As the aggregation of particles into chains under magnetic field progresses, the CNTs get trapped between the particles. This reduces the effective dipolar interaction between particles at points where the CNTs are present. The same occurs during zippering wherein the nanotubes get trapped between chains. The trapping of CNTs within the zippered structures is evident from the microscopic pictures shown in **Fig. 6.9**.

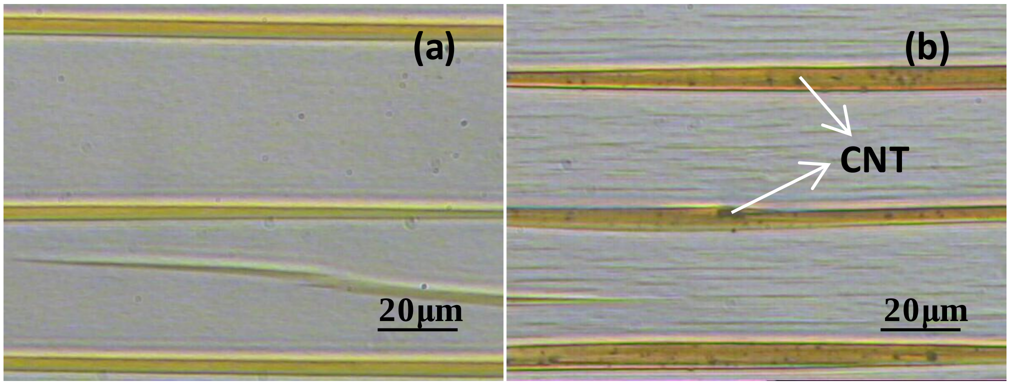

Figure 6.9: Phase contrast microscopic images of (a) FF and (b) CNT-FF in the presence of magnetic field.

The points where CNTs are present become points of preferred shear breakage. Thus in the presence of CNT, the overall field induced microstructure of the ferrofluid is weakened. This explains the observed decrease in viscosity, yield stress and storage modulus of the CNT-ferrofluid composite as compared to the pure ferrofluid under an external magnetic field.

6.4 Conclusions

The effect of multiwalled carbon nanotubes on the magnetorheological properties of oil based ferrofluid of $\varphi = 0.087$ was studied. Both the pure as well as the composite ferrofluid showed enhancement in viscosity with magnetic field due to the formation of heterogeneous structures like chains and columns. At larger magnetic field, a shear resistant microstructure develops in the pure ferrofluid due to a peculiar alignment of the chains with respect to the applied field direction (i.e. $\theta \le \theta_c$). This was followed by shear thinning of the suspension viscosity due to the dominant action of the shear force in disrupting the field induced structures. On the other hand, carbon nanotube-ferrofluid nanocomposite exhibited a weak microstructure indicated by the shifting of shear resistant plateau in the viscosity curve to higher magnetic fields. The yield stress dependence on the magnetic field strength for the pure and composite ferrofluid systems revealed that the presence of carbon nanotubes decreased the dipolar interaction strength of the ferrofluid and weakens their microstructure. Moreover, the composite system exhibited a lower yield stress than the pure system. Mason number scaling revealed very good collapse of the viscosity curves at different magnetic fields onto a single master curve for both the pure and composite ferrofluid systems for magnetic field above 80 mT, which showed that for such high magnetic fields, only the hydrodynamic and magnetic interactions were dominant. The composite system exhibited smaller hysteresis than the pure system which was attributed to the weakened microstructure of the ferrofluid in the presence of CNTs which relaxes faster when the magnetic field was decreased. The decrease in the hysteresis area with shear rate suggested that shear forces augment the relaxation phenomenon. The amplitude sweep measurements further confirm the weakening of the ferrofluid microstructure in the presence of carbon nanotubes. The observed lowering of yield stress and magnetic hysteresis in the presence of a small amount of CNT in ferrofluids has important implications in their technological applications.

Chapter 7 Effect of Hydrophilic Silica Nanoparticles on the Magnetorheological Properties of Ferrofluid

7.1 Introduction

The potential use of ferrofluids in technological applications depends on the coupling between the suspended magnetic nanoparticles and the hydrodynamics of the surrounding liquid.[158] Even modest values of externally applied magnetic fields are sufficient to increase the viscosity of the ferrofluid by several orders of magnitude due to the strong coupling. However due to the substantial decrease in the magnetoviscosity of ferrofluids under shear, their use in applications is limited. Zhenyu et al.[158] proposed a strategy to overcome this problem by replacing the conventional spherical magnetic particles with stiff magnetic nanotubes of Tobacco mosaic virus (TMV) coupled with magnetic nanoparticles. As the TMV-based structures are much longer and mechanically far more stable, the resulting viscosity enhancement is greater and is less susceptible to shear thinning. In a similar manner, the introduction of micron-sized silica in oil-based ferrofluids (inverse ferrofluids) has been found to enhance their magnetorheological properties.[98-100] Inverse ferrofluids produce viscosity enhancements comparable to MR fluids.[246] Dipolar interactions are induced between the nonmagnetic particles on application of a magnetic field.[101] The effect of hydrophobic and hydrophilic silica particles added to magnetorheological fluids were studied by Alves et al.[247] who observed that hydrophilic silica in MR fluid showed higher values of the viscosity, yield stress and viscoelastic moduli than those with hydrophobic silica. However, the effect of hydrophilic silica on the magnetorheological behavior of ferrofluids has not been studied. In the present work, the effect of hydrophilic fumed silica nanoparticles on the magnetorheology, yield stress, viscoelastic moduli, columnar aggregate formation and zippering transitions in ferrofluids were studied. The objective of this work was to probe and understand this relationship between the micro-nanostructures in the presence of non-magnetic additives and rheological properties under practical situations from a technological applications perspective.

Hydrophilic fumed silica particles contain silanol groups (Si-OH) on their surface and form stable nanofluids in polar medium.[248] However, under certain conditions, fumed metal oxide particles in aqueous media also undergo gelation. Cao et al.[249] have demonstrated the formation of silica gels by varying the ionic strength of the dispersion by the addition of salt solutions. Binks et al.[250] reported the stabilization of emulsions using a mixture of oppositely charged nanoparticles. The stabilization was achieved through heteroaggregation in two particles mixtures which increases the hydrophobicity of the particles resulting in their adsorption on oil droplets thereby increasing their stability. Recently, Weston et al.[251] have shown that pseudosolid gels are formed even at low concentrations (1.5 vol %) in aqueous dispersions of binary mixtures of fumed metal oxide nanoparticles in which one type of particle is positively charged and the other is negatively charged. The electrostatic interactions between the oppositely charged nanoparticles result in heteroaggregation of two different nanoparticle species creating a network of heteroaggregates spanning the entire fluid where the gel region lies between the isoelectric points of the two particles. When subject to shear, the binding forces are broken resulting in a flow. Such heteroaggregation in binary mixtures has been reported by several groups.[252-255] On the other hand, in a nonpolar medium the solvent does not interact with the hydrophilic fumed silica particles. The bridging between the silica particles through hydrogen bonding between the surface silanol groups results in the formation of 3D network and a consequent gellike behavior even at lower concentrations. Thus, in nonpolar medium particle-particle interactions dominate over the particle-solvent interactions while in polar medium vice-versa occurs.[248] The different behavior of hydrophilic fumed silica in different solvents depends on the hydrogen bonding capability of the solvent.[256] For liquids with strong hydrogen bonding ability, a solvation layer forms on the surface of silica through hydrogen bonding between liquid molecules and surface silanol groups (Si-OH) which gives rise to short-range non-DLVO repulsions while for liquids with no hydrogen bonding ability, the silanol groups on neighboring silica particles interact directly by hydrogen bonding leading to gelation.[256]

7.2 Experimental Details

Magnetite nanoparticles dispersed in kerosene at $\varphi = 0.087$ was used for the present study. The magnetite particles were synthesized by co-precipitation technique as discussed in **Chapter 2**. Hydrophilic Silica nanoparticles were dispersed in the ferrofluid as described by the method in **Chapter 2**. The pure ferrofluid and the ferrofluid containing silica are henceforth referred as FF and FF-silica, respectively. The suspensions were homogenized using a vortex mixer prior to the experiments. The magnetorheological measurements were performed as described in **Chapter 2**.

7.3 Results and Discussion

7.3.1 Properties of the Ferrofluid

Fig. 7.1 (a) shows the hydrodynamic size distribution of the magnetite nanoparticles obtained from dynamic light scattering measurement. The nanoparticles are found to be fairly monodisperse with an average size of ~10 nm. The VSM measurements (**Fig. 7.1(b)**) show that magnetite nanoparticles used in the ferrofluid are superparamagnetic in nature with a saturation magnetization of ~70 emu g^{-1}.

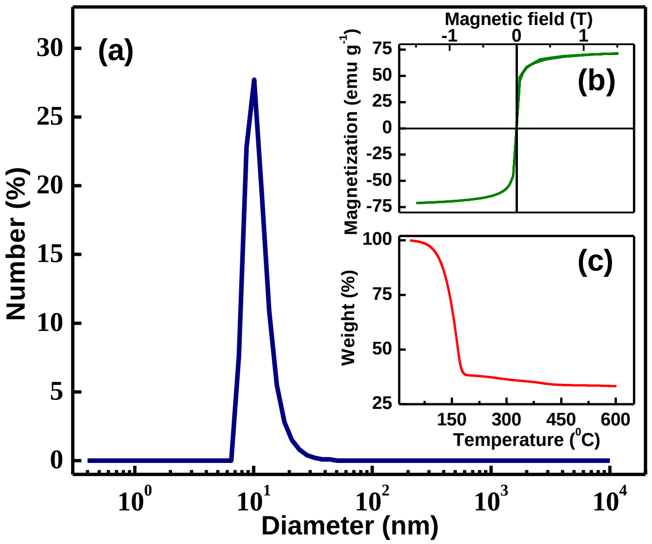

Figure 7.1: (a) Hydrodynamic size distribution (b) magnetization curve of Fe_3O_4 nanoparticles and (c) thermogravimetric curve of ferrofluid.

Fig. 7.1 (c) shows the weight loss curve obtained from TGA measurements indicating three step weight losses at 90, 185 and 450 °C. The first weight loss at 90 °C is due to the removal of the base fluid. The second and third steps are due to the removal of the free and bound surfactant (oleic acid) molecules, respectively.

7.3.2 Steady Shear Rheology

Fig. 7.2 (a) and **(b)** show the viscosity curves of FF and FF-silica under different magnetic fields. In the absence of magnetic field, the nanoparticles are under constant Brownian motion. On application of the magnetic field, the magnetic nanoparticles interact via dipolar interaction with the interaction energy given by **Eqn. (1.2)**.[124] When the dipolar interaction energy between the particles exceeds their thermal energy, the particles align in a tip-to-tip manner forming linear chainlike followed by zippering to form columnar aggregates aligned along the direction of the magnetic field.[119, 142]

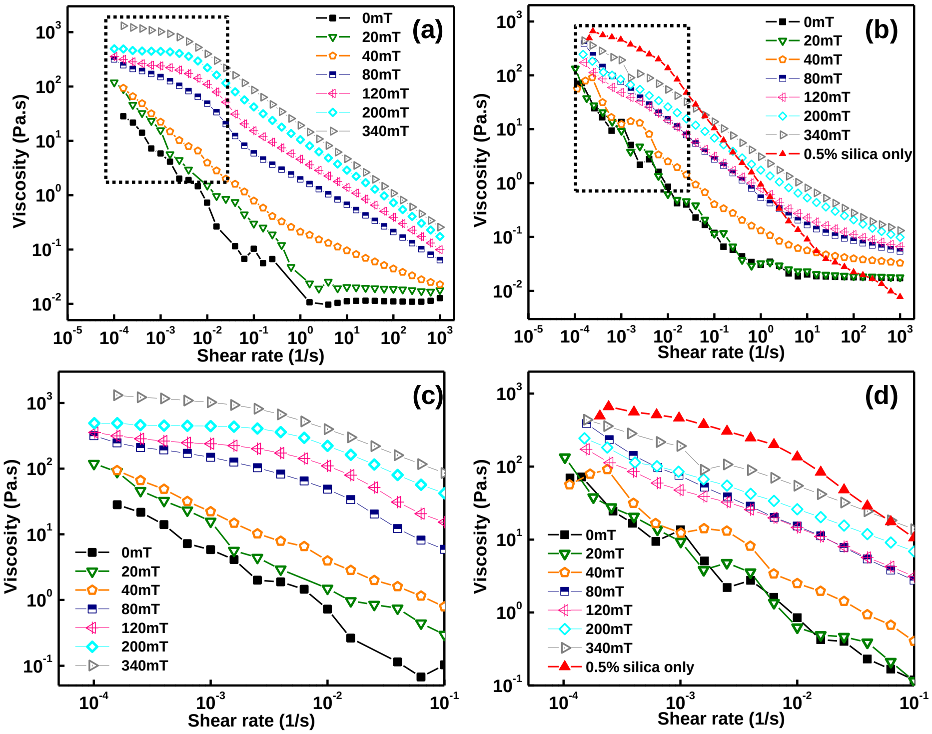

Figure 7.2: Viscosity curves at magnetic field of 0, 20, 40, 80, 120, 200 and 340 mT for (a) FF and (b) FF-silica. The viscosity curve of silica of volume fraction 0.098 in kerosene is shown in (b). The magnified view of the boxed regions of **(**a) and (b) are shown in (c) and (d), respectively.

The presence of chains and thick columns offer hindrance to the flow of the ferrofluid leading to an increase in the viscosity under magnetic field. In the presence of shear, the field induced chains and columns are broken down by the hydrodynamic force resulting in a decrease of viscosity.[116]

FF shows shear thinning behavior at all magnetic fields as seen in **Fig. 7. 2 (a)**. However at 80 mT and above, a small hump is seen at low shear rates followed by a shear thinning response. The hump develops into a plateau at higher magnetic fields. This is due to the arrangement of chains at a specific angle with respect to the magnetic field.[221] The FF-silica also exhibits an increase in viscosity with magnetic field and a shear thinning response (**Fig.**

7.2 (b)). However, the viscosity of FF-silica is lower than that of FF at all magnetic fields. Interestingly, the shear resistant plateau observed in FF disappeared in FF-silica. The shear resistant plateau in FF and its absence in FF-silica are shown magnified in **Fig. 7.2 (c)** and **(d)**.

7.3.3 Degree of Shear Thinning

The addition of silica nanoparticles to the ferrofluid has a profound effect on the degree of shear thinning. The degree of shear thinning is given by the exponent (*c*) of the power law fit ($\eta \propto \dot{\gamma}^c$) to the viscosity curves at different magnetic fields in the high shear rate region between 10 and 1000 s^{-1}. The exponents plotted as a function of magnetic field for FF and FF-silica are shown in **Fig. 7.3**.

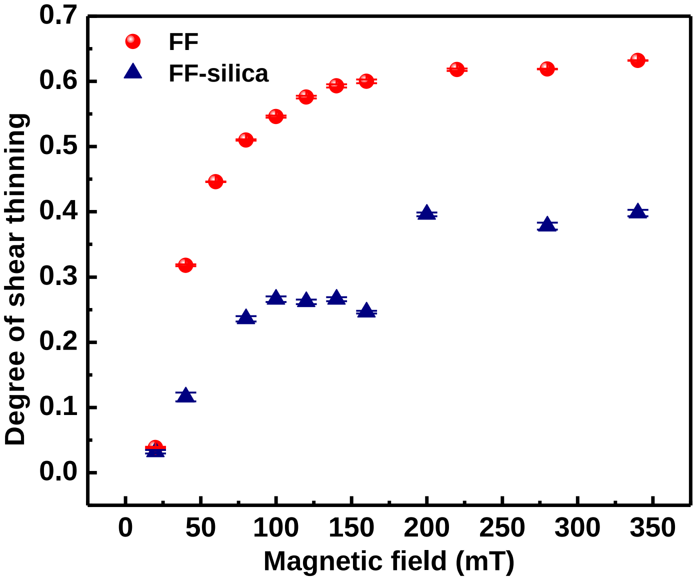

Figure 7.3: Degree of shear thinning at shear rate above 10 s^{-1} as a function of the magnetic field for FF and FF-silica.

It is observed that FF exhibits higher degree of shear thinning than FF-silica in the high shear rate region. The degree of shear thinning of both the systems increases with magnetic field and saturates above 200 mT.

7.3.4 Yield Stress Measurements

The influence of silica on the rheology of ferrofluid is seen in the yield stress values whose dependence on the magnetic field strength is shown in **Fig. 7.4**. The yield stress values were obtained by fitting the stress-shear rate plots to Herschel-Bulkley model.[196-198] It is observed that both the static and dynamic yield stresses of FF-silica are lower than that of FF for all values of magnetic field. The yield stress dependence on magnetic field strength for both FF and FF-silica follows a power law. The exponents of static yield stress for FF and FF-silica are 1.6 ± 0.002 and 1.02 ± 0.008, respectively. The exponents of dynamic yield stress for FF and FF-silica are 1.92 ± 0.002 and 1.59 ± 0.005, respectively.

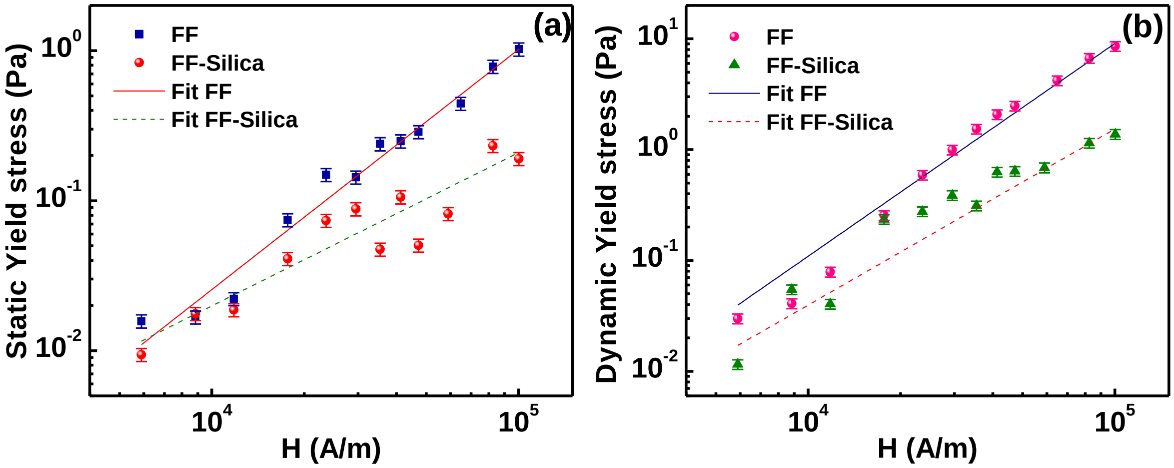

Figure 7.4: (a) Static yield stress and (b) dynamic yield stress of FF and FF-silica as functions of magnetic field strength.

Ginder et al.[199] reported that yield stress scaling with magnetic field strength depends on the magnetic field regimes as described in **Section 3.3.3**. In the linear magnetization regime, the yield stress depends on the square of the magnetic field strength as given by **Eqn. (3.8)**. In systems with interactions other than magnetic and hydrodynamic, the yield stress was found to depend on H in a sub quadratic manner by Lopez et al.[54] in organo-clay added magnetorheological fluids where $\tau_y \propto H^{1.4}$. The deviation from the quadratic dependence as reported by Ginder at al.[199] is attributed to the colloidal interactions between the iron particles, clay-clay and clay-iron. The decrease in exponent below 2 for the plot of yield stress vs. magnetic field strength was also reported by Fei et al.[61] in magnetorheological fluids containing carbonyl iron particles with single walled carbon nanotubes as filler material. This decrease is attributed to the saturation of the particle magnetization. As the field strength increases, the polarization forces between magnetic particles increase favoring the formation of chainlike structures and columns. At high magnetic fields, the particle magnetization saturates, which in turn leads to a saturation of the polarization force resulting in decrease in the exponent from 2.0 to 1.5 which occurred at a critical magnetic field H_c. In other words,

$$\tau_y \propto H^2, H < H_c \tag{7. 1}$$

$$\tau_y \propto H^{3/2}, H > H_c \tag{7. 2}$$

For the MR fluid studied by Fei et al.[61] the critical field strength for the exponent change was found to be 151.74 kA/m. Similar observations were reported in MR fluids containing carbonyl iron particles coated with polyaniline (PANI) shell and a multiwalled carbon nanotube nest.[59] In the present study, the magnetic fields used are below the saturation magnetic field and hence the lower exponents in both FF and FF-silica in the present work are attributed to contributions from the thermal motion and colloidal interactions between silica particles.

7.3.5 Mason Number Scaling

Fig. 7.5 shows the plots of the field specific viscosity as a function of the Mason number,[192-194] which signifies the ratio of the magnetic and hydrodynamic forces. If the rheology of a system is purely controlled by magnetic and hydrodynamic forces, then the viscosity curves at different magnetic fields will scale onto a single master curve. If additional forces like Brownian, colloidal, etc. act on the system, then the scaling will not be perfect.

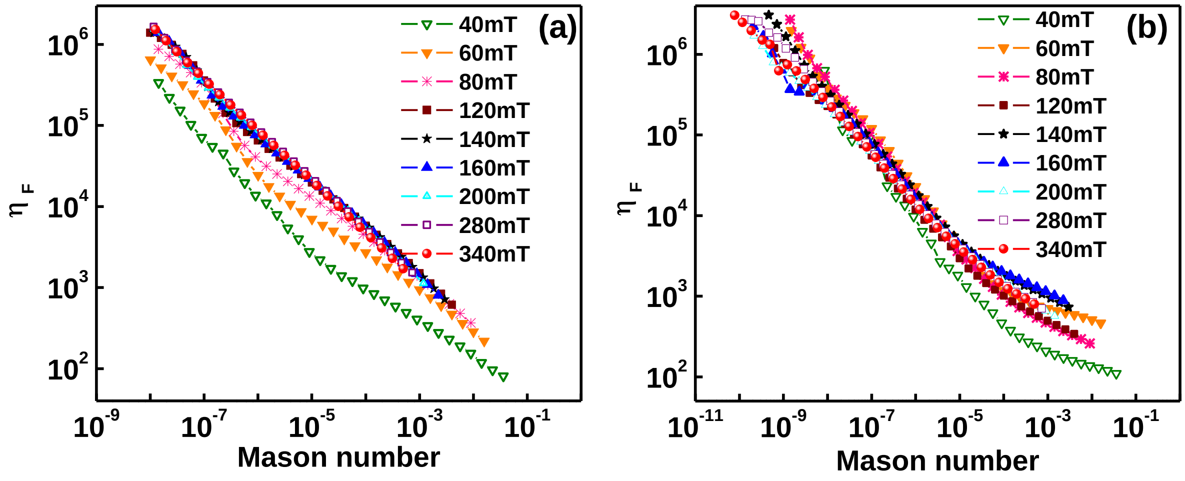

Figure 7.5: Field specific viscosity vs. Mason number at magnetic fields of 40, 60, 80, 120, 140, 160, 200, 280 and 340 mT for (a) FF and (b) FF-silica.

The viscosity curves at different magnetic fields collapse onto a single master curve above 80 mT for FF and 60 mT for FF-silica, which signifies that the rheology of the suspension is controlled entirely by the magnetic and hydrodynamic forces. The deviation from the master curve is an indication of the presence of additional interactions such as thermal, colloidal etc. in the system.[54] In the present study, the deviations observed in FF below 80 mT can be attributed to the dominant thermal energy contributions. In FF-silica, the silica-silica colloidal interactions show up as deviation in the low Mason number region, which is prominent at low magnetic field (40 mT).

7.3.6 Magnetic Hysteresis

The evolution of field induced structures and its effect on rheological properties is studied by performing magnetic field sweeps at constant shear rates, the results of which are shown in **Fig. 7.6**.

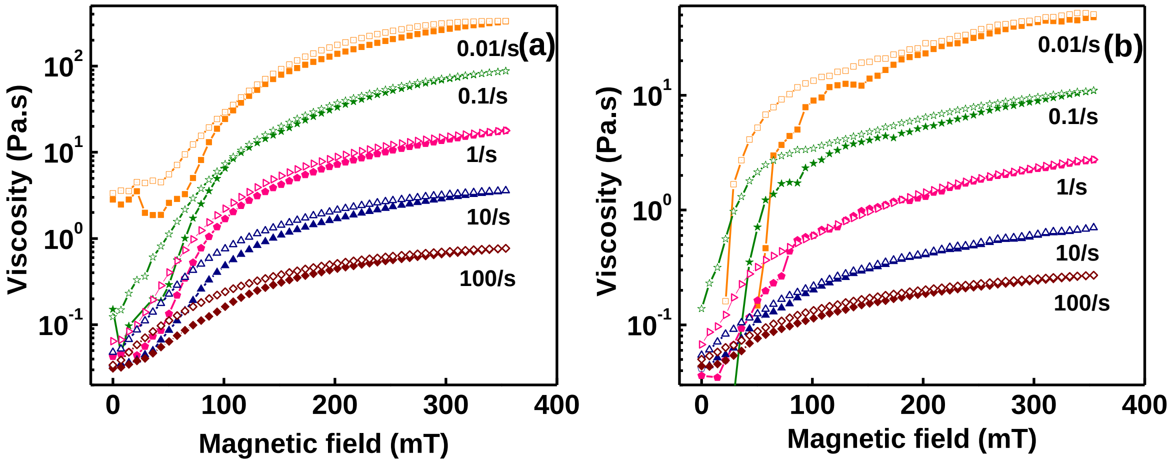

Figure 7.6: Viscosity as a function of magnetic field for (a) FF and (b) FF-silica at shear rate of 0.01, 0.1, 1, 10 and 100 s^{-1}. Closed and open symbols represent increasing and decreasing magnetic field, respectively.

The viscosities of both FF and FF-silica increase with magnetic field. On reversal of the field, the viscosities of both the systems decrease but with a hysteresis behavior, which is attributed to the higher relaxation time of the field induced structures than the measurement time (10 s).[71] The hysteresis area of FF-silica is smaller than that of FF. The reduction in hysteresis implies that the size of the field induced structures in FF-silica is lower than those present in FF as the colloidal interactions between silica particles dominate over the dipolar interactions between magnetic nanoparticles. In FF-silica, a 3D network is formed by silica particles which interact via hydrogen bonding between the silanol groups present on the particle surface. On application of magnetic field, the magnetic nanoparticles confined within the 3D network begin to interact through dipolar forces thereby forming chains aligned along the field direction. The structures thus formed are smaller and weaker as the silica network hinders the interaction between the magnetic nanoparticles.

7.3.7 Rheomicroscopic Experiments

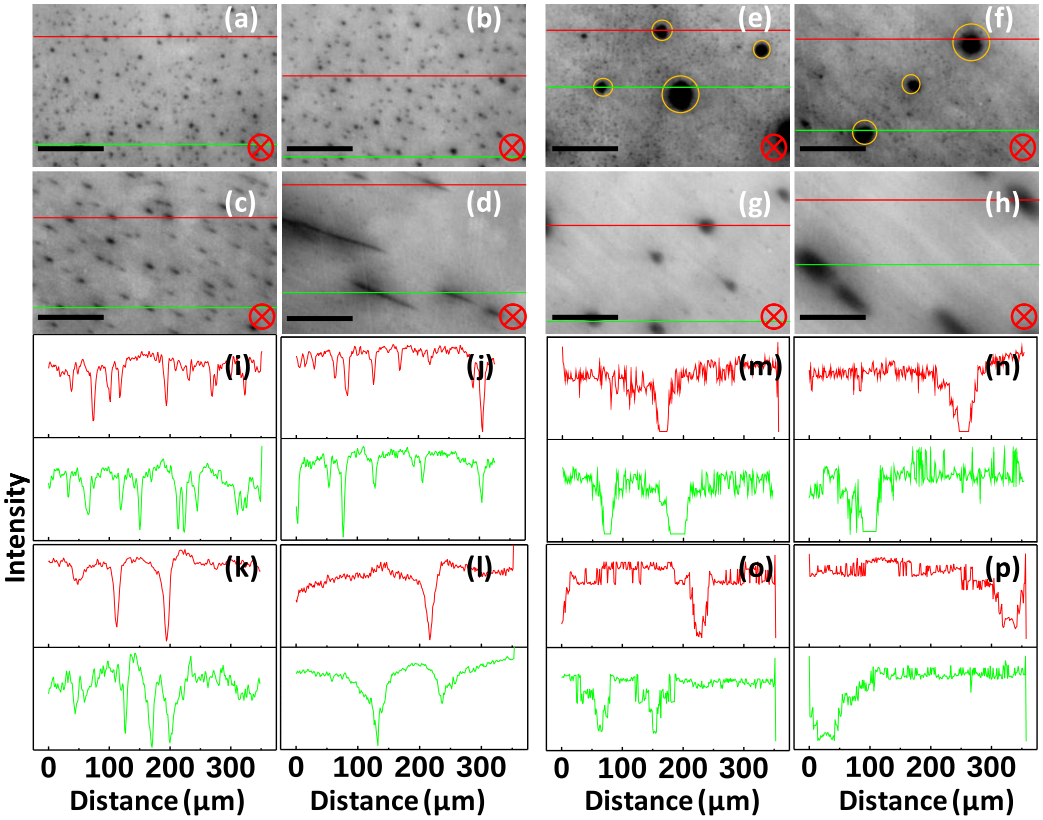

Figure 7.7: The rheomicroscopic images of FF and FF-silica at (a,e) 0.01 s^{-1} (b,f) 0.1 s^{-1} (c,g) 1 s^{-1} and (d,h) 10 s^{-1} at a magnetic field of 18.5 mT. The images were taken perpendicular to the plane of shear (top view) for diluted samples of FF and FF-silica. The scale bar corresponds to 100µm. The corresponding line profiles of the images for (i-l) FF and (m-p) FF-silica. The direction of the magnetic field is perpendicular to the plane of the images and is indicated by $\otimes$.

The field induced microstructures during rheological measurements were directly visualized using a rheomicroscope. The microstructural evolution of the field induced structures at a magnetic field of 18.5 mT is shown in **Fig. 7.7 (a) - (d)** for FF and **Fig. 7.7 (e) – (h**) for FF-silica. The images were taken perpendicular to the plane of shear (top view) for diluted samples. For FF, at 0.01 s^{-1} (**Fig. 7.7 (a)**), the microstructure consists of columnar structures seen as dots in the image. As the shear rate increases to 0.1 s^{-1} (**Fig. 7.7 (b)**), the columnar structures are disrupted and their number decreases. With further increase in shear rate, the structures begin to align along the shear flow direction as seen at 1 s^{-1} (**Fig. 7.7 (c)**) and 10 s^{-1} (**Fig. 7.7 (d)**). In the case of FF-silica, at 0.01 s^{-1} (**Fig. 7.7 (e)**) and 0.1 s^{-1} (**Fig. 7.7 (f)**) the columnar structures are seen as smaller dots and silica flocs are seen as big spheres (encircled). As the shear rate is increased to 1 s^{-1} (**Fig. 7.7 (g))** and then to 10 s^{-1} (**Fig. 7.7 (h)**), the columnar structures as well as the silica network are disrupted slightly and are aligned along the shear flow direction. The line profiles for the images are shown in **Fig. 7.7 (i) – (l)** for FF and **Fig. 7.7 (m) – (p)** for FF-silica. The diameter of the columns varies between 9.92 and 13.98 μm. For FF-silica, the average diameter of the field induced columns is 5.32 μm while the silica flocs appear larger with size of about 27 to 40 μm. The smaller diameters columnar structures observed in FF-silica indicates that the intervening silica matrix hamper the zippering transitions in FF-silica.

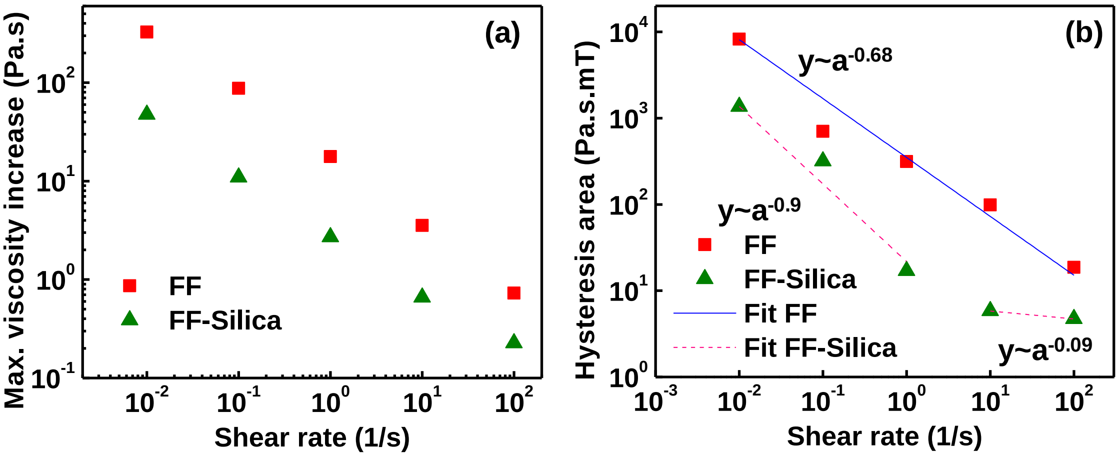

Figure 7.8: (a) Maximum increase in viscosity and (b) hysteresis area as functions of shear rate for FF and FF-silica. The exponent of the power law fit in (b) for FF is -0.68 ± 0.013. FF-silica (dotted line in (b)) has exponents of -0.9 ± 0.016 and -0.092, between the shear rates 10^{-2} to 1 s^{-1} and 10 to 100 s^{-1}, respectively.

Fig. 7.8 (a) shows that the maximum viscosity increase in FF-silica is almost an order of magnitude lower than that of FF at lower shear rates. The difference decreases at higher shear rates. The hysteresis area decreases with shear rate for both FF and FF-silica as shown in **Fig. 7.8 (b)**. The larger field induced structures are destroyed by the shear forces and the resulting smaller structures have lower relaxation times which lead to a decrease in the hysteresis effect. The hysteresis area exhibits a power law decay with shear rate (i.e., $y = ax^{q}$) with q = -0.68 ± 0.013 for FF. For FF-silica the plot shows two different regions 10^{-2} to 1 s^{-1} and 10 to 100 s^{-1} with exponents -0.9 ± 0.016 and -0.092, respectively. The smaller exponent above 10 s^{-1} indicates the insignificant hysteresis at higher shear rates.

7.3.8 Dynamic Rheology

The linear and nonlinear viscoelastic measurements were carried out on both FF and FF-silica under constant values of magnetic field.

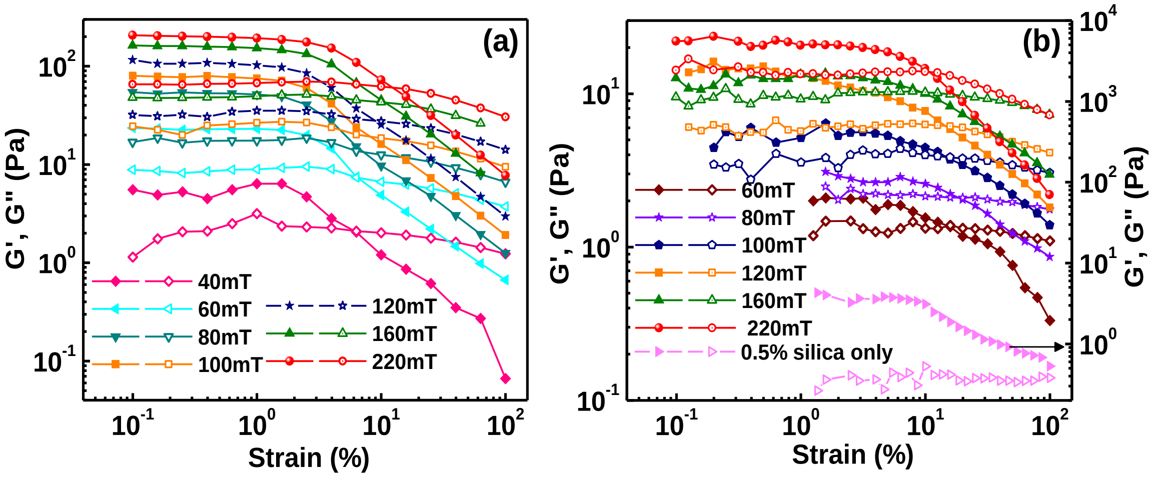

Figure 7.9: Storage (closed symbols) and loss (open symbols) moduli as function of strain amplitude at magnetic fields of 40, 60, 80, 100, 120, 160 and 220 mT for (a) FF and (b) for FF-silica. The right axis of (b) corresponds to storage and loss moduli for silica of volume fraction 0.098 in kerosene.

The amplitude sweep measurements in FF at a fixed angular frequency and magnetic field, (**Fig. 7.9 (a)**) show LVE region at lower strain amplitude with the strain independent storage modulus being greater than the loss modulus. In the LVE region, the system is predominantly elastic with *G'* > *G"*. The elastic or solidlike nature is attributed to the gap-spanning field induced structures, which undergo affine deformation. As the strain amplitude exceeds certain a critical value, *G'* begins to decrease and falls below *G"* due to the rearrangement of particles within the chains and also due to the destruction of the field induced structures. The system becomes predominantly viscous with *G"* > *G'*. The magnitudes of the storage and loss moduli increase with magnetic field as the number and the size of the field induced aggregates increase. At any given field there is a distribution of chain lengths.[187, 245] The gap-spanning structures contribute to the increase in *G'* while the unpinned or non gap-spanning ones contribute to *G"*.[103, 206] The increase in magnitude of the viscoelastic moduli with field and the elastic to viscous transition under increasing deformation are also observed in FF-silica (**Fig. 7.9 (b)**). However, the elastic behavior is evident in FF-silica only for fields above 60 mT (at low strains) while FF exhibits such behavior even at 40 mT. Also, the storage moduli in the LVE region at 220 mT are 187 and 20 Pa for FF and FF-silica, respectively. The almost one order reduction in the magnitude of *G'* in the presence of silica is attributed to the hindrance to the formation of field induced structures in the presence of the intervening silica and colloidal interactions.

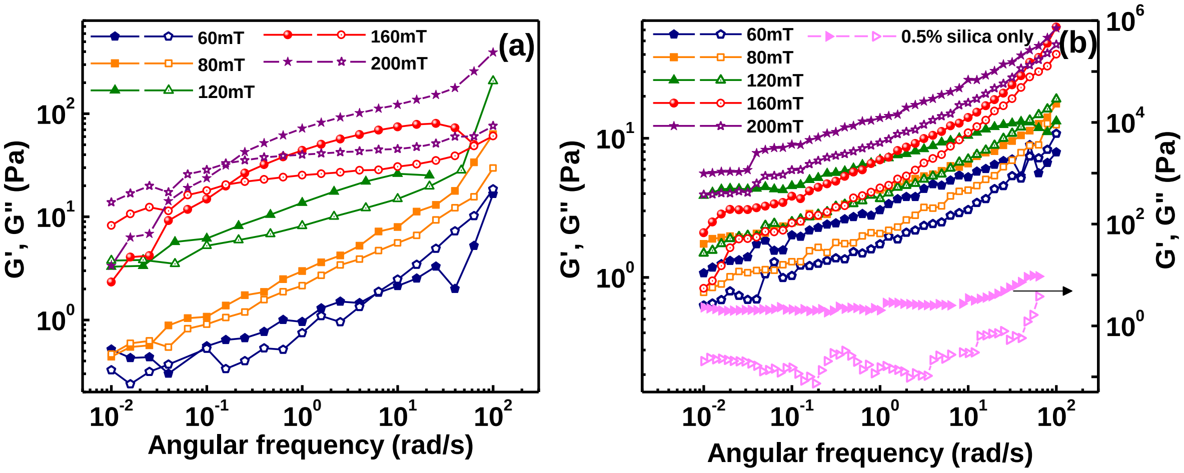

Figure 7.10: Storage (closed symbols) and loss (open symbols) moduli as function of angular frequency at magnetic fields of 60, 80, 120, 160 and 200 mT for (a) FF and (b) for FF-silica. The right axis of (b) corresponds to storage and loss moduli for silica of volume fraction 0.098 in kerosene.

The results of the linear viscoelastic measurements in **Fig. 7.10 (a)** show transition from elastic to viscous behavior in the presence of magnetic fields for FF. The storage modulus is greater than the loss modulus at high frequencies. As the frequency decreases, both the moduli decrease and the response of the ferrofluid becomes predominantly viscous (*G"* > *G'*) below a particular frequency. Thus a transition from elastic to viscous behavior is observed under a magnetic field. The transition is attributed to the rearrangement of particles within the zippered chains.[218] On the other hand, in FF-silica both the moduli decrease as the frequency decreases but with a fully elastic behavior (*G' > G"*) throughout the frequency region. The predominant elastic response in FF-silica is due to the presence of silica network. In FF-silica, the hydrophilic silica particles do not interact with the surrounding carrier fluid due to the inability of the latter to form hydrogen bonds. On the other hand, the silanol groups on the surface of the silica particles interact via hydrogen bonding forming aggregates which in turn results in the formation of a continuous 3D network of silica particles. On application of a magnetic field, the magnetite particles within the 3D network begin to form structures aligned along the direction of the magnetic field. When subject to an oscillatory shear, both the silica network and the field induced structures, undergo deformation. At higher frequencies, the time available for deformation is much smaller than the relaxation time of the silica network and that of the field induced structures and hence an elastic behavior is observed. At low frequencies, the time scale of deformation is larger than the time required for particle rearrangements within the field induced chains and hence relaxation occurs within the field induced structures. However, the surrounding silica network does not relax within the experimental time scale, which is evident from the frequency dependent measurements on pure silica ($\varphi = 0.098$) in the base fluid shown in **Fig. 7.10 (b)**. While the silica network does not relax, the field induced structures within the network do so at smaller frequencies. Thus, the observed decrease in *G'* with decrease in frequency is attributed to the particle rearrangements within the field induced structures while the predominant elastic behavior throughout the frequency region probed is due to the non relaxation of the surrounding silica network.

The results show that the addition of hydrophilic silica nanoparticles influences both the steady shear as well as the dynamic rheology of the ferrofluid significantly under a magnetic field. The presence of hydrophilic silica lowers the magnetoviscosity, the yield stress and the viscoelastic moduli of the ferrofluid. It also reduces the degree of shear thinning at high shear rates and improves the elastic nature under linear deformation which finds useful applications in ferrofluid seals, and ferrofluid based actuators.[164, 257] In FF-silica, the carrier fluid being nonpolar has no hydrogen bonding ability and hence does not interact with the silica particles. The silanol groups present on adjacent silica particles interact through hydrogen bonding to form a 3D network of silica aggregates. In the absence of magnetic field, the magnetic nanoparticles are interspersed within this 3D network. On application of magnetic field, the dipolar interactions come into picture. With increase in magnetic field, the microstructure of FF-silica develops from the one dominated by colloidal interactions to the one dominated by dipolar interactions. With increasing field strength, the microstructure of FF-silica evolves from 3D network of silica interspersed with magnetic particles to smaller field induced structures and ultimately to gap-spanning structures, all of them embedded within the silica matrix. The shear introduces an additional interaction in the system. The interplay among the three interactions namely, colloidal, magnetic and hydrodynamic determines the rheology of the FF-silica system.

In the presence of a magnetic field, the low shear rate region ($< 10\ s^{-1}$) in FF shows a strong shear thinning behavior. This region is dominated by the presence of 3D network with field induced structures embedded within them. The breakage of the silica network results in a strong shear thinning. This is in agreement with shear thinning observed in a dispersion of silica (φ = 0.098) in the carrier fluid as seen from **Fig. 7.2 (b)**. The destruction of the field induced structures also contributes to shear thinning. However, the major contribution is from the breakdown of silica network. Above 10 s^{-1}, the silica network is completely broken down and exists as isolated silica flocs along with the field induced structures that were destroyed by the hydrodynamic force (**Fig. 7.7**). The flocs prevent the dipolar aggregates from orienting along the shear planes leading to a decrease in the degree of shear thinning. The presence of silica lowers the yield stress of the ferrofluid as seen in **Fig. 7.4** indicating that FF-silica starts to flow at lower stresses than FF. In the presence of silica, the dipolar interactions between magnetic particles are weakened and the resultant microstructure starts to flow at lower stress than that required in FF and hence the static yield stress of FF-silica is lower than that of FF. The dynamic yield stress which corresponds to the stress required to break aggregates reforming in the presence of magnetic forces at high shear rates, is also lower for FF-silica due to the reduced dipolar aggregation in presence of the intervening silica. The yield stresses of FF-silica increase with magnetic field as a power law. The lower exponent of FF-silica (1.02 and 1.59 for static and dynamic, respectively) corroborates the prominent role of colloidal interactions in the system.

The colloidal interactions among silica aggregates hinder the formation of dipolar aggregates among magnetic particles. Hence, as in the case of viscosity, the viscoelastic moduli in FF-silica are lower than that of FF. The linear viscoelastic measurements show the absence of elastic to viscous transition in FF-silica. In ferrofluids and magnetorheological fluids, when the microstructure is composed of central gap-spanning chains with side chains attached to them (zippered structures), a transition from high frequency elastic to low frequency viscous response is observed. When the microstructure is subjected to an oscillatory deformation, the particles in the side chains undergo motion perpendicular to the shear direction.[218] At higher frequencies the time scale available for particle rearrangement is greater than the experimental time scale and hence no relaxation occurs, which leads to an elastic behavior.[216, 218] Single particle-width chains undergo affine deformation without any relaxation and hence *G'* in such case is independent of the frequency.[218] In FF-silica, under magnetic field, *G'* dominates over *G"* over the entire frequency regime probed and both the moduli decrease with decreasing frequency. The decrease in the moduli is attributed to the slight particle rearrangements within the field induced structures while the predominant elastic response over the entire frequency range probed is due to the non relaxation of the surrounding silica network. Relaxation may occur at larger time scales or at lower frequencies than that are probed here.

The amplitude sweep measurements in FF-silica shows purely viscous behavior below 40 mT. At 60 mT and above, the LVE region at lower strains becomes prominent, the reason being that the dipolar force is not strong enough to overcome the colloidal silica interactions. As the strain increases, the storage modulus begins to decrease and becomes smaller than the loss modulus at higher strains. The critical strain, at which *G'* decreases, is larger than that of FF at magnetic fields below 100 mT, above which the critical strain becomes smaller than that of FF. The pure silica in the base fluid shows a critical strain of ~9 %, which supports the argument that colloidal interactions dominate at low fields while dipolar interactions dominate at high fields.

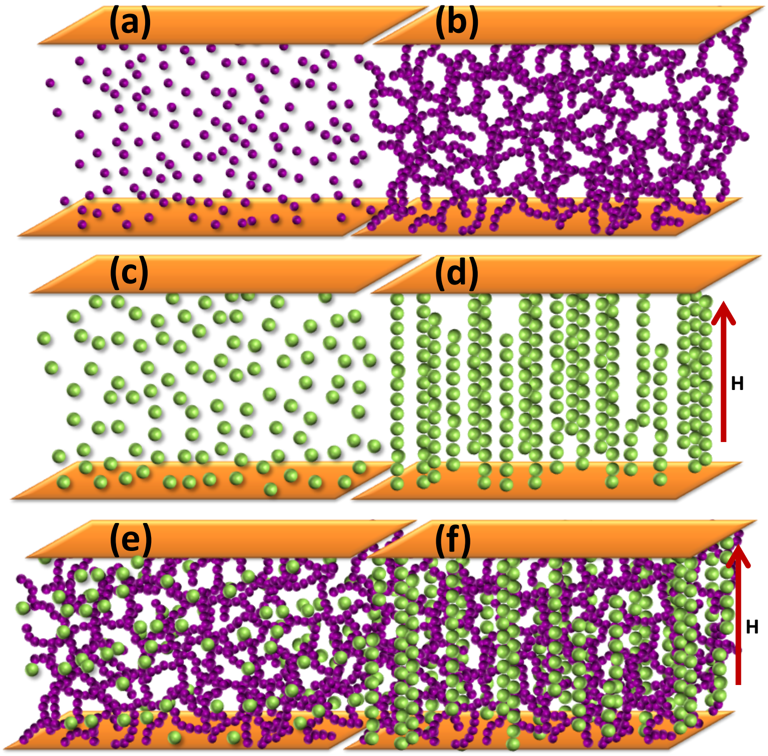

Figure 7.11: The schematic of the microstructure of hydrophilic silica nanoparticles in (a) polar and (b) nonpolar solvent, magnetic nanoparticles (c) in the absence and (d) in the presence of magnetic field, magnetic nanoparticles within silica network (e) in the absence and (f) in the presence of magnetic field.

The schematic of the ferrofluid microstructure drawn based on the findings of the present study is shown in **Fig. 7.11**. The schematic of the microstructures of hydrophilic silica particles alone in polar and nonpolar solvents are shown in **Fig. 7.11 (a)** and **(b)**, respectively. In polar solvents, the silanol (Si-OH) groups present on the particle surface form hydrogen bonds with the surrounding solvent molecules giving rise to a well dispersed suspension of particles as seen in **Fig. 7.11 (a)**. In nonpolar solvents, the adjacent silica particles interact through the formation of hydrogen bonds between the silanol groups due to the inability of the solvent molecules to form hydrogen bonds with the particles. Thus, a flocculated network of particles is formed as shown in **Fig. 7.11 (b)**. **Fig. 7.11(c)** and **(d)** show the schematic of the microstructure of pure FF in the absence and presence of magnetic field, respectively. In the absence of field, the magnetite particles are well dispersed in the base fluid while in the presence of field, chains and columnar structures are formed. **Fig. 7.11(e)** and **(f)** show the schematic of the microstructure of FF-silica in the absence and presence of magnetic field, respectively. In the absence of field, the magnetite particles are dispersed within the silica network. In presence of field, the field induced structures aligned along the magnetic field direction are formed within the 3D silica network. However, due to the presence of colloidal silica network, the field induced structures are smaller in size in FF-silica.

7.4 Conclusions

The effect of hydrophilic silica on the magnetorheological properties of an oil based ferrofluid containing Fe_3O_4 nanoparticles of size ~ 10 nm was studied. A small concentration of silica nanoparticles in ferrofluid is found to lower the yield stresses and viscoelastic moduli because of the weakening of dipolar interactions due to the intervening silica nanoparticles. Furthermore, the presence of silica also reduces the degree of shear thinning and the yield stresses power law exponents were < 2. The ferrofluid containing silica exhibits a dominant elastic behavior over the entire frequency region probed under the linear oscillatory shear, a reduced hysteresis during the magnetic field sweeps and a longer linear viscoelastic regime under nonlinear deformation. The rheomicroscopic images show that the columnar aggregate structures along the field directions at low shear rates are reoriented along the shear flow direction at high shear rates. The image analysis showed that the average diameter of the columnar aggregates in pure ferrofluid varies between 9.92 and

13.98 μm while it is ~ 5.32 μm in mixed FF-silica system. The lower size of the columnar aggregates shows that the intervening silica matrix hampers the zippering transition of columns at higher magnetic field and shear rates. Our results suggest that optimization of rheological properties of ferrofluids is possible by carefully adjusting the silica particle concentration and the results may find practical applications in dynamic seals, actuators, heat transfer, sensors and opto-fluidic devices, etc.

Chapter 8 Conclusions and Recommendations for Future Work

8.1 Conclusions

The magnetorheological properties of ferrofluids containing sterically stabilized magnetite nanoparticles dispersed in kerosene are studied in the absence and presence of additives.

The change in the microstructure is evident from the viscosity enhancement of the ferrofluid under the influence of a magnetic field. The application of magnetic field to the ferrofluid results in the alignment of the magnetic moments of the particles along the field direction leading to the formation of chains and columns when the coupling constant exceeds unity. When subjected to a shear force, the ferrofluid exhibits a shear thinning behavior due to the breaking of the field induced structures and their reorientation along the shear flow. Above a magnetic field of 40 mT, the low shear rate region of the viscosity curve shows a “plateau-like region” due to the peculiar alignment of the chains with respect to the field direction where the structure is stable against fragmentation. The size and number of the field induced structures increase with increase in magnetic field leading to an increase in the viscosity and yield stresses. By employing the Mason number for the first time in ferrofluids, it has been shown that the viscosity curves at different magnetic fields scale onto a single master curve because of the dominant magnetic and hydrodynamic forces over the thermal force. As the magnetic field is decreased gradually, the field induced structures relax back leading to a decrease in viscosity, with a hysteresis because of the mismatch between the relaxation time of these structures and the measurement time. The hysteresis area decreases with shear rate as a power law with an exponent of -0.64, indicating the augmentation of relaxation by the shear force. Under oscillatory shear, the ferrofluid exhibits a viscoelastic behavior. The amplitude sweep measurements show linear response at low strain amplitudes and a nonlinear behavior at higher strains due to the destruction of field induced structures. A transition from the high frequency elastic to low frequency viscous response is observed in the frequency dependent measurements, which is attributed to the movement of particles within the chains and columns.

The microstructure of the ferrofluid under magnetic field and shear is studied using a rheomicroscope. In the absence of shear, columnar aggregates, formed by particle aggregation, are observed under a magnetic field. The size of the columnar aggregates increases drastically with magnetic field for the concentration range φ = 0.0031 to 0.0063 while it increases slightly for the φ range of 0.00078 to 0.0012. The increase in the columnar size is attributed to the zippering transitions that occur when chains are in off registry undergo lateral coalescence to form larger size aggregates. For the ferrofluid concentrations studied, the typical diameter of the columns varies from 7 to 41 μm. Zippering is also confirmed from the decrease in the number density of the columns with magnetic field. The changes in the ferrofluid microstructure are reflected as increase in the macroscopic viscosity of the ferrofluid. Under shear, the columns begin to dealign from the direction of the magnetic field and reorient along the shear flow direction. The rheomicroscopic images show a disruption of columnar aggregates and their subsequent reorientation along the direction of shear. The corresponding macroscopic rheological behavior of the ferrofluids shows a shear thinning response.

Probing of field-induced structures and their dynamics in ferrofluid (φ = 0.046) using oscillatory rheology shows that the structural relaxation occurring at low frequencies can be shifted to an accessible frequency regime using the strain-rate frequency superposition. Using the scaling factors obtained from the frequency and modulus at the crossover point in oscillatory rheological measurements, the constant strain-rate frequency sweep data are superimposed onto a single master. The frequency scaling factor (ω_c) increases with the strain-rate as a power law with an exponent value close to unity, whereas the amplitude scaling factor (G_c) is almost strain-rate independent at high magnetic field strengths. The structural relaxation resulting from rearrangement of particles occurrs more easily as the strain-rate increases. These rearrangements occur when the particles in the side chains, attached to the single-sphere-width gap-spanning chain, undergo motion perpendicular to the shear flow due the competition between the hydrodynamic and magnetostatic forces. Such rearrangement is reflected as a transition from a solidlike to a liquidlike rheological response. The magnetic field dependence of the relaxation time and crossover modulus showed two distinct regions, indicating the different microstructures in those regions. These studies show that the ferrofluid exhibits a soft solidlike behavior whose relaxation is governed by the imposed strain-rate and the magnetic field.

The addition of multiwalled carbon nanotubes to an oil based ferrofluid of volume fraction $\varphi = 0.087$ shows a viscosity enhancement lower than that of pure ferrofluid which suggests a weakening of the ferrofluid microstructure by the CNTs. The onset of the shear resistant plateau observed at 120 mT in pure ferrofluid is shifted to 200 mT in the presence of CNTs. The weakening of the ferrofluid microstructure is evident from the decrease in the yield stress values of the composite system, indicating that a lower stress is sufficient to cause flow in CNT-FF. The static yield stress scales with magnetic field strength as a power law with exponents 1.6 and 1.3 for pure ferrofluid (FF) and composite system (CNT-FF), respectively against the theoretical value of 2. The lower exponent in case of CNT-FF is attributed to the influence of thermal fluctuations and the presence of CNT which weakens the magnetic field induced microstructure of the ferrofluid. The Mason number plots for both the pure and composite scale onto a single master curve for magnetic fields above 80 mT. The presence of CNT reduces the hysteresis behavior as a result of the weakened microstructure. The hysteresis area decreases with shear rate as a power law with exponents of -0.68 and -0.49 for FF and CNT-FF, respectively. The amplitude sweep measurements show that the linear viscoelastic region which is observed at 40 mT for FF is shifted to 80 mT for CNT-FF, which further confirms the weakening of the ferrofluid microstructure in the presence of CNTs.

Hydrophilic silica nanoparticles are found to modify the magnetorheological properties of ferrofluids. In a nonpolar oil based ferrofluid containing hydrophilic silica, the magnetic particles are embedded within the spanning silica network. On application of a magnetic field, the magnetic particles aggregate into chains and columns and are aligned along the field direction. The weakened dipolar interaction in presence of silica lowers the viscosity and yield stresses of the ferrofluid. The silica network hampers the zippering transition that is evident from the rheomicroscopic images. The diameter of the columns for pure ferrofluid varies between 9.9 and 13.9 μm and that for ferrofluid with silica is ~5.3 μm. The degree of shear thinning at high shear rates is reduced in the presence of silica owing to the intervening silica flocs. The evidence for colloidal interactions between silica particles is seen as lower power law exponents (1.02 and 1.59 for static and dynamic, respectively against the theoretical value of 2) of the yield stress-magnetic field strength curve. The weakened dipolar interactions in the presence of silica network results in an easy relaxation of field induced structures during the reversal of the magnetic field and hence a lower hysteresis. The oscillatory measurements show that the viscoelastic moduli are drastically reduced in FF-silica. Under linear oscillatory shear, the FF-silica exhibits a dominant elastic behavior over the entire frequency region due non relaxation of the silica network. During strain dependent measurements, a longer linear viscoelastic region (~9%) is observed at magnetic fields below 100 mT for FF-silica. These studies suggest dominant colloidal interactions at low magnetic fields and dipolar interactions at high fields.

The findings of this thesis show several new insights into the magnetorheological properties of oil based ferrofluids that would enable better utilization of these smart fluids for static and dynamic applications such as electronic cooling for micro and nanomechanical devices, smart dampers, dynamic liquid seals, etc. In particular for cooling applications, the fast switching of Brownian particles to linear structures and their retention under flow conditions is essential. Further, on reducing the temperature to desired level, the ferrofluid should undergo a reversible transition to Brownian particles. Similarly for dynamic sealing conditions, the 1-dimenional structures in the region of interest (radial gap for a shaft assembly) should remain intact under operation (shear forces). These results also suggest that optimization of rheological properties of ferrofluids is possible by carefully adjusting the additive concentration for use in practical applications such as in dynamic seals, heat transfer, sensors, and opto-fluidic devices, etc.

8.2 Recommendations for Future Work

- To optimize the magnetorheological properties of ferrofluids using additives.
- To study the magnetorheological properties of magnetic nanoparticle-polymer nanocomposites.
- To develop stimulus responsive magnetic gels by optimizing the properties of nanoparticle-polymer nanocomposites.
- To study temperature dependent magnetorheological properties of ferrofluids under different experimental conditions.

List of References

1. Kleman, M.; Lavrentovich, O. D., *Soft Matter Physics: An Introduction*. Springer-Verlag: New York, 2003.
2. Fraden, S.; Hurd, A. J.; Meyer, R. B., Electric-Field-Induced Association of Colloidal Particles. *Phys. Rev. Lett.* **1989,** 63, (21), 2373-2376.
3. Martin, J. E.; Odinek, J.; Halsey, T. C., Evolution of structure in a quiescent electrorheological fluid. *Phys. Rev. Lett.* **1992,** 69, 1524-1527.
4. Kumar, R.; Ketner, A. M.; Raghavan, S. R., Nonaqueous Photorheological Fluids Based on Light-Responsive Reverse Wormlike Micelles. *Langmuir* **2010,** 26, (8), 5405-5411.
5. Li, R.; Horgan, C. C.; Long, B.; Rodriguez, A. L.; Mather, L.; Barrow, C. J.; Nisbet, D. R.; Williams, R. J., Tuning the mechanical and morphological properties of self-assembled peptide hydrogels via control over the gelation mechanism through regulation of ionic strength and the rate of pH change. *RSC Adv.* **2015**, (5), 301-307.
6. Mortensen, K.; Pedersen, J. S., Structural Study on the Micelle Formation of Poly(ethylene oxide)-Poly(propylene oxide)-Poly(ethylene oxide) Triblock Copolymer in Aqueous Solution. *Macromolecules* **1993,** 26, 805-812.
7. Alexandridis, P.; Holzwarth, J. F.; Hatton, T. A., Micellization of Poly(ethylene oxide)-Poly(propylene oxide)-Poly(ethylene oxide) Triblock Copolymers in Aqueous Solutions: Thermodynamics of Copolymer Association. *Macromolecules* **1994,** 27, 2414–2425.
8. Maeda, T.; Kanda, T.; Yonekura, Y.; Yamamoto, K.; Aoyagi, T., Hydroxylated Poly(N-isopropylacrylamide) as Functional Thermoresponsive Materials. *Biomacromolecules* **2006,** 7, (2), 545-549.
9. Xia, L.-W.; Xie, R.; Ju, X.-J.; Wang, W.; Chen, Q.; Chu, L.-Y., Nano-structured smart hydrogels with rapid response and high elasticity. *Nature Communications* **2013,** 4, 2226.
10. Su, Z.; Yin, J.; Guan, Y.; Zhao, X., Electrically tunable negative refraction in core/shell-structured nanorod fluids. *Soft Matter* **2014,** 10, 7696-7704.
11. Espin, M. J.; Delgado, A. V.; Rejon, L., Electrorheological properties of hematite/silicone oil suspensions under DC fields. *J. Non-Newtonian Fluid Mech.* **2005,** 125, 1-10.
12. Yin, J.; Zhao, X., Electrorheology of nanofiber suspensions. *Nanoscale Res. Lett.* **2011,** 256, (6), 1-17.
13. Lengálová, A.; Pavlínek, V.; Sáha, P.; Stejskal, J.; Quadrat, O., Electrorheology of polyaniline-coated inorganic particles in silicone oil. *J. Colloid Interface Sci.* **2003,** 258, 174-178.
14. Parthasarathy, M.; Klingenberg, D. J., Electrorheology: mechanisms and models. *Mater. Sci. Eng., R* **1996,** R17, 57-103.
15. Jeong, J. H.; Schmidt, J. J.; Cha, C.; Kong, H., Tuning responsiveness and structural integrity of a pH responsive hydrogel using a poly(ethylene glycol) cross-linker. *Soft Matter* **2010,** 6, 3930-3938.
16. Feng, Y.; Taraban, M.; Yu, Y. B., The effect of ionic strength on the mechanical, structural and transport properties of peptide hydrogels. *Soft Matter* **2012,** 8, 11723-11731.
17. Joyner, K.; Taraban, M. B.; Feng, Y.; Yu, Y. B., An Interplay Between Electrostatic and Polar Interactions in Peptide Hydrogels. *Biopolymers* **2013,** 100, (2), 174–183.

18. Ketner, A. M.; Kumar, R.; Davies, T. S.; Elder, P. W.; Raghavan, S. R., A Simple Class of Photorheological Fluids: Surfactant Solutions with Viscosity Tunable by Light. *J. Am. Chem. Soc.* **2007,** 129, 1553-1559.

19. Ge, J.; Hu, Y.; Yin, Y., Highly Tunable Superparamagnetic Colloidal Photonic Crystals. *Angew. Chem.* **2007,** 119, 7572-7575.

20. Camargo, P. H. C.; Lib, Z.-Y.; Xia, Y., Colloidal building blocks with potential for magnetically configurable photonic crystals. *Soft Matter* **2007,** 3, 1215.

21. Bossard, F.; Aubry, T.; Gotzamanis, G.; Tsitsilianis, C., pH-Tunable rheological properties of a telechelic cationic polyelectrolyte reversible hydrogel. *Soft Matter* **2006,** 2, 510-516.

22. Zustiak, S. P.; Leach, J. B., Hydrolytically Degradable Poly(Ethylene Glycol) Hydrogel Scaffolds with Tunable Degradation and Mechanical Properties. *Biomacromolecules* **2010,** 11, (5), 1348-1357.

23. Swan, J. W.; Bauer, J. L.; Liu, Y.; Furst, E. M., Directed colloidal self-assembly in toggled magnetic fields. *Soft Matter* **2014,** 10, 1102-1109.

24. Byrom, J.; Biswal, S. L., Magnetic field directed assembly of two-dimensional fractal colloidal aggregates. *Soft Matter* **2013,** 9, (38), 9167-9173.

25. Solis, K. J.; Martin, J. E., Complex magnetic fields breathe life into fluids. *Soft Matter* **2014,** 10, 9136-9142.

26. An, H.; Picken, S. J.; Mendes, E., Enhanced hardening of soft self-assembled copolymer gels under homogeneous magnetic fields. *Soft Matter* **2010,** 6, 4497–4503.

27. Szabo, D.; Szeghy, G.; Zrınyi, M., Shape Transition of Magnetic Field Sensitive Polymer Gels. *Macromolecules* **1998,** 31, 6541-6548.

28. Reinicke, S.; Dohler, S.; Tea, S.; Krekhova, M.; Messing, R.; Schmidt, A. M.; Schmalz, H., Magneto-responsive hydrogels based on maghemite/triblock terpolymer hybrid micelles. *Soft Matter* **2010,** 6, 2760–2773.

29. Cha, G.; Ju, Y. S.; Ahuré, L. A.; Wereley, N. M., Experimental characterization of thermal conductance switching in magnetorheological fluids. *J. Appl. Phys.* **2010,** 107, 09B505.

30. An, H.-N.; Sun, B.; Picken, S. J.; Mendes, E., Long Time Response of Soft Magnetorheological Gels. *J. Phys. Chem. B* **2012,** 116, 4702-4711.

31. Xu, Y.; Gong, X.; Xuan, S., Soft magnetorheological polymer gels with controllable rheological properties. *Smart Mater.* **2013,** 22, 075029.

32. Liu, T.-Y.; Hu, S.-H.; Liu, T.-Y.; Liu, D.-M.; Chen, S.-Y., Magnetic-Sensitive Behavior of Intelligent Ferrogels for Controlled Release of Drug. *Langmuir* **2006,** 22, (14), 5974-5978.

33. Haghgooie, R.; Doyle, P. S., Transition from two-dimensional to three-dimensional behavior in the self-assembly of magnetorheological fluids confined in thin slits. *Phys. Rev. E* **2007,** 75, (6), 061406.

34. Shah, K.; Choi, S.-B., The field-dependent rheological properties of magnetorheological fluids featuring plate-like iron particles. *Front. Mater.* **2014,** 1, (21), 1-6.

35. Odenbach, S., *Ferrofluids: Magnetically Controllable Fluids and Their Applications*. Springer: 2010.

36. Rablau, C.; Vaishnava, P.; Sudakar, C.; Tackett, R.; Lawes, G.; Naik, R., Magnetic-field-induced optical anisotropy in ferrofluids: A time-dependent light-scattering investigation. *Phys. Rev. E* **2008,** 78, 051502

37. Gao, Y.; Huang, J. P.; Liu, Y. M.; Gao, L.; Yu, K. W.; Zhang, X., Optical negative refraction in ferrofluids with magnetocontrollability. *Phys. Rev. Lett.* **2010,** 104, 034501.

38. Mitsumata, T.; Nagata, A.; Sakai, K.; Taniguchi, T., Anisotropy in Storage Modulus of Magnetic Gels Induced by Magnetization. *Jpn. J. Appl. Phys.* **2004,** 43, (12), 8203-8207.

39. Mitsumata, T.; Wakabayashi, T.; Okazaki, T., Particle Dispersibility and Giant Reduction in Dynamic Modulus of Magnetic Gels Containing Barium Ferrite and Iron Oxide Particles. *J. Phys. Chem. B* **2008,** 112, 14132-14139.

40. Ahn, S.-k.; Kasi, R. M.; Kim, S.-C.; Sharma, N.; Zhou, Y., Stimuli-responsive polymer gels. *Soft Matter* **2008,** 4, 1151-1157.

41. M.Schmidt, A., Induction heating of novel thermoresponsive ferrofluids. *J. Magn. Magn. Mater.* **2005,** 289, 5-8.

42. Chen, C.-H.; Abate, A. R.; Lee, D.; Terentjev, E. M.; Weitz, D. A., Microfluidic Assembly of Magnetic Hydrogel Particles with Uniformly Anisotropic Structure. *Adv. Mater.* **2009,** 21, 3201-3204.

43. Lee, D.; Cohen, R. E.; Rubne, M. F., Antibacterial Properties of Ag Nanoparticle Loaded Multilayers and Formation of Magnetically Directed Antibacterial Microparticles. *Langmuir* **2005,** 21, (21), 9651-9659.

44. Rabinow, J., The Magnetic Fluid Clutch. *AIEE Trans.* **1948,** 67, 1308-1315.

45. Rabinow, J. Magnetic Fluid Shock Absorber. 2667237, 1954.

46. Park, B. J.; Fang, F. F.; Choi, H. J., Magnetorheology: materials and application. *Soft Matter* **2010,** 6, (21), 5246–5253.

47. Liu, B.; Li, W. H.; Kosasih, P. B.; Zhang, X. Z., Development of an MR-brake-based haptic device. *Smart Mater. Struct.* **2006,** 15, 1960-1966.

48. Bica, I., Damper with magnetorheological suspension. *J. Magn. Magn. Mater.* **2002,** 241, 196-200.

49. Felicia, L. J.; John, R.; Philip, J., Rheological Properties of Magnetorheological Fluid with Silica Nanoparticles Stabilizers - A Comparison with Ferrofluid. *2* **2013**, (75-84), 75.

50. Ewijk, G. A. v.; Vroege, G. J.; Philipse, A. P., Convenient preparation methods for magnetic colloids. *J. Magn. Magn. Mater.* **1999,** 201, 31-33.

51. Jang, I. B.; Kim, H. B.; Lee, J. Y.; You, J. L.; Choi, H. J.; Jhon, M. S., Role of organic coating on carbonyl iron suspended particles in magnetorheological fluids. *J. Appl. Phys.* **2005,** 97, 10Q912.

52. Viota, J. L.; Vicente, J. d.; Durán, J. D. G.; Delgado, A. V., Stabilization of magnetorheological suspensions by polyacrylic acid polymers. *J. Colloid Interface Sci.* **2005,** 284, 527-541.

53. Guerrero-Sanchez, C.; Lara-Ceniceros, T.; Jimenez-Regalado, E.; Rasa, M.; Schubert, U. S., Magnetorheological Fluids Based on Ionic Liquids. *Adv. Mater.* **2007,** 19, 1740-1747.

54. López-López, M. T.; Gómez-Ramírez, A.; Duran, J. D. G.; Gonzalez-Caballero, F., Preparation and Characterization of Iron-Based Magnetorheological Fluids Stabilized by Addition of Organoclay Particles. *Langmuir* **2008,** 24, (14), 7076-7084.

55. Lim, S. T.; Cho, M. S.; Jang, I. B.; Choi, H. J., Magnetorheological characterization of carbonyl iron based suspension stabilized by fumed silica. *J. Magn. Magn. Mater.* **2004,** 282, 170-173.

56. Choi, H. J.; Park, B. J.; Cho, M. S.; You, J. L., Core-shell structured poly(methyl methacrylate) coated carbonyl iron particles and their magnetorheological characteristics. *J. Magn. Magn. Mater.* **2007,** 310, 2835-2837.

57. Fang, F. F.; Kim, J. H.; Choi, H. J., Synthesis of core–shell structured PS/Fe_3O_4 microbeads and their magnetorheology. *Polymer* **2009,** 50, 2290-2293.

58. Jiang, W.; Zhu, H.; Guo, C.; Li, J.; Xue, Q.; Feng, J.; Gong, X., Poly(methyl methacrylate)-coated carbonyl iron particles and their magnetorheological characteristics. *Polym Int* **2010,** 59, 879-883.

59. Fang, F. F.; Liu, Y. D.; Choi, H. J.; Seo, Y., Core-Shell Structured Carbonyl Iron Microspheres Prepared via Dual-Step Functionality Coatings and Their Magnetorheological Response. *ACS Appl. Mater. Interfaces* **2011,** 3, 3487-3495.

60. Bell, R. C.; Karli, J. O.; Vavreck, A. N.; Zimmerman, D. T.; Ngatu, G. T.; Wereley, N. M., Magnetorheology of submicron diameter iron microwires dispersed in silicone oil. *Smart Mater. Struct.* **2008,** 17, 015028.

61. Fang, F. F.; Choi, H. J.; Jhon, M. S., Magnetorheology of soft magnetic carbonyl iron suspension with single-walled carbon nanotube additive and its yield stress scaling function. *Colloids Surf., A* **2009,** 351, 46-51.

62. Rabbani, Y.; Ashtiani, M.; Hashemabadi, S. H., An experimental study on the effects of temperature and magnetic field strength on the magnetorheological fluid stability and MR effect. *Soft Matter* **2015,** In Press.

63. Vicente, J. d.; Segovia-Gutiérrez, J. P.; Andablo-Reyes, E.; Vereda, F.; Hidalgo-Álvarez, R., Dynamic rheology of sphere- and rod-based magnetorheological fluids. *J. Chem. Phys.* **2009,** 131, 194902.

64. Lopez-Lopez, M. T.; Vertelov, G.; Bossis, G.; Kuzhir, P.; Duran, J. D. G., New magnetorheological fluids based on magnetic fibers. *J. Mater. Chem.* **2007,** 17, 3839-3844.

65. Molyet, K.; Yamamoto, H.; Vieira, S. L.; Naganathan, N. G., Magnetorheological Fluid Behavior Under Constant Shear Rates and High Magnetic Fields Over Long Time Periods. *J. Eng. Mater. Technol.* **2006,** 128, 163-168.

66. Tang, X.; Zhang, X.; Tao, R.; Rong, Y., Structure-enhanced yield stress of magnetorheological fluids. *J. Appl. Phys.* **2000,** 87, (5), 2634-2638.

67. Vereda, F.; Vicente, J. d.; Segovia-Gutierrez, J. P.; Hidalgo-Alvarez, R., Average particle magnetization as an experimental scaling parameter for the yield stress of dilute magnetorheological fluids. *J. Phys. D:Appl. Phys.* **2011,** 44, 425002.

68. Rosenzweig, R. E., *Ferrohydrodynamics*. Cambridge University Press: Cambridge, 1985.

69. Stephen, P. S. Low Viscosity Magnetic Fluid Obtained By The Colloidal Suspension Of Magnetic Particles. 1965.

70. Liao, W.; Chen, X.; Chen, Y.; Pu, S.; Xia, Y.; Li, Q., Tunable optical fiber filters with magnetic fluids. *Appl. Phys. Lett.* **2005,** 87, (15), 151122.

71. Shima, P. D.; Philip, J., Tuning of Thermal Conductivity and Rheology of Nanofluids Using an External Stimulus. *J. Phys. Chem. C* **2011,** 115, (41), 20097-20104.

72. - - - , J. D. G.; Iskakova, L.; Zubarev, A., Colloids on the Frontier of Ferrofluids. Rheological Properties. *Langmuir* **2012,** 28, 6232-6245.

73. Ochofiski, W., Dynamic Sealing with Magnetic Fluids. *Wear* **1989,** 130, 261-268.

74. Moskowitz, R.; Stahl, P.; Reed, W. R. Dynamic lip seal using ferrofluids as sealant/lubricant. 1979.

75. Rosensweig, R. E. Material separation using ferromagnetic liquid techniques. 1969.

76. Raj, K.; Moskowitz, B.; Casciari, R., Advances in ferrofluid technology. *J. Magn. Magn. Mater.* **1995,** 149, 174-180.
77. Rosensweig, R. E., Refrigeration aspects of magnetic particle suspensions. *Int. J. Refrig* **2006,** 29, 1250-1258.
78. Price, J. T.; Kruse, J. M. Magnetically controllable couplings containing ferrofluids 1990.
79. Moskowitz, R.; Stahl, P.; Reed, W. R. Inertia damper using ferrofluid 1978.
80. Philip, J.; Shima, P. D.; Raj, B., Nanofluid with tunable thermal properties. *Appl. Phys. Lett.* **2008,** 92, 043108.
81. Philip, J.; Jaykumar, T.; Kalyanasundaram, P.; Raj, B., A tunable optical filter. *Meas. Sci. Technol.* **2003,** 14, (8), 1289-1294.
82. Pu, S.; Chen, X.; Chen, L.; Liao, W.; Chen, Y.; Xia, Y., Tunable magnetic fluid grating by applying a magnetic field. *Appl. Phys. Lett.* **2005,** 87, (2), 021901.
83. Philip, J.; Rao, C. B.; Jayakumar, T.; Raj, B., A new optical technique for detection of defects in ferromagnetic materials and components. *NDT & E Int.* **2000,** 33, 289-295.
84. Stromberg, M.; Gunnarsson, K.; Johansson, H.; Nilsson, M.; Svedlindh, P.; Strømme, M., Interbead interactions within oligonucleotide functionalized ferrofluids suitable for magnetic biosensor applications. *J. Phys. D: Appl. Phys.* **2007,** 40, 1320-1330.
85. Wang, Y.; Dostalek, J.; Knoll, W., Magnetic Nanoparticle-Enhanced Biosensor Based on Grating-Coupled Surface Plasmon Resonance. *Anal. Chem.* **2011,** 83, (16), 6202-6207.
86. Inglis, D. W.; Riehn, R.; Austin, R. H.; Sturm, J. C., Continuous microfluidic immunomagnetic cell separation. *Appl. Phys. Lett.* **2004,** 85, 5093.
87. Jain, T. K.; Richey, J.; Strand, M.; Pelecky, D. L. L.; Flask, C.; Labhasetwar, V., Magnetic Nanoparticles with Dual Functional Properties: Drug Delivery and Magnetic Resonance Imaging. *Biomaterials* **2008,** 29, 4012.
88. Eberbeck, D.; Wiekhorst, F.; Steinhoff, U.; Trahms, L., Quantification of biomolecule agglutination by magnetorelaxometry. *Appl. Phys. Lett.* **2009,** 95, 213701.
89. Zimny, K.; Mascaro, B.; Brunet, T.; Poncelet, O.; Aristégui, C.; Leng, J.; Sandre, O.; Mondain-Monval, O., Design of a fluorinated magneto-responsive material with tunable ultrasound scattering properties. *J. Mater. Chem. B* **2014,** 2, (10), 1285-1297.
90. Pablico-Lansigan, M. H.; Situ, S. F.; Samia, A. C. S., Magnetic particle imaging: advancements and perspectives for real-time *in vivo* monitoring and image-guided therapy. *Nanoscale* **2013,** 5, (10), 4040-4055.
91. Liu, X. L.; Choo, E. S. G.; Ahmed, A. S.; Zhao, L. Y.; Yang, Y.; Ramanujan, R. V.; Xue, J. M.; Fan, D. D.; Fan, H. M.; Ding, J., Magnetic nanoparticle-loaded polymer nanospheres as magnetic hyperthermia agents. *J. Mater. Chem. B* **2014,** 2, (1), 120-128.
92. Ilg, P., Stimuli-responsive hydrogels cross-linked by magnetic nanoparticles. *Soft Matter* **2013,** 9, (13), 3465-3468.
93. Shen, W.; Lim, C. L.; Gao, Z., A ferrofluid-based homogeneous assay for highly sensitive and selective detection of single-nucleotide polymorphisms. *Chem. Commun.* **2013,** 49, (73), 8114-8116.
94. Zubarev, A. Y.; Iskakova, L. Y., Rheological properties of ferrofluids with microstructures. *J. Phys.: Condens. Matter* **2006,** 18, S2771–S2784.
95. Ilg, P.; Kröger, M., Anisotropic self-diffusion in ferrofluids studied via Brownian dynamics simulations. *Phys. Rev. E* **2005,** 72, 031504.
96. Barnes, H. A.; Hutton, J. F.; Walter, K., *An Introduction to Rheology*. Elsevier: 1989.

97. Popplewell, J.; Rosensweig, R. E.; Siller, J. K., Magnetorheology of ferrofluid composites. *J. Magn. Magn. Mater.* **1995,** 149, 53-56.

98. Gans, B. J. d.; Blom, C.; Philipse, A. P.; Mellema, J., Linear viscoelasticity of an inverse ferrofluid. *Phys. Rev. E* **1999,** 60, (4), 4518-4527.

99. Gans, B. J. d.; Duin, N. J.; Ende, D. v. d.; Mellema, J., The influence of particle size on the magnetorheological properties of an inverse ferrofluid. *J. Chem. Phys.* **2000,** 113, (5), 2032-2042.

100. Ramos, J.; Klingenberg, D. J.; Alvarez, R. H.; Vicente, J. d., Steady shear magnetorheology of inverse ferrofluids. *J. Rheol.* **2011,** 55, (1), 127-152.

101. Skjeltorp, A. T., One- and Two-Dimensional Crystallization of Magnetic Holes. *Phys. Rev. Lett.* **1983,** 51, (25), 2306-2309.

102. Gans, B.-J. d.; Hoekstra, H.; Mellema, J., Non-linear magnetorheological behaviour of an inverse ferrofluid. *Faraday Discuss.* **1999,** 112, 209-224.

103. Ramos, J.; Vicente, J. d.; Hidalgo-Alvarez, R., Small-Amplitude Oscillatory Shear Magnetorheology of Inverse Ferrofluids. *Langmuir* **2010,** 26, (12), 9334-9341.

104. McTague, J. P., Magnetoviscosity of Magnetic Colloids. *J. Chem. Phys.* **1969,** 51, 133.

105. Odenbach, S., Ferrofluids-magnetically controlled suspensions. *Colloids Surf., A* **2003,** 217, 171-178.

106. Shliomis, M. I., Effective Viscosity of Magnetic Suspensions. *J. Exp. Theor. Phys.* **1972,** 34, (6), 1291-1294.

107. Martsenyuk, M. A.; Raikher, Y. L.; Shliomis, M. I., On the kinetics of magnetization of suspensions of ferromagnetic particles. *J. Exp. Theor. Phys.* **1974,** 38, (2), 413-416.

108. Miguel, M. C.; Rubi, J. M.; Perez-Madrid, A., Dynamics of ferromagnetic particles in suspension; contribution of the energy of anisotropy. *Physica A* **1994,** 203, 24-32.

109. Felderhof, B. U.; Kroh, H. J., Hydrodynamics of magnetic and dielectric fluids in interaction with the electromagnetic field. *J. Chem. Phys.* **1999,** 110, 7403-7411.

110. Felderhof, B. U., Magnetoviscosity and relaxation in ferrofluids. *Phys. Rev. E* **2000,** 62, (3), 3848-3854.

111. Shliomis, M. I., Comment on ‘‘Magnetoviscosity and relaxation in ferrofluids’’. *Phys. Rev. E* **2001,** 64, 063501.

112. Muller, H. W.; Liu, M., Structure of ferrofluid dynamics. *Phys. Rev. E* **2001,** 64, 061405.

113. Patel, R.; Upadhyay, R. V.; Mehta, R. V., Viscosity measurements of a ferrofluid: comparison with various hydrodynamic equations. *J. Colloid Interface Sci.* **2003,** 263, 661-664.

114. Embs, J. P.; May, S.; Wagner, C.; Kityk, A. V.; Leschhorn, A.; Lücke, M., Measuring the transverse magnetization of rotating ferrofluids. *Phys. Rev. E* **2006,** 73, 036302.

115. Odenbach, S.; Gilly, H., Taylor vortex flow of magnetic fluids under the influence of an azimuthal magnetic field. *J. Magn. Magn. Mater.* **1996,** 152, 123-128.

116. Odenbach, S.; Stork, H., Shear dependence of field-induced contributions to the viscosity of magnetic fluids at low shear rates. *J. Magn. Magn. Mater.* **1998,** 183, 188-194.

117. Odenbach, S.; Rylewicz, T.; Heyen, M., A rheometer dedicated for the investigation of viscoelastic effects in commercial magnetic fluids. *J. Magn. Magn. Mater.* **1999,** 201, 155-158.

118. Odenbach, S., Magnetoviscous and Viscoelastic Effects in Ferrofluids. *Int. J. Mod. Phys. B* **2000,** 14, (16), 1615-1631.

119. Fermigier, M.; Gast, A. P., Structure Evolution in a Paramagnetic Latex Suspension. *J. Colloid Interface Sci.* **1992,** 154, (2), 522-539.

120. Furst, E. M.; Gast, A. P., Dynamics and lateral interactions of dipolar chains. *Phys. Rev. E* **2000,** 62, (5), 6916-6925.

121. Halsey, T. C.; Toor, W., Fluctuation-induced couplings between defect lines or particle chains. *J. Star. Phys.* **1990,** 61, (5-6), 1257-1281.

122. Halsey, T. C.; Toor, W., Structure of Electrorheological Fluids. *Phys. Rev. Lett.* **1990,** 65, 2820.

123. Laskar, J. M.; Philip, J.; Raj, B., Experimental investigation of magnetic-field-induced aggregation kinetics in nonaqueous ferrofluids. *Phys. Rev. E* **2010,** 82, 021402.

124. Laskar, J. M.; Philip, J.; Raj, B., Experimental evidence for reversible zippering of chains in magnetic nanofluids under external magnetic fields. *Phys. Rev. E* **2009,** 80, (4), 041401.

125. Shliomis, M. I.; Morozov, K. I., Negative viscosity of ferrofluid under alternating magnetic field. *Phys. Fluids* **1994,** 6, (8), 2855-2861.

126. Bacri, J.-C.; Perzynski, R.; Shliomis, M. I.; Burde, G. I., "Negative-Viscosity" Effect in a Magnetic Fluid. *Phys. Rev. Lett.* **1995,** 75, (11), 2128-2131.

127. Rosensweig, R. E., "Negative Viscosity" in a Magnetic Fluid. *Science* **1996,** 271, (5249), 614-615.

128. Andhariya, N.; Chudasama, B.; Patel, R.; Upadhyay, R. V.; Mehta, R. V., Field induced rotational viscosity of ferrofluid: Effect of capillary size and magnetic field direction. *J. Colloid Interface Sci.* **2008,** 323, 153-157.

129. Odenbach, S.; Raj, K., The Influence of Large Particles and Agglomerates on the Magnetoviscous Effect in Ferrofluids. *Magnetohydrodynamics* **2000,** 36, (4), 379-386.

130. Shahnazian, H.; Odenbach, S., Rheological investigations of ferrofluids with a shear stress controlled rheometer. *J. Phys.: Condens. Matter* **2008,** 20, 204137.

131. Thurm, S.; Odenbach, S., Magnetic separation of ferrofluids. *J. Magn. Magn. Mater.* **2002,** 252, 247-249.

132. Zeuner, A.; Richter, R.; Rehberg, I., Experiments on negative and positive magnetoviscosity in an alternating magnetic field. *Phys. Rev. E* **1998,** 58, (5), 6287.

133. Perez-Madrid, A.; Alarcon, T.; Vilar, J. M. G.; Rubi, J. M., A mesoscopic approach to the "negative" viscosity effect in ferrofluids. *Physica A* **1999,** 270, 403-412.

134. Zahn, M.; Pioch, L. L., Magnetizable fluid behaviour with effective positive, zero or negative dynamic viscosity. *Indian J. Eng. Mater. Sci.* **1998,** 5, 400-410.

135. Morimoto, H.; Maekawa, T.; Matsumoto, Y., Nonequilibrium Brownian dynamics analysis of negative viscosity induced in a magnetic fluid subjected to both ac magnetic and shear flow fields. *Phys. Rev. E* **2002,** 65, (6), 061508.

136. Rosensweig, R. E., Heating magnetic fluid with alternating magnetic field. *J. Magn. Magn. Mater.* **2002,** 252, 370-374.

137. Fannin, P. C.; Charles, S. W., The study of a ferrofluid exhibiting both Brownian and Neel relaxation. *J. Phys. D:Appl. Phys.* **1989,** 22, 187-191.

138. Zubarev, A. Y.; Iskakova, L. Y., Effect of chainlike aggregates on dynamical properties of magnetic liquids. *Phys. Rev. E* **2000,** 61, 5415-5421.

139. Odenbach, S., Microgravity research as a tool for the investigation of effects in magnetic fluids. *J. Magn. Magn. Mater.* 201, 149-154.
140. Zubarev, A. Y.; Iskakova, L. Y., Structural transformations in ferrofluids. *Phys. Rev. E* **2003,** 68, 061203.
141. Zubarev, A. Y.; Iskakova, L. Y., To the theory of rheological properties of ferrofluids: influence of drop-like aggregates. *Physica A* **2004,** 343, 65-80.
142. Chirikov, D. N.; Fedotov, S. P.; Iskakova, L. Y.; Zubarev, A. Y., Viscoelastic properties of ferrofluids. *Phys. Rev. E* **2010,** 82, (5), 051405.
143. Hosseini, S. M.; Fazlali, A.; E.Ghasemi; Moghaddam, H. A.; M.Salehi, Rheological properties of a γ-Fe_2O_3 paraffin-based ferrofluid. *J. Magn. Magn. Mater.* **2010,** 322, 3792-3796.
144. Pop, L. M.; Hilljegerdes, J.; Odenbach, S.; Wiedenmann, A., The microstructure of ferrofluids and their rheological properties. *Appl. Organometal. Chem.* **2004,** 18, 523-528.
145. Hong, R.-Y.; Li, J.-H.; Zhang, S.-Z.; Li, H.-Z.; Zheng, Y.; Ding, J.-m.; Wei, D.-G., Preparation and characterization of silica-coated Fe_3O_4 nanoparticles used as precursor of ferrofluids. *Appl. Surf. Sci.* **2009,** 255, 3485-3492.
146. Chen, H. J.; Wang, Y. M.; Qu, J. M.; Hong, R. Y.; Li, H. Z., Preparation and characterization of silicon oil based ferrofluid. *Appl. Surf. Sci.* **2011,** 257, 10802– 10807.
147. Paul, N.; Hazarika, S.; Saha, A.; Mohanta, D., Optical emission, vibrational feature, and shear-thinning aspect of Tb^{3+}-doped Gd_2O_3 nanoparticle-based novel ferrofluids irradiated by gamma photons. *J. Appl. Phys.* **2013,** 114, 134903.
148. Nowak, J.; Dohmen, E.; Odenbach, S., The Magnetoviscous Effect of a Biocompatible Ferrofluid at High Shear Rates. *IEEE Trans. Magn.* **2014,** 50, (11), 4600304.
149. Kroell, M.; Pridoehl, M.; Zimmermann, G.; Pop, L.; Odenbach, S.; Hartwig, A., Magnetic and rheological characterization of novel ferrofluids. *J. Magn. Magn. Mater.* **2005,** 289, 21-24.
150. Pacull, J.; Gonçalves, S.; Delgado, Á. V.; Durán, J. D. G.; Jiménez, M. a. L., Effect of polar interactions on the magnetorheology of silica-coated magnetite suspensions in oil media. *J. Colloid Interface Sci.* **2009,** 337, 254-259.
151. Yang, Y.; Li, L.; Chen, G.; Li, W., Magnetorheological Properties of Aqueous Ferrofluids. *J Soc. Rheol. Jpn.* **2006,** 34, (1), 25-31.
152. Brown, E.; Forman, N. A.; Orellana, C. S.; Zhang, H.; Maynor, B. W.; Betts, D. E.; DeSimone, J. M.; Jaeger, H. M., Generality of shear thickening in dense suspensions. *Nat. Mater.* **2010,** 9, 220-224.
153. Shahnazian, H.; Graf, D.; Borin, D. Y.; Odenbach, S., Rheology of a ferrofluid based on nanodisc cobalt particles. *J. Phys. D:Appl. Phys.* **2009,** 42, 205004.
154. Stoffelbach, F.; Aqil, A.; Jerome, C.; Jerome, R.; Detrembleur, C., An easy and economically viable route for the decoration of carbon nanotubes by magnetite nanoparticles, and their orientation in a magnetic field. *Chem. Commun.* **2005**, (36), 4532-4533.
155. Samouhos, S.; McKinley, G., Carbon Nanotube–Magnetite Composites, With Applications to Developing Unique Magnetorheological Fluids. *J. Fluids Eng.* **2007,** 129, 429-437.
156. Ko, S. W.; Yang, M. S.; Choi, H. J., Adsorption of polymer coated magnetite composite particles onto carbon nanotubes and their magnetorheology. *Mater. Lett.* **2009,** 63, (11), 861-863.

157. Korneva, G.; Ye, H.; Gogotsi, Y.; Halverson, D.; Friedman, G.; Bradley, J.-C.; Kornev, K. G., Carbon Nanotubes Loaded with Magnetic Particles. *Nano Lett.* **2005,** 5, (5), 879-884.

158. Wu, Z.; Mueller, A.; Degenhard, S.; Ruff, S. E.; Geiger, F.; Bittner, A. M.; Wege, C.; III, C. E. K., Enhancing the Magnetoviscosity of Ferrofluids by the Addition of Biological Nanotubes. *ACS Nano* **2010,** 4, (8), 4531-4538.

159. Wu, Z.; Zierold, R.; Mueller, A.; Ruff, S. E.; Ma, C.; Khan, A. A.; Geiger, F.; Sommer, B. A.; Knez, M.; Nielsch, K.; Bittner, A. M.; Wege, C.; III, C. E. K., Preparation and magnetoviscosity of nanotube ferrofluids by viral scaffolding and ALD on porous templates. *Phys. Status Solidi B* **2010,** 247, (10), 2412-2423.

160. Vekas, L.; Rasa, M.; Bica, D., Physical Properties of Magnetic Fluids and Nanoparticles from Magnetic and Magneto-rheological Measurements. *J. Colloid Interface Sci.* **2000,** 231, 247-254.

161. Brullot, W.; N.K.Reddy; J.Wouters; V.K.Valev; B.Goderis; J.Vermant; T.Verbiest, Versatile ferrofluids based on polyethyleneglycol coated iron oxide nanoparticles. *J. Magn. Magn. Mater.* **2012,** 324, 1919–1925.

162. Hong, R. Y.; Zhang, S. Z.; Han, Y. P.; Li, H. Z.; Ding, J.; Zheng, Y., Preparation, characterization and application of bilayer surfactant-stabilized ferrofluids. *Powder Technol.* **2006,** 170, 1-11.

163. Pastoriza-Gallego, M. J.; Lugo, L.; Legido, J. L.; Piñeiro, M. M., Rheological non-Newtonian behaviour of ethylene glycol-based Fe_2O_3 nanofluids. *Nanoscale Res. Lett.* **2011,** 6, 560.

164. Raj, K.; Moskowitz, R., Commercial applications of ferrofluids. *J. Magn. Magn. Mater.* **1990,** 85, 233-245.

165. Gnanaprakash, G.; Philip, J.; Jayakumar, T.; Raj, B., Effect of digestion time and alkali addition rate on physical properties of magnetite nanoparticles. *J. Phys. Chem. B* **2007,** 111, (28), 7978-7986.

166. Muthukumaran, T.; Gnanaprakash, G.; Philip, J., Synthesis of Stable Magnetic Nanofluids of Different Particle Sizes. *J. Nanofluids* **2012,** 1, (1), 85-92.

167. Newton, I., Philosophiae Naturalis Principia Mathematica. In 2009.

168. Tanner, R. I.; Walters, K., *Rheology: An Historical Perspective: An Historical Perspective*. Elsevier: 1998.

169. Schramm, G., *A Practical Approach to Rheology and Rheometry*. 1998.

170. Bergenholtz, J.; Brady, J. F.; Vicic, M., The non-Newtonian rheology of dilute colloidal suspensions. *J. Fluid Mech.* **2002,** 456, 239-275.

171. Wagner, N. J.; Brady, J. F., Shear thickening in colloidal dispersions. *Phys. Today* **2009,** 62, (10), 27-32.

172. Mewis, J., Thixotropy - A General Review. *J. Non-Newtonian Fluid Mech.* **1979,** 6, 1-20.

173. Barnes, H. A., Thixotropy - a review. *J. Non-Newtonian Fluid Mech.* **1997,** 70, 1-33.

174. Kanai, H.; Amari, T., Negative thixotropy in ferric-oxide suspensions. *Rheol. Acta* **1995,** 34, 303-310.

175. Whorlow, R. W., *Rheological Techniques*. Ellis Horwood Limited: 1992.

176. Wyss, H. M.; Miyazaki, K.; Mattsson, J.; Hu, Z.; Reichman, D. R.; Weitz, D. A., Strain-Rate Frequency Superposition: A Rheological Probe of Structural Relaxation in Soft Materials. *Phys. Rev. Lett.* **2007,** 98, (23), 238303.

177. Foner, S., Versatile and Sensitive Vibrating-Sample Magnetometer. *Rev. Sci. Instrum.* **1959,** 30, (7), 548-557.

178. Coats, A. W.; Redfern, J. P., Thermogravimetric analysis. A review. *Analyst* **1963,** 88, 906-924.

179. Tsenoglou, C., Scaling concepts in suspension rheology. *J. Rheol.* **1990,** 34, (1), 15-24.

180. Jones, D. A. R.; Leary, B.; Boger, D. V., The Rheology of a Concentrated Colloidal Suspension of Hard Spheres. *J. Colloid Interface Sci.* **1991,** 147, (2), 479-495.

181. Phuoc, T. X.; Massoudi, M., Experimental observations of the effects of shear rates and particle concentration on the viscosity of Fe_2O_3–deionized water nanofluids. *Int. J. Therm. Sci.* **2009,** 48, 1294–1301.

182. Veld, P. J. i. t.; Petersen, M. K.; Grest, G. S., Shear thinning of nanoparticle suspensions. *Phys. Rev. E* **2009,** 79, 021401.

183. Wilking, J. N.; Chang, C. B.; Fryd, M. M.; Porcar, L.; Mason, T. G., Shear-Induced Disruption of Dense Nanoemulsion Gels. *Langmuir* **2011,** 27, 5204-5210.

184. Odenbach, S., *Colloidal Magnetic Fluids: Basics, Development and Application of Ferrofluids*. Springer: 2009.

185. Haghgooie, R.; Doyle, P. S., Transition from two-dimensional to three-dimensional behavior in the self-assembly of magnetorheological fluids confined in thin slits. *Phys. Rev. E* **2007,** 75, 061406.

186. Zubarev, A. Y., Rheological Properties of Polydisperse Magnetic Fluids.Effect of Chain Aggregates. *J. Exp. Theor. Phys.* **2001,** 93, (1), 80-88.

187. Zubarev, A. Y.; Iskakova, L. Y., On the theory of rheological properties of magnetic suspensions. *Physica A* **2007,** 382, 378–388.

188. Zubarev, A. Y.; Iskakova, L. Y., Rheological properties of ferrofluids with microstructures. *J. Phys.: Condens. Matter* **2006,** 18, S2771-S2784.

189. Chirikov, D. N.; Fedotov, S. P.; Iskakova, L. Y.; Zubarev, A. Y., Viscoelastic properties of ferrofluids. *Phys. Rev. E* **2010,** 82, 051405.

190. Fermigier, M.; Gast, A. P., Structure Evolution in a Paramagnetic Latex Suspension. *J. Colloid Interface Sci.* **1992,** 154, (2), 522-539.

191. Martin, J. E.; Odinek, J.; Halsey, T. C.; Kamien, R., Structure and dynamics of electrorheological fluids. *Phys. Rev. E* **1998,** 57, (1), 756-775.

192. Martin, J. E.; Anderson, R. A., Chain model of electrorheology. *J. Chem. Phys.* **1996,** 104, (12), 4814-4827.

193. Espin, M. J.; Delgado, A. V.; Martin, J. E., Effects of electric fields and volume fraction on the rheology of hematite/silicone oil suspensions. *Rheol. Acta* **2004,** 44, 71-79.

194. Klingenberg, D. J.; Ulicny, J. C.; Golden, M. A., Mason numbers for magnetorheology. *J. Rheol.* **2007,** 51, (5), 883-893.

195. Ivey, M.; Liu, J.; Zhu, Y.; Cutillas, S., Magnetic-field-induced structural transitions in a ferrofluid emulsion. *Phys. Rev. E* **2000,** 63, 011403.

196. Volkova, O.; Bossis, G.; Guyot, M.; Bashtovoi, V.; Reks, A., Magnetorheology of magnetic holes compared to magnetic particles. *J. Rheol.* **2000,** 44, (1), 91-104.

197. López-López, M. T.; Kuzhir, P.; Bossis, G., Magnetorheology of fiber suspensions. I. Experimental. *J. Rheol.* **2009,** 53, (1), 115-126.

198. Vicente, J. d.; Klingenberg, D. J.; Hidalgo-Alvarez, R., Magnetorheological fluids: a review. *Soft matter* **2011,** 7, 3701–3710.

199. Ginder, J. M.; Davis, L. C.; Elie, L. D., Rheology of Magnetorheological Fluids: Models and Measurements. *Int. J. Mod. Phys. B* **1996,** 10, (23 & 24), 3293-3303.
200. Ramos, J.; Kingenberg, D. J.; Hidalgo-Alvarez, R.; Vicente, J. d., Steady shear magnetorheology of inverse ferrofluids. *J. Rheol.* **2011,** 55, (1), 127-152.
201. Viota, J. L.; Delgado, A. V.; Arias, J. L.; Durán, J. D. G., Study of the magnetorheological response of aqueous magnetite suspensions stabilized by acrylic acid polymers. *J. Colloid Interface Sci.* **2008,** 324, 199–204.
202. Vereda, F.; Vicente, J. d.; Segovia-Gutiérrez, J. P.; Hidalgo-Alvarez, R., On the effect of particle porosity and roughness in magnetorheology. *J. Appl. Phys.* **2011,** 110, 063520.
203. Soto-Aquino, D.; Rinaldi, C., Magnetoviscosity in dilute ferrofluids from rotational Brownian dynamics simulations. *Phys. Rev. E* **2010,** 82, 046310.
204. Shima, P. D.; Philip, J., Tuning of Thermal Conductivity and Rheology of Nanofluids Using an External Stimulus. *J. Phys. Chem. C* **2011,** 115, 20097-20104.
205. Wyss, H. M.; Larsen, R. J.; Weitz, D. A., Oscillatory Rheology Measuring the Viscoelastic Behaviour of Soft Materials. *G.I.T. Laboratory Journal* **2007,** 3-4, 68-70.
206. McLeish, T. C. B.; Jordan, T.; Shaw, M. T., Viscoelastic response of electrorheological fluids. I. Frequency dependence. *J. Rheol.* **1991,** 35, (3), 427-448.
207. Vicente, J. d.; López-López, M. T.; Durán, J. D. G.; Bossis, G., A slender-body micromechanical model for viscoelasticity of magnetic colloids: Comparison with preliminary experimental data. *J. Colloid Interface Sci.* **2005,** 282, 193-201.
208. Pop, L. M.; Odenbach, S.; Wiedenmann, A.; Matoussevitch, N.; Bonnemann, H., Microstructure and rheology of ferrofluids. *J. Magn. Magn. Mater.* **2005,** 289, 303-306.
209. Kruse, T.; Krautha¨user, H.-G.; Spanoudaki, A.; Pelster, R., Agglomeration and chain formation in ferrofluids: Two-dimensional x-ray scattering. *Phys. Rev. B* **2003,** 67, 094206.
210. Pastoriza-Gallego, M. J.; Pérez-Rodríguez, M.; Gracia-Fernández, C.; Piñeiro, M. M., Study of viscoelastic properties of magnetic nanofluids: an insight into their internal structure. *Soft Matter* **2013,** 9, (48), 11690-11698.
211. Kirkland-York, S.; Gallow, K.; Ray, J.; Loo, Y.-l.; McCormick, C., Temperature induced ordering and gelation of star micelles based on ABA triblocks synthesised via aqueous RAFT polymerization. *Soft Matter* **2009,** 5, 2179-2182.
212. Wang, S.; Yang, C.; Bian, X., Magnetoviscous properties of Fe_3O_4 silicon oil based ferrofluid. *J. Magn. Magn. Mater.* **2012,** 324, 3361-3365.
213. Ghasemi, E.; Mirhabibi, A.; Edrissi, M., Synthesis and rheological properties of an iron oxide ferrofluid. *J. Magn. Magn. Mater.* **2008,** 320, 2635-2639.
214. Pinho, M.; Brouard, B.; Genevaux, J. M.; Dauchez, N.; O.Volkova; Meziere, H.; Collas, P., Investigation into ferrofluid magnetoviscous effects under an oscillating shear flow. *J. Magn. Magn. Mater.* **2011,** 323, (18-19), 2386-2390.
215. Soto-Aquino, D.; Rosso, D.; Rinaldi, C., Oscillatory shear response of dilute ferrofluids: Predictions from rotational Brownian dynamics simulations and ferrohydrodynamics modeling. *Phys. Rev. E* **2011,** 84, 056306.
216. Parthasarathy, M.; Klingenberg, D. J., A microstructural investigation of the nonlinear response of electrorheological suspensions II. Oscillatory shear flow. *Rheol. Acta* **1995,** 34, 430-439.
217. Parthasarathy, M.; Klingenberg, D. J., A microstructural investigation of the nonlinear response of electrorheological suspensions I. Start-up of steady shear flow. *Rheol. Acta* **1995,** 34, 417-429.

218. Klingenberg, D. J., Simulation of the dynamic oscillatory response of electrorheological suspensions: Demonstration of a relaxation mechanism. *J. Rheol.* **1993,** 37, (2), 199-214.

219. Kuzhir, P.; Gómez-Ramírez, A.; López-López, M. T.; Bossis, G.; Zubarev, A. Y., Non-linear viscoelastic response of magnetic fiber suspensions in oscillatory shear. *J. Non-Newtonian Fluid Mech.* **2011,** 166, (7-8), 373-385.

220. Mohebi, M.; Jamasbi, N.; Liu, J., Simulation of the formation of nonequilibrium structures in magnetorheological fluids subject to an external magnetic field. *Phys. Rev. E* **1996,** 54, (5), 5407-5413.

221. Felicia, L. J.; Philip, J., Probing of Field-Induced Structures and Tunable Rheological Properties of Surfactant Capped Magnetically Polarizable Nanofluids. *Langmuir* **2013,** 29, (1), 110-120.

222. Mason, T. G.; Weitz, D. A., Linear Viscoelasticity of Colloidal Hard Sphere Suspensions near the Glass Transition. *Phys. Rev. Lett.* **1995,** 75, (14), 2770-2773.

223. Cloitre, M.; Borrega, R.; Leibler, L., Rheological Aging and Rejuvenation in Microgel Pastes. *Phys. Rev. Lett.* **2000,** 85, (22), 4819-4822.

224. Kowalczyk, A.; Hochstein, B.; Stahle, P.; Willenbacher, N., Characterization of complex fluids at very low frequency: experimental verification of the strain rate-frequency superposition (SRFS) method. *Appl. Rheol.* **2010,** 20, (5), 52340

225. Mohan, P. H.; Bandyopadhyay, R., Phase behavior and dynamics of a micelle-forming triblock copolymer system. *Phys. Rev. E* **2008,** 77, (4), 041803.

226. Shedge, A. S.; Wadgaonkar, P. P.; Lele, A. K.; Badiger, M. V., Hydrophobically Modified Poly(vinyl alcohol) Using Alkoxy-Substituted Methyl Gallate: Synthesis and Rheology. *J. Polym. Sci., Part B: Polym. Phys.* **2010,** 48, (10), 1054-1063.

227. Oliver, M.; Kovats, T.; Mijailovich, S. M.; Butler, J. P.; Fredberg, J. J.; Lenormand, G., Remodeling of Integrated Contractile Tissues and Its Dependence on Strain-Rate Amplitude. *Phys. Rev. Lett.* **2010,** 105, (15), 158102.

228. Krishnaswamy, R.; Majumdar, S.; Sood, A. K., Nonlinear Viscoelasticity of Sorbitan Tristearate Monolayers at Liquid/Gas Interface. *Langmuir* **2007,** 23, (26), 12951–12958.

229. Ferry, J. D., *Viscoelastic Properties of Polymers*. 3rd ed.; John Wiley & Sons: New York, 1980

230. Spruijt, E.; Sprakel, J.; Lemmers, M.; Stuart, M. A. C.; Gucht, J. v. d., Relaxation Dynamics at Different Time Scales in Electrostatic Complexes:Time-Salt Superposition. *Phys. Rev. Lett.* **2010,** 105, (20), 208301.

231. Cramer, C.; De, S.; Schonhoff, M., Time-Humidity-Superposition Principle in Electrical Conductivity Spectra of Ion-Conducting Polymers. *Phys. Rev. Lett.* **2011,** 107, (2), 028301.

232. Moctezuma, R. E.; Donado, F.; Arauz-Lara, J. L., Lateral aggregation induced by magnetic perturbations in a magnetorheological fluid based on non-Brownian particles. *Phys. Rev. E* **2013,** 88, (3), 032305.

233. Liu, Y. D.; Choi, H. J., Carbon nanotube-coated silicated soft magnetic carbonyl iron microspheres and their magnetorheology. *J. Appl. Phys.* **2012,** 111, (7), 07B502.

234. Fang, F. F.; Choi, H. J., Noncovalent self-assembly of carbon nanotube wrapped carbonyl iron particles and their magnetorheology. *J. Appl. Phys.* **2008,** 103, (7), 07A301.

235. Ko, S. W.; Lim, J. Y.; Park, B. J.; Yang, M. S.; Choi, H. J., Magnetorheological carbonyl iron particles doubly wrapped with polymer and carbon nanotube. *J. Appl. Phys.* **2009,** 105, (7), 07E703.

236. Fang, F. F.; Choi, H. J.; Seo, Y., Sequential Coating of Magnetic Carbonyliron Particles with Polystyrene and Multiwalled Carbon Nanotubes and Its Effect on Their Magnetorheology. *ACS Appl. Mater. Interfaces* **2010,** 2, (1), 54-60.

237. Duan, W. H.; Wang, Q.; Collins, F., Dispersion of carbon nanotubes with SDS surfactants: a study from a binding energy perspective. *Chem. Sci.* **2011,** 2, 1407-1413.

238. Wang, H., Dispersing carbon nanotubes using surfactants. *Curr. Opin. Colloid Interface Sci.* **2009,** 14, 364-371.

239. Chiu, C.-c.; Dieckmann, G. R.; Nielsen, S. O., Molecular Dynamics Study of a Nanotube-Binding Amphiphilic Helical Peptide at Different Water/Hydrophobic Interfaces. *J. Phys. Chem. B* **2008,** 112, 16326-16333.

240. Ji, Y.; Huang, Y. Y.; Tajbakhsh, A. R.; Terentjev, E. M., Polysiloxane surfactants for the dispersion of carbon nanotubes in nonpolar organic solvents. *Langmuir* **2009,** 25, (20), 12325-12331.

241. Shima, P. D.; Philip, J.; Raj, B., Magnetically controllable nanofluid with tunable thermal conductivity and viscosity. *Appl. Phys. Lett.* **2009,** 95, 133112.

242. Yearsley, K. M.; Mackley, M. R.; Chinesta, F.; Leygue, A., The rheology of multiwalled carbon nanotube and carbon black suspensions. *J. Rheol.* **2012,** 56, 1465-1490.

243. Bohlius, S.; Pleiner, H.; Brand, H. R., Pattern formation in ferrogels: analysis of the Rosensweig instability using the energy method. *J. Phys.: Condens. Matter* **2006,** 18, (38), S2671.

244. Tanvir, S.; Qiao, L., Surface tension of Nanofluid-type fuels containing suspended nanomaterials. *Nanoscale Res Lett* **2012,** 7, (1), 226.

245. Zubarev, A. Y., Rheological Properties of Polydisperse Magnetic Fluids. Effect of Chain Aggregates. *J. Exp. Theor. Phys.* **2001,** 93, (1), 80-88.

246. Bica, I.; Liu, Y. D.; Choi, H. J., Physical characteristics of magnetorheological suspensions and their applications. *J. Ind. Eng. Chem.* **2013,** 19, 394-406.

247. Alves, S.; Alcantara, M. R.; Neto, A. M. F., The effect of hydrophobic and hydrophilic fumed silica on the rheology of magnetorheological suspensions. *J. Rheol.* **2009,** 53, 651-662.

248. Khan, S. A.; Zoeller, N. J., Dynamic rheological behavior of flocculated fumed silica suspensions. *J. Rheol.* **1993,** 37, (6), 1225-1235.

249. Cao, X. J.; Cummins, H. Z.; Morris, J. F., Structural and rheological evolution of silica nanoparticle gels. *Soft Matter* **2010,** 6, 5425-5433.

250. Binks, B. P.; Liu, W.; Rodrigues, J. A., Novel Stabilization of Emulsions via the Heteroaggregation of Nanoparticles. *Langmuir* **2008,** 24, 4443-4446.

251. Weston, J. S.; Venkataramani, D.; Aichele, C. P.; Grady, B. P.; Harwell, J.; Resasco, D., Pseudosolid, Shear-Thinning Gel Formation in Binary Dispersions of Metal Oxide Nanoparticles at Low Volume Fractions. *Langmuir* **2014,** 30, 14982−14990.

252. Kim, A. Y.; Berg, J. C., Fractal Heteroaggregation of Oppositely Charged Colloids. *J. Colloid Interface Sci.* **2000,** 229, 607-614.

253. Kim, A. Y.; Hauch, K. D.; Berg, J. C.; Martin, J. E.; Anderson, R. A., Linear chains and chain-like fractals from electrostatic heteroaggregation. *J. Colloid Interface Sci.* **2003,** 260, 149-159.

254. Rasa, M.; Philipse, A. P.; Meeldijk, J. D., Heteroaggregation, repeptization and stability in mixtures of oppositely charged colloids. *J. Colloid Interface Sci.* **2004,** 278, 115-125.
255. Nallamilli, T.; Mani, E.; Basavaraj, M. G., A Model for the Prediction of Droplet Size in Pickering Emulsions Stabilized by Oppositely Charged Particles. *Langmuir* **2014,** 30, 9336-9345.
256. Raghavan, S. R.; Walls, H. J.; Khan, S. A., Rheology of Silica Dispersions in Organic Liquids: New Evidence for Solvation Forces Dictated by Hydrogen Bonding. *Langmuir* **2000,** 16, (21), 7920-7930.
257. Mitamura, Y.; Arioka, S.; Sakota, D.; Sekine, K.; Azegami, M., Application of a magnetic fluid seal to rotary blood pumps. *J. Phys.: Condens. Matter* **2008,** 20, (20), 204145.